METAL-LIGAND COOPERATION IN BIS(PHOSPHINIMINE)-SUPPORTED RHODIUM PINCER COMPLEXES: FROM DEHYDROGENATION TO VALUE-ADDED PRODUCTS

SHOU-JEN (EDWARD) HSIANG
Bachelor of Science, University of British Columbia, 2017

A thesis submitted
in partial fulfilment of the requirements for the degree of

DOCTOR OF PHILOSOPHY

in

EARTH, SPACE, AND PHYSICAL SCIENCE

Department of Chemistry and Biochemistry
University of Lethbridge
LETHBRIDGE, ALBERTA, CANADA

Metal-Ligand Cooperation in Bis(phosphinimine)-Supported Rhodium Pincer Complexes: From Dehydrogenation to Value-added Products

Shou-Jen (Edward) Hsiang

Date of Defense: March 18th, 2025

Dr. Paul G. Hayes	Professor	Ph.D.
Thesis Supervisor		
Dr. Michael Gerken	Professor	Ph.D.
Thesis Examination Committee Member		
Dr. Stacey D. Wetmore	Professor	Ph.D.
Thesis Examination Committee Member		
Dr. Hisako Hashimoto	Professor	Ph.D.
External Examiner, Tohoku University		
Dr. Jean-Denys Hamel	Assistant Professor	Ph.D.
Chair, Thesis Examination Committee		

Dedication

This thesis is dedicated to every person who has shown me kindness, generosity, and love when I have always had very little to offer in return.

These pages would be blank without you.

Abstract

Expansion of methodology towards the synthesis of pincer ligand (L = κ^3-NNN' = 2,5-[^{i}Pr$_2$P=N(4-^{i}PrC$_6$H$_4$)]$_2$-N'(C$_4$H$_2$)$^-$) supported rhodium tetrylene (κ^2-L(CO)Rh(ER$_2$); E = Si, Ge; κ^2-L = κ^2-NN'-Rh, κ^1-N-E) and borylene (κ^2-L(CO)Rh(BMes); Mes = mesityl) species is described, followed by investigations into the reactivity of these new complexes.

A metal-ligand cooperative approach was used to dehydrogenate group 14 starting materials of the form RR'EH$_2$ (E = Si, Ge; R = aryl or alkyl; R' = H, aryl or alkyl) and MesBH$_2$ (Mes = mesityl), and the resulting complexes were characterized by a variety of instrumentational techniques (NMR, IR, EA). X-ray crystallography was used to unambiguously confirm the solid-state structure within these species, establishing the hemilability of the R$_3$P=*N*Ar "phosphinimine" nitrogen-donor of the pincer ligand as well as its base-stabilization capabilities.

Diverse reaction chemistry was demonstrated for these species, starting with dehydrocoupling reactions with pinacol, which provided proof that the activated main group functionalities could be used as {BMes}, {SiRR'}, and {GeRR'} synthons and transferred to organic substrates. Additionally, reaction of a base-stabilized borylene complex with a variety of alkynes and CO gas yielded highly functionalized boron-containing heterocycles ($\overline{\text{PhC=CRBMesOC}}$=NPipp) that would be difficult to synthesize by alternative routes, showcasing the potential these systems have for applications. Finally, the H-substituted silylene complex, κ^2-L(CO)Rh(Si(H)Mes), was demonstrated to react with tris(pentafluorophenyl)borane to yield an elusive silylyne complex, the first of its kind with rhodium.

Altogether, a cohesive body of work encompassing the development of new methodologies, diverse reaction chemistry, and the presentation of future areas for pursuit are described herein.

Contribution of Authors and Preface

The following thesis chapters containing original research are reproduced from the listed publications with permissions from the corresponding publishers and co-authors.

Chapter 2 – MacNeil, C. S.; **Hsiang, S. J.**; Hayes, P. G.*, Dehydrogenation of a Primary Borane: A Source of :BR for Group Transfer Reactions. *Chemical Communications.* **2020**, *56*, 12323-12326.

Chapter 3 – **Hsiang, S. J.**; Hayes, P. G.*, Rhodium-mediated Dehydrogenation of Hydroboranes and Group 14 Compounds: Base-stabilized Silylene and Germylene Complexes vs. Transmetalation. *Chemistry – A European Journal.* **2023**, *30*, e202302925.

Chapter 4 – **Hsiang, S. J.**; Hayes, P. G.*, Rhodium-mediated Assembly of New Heterocycles: From Borylenes to Oxaboroles. *Angewandte Chemie International Edition.* **2025**, *178*, e202421302.

Chapter 5 – **Hsiang, S. J.**; Hayes, P. G.*, Synthesis and Reaction Chemistry of a Rhodium Silylyne Complex. Accepted for publication in the *Canadian Journal of Chemistry*, **2025**.

Aside from Chapter 2, which presents work by both me and Dr. Connor MacNeil, I am responsible for all experimental research reported in this thesis. Additional details delineating the contributions for Chapter 2 are provided within the preface for the chapter on page 32; the chapter has been re-written/paraphrased in my own words. As a publication-based thesis, the remaining first author publications are reproduced with only changes to formatting for Chapters 3-5 to fit the requirements of this document. Additional details regarding citation style, supplementary information, and sub-sections are elaborated upon within the abstract/preface page of each chapter. Compounds are numbered sequentially in order of appearance throughout the entire thesis document, a notable change from the original publications. This numbering of compounds has been established to improve readability and make references to specific compounds easier to follow. References, and numbers thereof, are reset at the start of each chapter.

Dr. Dylan J. Webb and I performed all combustion measurements for new and published compounds listed in this document. With the exception of compounds **3** and **4** collected by Dr. Connor MacNeil, all X-ray crystallographic data was collected and processed by me. IR spectroscopy requiring inert atmosphere conditions was conducted with aid from Nathan Hill and Prof. René Boeré, while Orbitrap mass spectrometry experiments were conducted with the aid of Carl Holland. I performed all other experimental techniques, including NMR spectroscopy and GC-MS. Computational work was also performed myself with resources provided by the Digital Research Alliance of Canada (alliancecan.ca) and suggestions from Dr. Austin Pounder. No use of generative AI was used in either the writing of this thesis or the experimental/computational work described.

Acknowledgements

Paul, who has given me so many opportunities to learn, grow, and explore. Without his enthusiastic support since our very first phone call, I would not have made it this far. I thank him for his encouragement throughout this long degree, his endless excitement for new discoveries even when I've been discouraged in my progress, and for being my biggest advocate in everything I've wanted to pursue. I firmly believe that I would not have had the same opportunities, skills, or confidence in what I do without his guidance. Thanks for having me as a student Paul.

It takes a village to raise a PhD student, and what a great village I wound up in here at the University of Lethbridge. I am forever grateful for the friendship and kindness fellow students in the Hayes lab have shown me.

Dylan Webb, you were the first face I saw coming into campus and have been a mainstay in my life since. Your friendship means the world. Thanks for making the workplace a joy to be in and for looking out for me over the years.

Sam Dresher, watching you transition from our neuroscience independent study student to the accomplished chemist you are today was truly inspiring. From being a friend to being a colleague, your support was unwavering and your compassion got me through a lot. Thanks for all the discussions we've had on chemistry as well as life, I cherish them greatly.

Jackson Knott, you were there to meet me for Thai food in Vancouver before this degree even began, and I'll probably be staying with you at the end when I defend it. You already know how special you are to me. Sorry I didn't carry on through with your research, but thanks for being a light in my life along the way.

Daisy Cruz-Milette, your work ethic was insane and your passion for chemistry contagious. Thanks for your company and support when I was struggling, and your endless generosity towards your friends.

Connor MacNeil and Tara Dickie, thanks for your help and support throughout the start of my degree. A special thanks to Connor for laying the foundations of this project and advocating for me to be a part of it.

To the new blood of the lab, thanks for putting up with my chaos within the lab, and for your support as I've been finishing up. Thamara Salazar, thanks for being a great and passionate friend and co-worker, I wish you all the success in carrying on the Hayes lab torch.

Finally, to the undergraduate students who have had to deal with me, Ashraf Aborawi, Bryan Mills, Corey Wiltse, Marc Tardiff, and Elise Green, as much or little as I've been able to teach you, you've all repaid me in friendship and support and I thank you for that. I take pride in knowing that all of you like me enough to hang out with me outside of work.

To my other friends within the department, Austin Pounder, Makay Murray, and Nathan Hill, you've all helped and supported me in some way or another throughout my degree. Thanks for being my friends, and good luck with your future endeavors.

The faculty and staff at this university have been amazing to work alongside of and have offered me many opportunities I doubt I would have had access to otherwise. I would like to thank Prof. René Boeré for his help with X-Ray Crystallography and his words of support throughout my degree. I'd also like to thank Tony Montina, Vince Weiler, and Mike Opyr for their help with the NMR instruments so essential to our work. The teaching faculty I've worked with, including Dr. Greg Patenaude and Dr. Susan Findlay, have inspired much of my desire to pursue opportunities in lecturing outside of my normal TA-ship duties. Support staff, including Heather Weiler and Susan Hill, are a backbone for our department and I thank them for their help as well. Finally, my committee members Prof. Michael Gerken and Prof. Stacey Wetmore have been nothing but supportive of me, and I thank them for their guidance.

Table of Contents

List of Figures

List of Schemes

List of Tables

List of New Compounds

Base-stabilized borylene, silylene, silylyne, and germylene species depicted in two canonical resonance structures. Non-isolable compounds denoted with (*). Compounds **1** and **2** were previously published by Dr. Connor MacNeil, and included here for completeness.

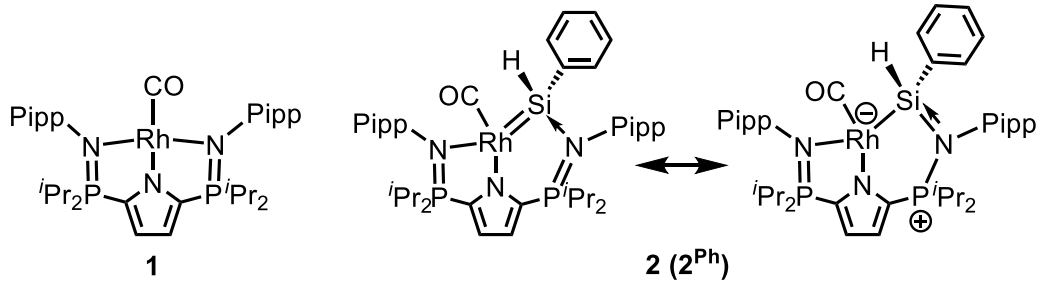

1 **2 (2^{Ph})**

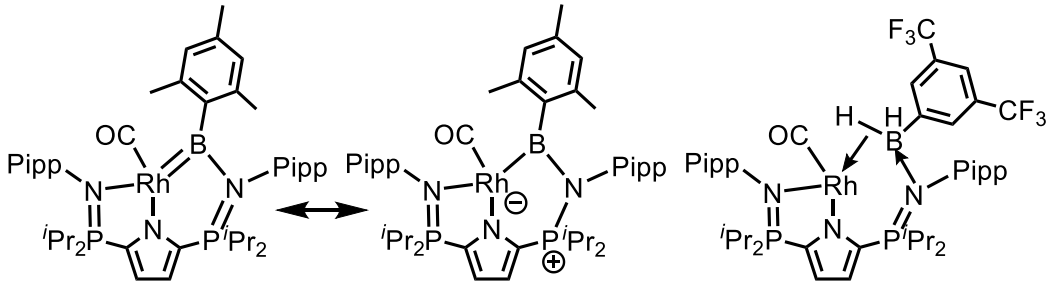

3 **4**

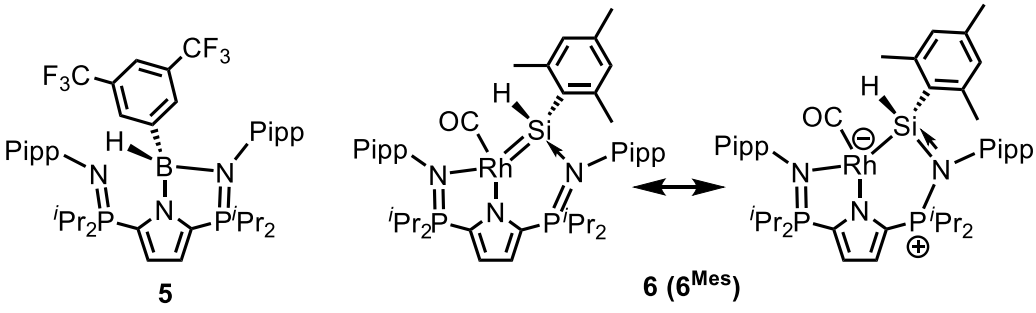

5 **6 (6^{Mes})**

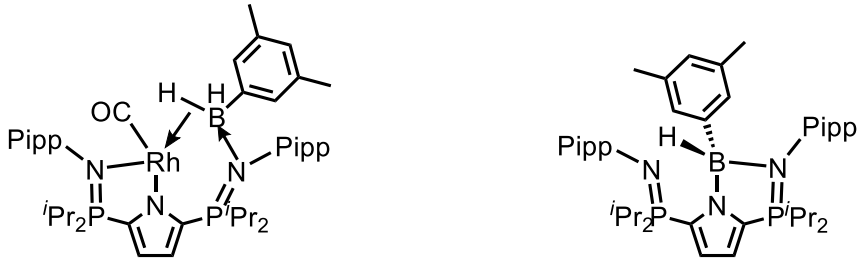

7 **8**

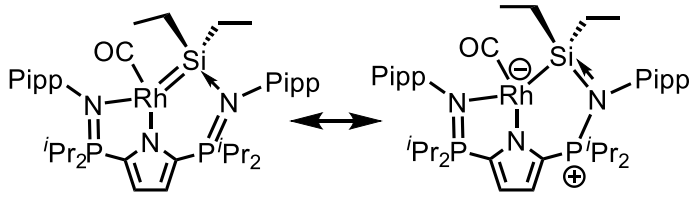

9

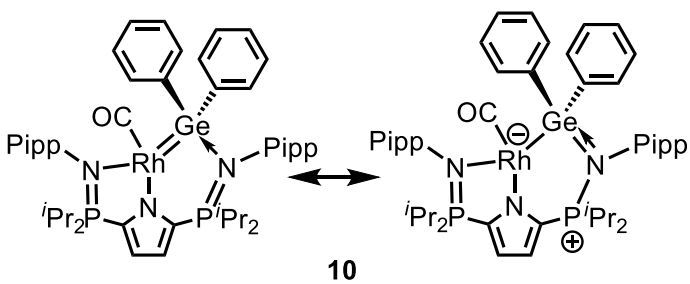

10

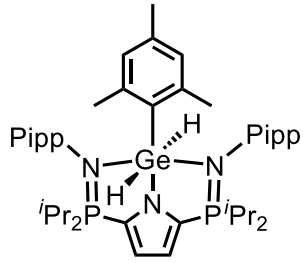

11*

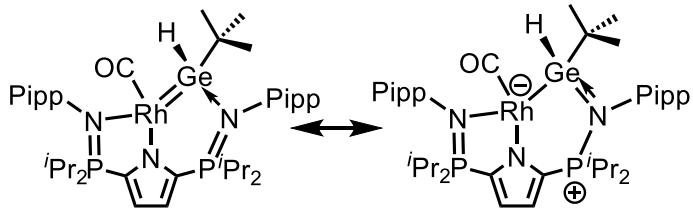

12

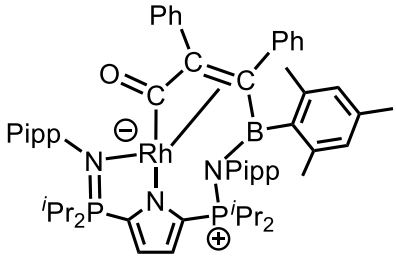

13^{Ph}

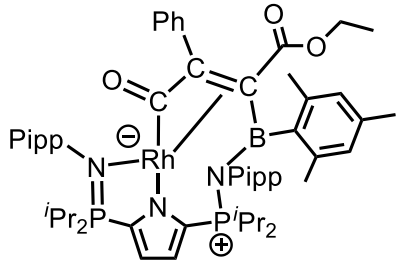

13^{CO2Et}

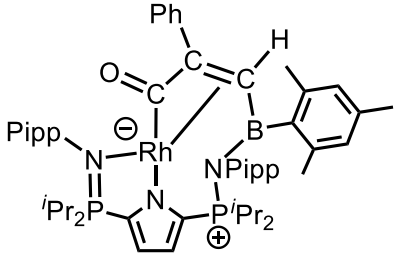

13^{H}

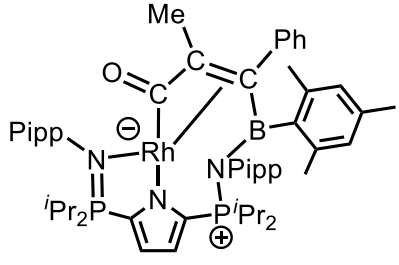

13^{Me}

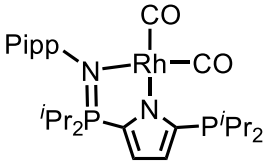

14

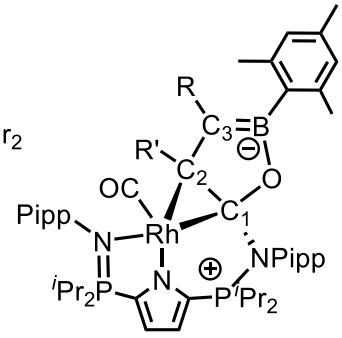

15-16^{Ph} (R = R' = Ph)
15-16^{CO2Et} (R = CO_2Et, R' = Ph)
15-16^{H} (R = H, R' = Ph)
15-16^{Me} (R = Ph, R' = Me)

15* (**15^{Ph}** not observed)

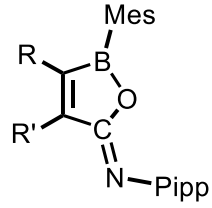

16*

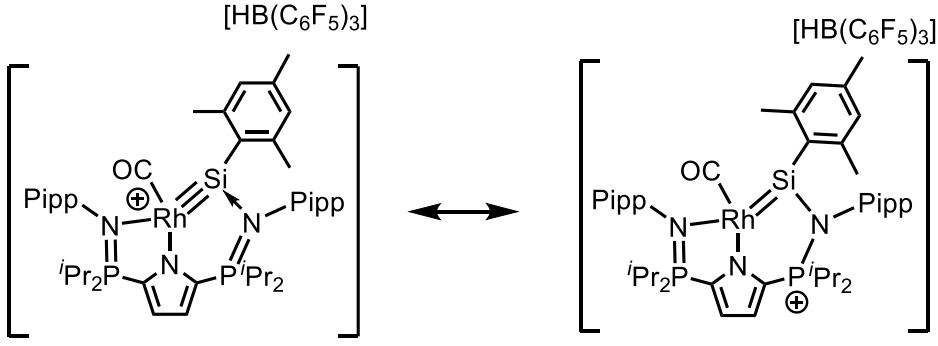

17^{Mes}

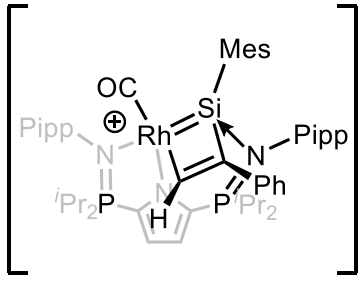

18^{Mes*}

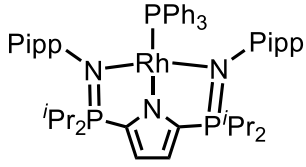

19

List of Abbreviations and Symbols

Å	Angstrom
Anal Calcd	calculated (elemental analysis)
APT	attached proton test (NMR spectroscopy)
Ar	aryl
atm	atmosphere
BDE	bond dissociation energy
br	broad
C	Celsius
CCDC	Cambridge Crystallographic Data Center
COE	cyclooctene
COD	1,5-cyclooctadiene
COSY	correlated spectroscopy (NMR spectroscopy)
Cp	cyclopentadienyl ligand
Cp*	pentamethylcyclopentadienyl ligand
Cy	cyclohexyl (C_6H_{11})
d	doublet
°	degree
δ	delta (chemical shift in NMR spectroscopy or partial charge)
Δ	delta (change in)
DBU	1,8-diazabicyclo[5.4.0]undec-7-ene
DEPT	distortion-less enhancement by polarization transfer
DFT	density functional theory
Dipp	2,6-diisopropylphenyl
dmp	2,6-dimesitylphenyl
η	eta (hapticity)
E	main group element (typically group 13/14)
FLP	frustrated Lewis pair
g	grams
G	Gibb's free energy
GC-MS	gas chromatography – mass spectrometry

h	hours
HOMO	highest occupied molecular orbital
HMBC	heteronuclear multiple bond correlation
HSQC	heteronuclear single quantum coherence
Hz	Hertz
^{i}Pr	isopropyl
IR	infrared
J	symbol for coupling constant (Hz)
K	Kelvin
κ	kappa (denticity)
λ	lambda (wavelength)
L_n	ligand(s)
LA	Lewis acid
LB	Lewis base
lp	lone pair (computational)
LUMO	lowest unoccupied molecular orbital
m	multiplet
Me	methyl
Mes	mesityl
^{meta}Xyl	3,5-$Me_2(C_6H_3)$
^{meta}Xyl^{F}	3,5-$(CF_3)_2(C_6H_3)$
MLC	metal ligand cooperation
MLMB	metal ligand multiple bond(ing)
min	minutes
MS	mass spectrometry
NBO	natural bond order (computational)
^{n}Bu	*n*-butyl
NHC	N-heterocyclic
ν	nu (wavenumber)
NMR	nuclear magnetic resonance
ov	overlapping

Ph	phenyl
π	pi
Pin	pinacol
Pipp	*para*-isopropylphenyl
ppm	parts per million
PTFE	polytetrafluoroethylene
q	quartet
R	alkyl or aryl substituent
s	singlet
σ	sigma
Σ	sigma (sum)
Sol	solvent
sp	septet
τ	tau (geometry index)
t	time or triplet (spectroscopy)
T	temperature
^{t}Bu	*tert*-butyl
THF	tetrahydrofuran
TM	transition metal
Tol/tol	toluene
X	halogen
xs	excess
WBI	Wiberg bond index
1D	one dimensional
2D	two dimensional
{}	decoupled (NMR spectroscopy)

Chapter 1. Introduction

1.1. Thesis Overview

Discrete metal complexes leveraged towards the synthesis of complex molecular structures have revolutionized our world and are responsible for most of the pharmaceuticals and polymer materials we use everyday. As metal ions impart little selectivity on their own, the necessity of ligands, used to fine-tune the steric and electronic environment around the metal center, is well established. Additionally, the use of ligands as reactive sites complimentary to the transition metal has led to Nobel prize winning discoveries, including the 2005 prize for olefin metathesis that relies on the incorporation of a metal-bound carbene (M=C) ligand. While metal-carbon multiple bonding has been thoroughly studied over the past few decades, multiple bonding to the heavier group 14 elements (tetrylenes) has lagged, owing to synthetic challenges in isolating stable examples. The work detailed in this thesis aimed to address that paucity by developing new methodologies for preparing these elusive tetrylene functionalities. The reactivity of the resulting complexes has been studied in depth, complimenting existing work and showcasing the high potential of these systems for use in the synthesis of value-added products.

1.2. Transition Metal Catalysis and Ligand Design

Catalysis has been a cornerstone to the development of new technologies in the field of chemistry, allowing the construction of molecular complexity with increasing selectivity and efficiency. Synthetic methodologies developed with catalysis in mind usually lead to greener processes (increased atom economy and use of sustainable reagents) that cut down on cost, time, and production steps.[1]

This field can be split largely into the categories of homogeneous vs heterogeneous catalysis, which distinguish between whether the substrate and catalyst are in the same or different physical phase; as well as organo- vs. transition metal (TM) catalysis which differentiate between whether the

active site of the catalyst is carbon or transition metal-based.[1a, 1c] For systems that utilize main group elements other than carbon, such as in frustrated Lewis pair (FLP) catalysis, these examples are generally grouped with organo-catalysts as a broader family of transition metal-free systems. High-throughput industrial processes often favor heterogeneous catalysis (90% of industrial chemicals by volume), where solubilized or even vaporized substrate can pass through solid catalyst interfaces.[1a] When more delicate transformations are required, such as in the pharmaceutical industry, homogeneous catalysis prevails due to the increased active site-specificity and selectivity these catalysts can provide.[1a, 1c]

When compared to organo-catalysts, transition metal-catalysts are marked by the ease at which they can shuttle between oxidation states, as well as their ability to accommodate novel bonding motifs to bring substrates together. Nobel prize acknowledgements in this field include the 2001 prize for stereoselective catalysis awarded to Knowles, Noyori, and Sharpless; as well as the 2010 prize for palladium catalyzed cross-coupling awarded to Heck, Negishi, and Suzuki.[2] These processes feature redox cycles that rely on the ability of transition metals to break apart existing bonds in the activation of substrates, facilitate the formation of new bonds, and finally, eliminate the intended product in an atom-economic manner (Scheme 1.1). The 2005 Nobel Prize for olefin metathesis, awarded to Schrock, Grubbs, and Chauvin, does not undergo a redox cycle but instead highlights the merits of novel bonding motifs in the form of metal–carbon multiple bonds.[3] Nonetheless, the ability of transition metals to bring molecular building blocks together in proximity, and electronically activate them, is essential in these metathesis strategies.

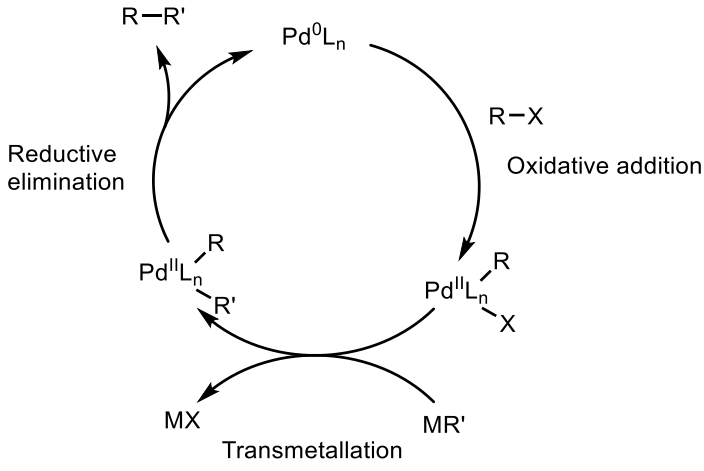

Scheme 1.1. Generic mechanism for palladium catalyzed cross-coupling. Oxidative addition activates the substrate by breaking the R–X bond. Transmetallation introduces the R' group to the system, where M = Zn, Zr, Al (Negishi); B (Suzuki); Sn (Stille). In Heck systems, a metal free, olefinic substrate coordinates independently. By bringing the R and R' groups into close proximity, the system is able to form new C–C bonds in a reductive elimination step, releasing R–R'.

1.2.1. Introduction to Ligands

With these significant contributions in mind, it is important to note that the field of homogenous transition metal catalysis necessitates the inclusion of ligand moieties that allow for the isolation of discrete metal coordination complexes. These ligands are not only stabilizing towards the metal center, but also allow for the fine tuning of steric and electronic environments about the active sites.[4] It is the development of new and varied ligands that have allowed for the incredible stereo/regio-selectivity of these systems, as well as their reaction specificity. These groups can vary in their utility; some serving as bulky rigid scaffolds that influence the steric geometry of the metal active site, while others can be modified or displaced during the catalytic cycle. Chiral ligands like (2*S*,3*S*)-(–)-bis(diphenylphosphino)butane (Chiraphos), for example, offer steric shielding about specific "quadrants" of the metal active site, which encourages the substrate to coordinate about a specific face that imparts enantioselectivity (Figure 1.1).[5]

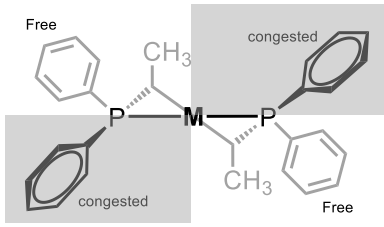

Figure 1.1. Diagram of Chiraphos coordinated to a generic metal center. Shaded areas denote sterically congested quadrants blocked off by the protruding phenyl groups. Light areas denote sterically accessible quadrants due to planar phenyl groups.

Ligands which do not readily undergo chemical changes or substitution are considered to be "spectator" or "auxiliary" ligands and can have varied influence on catalyst behaviour. In the case of the Heck process, triphenylphosphine ligands are used primarily to stabilize the *in situ* generated palladium (0) catalyst and have significantly less interaction with the substrate compared to the example above.[6] Other ligands, such as H^-, CH_3^-, and RO^- can actively participate in the catalytic process and are considered reactive ligands, such as in the oxo process for hydroformylation.[7] Some groups, such as CO or olefins, can be either reactive or auxiliary depending on the context of the catalytic system, giving rise to the concept of non-innocent or cooperative ligands which will be discussed further on in Section 1.3.[4]

1.2.2. Ligand Properties

The careful design and selection of the ligand environment is therefore paramount in the development of new transition metal-catalyzed technologies. Some key considerations when discussing ligand features are highlighted herein, including ligand hapticity and denticity, donor and acceptor qualities, and ligand charge.

Hapticity is defined as the number of atoms simultaneously binding to a metal center in a contiguous series, typically in a conjugated pi-system. Pioneering work in the field of coordination chemistry relied heavily on the use of carbon-based cyclopentadienyl (Cp) ligands which can sterically and electronically saturate the coordination sphere of various metals (Figure 1.2, left).[8]

These Cp ligands bind η^5 to most metal centers, where the η^x designation describes the hapticity of the ligand. This is in contrast to denticity, which similarly describes the number of atoms in a ligand binding or "chelating" to the metal, but in this case, discrete, non-contiguous donor sites are highlighted. The κ^x notation is used to describe these multi-dentate ligands, such as in κ^2-ethylenediamine (Figure 1.2, right). The greater affinity of multidentate ligands for a metal ion, compared to monodentate ligands, is described as the chelate effect, increasing the resilience of the active catalyst to irreversible ligand loss.[4, 8] Geometric constraints imposed by the backbone of multi-dentate ligands can also have a profound impact on how close their donor groups can approach the metal center, further influencing the level of orbital overlap and resultant electronic environment.

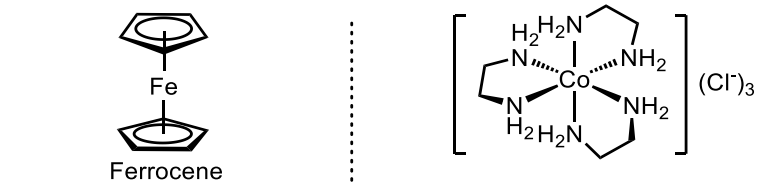

Figure 1.2. Ferrocene demonstrating η^5-coordination of the cyclopentadienyl (Cp) ligand to iron (left). Tris-(κ^2-ethylenediamine)cobalt(III)chloride demonstrating non-contiguous bidentate coordination of ethylenediamine (right).

From a historical perspective, Cp ligands and their derivatives have largely fallen out of favour for modern investigations. The relatively few geometries that allow for accommodation of η^5-coordination (*e.g.* piano stool, sandwich, *etc*.), as well as the fact that derivations are limited to the addition of various substituents on the 5-membered ring, have led to a saturation of examples in the literature. Multidentate ligands, that can have their donor sites spread further apart, allow for more varied substitution patterns and geometries, replacing metallocenes as the norm.

The coordination mode of ligands is also governed by their σ and π donor and acceptor qualities. Most ligands are σ-donors that contribute a lone pair of electrons to interact with the metal center.

While some exceptions exist for Lewis acidic groups such as BR_3 or SO_2, which can exhibit varying degrees of σ-acceptor type interactions, examples such as these are rare.[9] The extent of π-donor and acceptor capabilities has a pronounced impact on the electronic structure, influencing the energy gap between the valent d-orbitals of the metal. For example, ligands like Cl^- or RO^-, that have filled orbitals of correct π-symmetry, can donate electron density, and reduce the energy gap between the e_g and t_{2g} sets of d-orbitals in octahedral complexes. Conversely, a ligand like CO can cause a larger splitting parameter due to its ability to accept electron density from the metal into its C–O σ-antibonding orbital through back-bonding interactions. Similar effects are widely accepted for other well-known geometries (*e.g.* square planar, trigonal bipyramidal, tetrahedral, *etc*.).[8]

Finally, the formal charge of the ligands must also be accounted for when describing transition metal coordination complexes. The redox cycle available to transition metals is one of the distinguishing features being leveraged for catalytic processes. Careful consideration of ligand charge, and consequently the formal charge of the metal center, is therefore vital for isolating stable complexes due to the preferred oxidation states of transition metals.[8] Neutral donors can be employed as auxiliary ligands to saturate the steric and electronic environment without affecting the formal charge, while anionic substituents are often required to gain access to requisite redox cycles.

1.2.3. Pincer Ligands

With these considerations in mind, pincer ligands have become increasingly popular in the post-metallocene era of transition metal chemistry.[4, 10] Defined as being a planar tridentate ligand that chelates to the metal center in a meridional fashion (Figure 1.3), pincer ligands impart similar thermal stability and resistance to displacement as cyclopentadienyl ligands through the chelate effect, while allowing for the versatility of different donor groups, fine tuning of steric quadrants, and modular charge distribution about the three donor sites.[4, 10] Informally grouped by abbreviations corresponding to the three donor atoms, popular PNP, POP, NCN, or PCP ligands

often employ a mix of neutral and anionic donors to accommodate oxidation state requirements. Combinations of strong and weak donor groups on multidentate ligands can also allow for facile coordination/de-coordination events to occur without the loss of the pincer ligand as a whole. This concept of hemi-lability will be core to the theme of metal-ligand cooperation throughout this thesis and further expanded upon in the following section.

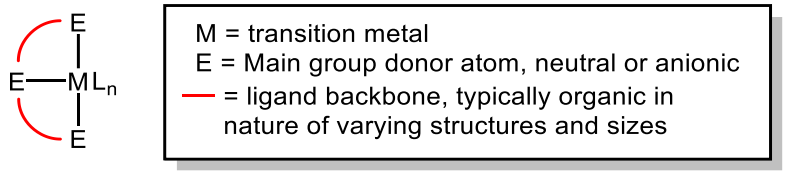

Figure 1.3. Generic depiction of a pincer ligand coordinating meridionally to a transition metal center through three separate donors. The three donor atoms can differ in element, charge, and number of additional substituents. The connecting backbone is often aromatic in nature to increase the planarity of the ligand.

1.3. Metal Ligand Cooperation and Hemilability

The "redox-innocence" of main-group elements precludes oxidative addition and reductive elimination steps that are fundamental to most transition metal-catalyzed technologies. Nonetheless, chemists have still been able to develop novel ways to elicit the breaking of chemical bonds in a controlled and specific manner, crucial for the synthesis of new value-added compounds. Frustrated Lewis Pair chemistry, for example, combines a strongly donating and sterically bulky Lewis base (*e.g.* PCy_3, Cy = C_6H_{11}), with a Lewis acid (*e.g.* $B(C_6F_5)_3$) to activate H_2 and form [*H*PCy_3][*H*$B(C_6F_5)_3$], as disclosed by Stefan *et al*. in their landmark contributions (Scheme 1.2, left).[11] In contrast to processes highlighted in the previous section, which occur only at the metal center, main-group and organo-catalyzed processes rely more heavily on the cooperation between multiple active centers with contrasting electronic properties. Combining this multi-centered approach with conventional organometallic systems results in the research area of metal-ligand cooperation (MLC).

Processes involving MLC utilize specifically designed systems that allow for the ligand groups to participate cooperatively in the activation of substrates.[12] Take for example, the activation of the X–Y bond of a generic substrate through oxidative addition at only the metal center. By careful selection of the coordination environment about the metal, we can envision an MLC counterpart wherein the X–Y bond is instead added to both the metal and a reactive ligand, allowing for an overall redox neutral transformation (Scheme 1.2, right).

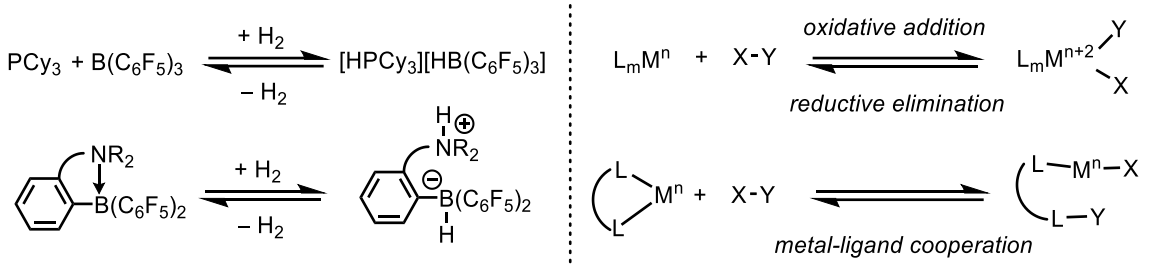

Scheme 1.2. H_2 activation by an FLP system that limits adduct formation through bulky substituents (left, top). H_2 activation by an FLP system that utilizes a hemilabile pendant amine donor (left, bottom). Oxidative addition of a generic substrate X–Y to a metal, resulting in an increase in both oxidation state and coordination number by two (right, top). Activation of a generic substrate X–Y through metal ligand cooperation, resulting in modification to both the metal center and the ligand (right, bottom).

1.3.1. Relevant Examples in MLC

A recent review of MLC systems by Harutyunyan *et al.* defines them as "reactions catalysed by transition metal complexes that involve active participation of both ligand and metal in at least one mechanistically relevant bond-forming or bond-breaking step".[12b] While this definition broadly encompasses a wide range of modes through which a ligand can participate in processes, this section will highlight specific examples that help introduce the subsequent chemistry.

Perhaps the most famous example of MLC comes from the Noyori process for the enantioselective hydrogenation of arylketones. Shown below in Scheme 1.3, the NH functionality of the κ^2-diamine

ligand was found to be essential for catalytic hydrogenation, with tertiary amines being inactive. Early studies by Noyori and Ikariya described how the ligand nitrogen undergoes protonation and deprotonation steps throughout the catalytic cycle and cooperatively activating H_2.[12b, 13] This example highlights the use of the ligand as a hydrogen-shuttle, and also illustrates the high impact MLC systems can have (Nobel prize 2001, *vide supra*).

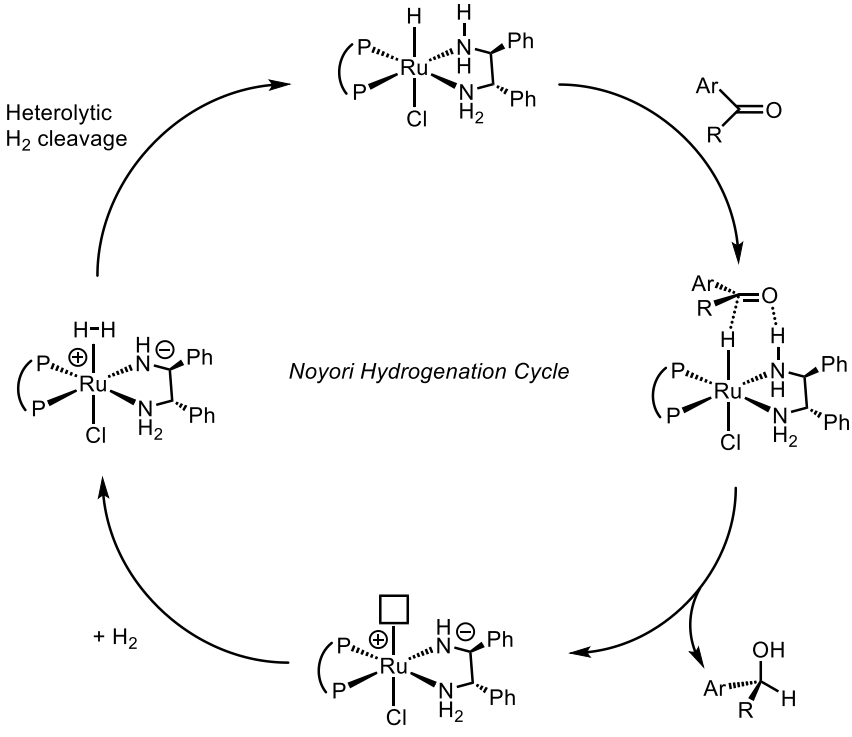

Scheme 1.3. Catalytic cycle established for the Noyori hydrogenation of arylketones. The non-innocence of the diamine ligand allows for both cooperative H_2 activation, and the transfer of the amine bound proton to the aryl ketone.

Milstein and colleagues have disclosed PNN and PNP pincer ligands that work with either ruthenium or iridium to achieve bond activation through aromatization/de-aromatization of the ligand's pyridine ring (Scheme 1.4, top).[12a] When a similar PNP system is applied to zinc, the complex is able to activate H_2 and hydrogenate a series of ketones and imines (Scheme 1.4, bottom).[12c] Notably, the zinc metal center remains in the 2+ oxidation state throughout the transformation, and the hemilability of one of the phosphorus donors on the ligand is demonstrated.

Rather than the donor atom acting as a proton shuttle, like in the Noyori example, the ligand backbone actively participates in the chemistry.

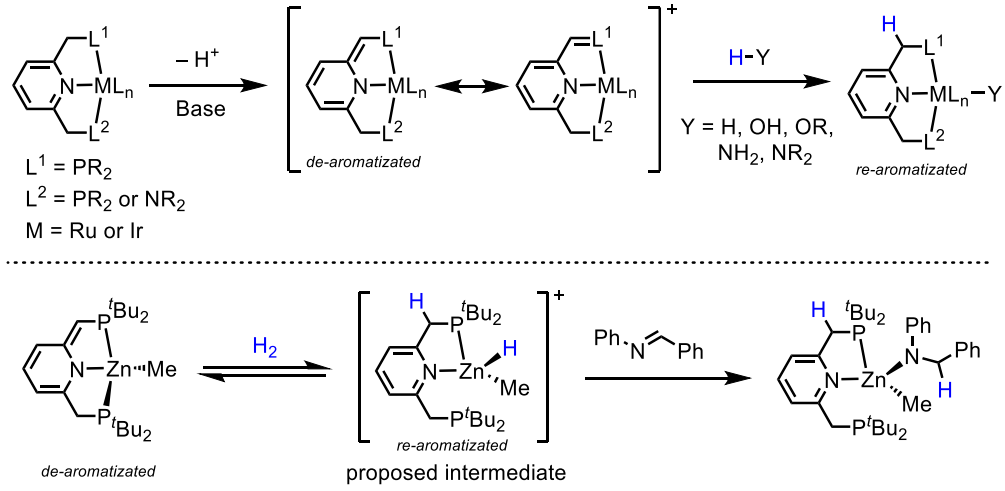

Scheme 1.4. Ruthenium and iridium complexes supported by PNP or PNN pincer ligands that achieve bond activation through aromatization/de-aromatization of the pyridine ring (top). Zinc complex supported by a PNP pincer ligand that is able to activate H_2 through an aromatization step, followed by hydrogenation of an imine substrate (bottom).

Another fundamental concept that both of these examples highlight is the necessity of open coordination sites on the metal center. In the Noyori cycle, H_2 is able to coordinate due to the vacant site on ruthenium after hydride transfer to the ketone. In Milstein's work, we see that dissociation of one of the phosphine donors allows for the aromatized complex to maintain a four-coordinate zinc center. In the context of this section, the ability of a ligand to exhibit both hemilabile properties to free up a coordination site on the metal, as well as reactive properties to interact cooperatively with the substrate, allows for elegant and efficient catalyst systems to be designed. This final example from Gandelman *et al*. highlights this interplay when a ruthenium complex supported by a triazole-based phosphine ligand is shown to catalytically couple terminal alkynes with carboxylic acids in a regioselective fashion (Scheme 1.5).[14] Based on the stereo-selectivity observed, as well as mechanistic investigations involving isotope labelling at either the terminal alkyne or carboxylic

acid hydrogens, the group proposed an MLC-mediated cycle that involves the triazole nitrogen as an internal base. Retention of the hemilabile triazole moiety is accomplished due to the bidentate nature of the ligand. Regioselectivity can be rationalized through the unsymmetric nature of the aryl-substituted alkyne, encouraging nucleophilic attack on the substituted end in step II. Head-to-head alkyne coupling in step IV is postulated to be due either to an allyl-like interaction between the Ph–C–C π-system and ruthenium, or steric hindrance between the two aryl groups.

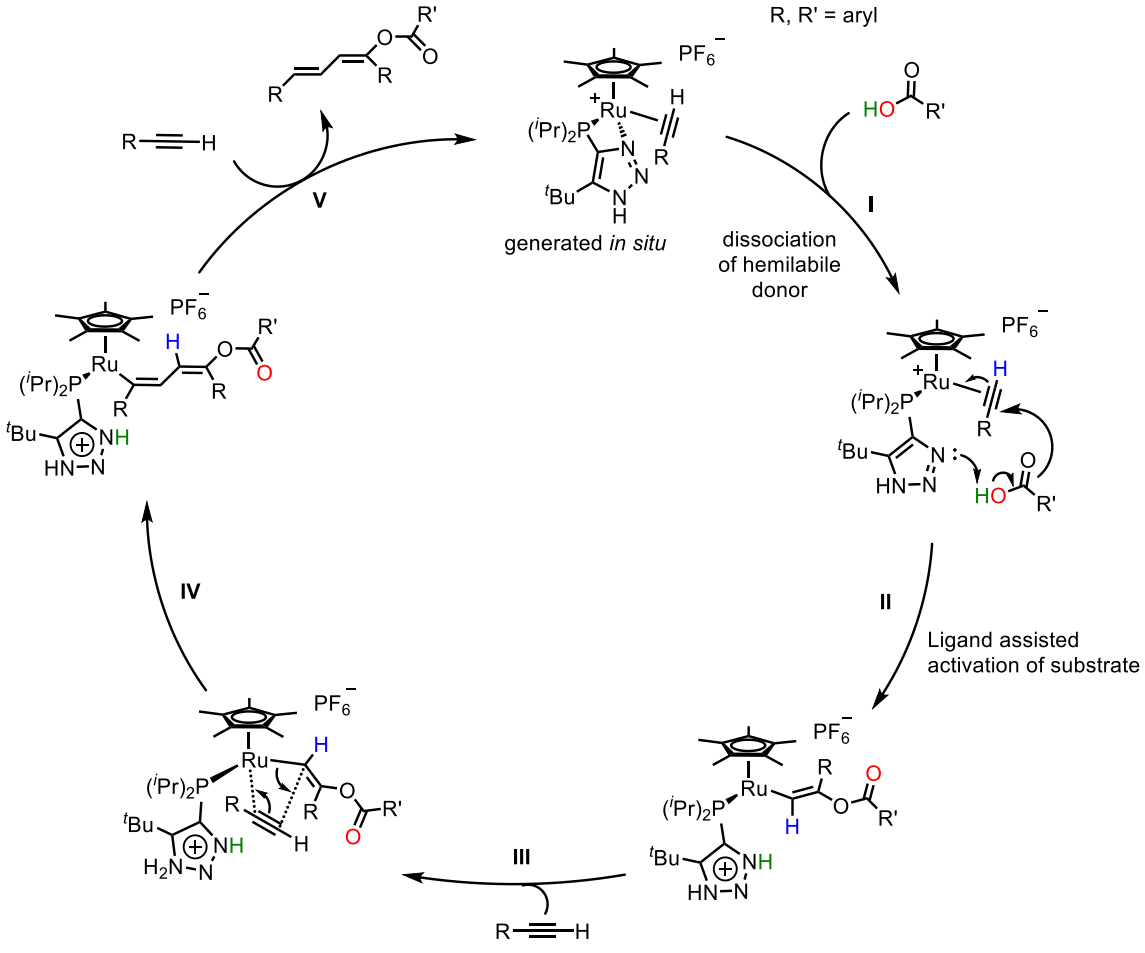

Scheme 1.5. Proposed catalytic cycle for the MLC mediated coupling of terminal alkynes and carboxylic acids.

Noted by both Milstein's 2015 review, as well as Harutyunyan's 2024 review, the topic of MLC finds most of its success in hydrogenation/dehydrogenation applications.[12b, 12d] Indeed, the

breaking of element–H or H–H bonds will also be a significant focus for this body of work, which aims to not only supplement existing examples, but also push the envelope one step further in the development of new MLC mediated technologies.

1.4. Metal–Main Group Element Multiple Bonding

Another approach that involves both the metal and a non-innocent ligand deals with the reactivity of transition metal–main group element multiple bonds (MLMB, M=E). A famous example involves the aforementioned olefin metathesis catalysts wherein a transition metal carbene ($L_nM=CR$) is able to interact with other unsaturated substrates in a [2+2] cycloaddition. While processes such as olefin metathesis can technically be considered MLC systems due to the fact that both metal and ligand fragments are altered in a redox-neutral transformation (Scheme 1.6), the loss of the original donor atom as part of the product leads to some contention for their grouping with the previous examples. Nonetheless, ruthenium-based olefin metathesis catalysts have found widespread success in both academic and industrial applications due to their functional group, air, and moisture tolerance.[15] Investigations into analogous complexes where metals form multiple bonds with carbon-adjacent elements on the periodic table are therefore appealing for the development of new and varied systems.

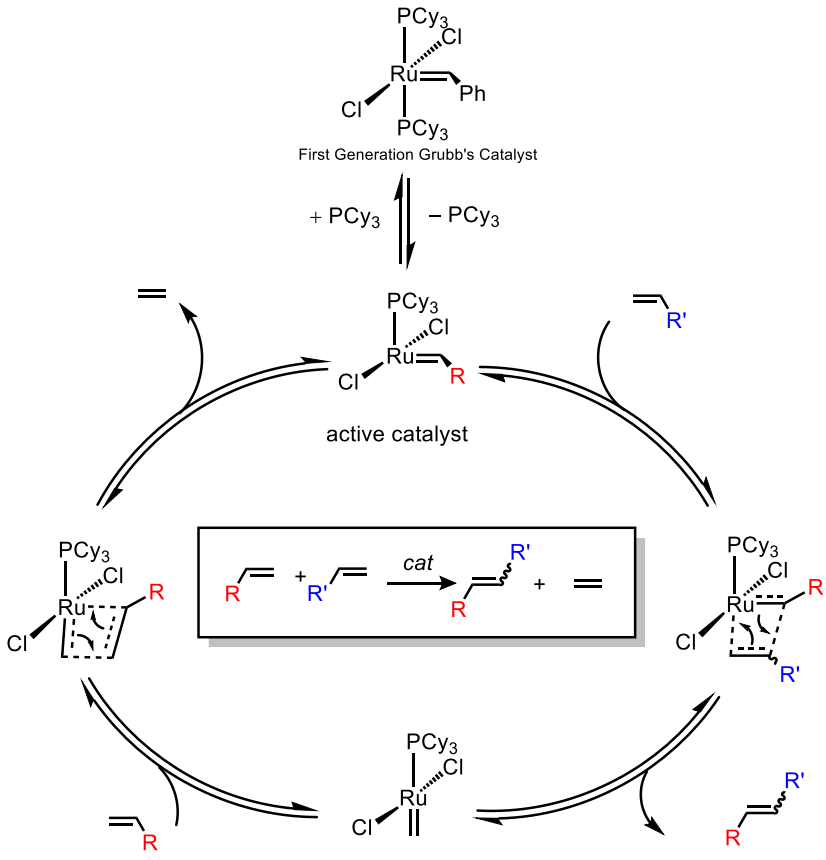

Scheme 1.6. Generic cycle for the catalytic cross-metathesis of olefins using Grubb's first-generation catalyst. After the first cycle, the phenyl group of the pre-catalyst is replaced by the red R group.

Cooperative bond activation at metal–nitrogen multiple bonds is well documented; however, such examples are generally hindered catalytically by their inability to reform the imide functionality.[12d] Early transition metal imido complexes, for example, have been demonstrated to activate challenging substrates, such as the C–H bond of benzene (Scheme 1.7, top) or undergo similar [2+2] cycloadditions with alkynes (Scheme 1.7, bottom).[12d, 16] Addition of H_2 across Ti=S bonds in titanocene sulfido complexes have also been reported since the late 1990's.[17]

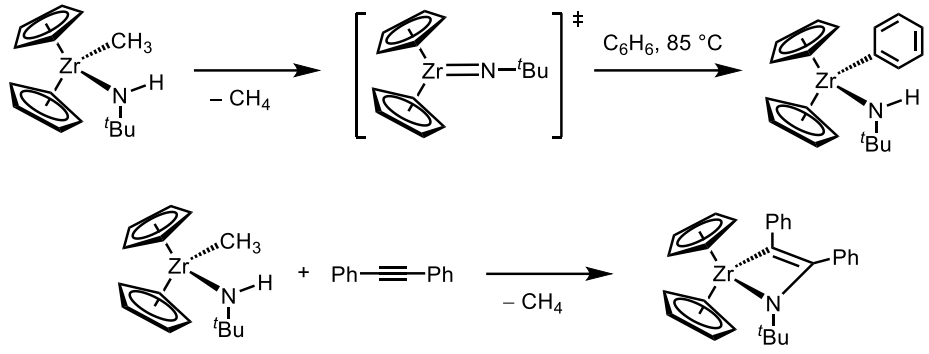

Scheme 1.7. Metal ligand cooperation between an *in situ* generated zirconium imido complex in the activation of benzene (top). [2+2] cycloaddition between *in situ* generated zirconium imido complex and diphenylacetylene.

Looking at literature trends, successful transformations often utilize either electron poor early transition metals ($M^{\delta+}$) with π-basic ($E^{\delta-}$) ligands or electron rich late transition metals ($M^{\delta-}$) with π-acidic ($E^{\delta+}$) ligands.[18] While the former pairing of ($M^{\delta+}$=$E^{\delta-}$) is clearly demonstrated in the examples involving zirconium and titanium, a greater emphasis on the latter ($M^{\delta-}$=$E^{\delta+}$) pairing in the form of late transition metal tetrylenes will be presented in this body of work.

1.5. Transition Metal Tetrylenes (M=E, E = Si, Ge, Sn, Pb)

At first glance, one might expect compounds of the form of ($M^{\delta-}$=$E^{\delta+}$) to be rare, as transition metal complexes are typically formulated as metal cations and are more electropositive than the main group elements bound to them. The concept of metal basicity is, however, well known for electron rich late transition metals in low oxidation states.[18-19] Late metal silylene complexes reported by Tilley *et al*., for example, display substantial positive character at silicon, with reactivity predominantly governed by the electrophilicity of silicon, rather than the metal center (Scheme 1.8).[18, 20]

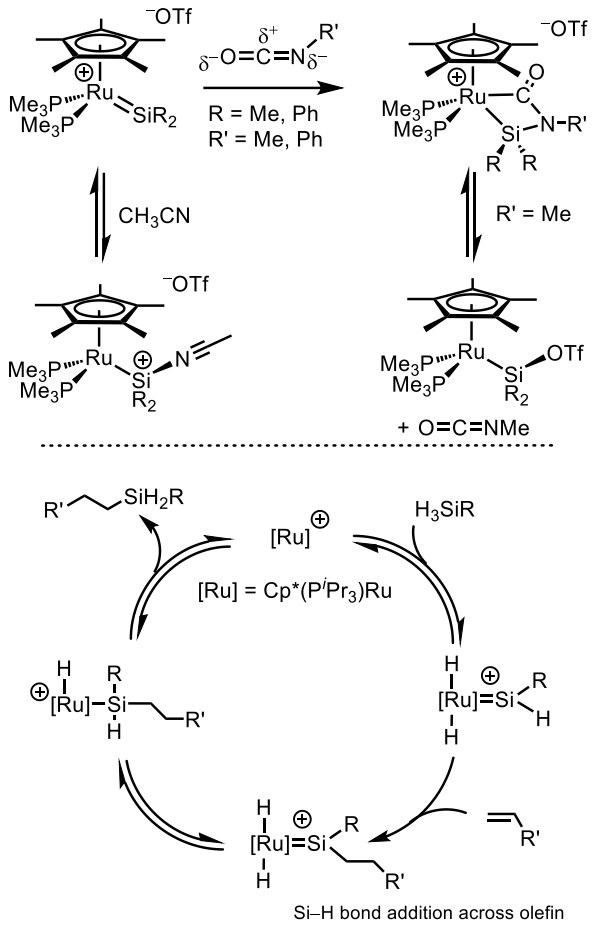

Scheme 1.8. Cyclopentadienyl ruthenium silylene complexes from Tilley *et al*. that showcase the electrophilicity at silicon.

1.5.1. Electronic Structure and Properties of Carbenes and Carbene Analogues

When carbon, the lightest group 14 element, is multiply bonded to a transition metal, the complex can exist in singlet (no unpaired electrons, *i.e.* Fischer carbene) or triplet (two unpaired electrons, *i.e.* Schrock carbene) forms. The former singlet state results in a partial positive charge at an electrophilic carbon, while the latter shows the flexibility of carbon as an element to also be a nucleophilic donor.[8] Transition metal complexes featuring multiple bonds to heavier group 14 elements (tetrylene complexes) however, display almost exclusively electrophilicity at the main group atom ($M^{\delta-}=E^{\delta+}$). This polarization is substantially more pronounced in metal-silylenes compared to Fischer carbenes, and the trend persists when going further down the group, prompting

further study of these tetrylene complexes from contributors such as Tilley, Power, Hashimoto, Filippou, and Hayes. Rationalization stems primarily from the increased size of the atoms going down the group which discourages the more diffuse *p*-orbitals from hybridizing.[20a] This results in mostly singlet ground states where an unfilled *p*-orbital confers the strong electrophilicity, and a lone pair of mainly *s*-character allows for σ-donation. Moreover, multiple bonding between transition metals and group 14 donors leads to a smaller HOMO-LUMO gap of the tetrylene, giving rise to increased reactivity at the electrophilic site.[20a, 21]

1.5.2. Relevant Examples of MLC in Transition Metal Tetrylene Complexes

A 2021 review by Campos and Somerville entitled "Cooperativity in Transition Metal Tetrylene Complexes" corroborates the premise of MLC presented in this introductory chapter.[20a] While a wide range of transformations are detailed (oxidative addition across the metal tetrylene bond, cycloadditions, 1,2-migrations, and activation of alkynes/ketones/heteroallenes), select examples have been chosen for discussion.

Tilley *et al*. disclosed the reaction between a pincer-ligand supported PNP-iridium silylene complex that reacts with a variety of aldehydes, ketones, alcohols, and anilines.[22] Protonation at the nitrogen donor of the PNP ligand occurs when acetophenone, dimethylformamide, alcohols, and anilines were used as substrates, demonstrating that the pincer ligand is non-innocent in the process. When deuterated 3,5-di-*tert*-butylphenol was employed as a substrate, deuteration at both the hydride and amine positions, in an approximately 45:55 ratio, was observed (Scheme 1.9).

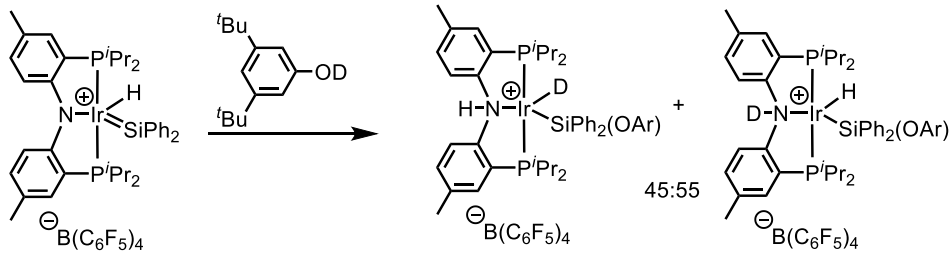

Scheme 1.9. Reaction between Tilley's PNP-iridium silylene complex and deuterated 3,5-di-tert-butylphenol resulting in deuterium incorporation at both the hydride and amine sites.

Whited *et al*. demonstrated ethylene and CO_2 reductions using two equivalents of a cationic cobalt silylene complex (Scheme 1.10).[23] A metal-ligand cooperative approach was clearly demonstrated where the substrate is first activated by the electrophilic silicon. The author's propose one-electron reduction at each of the two Co(I) metal centers in the silylene starting material to Co(II) in the dinuclear products.

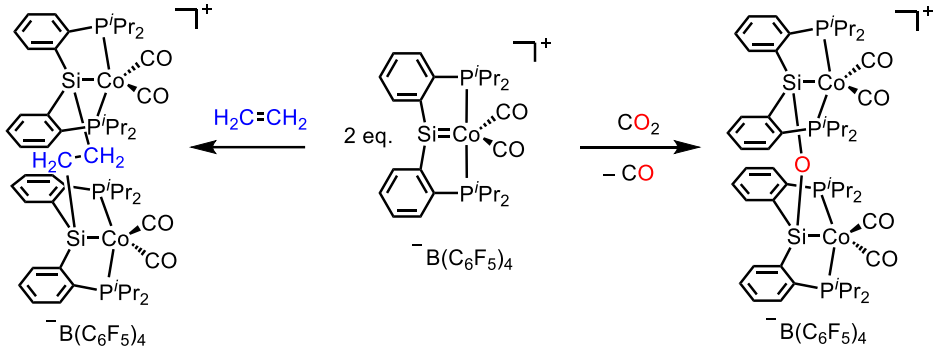

Scheme 1.10. Dinuclear CO_2 and ethylene reduction at a cobalt silylene complex.

Extension of the tetrylene terminology to include parent compounds of the form ":ER_2" leads to complexes from Banaszak Holl and co-workers where isolable :GeR_2 moieties are used as neutral, two electron, donor ligands to platinum and palladium metal centers.[24] Rich [2+2] cycloaddition chemistry across the metal germanium bond was demonstrated with CO_2, nitrosobenzene, formaldehyde, and O_2 (Scheme 1.11). In the case of nitrosobenzene, preference for the more

electronegative oxygen to coordinate to germanium confirms the Lewis acidity of the main group element.

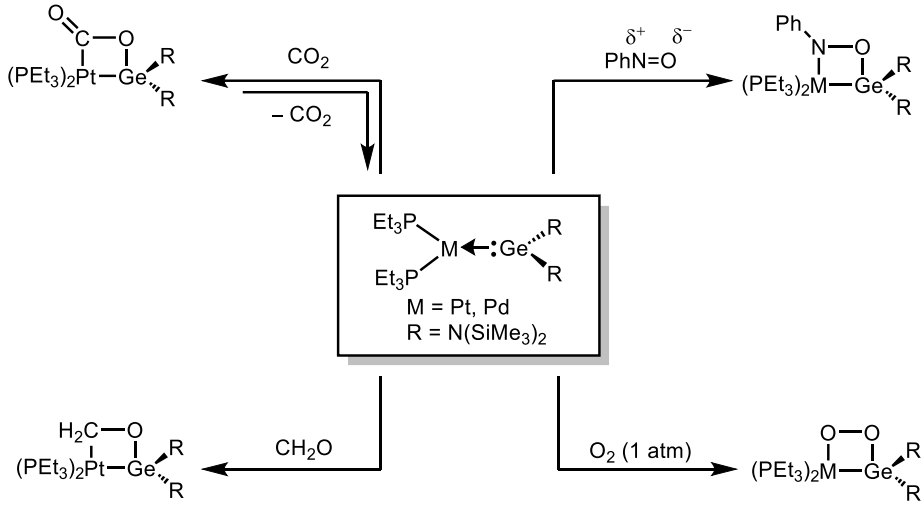

Scheme 1.11. [2+2] cycloadditions across platinum and palladium germylene compounds.

These reactions serve to illustrate the wide range of substrates that can be activated by transition metal tetrylene complexes. Metal–main group element cooperation, as well as the Lewis acidity of the bound group 14 element, are emphasized across several different binding motifs. Aside from prominent examples from Tilley *et al*. regarding transition metal silylene complexes capable of catalytic hydrosilation,[25] the majority of transformations involving this class of compound are stoichiometric. This is primarily due to the thermodynamic stability of four-coordinate E(IV) oxidized species that similarly poses challenges in the synthesis of transition metal tetrylenes.

1.5.3. Conventional Strategies for Tetrylene Synthesis

Three main synthetic strategies towards generating transition metal silylene and germylene compounds have been established over the past few decades. The first involves abstraction of an anionic substituent from the silicon atom of a transition metal silyl compound. Initial examples of isolable base-free silylene compounds come from the Tilley group in 1990, where lithium tetraphenylborate was used to abstract a triflate group from a piano-stool ruthenium complex

(Scheme 1.12a).[20c] While this methodology is tolerant of various substituents on the main group element, the resulting complexes are inherently cationic.[20b]

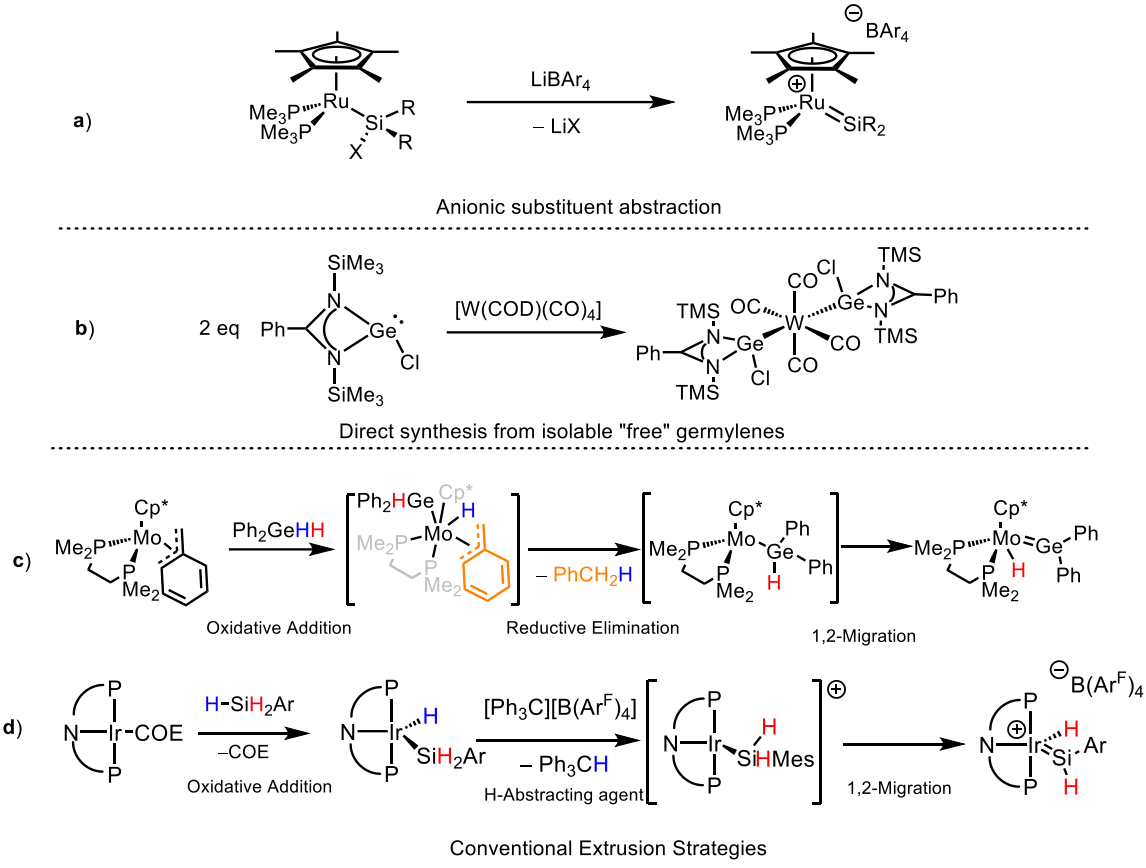

Scheme 1.12. Established methods for the generation of terminal tetrylene complexes. a) Abstraction of an anionic substituent on the group 14 atom. b) Direct synthesis from isolable “free” germylenes. c) Extrusion strategy that involves a reductive elimination which induces 1,2-migration, forming a neutral germylene. d) Extrusion strategy that relies on using a hydride-abstracting agent to induce 1,2-migration, forming a cationic silylene complex.

“Free” silylene and germylene starting materials, as mentioned in Section 1.5.2, have been isolated using bulky, π-donating, amido groups to stabilize the divalent silicon and germanium centers. Direct coordination of these substrates can lead to neutral transition metal tetrylene compounds that have a decreased Lewis acidity, and spectral characteristics more similar to base-stabilized

examples of the form [$L_nM{=}ER_2{\leftarrow}LB$] (LB = Lewis Basic 2-electron donor) (Scheme 1.12b).[20b, 26]

A third route comes from induced 1,2-migration of an α-substituent on the silyl/germyl ligand, typically a hydrogen, through removal of a separate metal bound group. These processes, coined as extrusion methods, typically proceed *via* oxidative addition of an E–H bond, reductive elimination of an RH molecule, which frees up a metal coordination site, and finally, α-hydrogen migration to form the M=E multiple bond (Scheme 1.12c).[20b, 27] The driving force of these reactions comes from the thermodynamic stability of the departing molecule, often methane or toluene. An alternative to the oxidative addition/reductive elimination strategy requires abstraction of an anionic ligand from the metal center to free up the coordination site. These methods employ salts, such as $Na[B(C_6F_5)_4]$, that contain weakly-coordinating anions to remove transition metal hydrides and halides, prompting α-hydrogen migration to form cationic tetrylene complexes similar to those described above (Scheme 1.12d). The general appeal of this third method stems from the use of simple organo-dihydrosilanes and germanes (H_2ER_2) as starting materials which can be synthesized using conventional Grignard/lithium reagents.

1.5.4. Modern Routes to Tetrylenes

While the aforementioned methods are widely established and covered in Tilley *et al.*'s seminal 2007 review, improvements in the methodology towards transition metal tetrylenes and extension towards tetrylyne complexes (M≡E) have been explored by Hashimoto and Tobita, as well as Fillipou and coworkers. The former group has taken a complementary approach to extrusion, where photochemically labile CO ligands are lost concurrently with reductive elimination of MeH, allowing for the isolation of neutral H-substituted silylenes (Scheme 1.13, top).[28] The loss of CO leads to undersaturated metal centers, facilitating the subsequent loss of H_2 to form neutral tetrylyne complexes without the need for an anion-abstraction agent (Scheme 1.13, bottom).[28c, 28d]

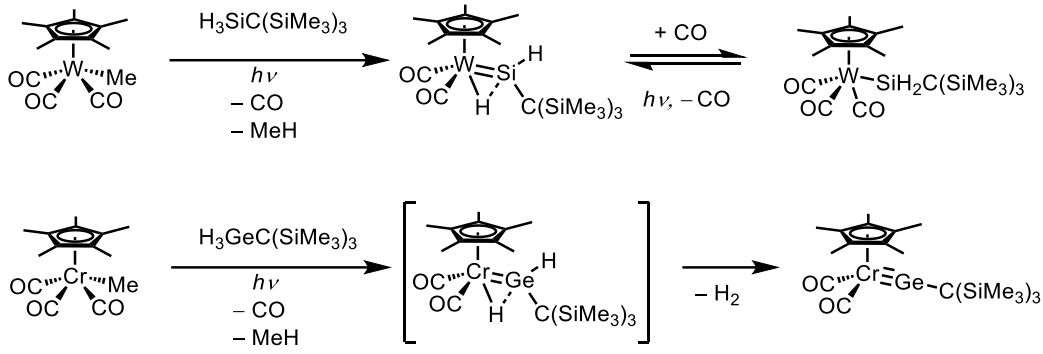

Scheme 1.13. Photochemically induced silylene extrusion with a cyclopentadienyl tungsten complex bearing CO ligands (top). Photochemically induced germylene extrusion followed by subsequent H_2 loss which yields a chromium germylyne species (bottom).

Filipou *et al.* have capitalized on the high nucleophilicity of divalent group 14 substrates and paired them with early transition metals. Reaction of an 18-electron manganese dihydrogen complex with a bulky $ArSn^{II}Cl$ species is hypothesized to go first through loss of the dihydrogen ligand to yield an electrophilic 16-electron intermediate capable of trapping the chlorostannane as a terminal stannylidene (Scheme 1.14, top).[29] Similar direct reaction between a divalent arylchlorogermane starting material and rhenium complexes are able to generate germylidene species after loss of a neutral PMe_3 ligand (Scheme 1.14, middle).[30] In both cases, migration or removal of the tetrylidene bound halide leads to tetrylidyne formation. Finally, the group has demonstrated salt metathesis strategies between NHC-stabilized dibromosilanes (NHC→$SiBr_2$) and $Li[CpCr(CO)_3]$ to afford neutral bromosilylidene complexes (Scheme 1.14, bottom). The authors use terminology consistent with Schrock alkylidenes to describe their compounds, implying a reversal of polarity from previous examples wherein the electron deficient early/mid-transition metal now holds the partial positive charge, and the tetrylidene maintains nucleophilicity ($M^{\delta+}=E^{\delta-}$). Reaction chemistry from the group however focuses on the tetrylidyne species where the main group element is still found to be electrophilic, as would be expected for Fischer carbynes.[31]

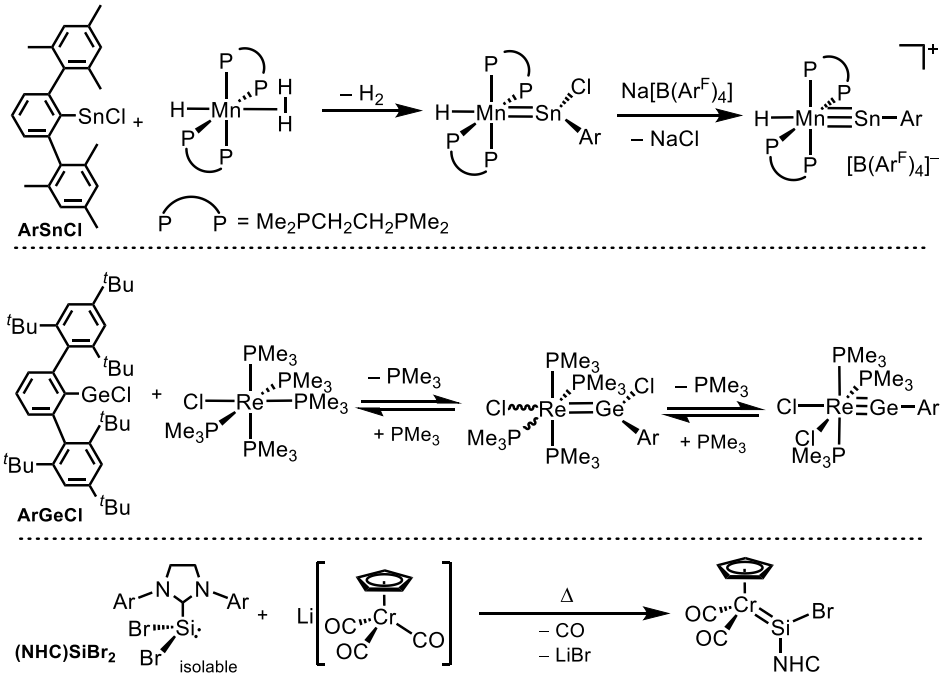

Scheme 1.14. Representative work from Filippou *et al*. that pairs divalent group 14 starting materials with early/mid-transition metals. A manganese dihydrogen complex supported by bidentate phosphine ligands reacts directly with a bulky Sn(II) compound to yield a neutral stannylidene, followed by halide-abstraction to form a cationic stannylidyne (top). A rhenium complex bearing labile PMe_3 ligands is able to react directly with a bulky Ge(II) substrate to form neutral germylidene and germylidyne species through sequential ligand displacement steps (middle). Salt metathesis between an isolable, NHC-stabilized, Si(II) precursor and $Li[CpCr(CO)_3]$ yields a neutral chromium silylidene (bottom).

While the synthetic protocols shown in this chapter involve fairly elementary chemical steps, the high reactivity of transition metal tetrylene complexes renders isolation of discrete examples non-trivial. Tailored environments, bulky substituents, or stabilization using Lewis bases are often crucial requirements that require a careful balance to achieve.

1.6. Relevant Hayes Lab Chemistry

The overarching themes of pincer ligands, metal ligand cooperation, and the synthesis of transition metal tetrylene complexes are all relevant to research being done in the Hayes group. In

particular, pioneering work by Dr. Connor MacNeil in our lab has served as a starting point for the chemistry that will be presented in this thesis.

Beginning from the mention of pincer ligands, an *NNN*-pincer ligand of general structure (2,5-$[R_2P{=}N(Ar)]_2$-N'$(C_4H_2)^-$) (R = alkyl/Ph, Ar = Aryl) has been used extensively to support a variety of metals throughout the periodic table (Figure 1.4).[32] The "phosphinimine" or iminophosphorane ($R_3P{=}NAr$) functional group has been demonstrated to be a strong σ- and π-donor, and can be more accurately depicted as $R_3P^{(+)}–N^{(-)}Ar$ wherein the polarized P–N bond precludes π-acceptor properties one would expect for analogous imido ($R_2C{=}NR$) moieties.[33] Additionally, when coordinated to a metal center through the phosphinimine nitrogen, the electronic environment can be monitored by ^{31}P NMR spectroscopy. For example, the proteo-ligands (2,5-$[R_2P{=}N(Ar)]_2$-***H***N'(C_4H_2)) have ^{31}P NMR chemical shifts in the 0-15 ppm range.[32] Following deprotonation of the central pyrrole nitrogen with NaH, a downfield shift can be observed to 17-28 ppm, and finally, coordination to a metal center results in further deshielding of the phosphorus nuclei resulting in resonances between δ 30 and 60.[32] While the substituents on both phosphorus and nitrogen can be changed to alter the steric and donor properties of the ligand, the work presented in this document will focus on *L* = κ^3-NNN' = 2,5-$[^iPr_2P{=}N(4\text{-}^iPrC_6H_4)]_2$-N'$(C_4H_2)^-$), where R = isopropyl and Ar = para-isopropylphenyl. This particular iteration of the ligand appears to impart substantial chemical stability and resistance to cyclometallation pathways that have been previously observed,[34] while also allowing substrates sufficient accessibility to the metal center. Other Hayes lab students have, and are currently exploring the effects of ligand alteration, so those discussions will be reserved for the future work section of this thesis.

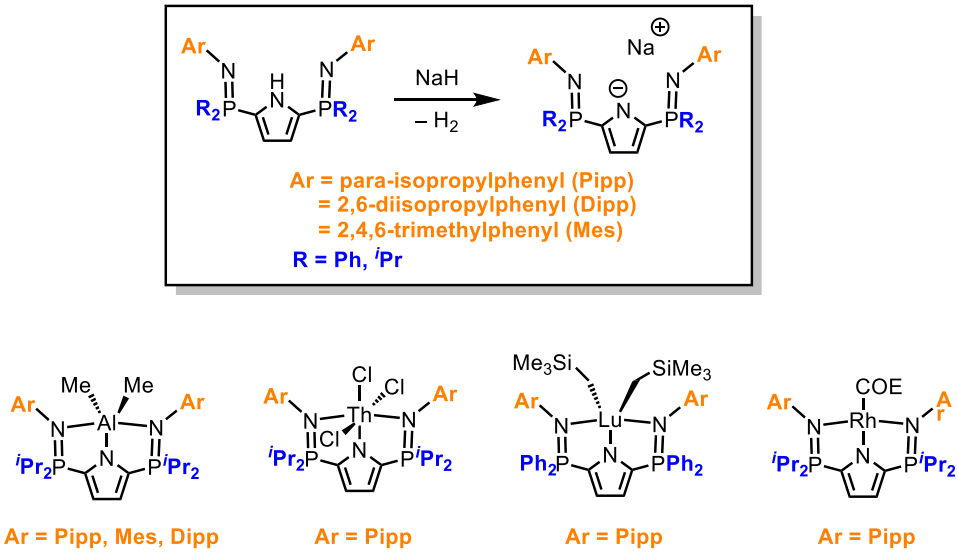

Figure 1.4. Generic depiction of the NNN-pincer ligand used in the Hayes Lab (top), along with representative complexes with aluminum, thorium, lutetium, and rhodium.

1.6.1. Metal Ligand Cooperation in the Hayes Lab

Exploration of these *NNN*-pincer ligands towards MLC systems was first conducted by MacNeil, Hänninen, and Zamora who sought to contrast hard-nitrogen donors with soft electron-rich metals in their successful attempts at small molecule activation.[32c, 35] In particular, the juxtaposition in reactivity between the alkene coordination complex *L*Rh(COE) (COE = cyclooctadiene) and the mono-carbonyl *L*Rh(CO), compound **1**, highlights some particular requirements towards MLC in these systems (Scheme 1.15).[35] Rationale provided for this interesting deviation compares the donor/acceptor qualities of the ligand sitting *trans*- to the central pyrrole donor (COE and CO) with that of the flanking phosphinimine donors. When the larger, and more labile cyclooctene was employed, reaction with phenylsilane led to oxidative addition, displacing the COE ligand to generate the 5-coordinate Rh(III) complex *L*Rh(H)(SiH_2Ph). Using the smaller CO ligand, which has better orbital overlap for back-bonding, preference for de-chelating the phosphinimine nitrogen (σ- and π-donor) leads instead to ligand-assisted

dehydrogenation, resulting in isolation of the base-stabilized silylene compound κ^2-*L*RhSi(H)Ph, (**2**; κ^2-*L* = κ^2-NN'-Rh, κ^1-N-E; E = Group 13 or 14 element).

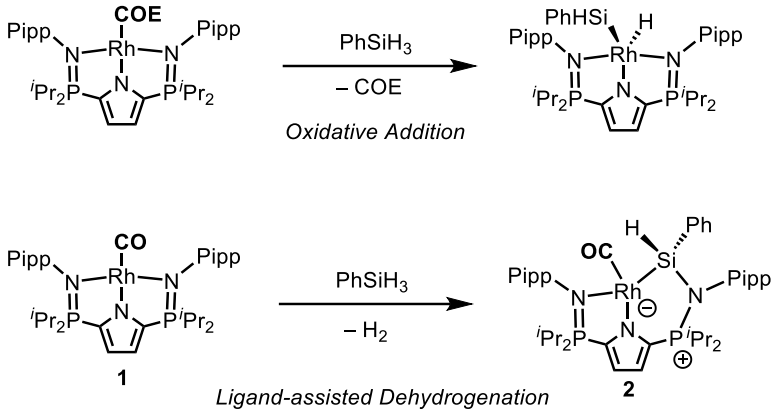

Scheme 1.15. Divergent reactivity between LRhCOE (top) and LRhCO (bottom) with $PhSiH_3$ to yield oxidative addition and base-stabilized silylene products, respectively.

This methodology for silylene extrusion does not require the use of a designated leaving group on rhodium, like previous examples from Tilley (*vide supra*), as H_2 is spontaneously released through an intramolecular pathway. This allows for the atom economic synthesis of neutral rhodium silylene compounds from simple organosilanes that may allow for facile regeneration of the active monocarbonyl complex **1**. While other research groups have boasted fully terminal silylenes rather than base-stabilized derivatives, we aim to be able to establish that these species still serve as silylene synthons that can readily transfer the :SiR_2 moiety.

1.7. Thesis Goals and Outcomes

The expansion of the MLC-assisted dehydrogenation methodology towards a wider range of substrates allows for a better understanding of transition metal tetrylenes and their reactivity. The use of phosphinimine donors as non-innocent ligands fulfills an unexplored niche in the literature for these types of extrusion methods and highlights the synergistic pairing of electron rich metals with purely donating ligands.

In Chapter 2 of this thesis, work done jointly with Dr. Connor MacNeil, describes the extension of our ligand-assisted dehydrogenation to the group 13 element boron, which has wide applications in cross-coupling technologies. Mechanistic considerations, chemical reversibility, as well as formal borylene transfer in cross-dehydrogenative coupling reactions, are addressed.[36]

Chapter 3 serves as a follow-up to the Chapter 2 as well as the pioneering work done by Dr. Connor MacNeil.[35] Base-stabilized silylene and germylene compounds are presented, highlighting particularities in substrate scope and the potential for undesirable transmetalation reactions. Specifically, the ability of our system to accommodate alkyl-substituents on silicon and germanium, without the need for bulky aryl groups, fills a prominent gap in the literature.[37]

To demonstrate the utility of our complexes, and expand this body of work beyond just our synthetic protocol, Chapter 4 takes the base-stabilized borylene compound presented in Chapter 2 and demonstrates unprecedented reactivity with a variety of alkynes. The auxiliary CO ligand of complex **1**, as well as the {NPipp} group of the pincer ligand are incorporated in the final product to yield highly functionalized heterocycles which are structurally analogous to rare examples of new anti-fungal therapeutics recently approved by the FDA.

Chapter 5 describes preliminary attempts to generate and study a rhodium silylyne complex by abstraction of a silicon bound hydride from silylene complexes described in Chapter 3. This chapter represents foundational groundwork towards these elusive species, and serves as an accessible continuation point for future students.

Finally, Chapter 6 features proposed avenues of continuation for the chemistry described in this thesis. An emphasis will be placed on potential modifications to the ligand structure and the isolation of new main group coordinated complexes to support current and future work. Additionally, substrates that could be targeted for activation *via* metal ligand cooperation are presented.

As this thesis is based on a collection of publications/paper submissions, each chapter will include a more detailed introduction to the chemistry at hand. It is my intention that this compilation will portray a cohesive and comprehensive body of work, with each chapter building off the previous one in a continuous stream of experimental design.

1.8. References

[1] a) G. Rothenberg, *Catalysis : concepts and green applications*, Wiley-VCH, Weinheim [Germany], **2008**; b) J. Twilton, C. Le, P. Zhang, M. H. Shaw, R. W. Evans, D. W. C. MacMillan, *Nat. Rev. Chem.* **2017**, *1*, 0052; c) H. Yorimitsu, M. Kotora, N. T. Patil, *The Chem. Rec.* **2021**, *21*, 3335-3337.

[2] a) A. Ault, *J. Chem. Educ.* **2002**, *79*, 572; b) C. C. C. Johansson Seechurn, M. O. Kitching, T. J. Colacot, V. Snieckus, *Angew. Chem. Int. Ed.* **2012**, *51*, 5062-5085.

[3] C. P. Casey, *J. Chem. Educ.* **2006**, *83*, 192.

[4] R. J. Lundgren, M. Stradiotto, in *Ligand Design in Metal Chemistry*, **2016**, pp. 1-14.

[5] a) M. Berthod, G. Mignani, G. Woodward, M. Lemaire, *Chem. Rev.* **2005**, *105*, 1801-1836; b) I. D. Gridnev, T. Imamoto, *Acc. Chem. Res.* **2004**, *37*, 633-644.

[6] W. Cabri, I. Candiani, *Acc. Chem. Res.* **1995**, *28*, 2-7.

[7] D. Evans, J. A. Osborn, G. Wilkinson, *J. Chem. Soc. A* **1968**, 3133-3142.

[8] J. F. Hartwig, *Organotransition metal chemistry: from bonding to catalysis*, University Science Books, Sausalito, Calif, **2010**.

[9] A. Amgoune, D. Bourissou, *Chem. Commun.* **2011**, *47*, 859-871.

[10] a) C. Gunanathan, D. Milstein, *Chem. Rev.* **2014**, *114*, 12024-12087; b) M. M. Hänninen, M. T. Zamora, P. G. Hayes, in *The Privileged Pincer-Metal Platform: Coordination Chemistry & Applications* (Eds.: G. van Koten, R. A. Gossage), Springer International Publishing, Cham, **2016**, pp. 93-177; c) S.-J. Hsiang, P. G. Hayes, in *Comprehensive Coordination Chemistry III* (Eds.: E. C. Constable, G. Parkin, L. Que Jr), Elsevier, Oxford, **2021**, pp. 40-72; d) K. Kirchner, *Angew. Chem. Int. Ed.* **2015**, *54*, 4706-4707.

[11] D. W. Stephan, *Org. Biomol. Chem.* **2008**, *6*, 1535-1539.

[12] a) C. Gunanathan, D. Milstein, *Acc. Chem. Res.* **2011**, *44*, 588-602; b) T.-F. Ramspoth, J. Kootstra, S. R. Harutyunyan, *Chem. Soc. Rev.* **2024**, *53*, 3216-3223; c) M. Rauch, S. Kar,

A. Kumar, L. Avram, L. J. W. Shimon, D. Milstein, *J. Am. Chem. Soc.* **2020**, *142*, 14513-14521; d) J. R. Khusnutdinova, D. Milstein, *Angew. Chem. Int. Ed.* **2015**, *54*, 12236-12273.

[13] C. A. Sandoval, T. Ohkuma, K. Muñiz, R. Noyori, *J. Am. Chem. Soc.* **2003**, *125*, 13490-13503.

[14] A. Hassin, R. Levy, N. Fridman, M. Gandelman, *Organometallics* **2024**, *43*, 368-380.

[15] O. M. Ogba, N. C. Warner, D. J. O'Leary, R. H. Grubbs, *Chem. Soc. Rev.* **2018**, *47*, 4510-4544.

[16] a) J. R. Webb, S. A. Burgess, T. R. Cundari, T. B. Gunnoe, *Dalton Trans.* **2013**, *42*, 16646-16665; b) P. J. Walsh, F. J. Hollander, R. G. Bergman, *J. Am. Chem. Soc.* **1988**, *110*, 8729-8731.

[17] Z. K. Sweeney, J. L. Polse, R. G. Bergman, R. A. Andersen, *Organometallics* **1999**, *18*, 5502-5510.

[18] M. T. Whited, *Beilstein J. Org. Chem.* **2012**, *8*, 1554-1563.

[19] D. F. Shriver, *Acc. Chem. Res.* **1970**, *3*, 231-238.

[20] a) R. J. Somerville, J. Campos, *Eur. J. Inorg. Chem.* **2021**, *2021*, 3488-3498; b) R. Waterman, P. G. Hayes, T. D. Tilley, *Acc. Chem. Res.* **2007**, *40*, 712-719; c) D. A. Straus, S. D. Grumbine, T. D. Tilley, *J. Am. Chem. Soc.* **1990**, *112*, 7801-7802; d) P. B. Glaser, T. D. Tilley, *J. Am. Chem. Soc.* **2003**, *125*, 13640-13641.

[21] a) A. C. Filippou, B. Baars, O. Chernov, Y. N. Lebedev, G. Schnakenburg, *Angew. Chem. Int. Ed.* **2014**, *53*, 565-570; b) K. Inomata, T. Watanabe, Y. Miyazaki, H. Tobita, *J. Am. Chem. Soc.* **2015**, *137*, 11935-11937; c) Y. N. Lebedev, U. Das, G. Schnakenburg, A. C. Filippou, *Organometallics* **2017**, *36*, 1530-1540; d) P. Wilfling, K. Schittelkopf, M. Flock, R. H. Herber, P. P. Power, R. C. Fischer, *Organometallics* **2015**, *34*, 2222-2232.

[22] E. Calimano, T. D. Tilley, *Organometallics* **2010**, *29*, 1680-1692.

[23] M. T. Whited, J. Zhang, A. M. Conley, S. Ma, D. E. Janzen, D. Kohen, *Angew. Chem. Int. Ed.* **2021**, *60*, 1615-1619.

[24] a) K. E. Litz, M. M. Banaszak Holl, J. W. Kampf, G. B. Carpenter, *Inorg. Chem.* **1998**, *37*, 6461-6469; b) K. E. Litz, J. E. Bender, R. D. Sweeder, M. M. Banaszak Holl, J. W. Kampf, *Organometallics* **2000**, *19*, 1186-1189; c) K. E. Litz, K. Henderson, R. W. Gourley, M. M. B. Holl, *Organometallics* **1995**, *14*, 5008-5010; d) K. E. Litz, J. W. Kampf, M. M. Banaszak Holl, *J. Am. Chem. Soc.* **1998**, *120*, 7484-7492.

[25] a) E. Calimano, T. D. Tilley, *J. Am. Chem. Soc.* **2008**, *130*, 9226-9227; b) E. Calimano, T. D. Tilley, *J. Am. Chem. Soc.* **2009**, *131*, 11161-11173; c) M. E. Fasulo, M. C. Lipke, T. D. Tilley, *Chem. Sci. J.* **2013**, *4*, 3882-3887; d) P. G. Hayes, C. Beddie, M. B. Hall, R. Waterman, T. D. Tilley, *J. Am. Chem. Soc.* **2006**, *128*, 428-429; e) D. S. Levine, T. D. Tilley, R. A. Andersen, *Chem. Commun.* **2017**, *53*, 11881-11884.

[26] L. Álvarez-Rodríguez, J. A. Cabeza, P. García-Álvarez, D. Polo, *Coord. Chem. Rev.* **2015**, *300*, 1-28.

[27] a) T. P. Dhungana, H. Hashimoto, M. Ray, H. Tobita, *Organometallics* **2020**, *39*, 4350-4361; b) J. D. Feldman, J. C. Peters, T. D. Tilley, *Organometallics* **2002**, *21*, 4065-4075; c) P. G. Hayes, R. Waterman, P. B. Glaser, T. D. Tilley, *Organometallics* **2009**, *28*, 5082-5089.

[28] a) H. Hashimoto, K. Nagata, *Chem. Lett.* **2021**, *50*, 778-787; b) H. Hashimoto, H. Tobita, *Coord. Chem. Rev.* **2018**, *355*, 362-379; c) M. Matsuoka, K. Nagata, R. Ohno, T. Matsuo, H. Tobita, H. Hashimoto, *Chem. Eur. J.* **2024**, *30*, e202303765; d) K. Nagata, H. Omura, M. Matsuoka, H. Tobita, H. Hashimoto, *Organometallics* **2023**, *42*, 1131-1138; e) T. Watanabe, H. Hashimoto, H. Tobita, *Angew. Chem. Int. Ed.* **2004**, *43*, 218-221.

[29] A. C. Filippou, P. Ghana, U. Chakraborty, G. Schnakenburg, *J. Am. Chem. Soc.* **2013**, *135*, 11525-11528.

[30] a) A. C. Filippou, U. Chakraborty, G. Schnakenburg, *Chem. Eur. J.* **2013**, *19*, 5676-5686; b) A. C. Filippou, N. Weidemann, A. I. Philippopoulos, G. Schnakenburg, *Angew. Chem. Int. Ed.* **2006**, *45*, 5987-5991.

[31] A. C. Filippou, K. W. Stumpf, O. Chernov, G. Schnakenburg, *Organometallics* **2012**, *31*, 748-755.

[32] a) D. T. Chisholm, P. G. Hayes, *New J. Chem.* **2021**, *45*, 15043-15052; b) T. K. K. Dickie, A. A. Aborawi, P. G. Hayes, *Organometallics* **2020**, *39*, 2047-2052; c) M. M. Hänninen, M. T. Zamora, C. S. MacNeil, J. P. Knott, P. G. Hayes, *Chem. Commun.* **2016**, *52*, 586-589.

[33] a) S. S. Hanson, E. Doni, K. T. Traboulsee, G. Coulthard, J. A. Murphy, C. A. Dyker, *Angew. Chem. Int. Ed.* **2015**, *54*, 11236-11239; b) S. S. Hanson, N. A. Richard, C. A. Dyker, *Chem. Eur. J.* **2015**, *21*, 8052-8055; c) I. M. Marin, A. Auffrant, *Eur. J. Inorg. Chem.* **2018**, *2018*, 1634-1644.

[34] a) M. T. Zamora, K. R. D. Johnson, M. M. Hänninen, P. G. Hayes, *Dalton Trans* **2014**, *43*, 10739-10750.; b) J. P. Knott, M. M. Hänninen, J. M. Rautiainen, H. M. Tuononen, P. G. Hayes, *J. Organomet. Chem.* **2017**, *845*, 135-143.

[35] C. S. MacNeil, P. G. Hayes, *Chem. Eur. J.* **2019**, *25*, 8203-8207.

[36] C. S. MacNeil, S.-J. Hsiang, P. G. Hayes, *Chem. Commun.* **2020**, *56*, 12323-12326.

[37] S.-J. Hsiang, P. G. Hayes, *Chem. Eur. J.* **2024**, *30*, e202302925.

Chapter 2. Metal Ligand Cooperation Towards the Dehydrogenation of a Primary Borane

Abstract and Preface

The reversible dehydrogenation of a primary aryl borane, $MesBH_2$ (Mes = 2,4,6-$(CH_3)_3C_6H_2$), by a 16-electron, mono-carbonyl rhodium (I) complex *L*Rh(CO) (**1**; *L* = κ^3-NNN' = 2,5-[^{i}Pr$_2$P=N(4-^{i}PrC$_6$H$_4$)]$_2$-N'$(C_4H_2)^-$), is communicated. The resulting complex, κ^2-*L*(CO)Rh(BMes) (**3**; κ^2-*L* = κ^2-NN'-Rh, κ^1-N-B), is described as a neutral, ligand-stabilized rhodium borylene. Addition of H_2 gas to a solution of **3**, reforms compound **1**, highlighting the reversibility of the reaction, as well as the ability of **3** to facilitate small molecule activation. In contrast, reaction between a *meta*-substituted borane, $^{meta}Xyl^FBH_2$ (Ar^F = 3,5-$(CF_3)_2C_6H_3$), and complex **1** resulted in isolation of a Lewis acid/base adduct, κ^2-*L*'(CO)Rh($^{meta}Xyl^FBH_2$), **4**, which we propose to be a key reaction intermediate. Without sufficient steric bulk about boron, compound **4** undergoes a transmetalation pathway rather than borylene extrusion, highlighting the sensitivity of the system to subtle changes. Formal transfer of the {BMes} group to pinacol in a display of dehydrogenative coupling results in reformation of mono-carbonyl **1**, and release of MesBPin (Pin = pinacol).

The contents of this chapter are adapted from a publication in which I am the secondary author. Connor MacNeil was responsible for initial findings, including the characterization and synthesis of compounds **1** and **3**, as well as the computational work. I was responsible for the synthesis and characterization of compounds **4** and **5**, H/D scrambling reactions with **3**, as well as the reaction chemistry between **3** and pinacol. We jointly performed the variable temperature NMR experiments to support the agostic interaction between the captured $^{meta}Xyl^FBH_2$ moiety and rhodium. While Connor MacNeil wrote the majority of the published manuscript, this chapter has been rewritten, paraphrased, and reformatted for inclusion in my own words.

The experimental insights in this chapter help describe the bonding in our base-stabilized borylene compound and establish precedent towards transmetalation pathways discussed in further chapters. Proof of concept transfer of the {BMes} moiety also paved the way forward for subsequent reaction chemistry discussed in Chapter 4.

In an effort to be consistent, the citation style utilized in this chapter follows those detailed for *Angewandte Chemie, International Edition*, published by Wiley. Experimental details, including the preparation and characterization of novel compounds, X-ray crystallography, additional NMR spectra, computational details, and additional references are provided in Appendix I, and are reproduced from the manuscript: "MacNeil, C.S.; Hsiang, S.J.; Hayes, P.G.*, Dehydrogenation of a Primary Borane: A Source of :BR for Group Transfer Reactions. *Chemical Communications***.** **2020**, *56*, 12323-12326."

2.1. Introduction

While the oxidative addition of B–H bonds to electron-rich metal centres is well-precedented for common secondary boranes (*e.g.* 9-borabicylo[3.3.1]nonane, pinacol-, catechol- and dialkylboranes),[1] examples where a primary dihydroborane (H_2BR) undergoes consecutive B–H activations are few and far between.[2] The methodology rarely follows conventional extrusion strategies previously discussed for the dehydrogenation of dihydrosilanes and germanes (See Chapter 1. Section 1.5.3), whereby the initial oxidative addition step yields the transition metal boryl species (*e.g.* Aldridge and co-workers' $L_nIr(H)[B(H)=N(Cy)_2]$), followed by a boron to metal α-hydride migration to yield a metal borylene (*e.g.* $[L_nIr(H)_2[B=N(Cy)_2]]^+$, Scheme 2.1a).[3] Instead, generation of σ-complexes where both of the σ-H−B bonds are coordinating to the metal prevails.[2b, 4] Nonetheless, both Sabo-Etienne and Braunschweig have demonstrated that such σ-complexes are capable of releasing H_2 gas to generate terminal borylene species without the need for a supporting donor (Scheme 2.1b,c).[2b, 4b] The former group gives valuable insight towards the nature of these σ-complexes, describing them as true three-centered two-electron interactions between the H−B bond and the metal, with no other intramolecular interactions, such as back-bonding, present, noting that excessive back-donation results in formal oxidative addition and breaking of the H−B bond.[4] When primary boranes are involved, formation of dihydroborates can also be competitive, further complicating the matter. Braunschweig's contribution on the other hand, showcased the steric effects of the aryl group on primary borane substrates, suggesting that substituents in the *ortho* position were key for moving from these bis-σ-borane complexes to terminal borylenes.[2b] Certainly, many additional considerations must be made in generating transition metal borylene complexes compared to their carbene and silylene analogues. The activation of primary boranes to form transition metal borylene species as {BR} synthons however, remains an appealing alternative to hydroboration, giving access to reactive monosubstituted alkyl and aryl boryl fragments sourced directly from RBH_2.

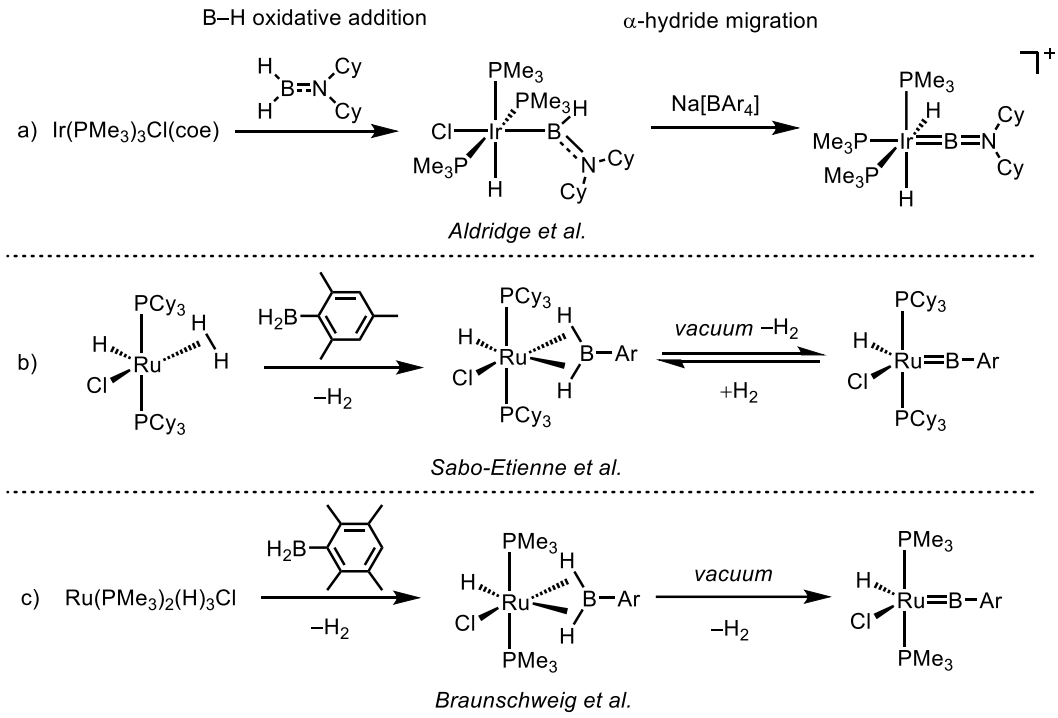

Scheme 2.1. a) Aldridge and co-workers example of double B–H bond activation through conventional extrusion methods. b) Sabo-Etienne's isolation of a formal bis σ-borane ruthenium complex capable of reversibly losing H_2 to generate a terminal ruthenium borylene. c) Braunschweig's example that showcases the necessity of ortho-substitutents on the aryl borane for H_2 loss.

2.2. Results and Discussion

As mentioned in Chapter 1. Section 1.6 of this document, preliminary work has been established for the dehydrogenation of H_2SiPh_2 and H_3SiPh to form rhodium silylene compounds stabilized by the Lewis basic phosphinimine of our ligand system.[5] The phosphinimine functionality can be considered to be both σ- and π- donating, compared to common phosphine and imine donors that are capable of π-backbonding interactions. The donor strength has been explored by Dyker and co-workers who isolated a tetra(iminophosphorano)-substituted bispyridinylidene that they claimed as the strongest neutral electron donor in 2015 in consideration of its intense redox potential.[6] Through previous studies, we have proposed that this purely donating characteristic is what allows for the metal-ligand cooperation in the activation of silanes.

Recognizing the diagonal relationship between boron and silicon on the periodic table, as well as the literature precedent described above, we sought to extend this methodology towards the dehydrogenation of primary aryl boranes using the same mono-carbonyl rhodium (I) species, *L*Rh(CO) (**1**; *L* = κ^3-NNN' = 2,5-[^{i}Pr$_2$P=N(4-^{i}PrC$_6$H$_4$)]$_2$-N'(C$_4$H$_2$)$^-$).

As Sabo-Etienne had success using the 2,4,6-trisubstituted mesityl borane, and Braunschweig implied the importance of *ortho*-substituted aryl boranes, we first reacted **1** with MesBH$_2$ as our model substrate. Analysis by ^{1}H and ^{31}P NMR spectroscopy in a solution of benzene-d_6 gave a mixture of compound **1**, H$_2$, and a new asymmetric product as evidenced by two distinct phosphorus signals in a 1 : 1 ratio at δ 52.7 and 37.9. X-ray diffraction experiments performed on single crystals grown from a saturated Et$_2$O solution at −35 °C revealed the anticipated base-stabilized borylene complex κ^2-*L*(CO)Rh(BMes) (**3**; κ^2-*L* = κ^2-NN'-Rh,κ^1-N-B), where the {BMes} fragment is suspended between the rhodium metal center and the phosphinimine nitrogen (Scheme 2.2).

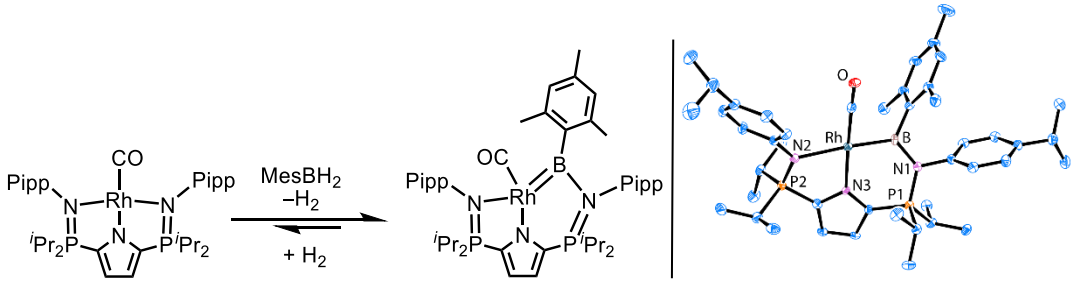

Scheme 2.2. Reaction between compound **1** and H$_2$BMes to form base-stabilized borylene compound **3** (left). Solid-state structure of **3** at 35% ellipsoid probability with hydrogen atoms removed for clarity (right).

The geometry at the 3-coordinate boron center (Σ_{angles} = 359.8°) is trigonal planar, with the mesityl group sitting perpendicular to the plane of the molecule defined by the phosphinimine nitrogen (N1), mesityl *ipso*-carbon, and rhodium centre. The rhodium-boron distance of 2.024(5) Å is notably elongated compared to ruthenium terminal borylene complexes (1.780(4) Å in Sabo-Etienne's [(PCy$_3$)$_2$(H)$_2$Ru=BMes], and 1.795(2) Å in Braunschweig's [(PCy$_3$)$_2$(Cl)(H)Ru=B(Dur)],

Dur = 2,3,5,6-Me_4C_6H).[2b, 4b] The ^{11}B resonance is broad at δ 32.6, and upfield compared to known rhodium aminoborylene complexes (δ 75-120),[7] suggesting a strong shielding effect from the nitrogen to boron π-donation. Infrared (IR) spectroscopic analysis of **1** (1930 cm^{-1}) and **3** (1909 cm^{-1}) revealed a redshift of the ν_{CO} stretch resulting from borylene formation, emphasizing the σ-donor ability of borylene relative to phosphinimine. DFT calculations were performed to better understand the orbital interactions between rhodium, boron, and nitrogen. The gas-phase structure of **3** was optimized at the B3LYP/aug-cc-pVDZ level of theory with associated pseudopotentials for Rh (See Appendix I. V for details). The B−Rh σ-bonding NBO is slightly polarized towards boron, further corroborating the IR analysis. Second order perturbation analysis indicates a strong N(lp) → B(p) interaction [$E^{(2)}$: 35.2 kcal mol^{-1}] between the nitrogen lone pair and the vacant boron p-orbital, as well as a weaker Rh-backdonation interaction [$E^{(2)}$: 10.3 kcal mol^{-1}] from the Rh $4d_{xz}$ donor NBO. The stronger nitrogen to boron interaction is consistent with what our group has proposed for similar base-stabilized rhodium silylene compounds, and the rhodium borylene depiction is drawn for consistency.[5]

To better understand why the initial reaction between **1** and $MesBH_2$ did not go to completion, we reasoned that the reversible H_2 activation pathway was likely accessible, resulting in an equilibrium between **1** and **3** in solution. Putting a benzene-d_6 solution of **3** under 4 atmospheres of H_2 confirmed the reversibility of the process at ambient temperatures (>80% formation of **1** in 10 minutes). Additionally, when a 1 : 1 mixture of $MesBH_2$ and $MesBD_2$ (1 total equivalent) was combined with mono-carbonyl rhodium **1**, both H_2 and HD gas were identified in the ^1H NMR spectrum (Figure 2.1). The isotope mixing in this study supports the formation of a rhodium boryl hydride species that is capable of intermolecular Rh−H(D) and/or B−D(H) exchange. The control reaction between only $MesBH_2$ and $MesBD_2$ showed no sign of H/D scrambling or evolution of HD gas.

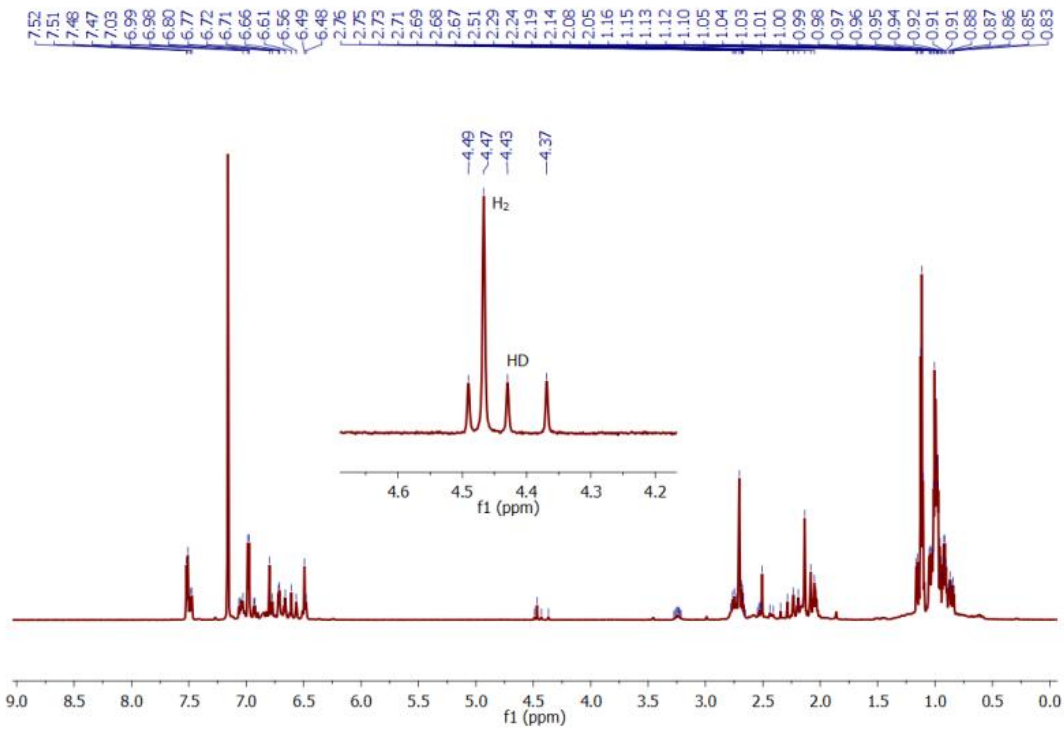

Figure 2.1. ^{1}H NMR (700 MHz) spectrum of compound **1** + a 1:1 mixture of mesitylborane and mesitylborane-d_2. Inset: enlarged region showing H_2 and HD gas in benzene-d_6.

Following these experiments, variable temperature NMR spectroscopy was employed with toluene-d_8 as the solvent system for the reaction between **1** and $MesBH_2$. $^{31}P\{^{1}H\}$ spectra obtained at −40 °C showed two new resonances in a 1 : 1 ratio at δ 50.4 and 47.8, and a broad resonance at δ −2.7 in the accompanying ^{1}H NMR spectrum. These resonances, attributed to an intermediate species, were consumed upon warming of the solution to 22 °C, while those attributed to the borylene complex **3**, grew in intensity (*vide infra*).

The generality of dehydrogenation was studied by reacting mono-carbonyl **1** with the trifluoromethylated borane, $^{meta}Xyl^{F}BH_2$ ($^{meta}Xyl^{F}$ = 3,5-$(CF_3)_2C_6H_3$), which has both a reduced steric profile about boron, and electron withdrawing substituents on the aromatic ring. Rather than generating the analogous borylene compound to **2** however, the reaction stalled at a product with

^{31}P NMR resonances at δ 51.2 and 48.8, more closely resembling the intermediate observed in the low temperature experiment between **1** and $MesBH_2$. Single crystals grown from a saturated Et_2O solution at −30 °C allowed for X-ray diffraction analysis to reveal a Lewis acid-base adduct between the unaltered $^{meta}Xyl^FBH_2$ moiety and the phosphinimine nitrogen (Figure 2.2). The rhodium center in κ^2-*L*'(CO)Rh($^{meta}Xyl^FBH_2$), **4**, appears to be stabilized by a B−H end on interaction as suggested by an upfield B−*H* signal at δ −3.8 in the ^{1}H NMR spectrum (H−Rh = 1.61(2) Å).

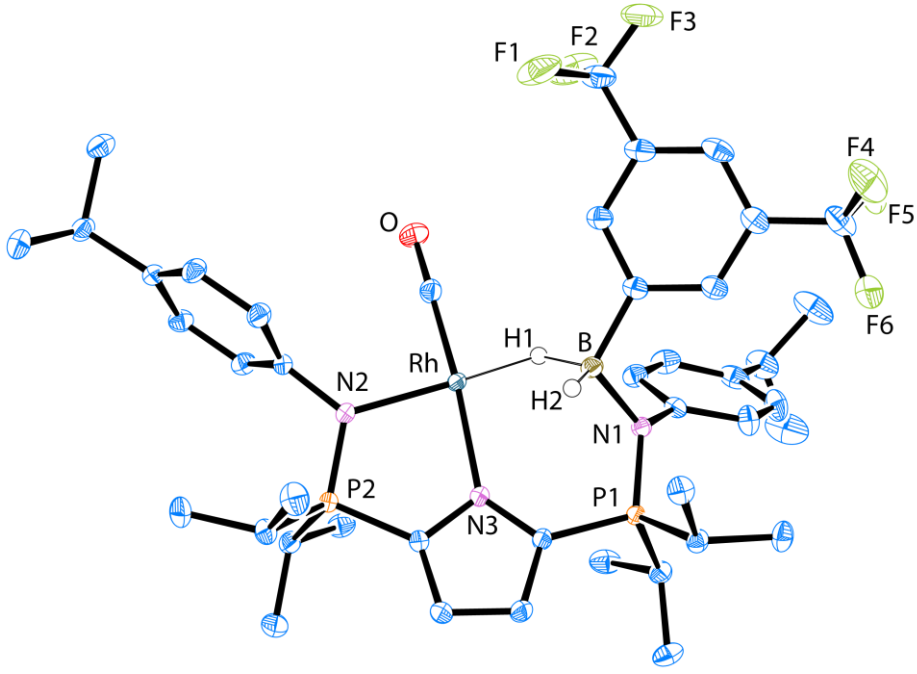

Figure 2.2. Solid-state structure of compound **4** at 35% ellipsoid probability. Hydrogen atoms, aside from BH_2, as well as co-crystallized solvent (benzene) molecules, removed for clarity. H1 and H2 were located using Q-peaks in the difference Fourier map.

Variable temperature NMR spectroscopy performed on a toluene-d_8 solution of **3** at −80 °C collapses the broad signal attributed to the two rapidly exchanging BH_2 environments at δ −3.8 into distinct resonances at δ 3.8 (B–*H*) and δ –9.8 (Rh–*H*–B). The two signals coalesce at –25 °C ($\Delta G^{\ddagger}$ = 9.9(4) kcal mol^{-1}), and reappear as the original resonance near 0 °C (Figure 2.3).

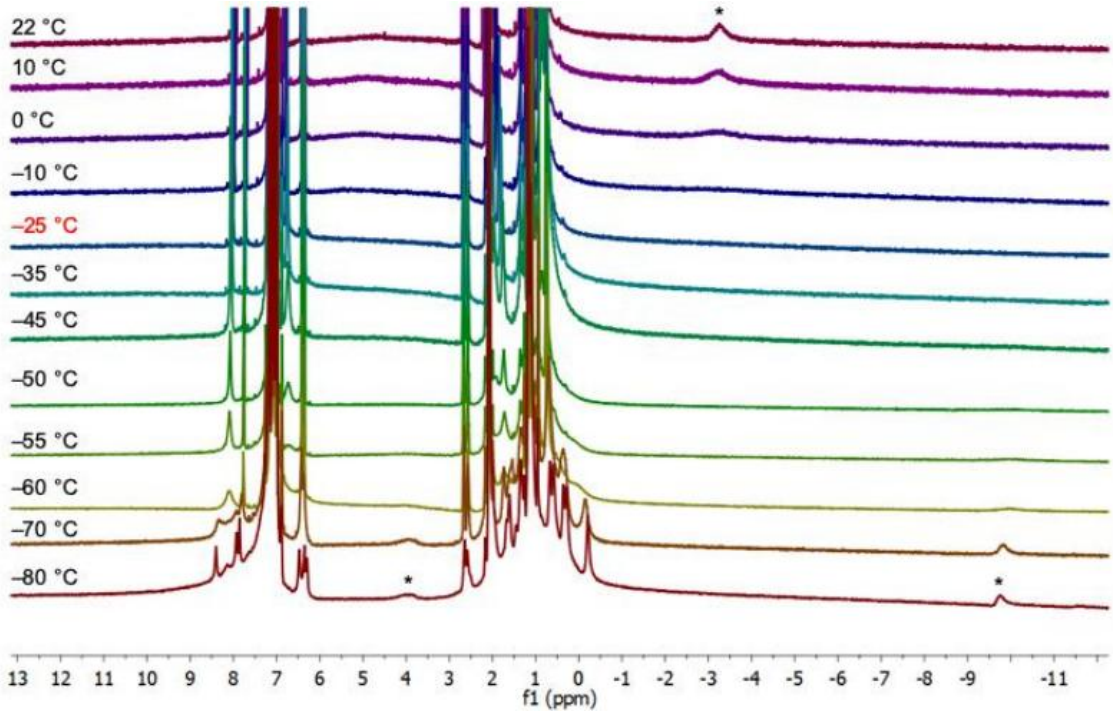

Figure 2.3. Variable temperature ^{1}H NMR (700 MHz) spectra of **4** in toluene-d_8. The peaks corresponding to the borane BH_2 protons are marked with an asterisk (*) and the coalescence temperature (–25 °C) is highlighted in red.

Computational studies were also performed on **4** at the same B3LYP/aug-cc-pVDZ level of theory, and second-order perturbation analysis show back-donation from the Rh $4d_{xy}/4d_{xz}$ orbitals to the (B–H)σ* orbital comparable with a sigma-complex interaction (*vide supra*). The blue-shifted ν_{CO} stretching frequency (1950 cm^{-1}) compared to both compounds **1** and **3** further corroborates increased donation from the metal center.

Similar to the findings from Braunschweig *et al.*, the decreased steric profile of ^{meta}Xyl^{F}BH$_2$ prevented the dehydrogenation step from occurring to form the desired base-stabilized borylene.[2b] When left in solution at ambient temperatures, the ^{31}P NMR spectrum instead revealed a gradual transition to a new unsymmetric product with resonances at δ 52.0 and 10.6. The upfield resonance is diagnostic of a dissociated phosphinimine as shown in previous work in our group, implying a κ^2-bound ligand.[5] Additionally, when **4** was prepared with a ^{13}C-labelled CO group, the diagnostic

doublet ($^1J_{CRh}$ = 73.4 Hz) centered at δ 190.6 gradually disappears after 12 h at ambient temperatures in the ^{13}C NMR spectrum. This new species was identified as the product of a transmetalation pathway whereby the ligand is κ^2-bound to a moiety of B(H)(^{meta}Xyl^F) in the form of κ^2-NN'-2,5-[^{i}Pr$_2$P=N(4-^{i}PrC$_6$H$_4$)]$_2$-N'(C$_4$H$_2$)$^-$)B(H)(^{meta}Xyl^F), **5** (Scheme 2.3). Independent synthesis of this compound through reaction of the proteo-ligand (HL), 2,5-[^{i}Pr$_2$P=N(4-^{i}PrC$_6$H$_4$)]$_2$-HN'(C$_4$H$_2$), and ^{meta}Xyl^{F}BH$_2$ further confirms the absence of rhodium in the compound. Further details for this transmetalation are discussed in Chapter 3, but the fate of the {RhCO} moiety is unknown.

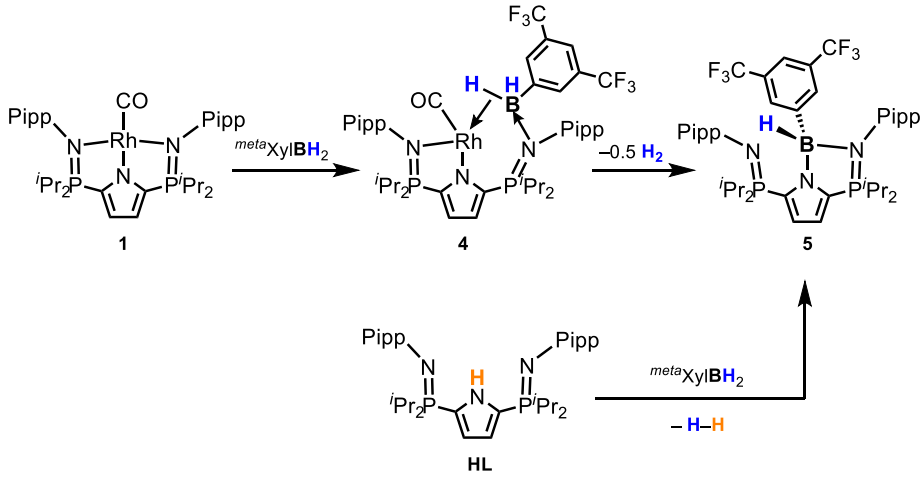

Scheme 2.3. Reaction between compound **1** and ^{meta}XylBH$_2$ to form intermediate **4**, followed by a transmetallation step that results in the formation of **5**. Independent synthesis between HL and ^{meta}XylBH$_2$ result in the same product.

Based on these findings, we propose that MesBH$_2$ forms a similar adduct when reacting with **1**, where extensive back-donation from rhodium results in formal oxidative addition as described by Sabo-Etienne (*vida supra*) to form a Rh(III) boryl hydride species.[4b] H$_2$ loss then occurs *via* either a 4-centered transition state involving the Rh–H $^{(\delta+)}$ and hydridic B–H $^{(\delta-)}$, or a Brønsted pathway involving protonation of the phosphinimine nitrogen.[5]

Given the ability of **3** to activate H_2 and release $MesBH_2$, we were inspired to attempt the dehydrocoupling of pinacol with our borylene species. Addition of pinacol (0.17 mmol) to an equimolar benzene-d_6 solution of **3** resulted in immediate effervescence of H_2 gas, and MesBpin as well as **1** were identified as the resulting products *via* NMR spectroscopy, which showed full conversion within 15 min (Scheme 2.4). This proof-of-principle reaction demonstrates formal transfer of the {BMes} fragment to small molecules, regenerating the initial monocarbonyl rhodium complex in the process. Unfortunately, the direct reaction of $MesBH_2$ and pinacol also affords the MesBpin product in quantitative yields, discouraging attempts at making this process catalytic.

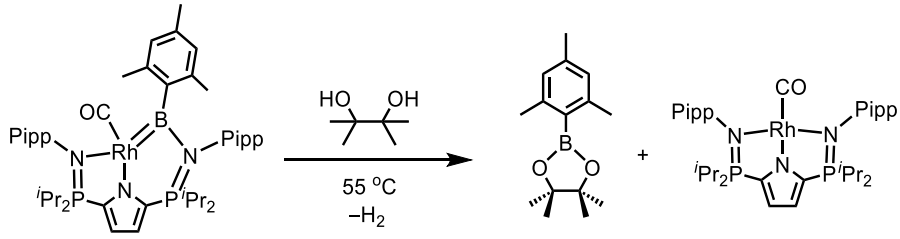

Scheme 2.4. Reaction between complex **3** and pinacol to form MesBPin and regenerate monocarbonyl **1**.

2.3. Conclusions

This work show-cases the importance of metal-ligand cooperation in the dehydrogenation of primary aryl boranes. To the best of our knowledge, this is the first example of consecutive B–H bond activations to form a borylene species at rhodium; and mechanistic studies show how the process proceeds first through a Lewis acid/base adduct formed between the borane and the phosphinimine nitrogen of the ligand. Reaction with the less sterically encumbered and electron deficient $^{meta}Xyl^{F}BH_2$ results only in the isolation of this intermediate species, highlighting the sensitivity of the system to subtle changes. In the scope of this thesis document, the insights towards the bonding between rhodium, boron, and nitrogen will be key in the discussion of subsequent chemistry.

2.4. References

[1] a) K. Burgess, W. A. Van der Donk, S. A. Westcott, T. B. Marder, R. T. Baker, J. C. Calabrese, *J. Am. Chem. Soc.* **1992**, *114*, 9350-9359; b) A. Caballero, S. Sabo-Etienne, *Organometallics* **2007**, *26*, 1191-1195; c) Cathleen M. Crudden, D. Edwards, *Eur. J. Org. Chem.* **2003**, *2003*, 4695-4712; d) C. N. Muhoro, X. He, J. F. Hartwig, *J. Am. Chem. Soc.* **1999**, *121*, 5033-5046; e) S. A. Westcott, H. P. Blom, T. B. Marder, R. T. Baker, *J. Am. Chem. Soc.* **1992**, *114*, 8863-8869.

[2] a) N. Arnold, H. Braunschweig, R. D. Dewhurst, W. C. Ewing, *J. Am. Chem. Soc.* **2016**, *138*, 76-79; b) C. Lenczyk, D. K. Roy, J. Nitsch, K. Radacki, F. Rauch, R. D. Dewhurst, F. M. Bickelhaupt, T. B. Marder, H. Braunschweig, *Chem. Eur. J.* **2019**, *25*, 13566-13571.

[3] M. O'Neill, D. A. Addy, I. Riddlestone, M. Kelly, N. Phillips, S. Aldridge, *J. Am. Chem. Soc.* **2011**, *133*, 11500-11503.

[4] a) G. Alcaraz, E. Clot, U. Helmstedt, L. Vendier, S. Sabo-Etienne, *J. Am. Chem. Soc.* **2007**, *129*, 8704-8705; b) G. Alcaraz, M. Grellier, S. Sabo-Etienne, *Acc. Chem. Res.* **2009**, *42*, 1640-1649.

[5] C. S. MacNeil, P. G. Hayes, *Chem. Eur. J.* **2019**, *25*, 8203-8207.

[6] S. S. Hanson, E. Doni, K. T. Traboulsee, G. Coulthard, J. A. Murphy, C. A. Dyker, *Angew. Chem., Int. Ed.* **2015**, *54*, 11236-11239.

[7] a) H. Braunschweig, M. Forster, T. Kupfer, F. Seeler, *Angew. Chem. Int. Ed.* **2008**, *47*, 5981-5983; b) H. Braunschweig, M. Forster, F. Seeler, *Chem. Eur. J.* **2009**, *15*, 469-473.

Chapter 3. Rhodium-mediated Dehydrogenation of Hydroboranes and Group 14 Compounds: Base-stabilized Silylene and Germylene Complexes vs. Transmetalation

Abstract and Preface

Monocarbonyl rhodium complex *L*Rh(CO), **1**, which is stabilized by a pyrrole-based bis(phosphinimine) pincer ligand ($L = \kappa^3$-*NNN*' = 2,5-[^{i}Pr$_2$P=N(4-^{i}PrC$_6$H$_4$)]$_2$-N'(C$_4$H$_2$)$^-$), serves as a versatile platform for the dehydrogenation of Group 14 substrates. Reaction with primary and secondary silanes and germanes (MesSiH$_3$, Et$_2$SiH$_2$, Ph$_2$GeH$_2$, ^{t}BuGeH$_3$; Mes = mesityl) liberates H$_2$ and yields base-stabilized tertylene compounds of the form κ^2-*L*(CO)Rh(ER$_2$) (E = Si: R = Mes, H, **6**; R = Et, **9**; E= Ge: R = Ph, **10**; R = ^{t}Bu, H, **12**). The ":ER$_2$" fragment in these species bridges between the rhodium center and a phosphinimine donor. Preliminary reactions between pinacol (Pin) and κ^2-*L*(CO)Rh(ER$_2$), E = Si, Ge, indicate that such complexes can serve as silylene and germylene synthons, releasing :ER$_2$ and catalytically generating PinER$_2$. In contrast, combination of complex **1** and MesGeH$_3$ does not yield the anticipated dehydrogenation product, but rather, transmetalation similar to that observed upon reaction between **1** and 3,5-dimethylphenylborane prevails.

This chapter serves as a continuation from Chapter 2, where the methodology of silylene and borylene extrusion through dehydrogenation is expanded towards additional silanes as well as germanes. In particular, the work in this chapter showcases rare examples of alkyl substituted silylene and germylene compounds, as well as preliminary accounts of reaction chemistry wherein the R$_2$E: fragment is catalytically transferred from the metal to another compound. By presenting a use-case for silylene and germylene complexes, the chapter provides rationalization of why this class of compounds are worth pursuing. The substrate scope presented highlights the advantages of our specific system compared to others in the literature.

The chapter is reproduced from "Hsiang, S.J.; Hayes, P.G.*, Rhodium-mediated Dehydrogenation of Hydroboranes and Group 14 Compounds: Base-stabilized Silylene and Germylene Complexes vs. Transmetalation. *Chemistry – A European Journal.* **2023**, *30*, e202302925." The citation style follows that of *Chemistry – A European Journal*, published by Wiley. The experimental section for this chapter is provided in the body of the text, including characterization details and general procedures. Additional NMR spectra, as well as X-ray crystallographic details and computational details, are provided in Appendix II.

3.1. Introduction

Marked by a decreased tendency to engage in multiple-bonding, larger size, and higher-energy valence orbitals, silicon, germanium, and tin possess unique properties when compared to carbon, the lightest group 14 element.[1] Accordingly, mid-late transition metal complexes bearing silylene ($L_nM{=}SiR_2$) functionalities exhibit different reaction chemistry than their much better known carbon-based congeners, partly due to the umpolung $M^{\delta-}$–$Si^{\delta+}$ bond.[2] Notably, silylene complexes are important intermediates in the Direct Process which generates chlorosilanes that are essential for the production of silicones.[3] Transition metal germylene and stannylene complexes are less well studied, and given the diverse chemistry they exhibit, efforts to better understand these classes of compound, and the potential value they offer the chemical industry, is warranted.[4]

There are several established routes for generating heavier tertylene complexes, including anionic substituent abstraction, coordination or transfer of stable R_2E: moieties (E = Group 14 element), and sequential E–H bond oxidative addition/α–hydrogen migration.[2a, 4e] While the latter method is appealing because one can use simple organic substrates (*e.g.,* R_2EH_2), it affords species that retain reactive metal hydride functionalities that can participate in undesired reactions and obfuscate the extent of formal M=E multiple bond character. For example, the reaction between Cp*(dmpe)Mo(η^3-CH_2Ph) (dmpe = $Me_2PCH_2CH_2PMe_2$) and Et_2GeH_2 leads to Cp*(dmpe)Mo(H)$GeEt_2$ which contains a bridging hydride that is well within the van der Waals radii of both the Mo and Ge atoms (Scheme 3.1A).[4c]

Previously, our group disclosed the dehydrogenation of primary and secondary aryl silanes by reaction with the monocarbonyl rhodium (I) species *L*Rh(CO) (**1**; *L* = κ^3-NNN**'** = 2,5-[^{i}Pr$_2$P=N(4-^{i}PrC$_6$H$_4$)]$_2$-N**'**(C$_4$H$_2$)$^-$) to afford base-stabilized rhodium silylene species of the form κ^2-*L*(CO)Rh(SiRPh) (R = Ph, H; κ^2-*L* = κ^2-NN'-Rh,κ^1-N-E; E = Si) (Scheme 3.1B).[5] Additionally, reaction between complex **1** and the primary borane $MesBH_2$ (Mes = 1,3,5-$Me_3C_6H_2$) generates the base-stabilized rhodium borylene κ^2-*L*(CO)Rh(BMes) (Scheme 3.1C).[6] This general methodology

is unique for silanes in that the consecutive Si–H bond activation leads to loss of molecular H_2, creating a neutral, hydride-free product.

Base stabilization of a formal metal silylene species is not uncommon, owing to the substantial Lewis acidity of the silicon atom. Accordingly, coordination of Lewis bases to metal silylenes is an archetypal reaction of this class of compound.[2] As with similar base-stabilized species, NBO analysis indicates that our compounds have limited Rh–Si and Rh–B π-bonding interactions, partly due to the strong σ- and π- donating properties of the phosphinimine groups.[5-6] Nonetheless, these complexes can be considered as silylene and borylene synthons, respectively. The silicon- and germanium-containing complexes reported herein are described as "base-stabilized silylenes/germylenes"[2c] and depicted with a M=E double bond (E = Si, Ge), in accordance with common practice in the relevant scientific literature.[2a,b]

Extension of known silylene extrusion methods to germanium and tin poses additional challenges that typically require increasingly stringent reaction conditions and substrate choice. For example, the Tilley group reported that while $[PhB(CH_2PPh_2)_3]Ir(H)(\eta^3\text{-}C_8H_{13})$ reacted with Mes_2GeH_2 to yield the terminal germylene $[PhB(CH_2PPh_2)_3](H)_2Ir{=}GeMes_2$, reaction with Mes_2SnH_2 rapidly led to a mixture of iridium-containing products.[7] Below, we detail a systematic study wherein we probe the generality of our protocol for the dehydrogenation of main group compounds. Specifically, reaction between our electron-rich, monomeric, rhodium complex *L*Rh(CO) (**1**) and silane, germane, and stannane substrates revealed that while the system is tolerant of all employed aryl/alkyl silanes, substantial steric bulk precludes H_2 loss from certain germanes, as well as diphenylstannane. Such findings draw parallels to an unexpected transmetalation pathway found upon reaction of complex **1** with *meta*-substituted aryl boranes.

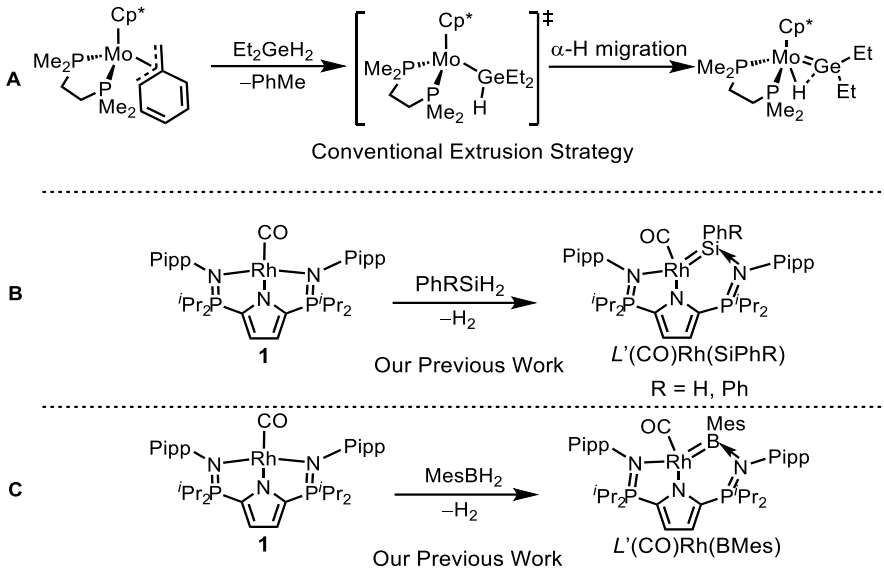

Scheme 3.1 A) Double Si–H activation extrusion strategy B) Reaction of complex **1** with silanes C) Reaction of **1** with $MesBH_2$

3.2. Results and Discussion

3.2.1. Synthesis of Base-stabilized Silylenes and Comparison to Analogous Borylene

Complex **1** has been previously demonstrated to react with primary and secondary phenyl silanes to yield base-stabilized silylenes (*vide supra*).[5] In the case of the addition of $PhSiH_3$ to **1**, a rare example of a neutral Si–H substituted silylene was isolated.[5] In an effort to garner a deeper understanding of this unusual type of compound, complex **1** was reacted with $MesSiH_3$ in toluene at 50 °C. The product of this reaction exhibits two equal intensity peaks at δ 50.2 and *δ* 41.1 in its ^{31}P NMR spectrum. Resonances attributed to H_2 (δ 4.47) and Si–*H* were observed (δ 6.51, $^{1}J_{SiH}$ = 182 Hz) in the ^{1}H NMR spectrum, suggesting formation of the anticipated silylene κ^2-*L*(CO)Rh(Si(H)Mes), (**6**). Free rotation about the Si–Mes bond is restricted on the ^{1}H NMR timescale, leading to three distinct mesityl CH_3 resonances. Similarly, four separate aromatic peaks were found for the *para*-isopropylphenyl (Pipp) substituent on the phosphinimine nitrogen coordinated to silicon. The ^{29}Si NMR signal was located at δ 38.0, which is substantially upfield-

shifted compared to the resonances for κ^2-*L*(CO)Rh(Si(H)Ph) and κ^2-*L*(CO)Rh($SiPh_2$), which appear at δ 54.6 and δ 51.4, respectively. Crystals suitable for X-ray diffraction analysis were grown from a –35 °C Et_2O solution saturated with complex **6**; the solid-state structure confirmed the identity of **6** as the mesityl-substituted, base-stabilized, silylene κ^2-*L*(CO)Rh(Si(H)Mes) (Figure 3.1A). The Rh–Si distance of 2.272(1) Å in **6** is marginally longer than the Rh–Si length (2.262(1) Å) in isostructural κ^2-*L*(CO)Rh(Si(H)Ph), presumably due to the increase in steric bulk at silicon (Table 3.1).[5]

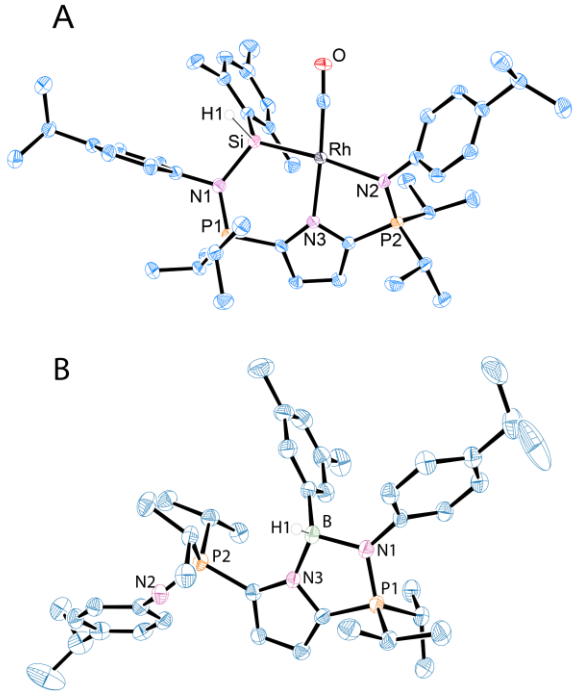

Figure 3.1 ORTEP diagram of A) complex **6** and B) compound **8**, with thermal ellipsoids depicted at the 50% probability level. All carbon-bound hydrogens, as well as co-crystallized solvent molecules and disorder models, have been omitted for clarity. Selected bond distances (Å) and angles [º] for **2**: Rh–Si 2.272(1), Si–N1 1.835(3), N1–Si–Rh 115.1(1). Selected bond distances (Å) for **8**: B–N1 1.5997(1), B–N3 1.5859(1).

The observed generality of dehydrogenating silane substrates is in direct contrast with attempts to prepare borylene species from $^{meta}Xyl^FBH_2$ and $MesBH_2$ ($^{meta}Xyl^F$ = 3,5-$(CF_3)_2C_6H_3$).[6] While reaction of **1** with $MesBH_2$ indeed affords the anticipated dehydrogenation product κ^2-

L(CO)Rh(BMes), an unexpected compound was obtained when the *meta*-substituted borane ^{meta}Xyl^{F}BH$_2$ was employed.[6] Specifically, further study revealed that regardless of the electronic nature of the xylyl substituents (CF_3 vs. CH_3), reduction of steric bulk about boron leads to a Lewis acid-base adduct between the borane and a phosphinimine nitrogen. Similar to that previously reported for κ^2-*L*'(CO)Rh(^{meta}Xyl^{F}BH$_2$), the rhodium centre in κ^2-*L*(CO)Rh(^{meta}XylBH$_2$) (**7**, ^{meta}Xyl = 3,5-$Me_2C_6H_3$) appears to be stabilized by a B–H agostic interaction as suggested by an upfield B–*H* signal in the ^{1}H NMR spectrum (δ –3.10).[6] Allowing this species to sit in quiescent benzene-d_6 solution for 12 hours at ambient temperature led to complete conversion into (κ^2-NN'-2,5-[^{i}Pr$_2$P=N(4-^{i}PrC$_6$H$_4$)]$_2$-N'(C$_4$H$_2$)$^-$)B(H)(^{meta}Xyl), (**8**), as indicated by multinuclear NMR spectroscopy (Scheme 3.2). An isotopic labelling experiment using κ^2-*L*(^{13}CO)Rh(^{meta}XylBH$_2$), **7-^{13}CO**, confirmed that the formation of compound **8** was coupled with loss of the ^{13}CO resonance in the ^{13}C NMR spectrum, as well as the precipitation of an intractable black solid. In addition, an upfield signal in the ^{31}P NMR spectrum (δ 13.4) was consistent with a dissociated phosphinimine donor. Single crystals of compound **8** grown from a saturated pentane/toluene (5:1) solution unambiguously established that a transmetalation process afforded the borane ligated species (κ^2-NN'-2,5-[^{i}Pr$_2$P=N(4-^{i}PrC$_6$H$_4$)]$_2$-N'(C$_4$H$_2$)$^-$)B(H)(^{meta}Xyl) (Figure 3.1B, *vide supra*). The fate of rhodium is not known.

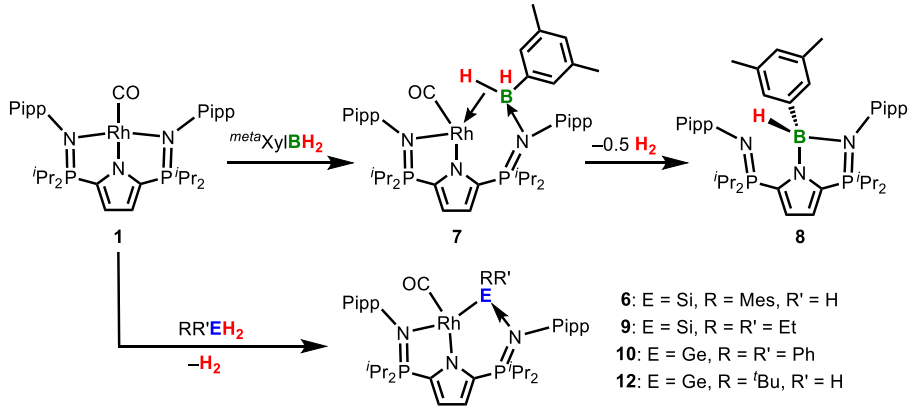

Scheme 3.2 Generation of complexes **6-10** and **12**.

Extrusion processes appear to be highly sensitive to the steric profile of the main group substrates. For example, Braunschweig *et al.* have found that *ortho*-substituted aryl boranes are necessary for dehydrogenative borylene formation from their ruthenium complex $Ru(PCy_3)_2HCl(H_2)$.[8] Meanwhile, the Tilley and Hashimoto groups utilize sterically demanding reagents, such as Mes_2SiH_2 and $TsiGeH_3$ to generate terminal silylene ($[(dippe)Pt(H)=SiMes_2][BAr^f_4]$, dippe = 1,2-bis(diisopropylphosphino)ethane; Ar^f =3,5-$(CF_3)_2C_6H_3$) and germylene ($[Cp^*(OC)_2Fe(H)=Ge(H)Tsi]$, Tsi = $C(SiMe_3)_3$) complexes, respectively.[4e, 9] In our system, primary and secondary silanes appear to sit in a "goldilocks" zone that permit access to a wide array of silylene complexes.

3.2.2. Synthesis of Alkyl-substituted Silylenes

While routes to silylene complexes have been reported from a variety of primary and secondary aryl silanes, to the best of our knowledge the synthesis of stable alkyl-substituted silylenes from their respective alkyl silanes is exceedingly rare. While Tilley *et al*. were able to prepare $[PhBP_3](H)_2Ir{=}SiR_2$ (R = Mes, Ph, Et, Me) *in situ*; the compounds where R ≠ Mes were deemed thermally unstable and decomposed upon removal of solvent.[7] With this in mind, an excess of Et_2SiH_2 was added to complex **1** in toluene and the reaction mixture was heated to 45 °C for one hour. Monitoring by ^{31}P NMR spectroscopy indicated complete consumption of the monocarbonyl **1**, along with concomitant generation of a single product that resonates at δ 49.5 and δ 39.9. Although signal overlap rendered it difficult to ascertain $^{29}Si–^{1}H$ coupling constants, 2D COSY, HSQC, and HMBC experiments corroborated the presence of Si–CH_2CH_3 groups. The $^{29}Si\{^{1}H\}$ NMR spectrum exhibited a doublet of doublet of doublets (ddd) at δ 67.5, due to coupling to both phosphorus nuclei, as well as rhodium (^{103}Rh = 100%, I = ½). Notably, this signal is downfield shifted by 16 ppm compared to κ^2-*L*(CO)Rh($SiPh_2$) and is consistent with the targeted base-stabilized, alkyl-substituted, silylene complex κ^2-*L*(CO)Rh($SiEt_2$), (**9**). Complex **9** is stable in aromatic solvents at ambient temperature and can be isolated as a yellow powder in high yield

(81%). X-ray quality crystals grown from a saturated Et_2O solution at –35 °C confirmed the structure of **9**, which has a slightly longer Rh–Si distance (2.282(1) Å) than that found in our other silylenes (Figure 3.2, Table 3.1).

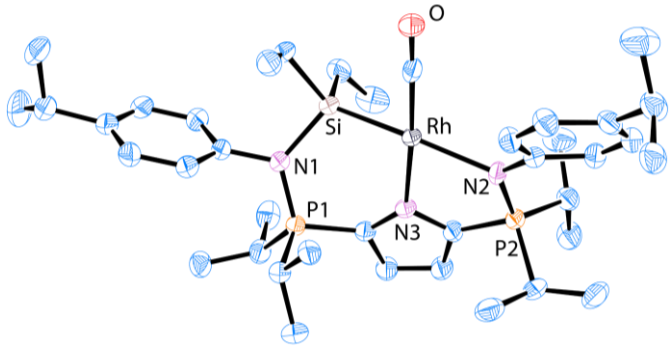

Figure 3.2 ORTEP diagram of **9** with thermal ellipsoids drawn at the 50% probability level. Hydrogen atoms and disorder model omitted for clarity. Selected bond distances (Å) and angles [°]: Rh–Si 2.282(1), Si–N1 1.857(3), N1–Si–Rh 112.8(1).

The ability of this platform to incorporate alkyl-substituted silanes expands the subsequent breadth of available chemistry. Previously reported dialkylsilylene complexes were often accessed *via* salt metathesis strategies. For example, Müller reacted Me_2SiCl_2 and $[Na_2Fe(CO)_4]$ to yield the base-stabilized iron silylene $(CO)_4Fe{=}Si(Me)_2{\leftarrow}$HMPT (HMPT = hexamethylphosphoramide). As previously mentioned, Tilley *et al*. have exploited *in situ* extrusion processes.[7, 10] Unlike our system, both of these methods generate a metal-based by-product which complicates the conversion of stoichiometric chemical reactions into catalytic processes.

Table 3.1 Selected bond distances (Å), angles (°), and solution-state ^{31}P and ^{29}Si NMR chemical shifts (δ) of silylene and germylene compounds.

Compound	Rh–E[a]	P=N$_{(E)}$[a]	P=N$_{(Rh)}$	N–E (Å)[a]	N$_{(Pipp)}$–Rh	CO	Rh–E–N[a] ∠ (°)	^{31}P (ppm)	^{29}Si (ppm)
6 (SiHMes)	2.272(1)	1.637(3)	1.606(2)	1.835(3)	2.225(3)	1.162(4)	115.1(1)	50.2, 41.1	38.0
9 (SiEt$_2$)	2.278(1)	1.640(4)	1.616(3)	1.857(3)	2.235(3)	1.160(5)	112.8(1)	49.4, 39.9	67.5
10 (GePh$_2$)	2.3438(4)	1.630(2)	1.611(2)	1.980(2)	2.189(1)	1.163(3)	111.96(5)	47.6, 43.8	N/A
(SiPh$_2$)[5]	2.2702(7)	1.636(2)	1.607(2)	1.842(2)	2.224(2)	1.149(4)	113.61(9)	53.1, 43.1	51.4
(SiHPh)[5]	2.262(1)	1.637(2)	1.596(2)	1.834(3)	2.196(3)	1.161(4)	113.54(8)	53.0, 43.5	54.6

[a] E = Group 14 element, Si or Ge

3.2.3. Silylene Transfer

Previously we reported that reaction of our base-stabilized borylene complex κ^2-*L*(CO)Rh(BMes) with pinacol causes :BMes group transfer to yield the boronic ester PinBMes, along with regeneration of complex **1**.[6] We therefore anticipated that a similar pathway might be viable for our silylene complexes. Such a transformation was particularly attractive because unlike hydroboranes, hydrosilanes do not spontaneously react with pinacol. Furthermore, catalytic generation of $PinSiR_2$ can be readily envisioned. To this end, a PTFE-sealed NMR tube was charged with pinacol and diphenylsilane as a 1:1 mixture in benzene-d_6. As expected, after 16 hours at 80 °C no reaction was observed by NMR spectroscopy. Upon cooling to ambient temperature, 0.1 equivalents of complex **1** was added to the reaction mixture, resulting in immediate effervescence of a gas (presumably H_2). Within 5 minutes ^1H and ^{13}C NMR spectra indicated formation of 4,4,5,5-tetramethyl-2,2-diphenyl-1,3-dioxa-2-silacyclopentane ($PinSiPh_2$). Full conversion of the hydrosilane was achieved after 30 minutes at 40 °C (Scheme 3.3). In order to demonstrate generality, the alkylsilane Et_2SiH_2 was reacted with pinacol and 10 mol% complex **1** (Scheme 3.3) in benzene-d_6. Spontaneous liberation of H_2 was observed, though the catalysis was substantially slower than with Ph_2SiH_2, requiring 1.2 hours at 40 °C to reach completion, as indicated by multinuclear NMR spectroscopy.

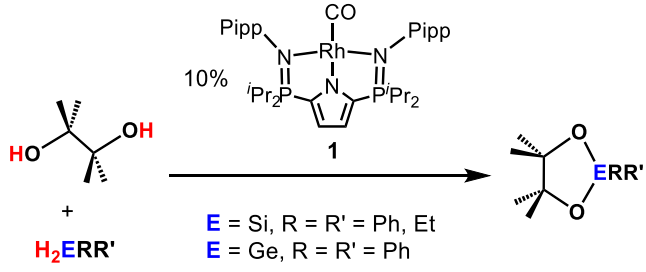

Scheme 3.3 Catalytic dehydrocoupling of pinacol and group 14 compounds.

Dehydrocoupling reactions catalyzed by rhodium species are well documented and typically involve oxidative addition as the first step in the catalytic cycle. For instance, Wilkinson's catalyst,

$(PPh_3)_3RhCl$, can couple sterically hindered organosilanes and alcohols at ambient temperature.[11] The authors reported rapid H/D scrambling when Et_3SiH and Ph_3SiD were added to the active catalyst. Recent advances in the dehydrocoupling of hydrosilanes with alcohols demonstrate that the process can be accomplished by Lewis acid (*e.g.* $B(C_6F_5)_3$) Si–H activation, addition of a strong base (*i.e.* NaOH) to form a pentacoordinate Si intermediate, and Lewis-base activation of the silicon atom.[12] As previously mentioned, the strongly basic phosphinimine donor is a ready participant in the activation of small molecules, and may partake in Lewis base-catalyzed hydrosilane functionalization.[5-6] Accordingly, we postulated that pinacol might initially react with a phosphinimine-activated silane ($R_3PArN\cdots SiH_2R_2$),[12b,c] rather than with a fully dehydrogenated $:SiR_2$ moiety.

In an effort to probe the reaction mechanism of catalytic $PinSiPh_2$ generation, 0.1 equivalents of κ^2-*L*(CO)Rh($SiPh_2$) was reacted with pinacol and diphenylsilane. Although $PinSiPh_2$ was produced, the reaction was much slower than when 10 mol% of complex **1** was utilized—4 hours at 80 °C was required to reach completion. Careful monitoring *via* NMR spectroscopy over the course of the reaction revealed a slow initial rate that increased over time, presumably due to an accumulation of **1** *in situ*. When stoichiometric quantities (1:1) of κ^2-*L*(CO)Rh($SiPh_2$) and pinacol were combined in benzene-d_6, heated at 80 °C, and monitored by NMR spectroscopy, Ph_2SiPin and complex **1** indeed formed, but the process required 32 hours to consume ~90% of the reactants. These experiments suggest that the operative pathway between monocarbonyl complex **1**, Ph_2SiH_2, and pinacol does not involve κ^2-*L*(CO)Rh($SiPh_2$). Finally, it is important to note that the control reaction between pinacol, Ph_2SiH_2 and metal-free proteo-ligand, HL, did not afford product, even after heating at 80 °C for 24 hours.

3.2.4. Reaction of Complex 1 with Aryl and Alkylgermanes

Encouraged by the ability of complex **1** to dehydrogenate a variety of silanes, we sought to expand the substrate scope to include the heavier Group 14 element germanium. Reaction of **1**

with the secondary germane Ph_2GeH_2 in toluene at 50 °C for three hours led to formation of κ^2-*L*(CO)Rh($GePh_2$), (**10**), as the sole rhodium-containing product. The ^{31}P NMR spectrum exhibits two equal intensity singlets at δ 47.6 and δ 43.8, consistent with the targeted C_s-symmetric base-stabilized germylene. Complex **10** readily crystallized from a saturated Et_2O solution at –35 °C; X-ray diffraction experiments confirmed the identity of κ^2-*L*(CO)Rh($GePh_2$) (Figure 3.3).

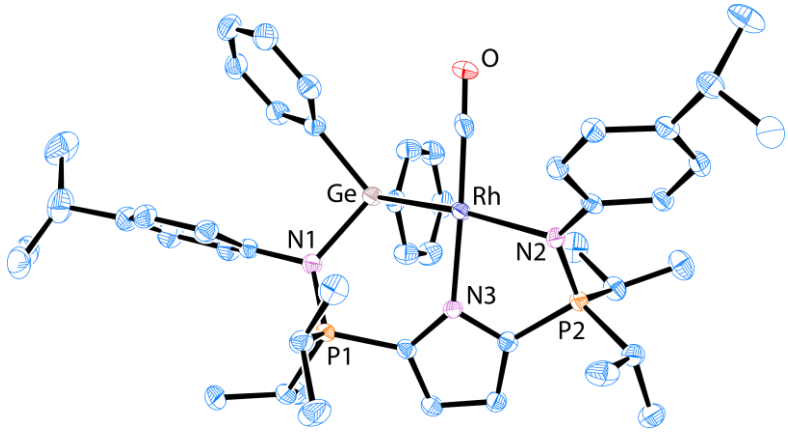

Figure 3.3 ORTEP diagram of complex **10** with thermal ellipsoids drawn at the 50% probability level. Hydrogen atoms and disorder model omitted for clarity. Selected bond distances (Å) and angles [°]: Rh–Ge 2.3438(4), Ge–N1 1.980(2), N1–Ge–Rh 111.96(5).

Selected bond distances given in Table 3.1 demonstrate that germylene **10** is isostructural with the diphenylsilylene congener κ^2-*L*(CO)Rh($SiPh_2$). The angles about germanium range from 98.75(8)° to 125.55(7)°, indicating distorted tetrahedral geometry (τ_4 = 0.86) due to strong phosphinimine N→Ge σ-donation that presumably minimizes Rh→Ge π-interactions.[13] The Rh–Ge distance of 2.3438(4) Å is similar to the terminal Ir=Ge bond (2.339(1) Å) in aforementioned [$PhB(CH_2PPh_2)_3$](H)$_2$Ir=$GeMes_2$, and longer than the Ru=Ge length of 2.2821(6) Å in Cp*(^{i}Pr_2MeP)(H)Ru=GeH(2,4,6-^{i}Pr_3-C_6H_2).[7, 14] Nonetheless, a search of the Cambridge Crystal Structure Database, revealed that the rhodium germanium bond in complex **10** is amongst the shortest reported.[15]

In order to establish if hydrogen-substituted germylenes are accessible, $MesGeH_3$ was added to monocarbonyl rhodium complex **1** at ambient temperature in benzene-d_6 solvent. Initial monitoring *via* ^{31}P NMR spectroscopy revealed formation of a new species with peaks at δ 57.1 and δ 46.9 in a 1:1 ratio. However, over several hours an insoluble black solid precipitated and the only ^{31}P NMR resonance remaining was a singlet at δ 34.4. Numerous attempts to seek reaction parameters conducive to generation of the targeted compound proved unsuccessful. An experiment utilizing ^{13}CO labelled **1** (*L*Rh(^{13}CO), **1-^{13}CO**) and $MesGeH_3$ indicated a lack of CO in the final product, suggesting that a transmetalation process similar to that which generated compound **8** (*vide supra)* had occurred (Scheme 3.4). The ^1H NMR spectrum of a crude mixture contained signals that can be attributed to ligand *L* and the germanium mesityl group, as would be expected for the anticipated product *L*GeH_2Mes, (**11**). In addition, a sharp singlet at δ 4.21, which integrates to 2H, lacks crosspeaks in ^1H–^{13}C HSQC experiments, and hence, has been assigned to GeH_2. Finally, it should be noted that over the course of the reaction liberated H_2 was observed in the ^1H NMR spectrum. Unfortunately, all efforts to isolate analytically pure samples of compound **11** resulted in decomposition to unidentified products.

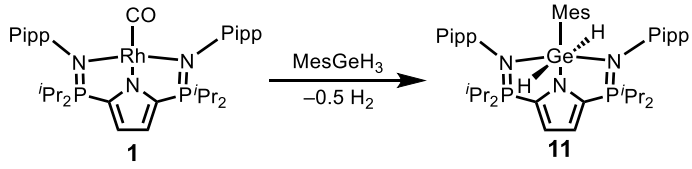

Scheme 3.4 Presumed generation of compound **11** by transmetalation

Since efforts to prepare κ^2-*L*(CO)Rh(Ge(H)Mes) were unsuccessful, we targeted an alkyl-substituted germylene, in an attempt to inductively stabilize the Lewis acidic germylene. Specifically, addition of the primary germane ^{t}BuGeH_3 to **1** afforded κ^2-*L*(CO)Rh(Ge(H)^{t}Bu), (**12**), after 5 hours in toluene at 50 °C. Despite the different steric and electronic properties of the germanium substituents in complexes **10** and **12**, the chemical shifts of the ^{31}P NMR signals are similar (**10**: δ 47.6 and δ 43.8; **12**: δ 47.4 and δ 43.5). A pseudotriplet ($^3J_{HP} = {}^2J_{HRh}$ = 10.6 Hz) in

the ^{1}H NMR spectrum was assigned to the germanium bound hydrogen. Low quality crystals, grown from a saturated pentane solution, established the anticipated connectivity in germylene **12**. Complex **12** represents a rare example of a neutral, H-substituted tertylene accessed from a primary main group substrate. Normally, the kinetic stability of such species mandates extremely bulky substituents on the main group element; for example, $Cp^{*}(OC)_2(H)M{=}Ge(H)Tsi$ (M = Cr, Mo), reported by Hashimoto and colleagues.[9, 16]

3.2.5. Germylene Transfer

Following the synthesis of these germylene species, the catalytic dehydrocoupling of diphenyl germane with pinacol using 10 mol% complex **1** as a catalyst, was attempted. No reaction was observed after 30 minutes at ambient temperature, though partial conversion from complex **1** to **10** became apparent spectroscopically after one hour at 40 °C. Heating the mixture to 80 °C for 16 hours led to complete consumption of complex **1**, along with approximately 5% production of $PinGePh_2$. Another 24 hours under the same conditions afforded an additional 5% of $PinGePh_2$ (Scheme 3.3, *vide supra*). Although catalytic dehydrocoupling appears to work with Ph_2GeH_2, the reaction is obviously quite sluggish and the reasons behind the drastic change in reaction rate are not yet understood. Detailed studies into substituent and group 14 element effects on this process are ongoing.

3.2.6. Reaction of Complex 1 with Ph_2SnH_2

The mixed results encountered when attempting to dehydrogenate germanes prompted study of the reaction between complex **1** and Ph_2SnH_2. Upon addition of the secondary stannane to a benzene-d_6 solution of **1** at ambient temperature, an immediate change in color from bright orange to dark red was observed. Analysis of the mixture by ^{31}P NMR spectroscopy after removal of solvent and extraction by diethyl ether revealed the presence of multiple phosphorus-containing products. The major product of this mixture displays a single peak located at δ 33.5 in the ^{31}P NMR spectrum, suggesting that it possesses C_2 symmetry. Similar to compounds **8** and **11**, no evidence

could be obtained for the retention of CO. These results lead us to hypothesize a transmetalation product analogous to **11**. ^{1}H NMR spectroscopy reveals many overlapping peaks in the aromatic region between δ 6-8, but diagnostic resonances attributed to ligand ^{i}Pr groups are retained. Attempts at acquiring ^{119}Sn NMR spectra across a wide range of chemical shifts unfortunately yielded no discernable resonances.

3.3. Conclusions

A series of neutral, base-stabilized rhodium silylene and germylene complexes has been prepared *via* dehydrogenation of primary and secondary silanes and germanes. The system appears to tolerate a wide array of both alkyl and aryl silanes, but is incompatible with mesityl germane and diphenylstannane. The products of the latter reactions are presumed to be the result of a transmetalation pathway wherein the monoanionic pincer ligand is captured by the main group element. The mechanism for this process is unknown and it is possible that different pathways are responsible for the formation of boron-containing **8** *vs*. that which leads to compound **11**. Regardless, the fact that only 0.5 equivalents of H_2 is liberated from the main group fragment, implies that the operative mechanism is unlikely to include κ^2-*L*(CO)Rh(ER$_x$).

Proof of concept experiments indicate that stoichiometric and catalytic silylene group transfer is possible. Ongoing studies aim to exploit this reactivity to create value-added silyl- and germyl-containing compounds. Additional efforts aim to garner a deeper understanding of the rich chemistry available to the little-known hydrogen-substituted tertylenes described above.

3.4. Experimental Section

General Considerations

All air- and moisture-sensitive manipulations were carried out using vacuum line, Schlenk and cannula techniques, or in an MBraun inert atmosphere (argon) glove box unless otherwise noted. All glassware was stored in a pre-heated (110 °C) oven or flame-dried prior to use. Solvents used for air-sensitive procedures were purified using an MBraun solvent purification system (SPS), stored in PTFE-sealed glass vessels over sodium benzophenone ketyl (THF, diethylether, pentane, benzene, and toluene), and distilled at the time of use. Benzene-d_6 was dried over sodium benzophenone ketyl, distilled *in vacuo* and stored over 4 Å molecular sieves in PTFE-sealed glass vessels under argon. $MesSiH_3$ and $MesGeH_3$ were prepared according to literature procedures.[17] Diphenyltin was prepared *via* reduction of diphenyltindichloride with lithium aluminum hydride in diethyl ether solution following literature procedures.[18] Diethylsilane, tetrachlorogermane, and *tert*-butylgermane were purchased from Gelest, degassed and stored over 4 Å molecular sieves in PTFE-sealed glass vessels. Pinacol, tetrachlorosilane, diphenyltindichloride and 2-bromomesitylene were purchased from Sigma-Aldrich and used without further purification. Complexes **1,** κ^2-*L*(CO)Rh(Si(H)Ph), and κ^2-*L*(CO)Rh($SiPh_2$) were synthesized according to previous literature procedures.[5] Unless otherwise noted, all NMR spectra were recorded at ambient temperature with a Bruker Avance II NMR spectrometer (300.13 MHz for ^{1}H, 75.47 MHz for ^{13}C, 96.29 MHz for ^{11}B and 121.48 MHz for ^{31}P) or Avance III NMR spectrometer (700.44 MHz for ^{1}H, 139.10 MHz for ^{29}Si, 224.63 MHz for ^{11}B, 176.13 MHz for ^{13}C, and 283.54 MHz for ^{31}P). All ^{1}H and ^{13}C NMR chemical shifts are reported in ppm relative to $SiMe_4$ using the ^{1}H (benzene-d_6: 7.16 ppm) and ^{13}C (benzene-d_6: 128.06 ppm) chemical shifts of the solvent as reference. ^{11}B NMR chemical shifts were referenced externally to $BF3{\cdot}Et_2O$ (δ 0.0). ^{31}P NMR chemical shifts were referenced to external 85% H_3PO_4 in H_2O (δ 0.0). ^{1}H and ^{13}C NMR data are

reported as follows: chemical shift, multiplicity (s = singlet, d = doublet, t = triplet, q = quartet, quin = quintet, sp = septet, m = multiplet, br = broad, ov = overlapping), coupling constant(s) (Hz), integration, assignment. Assignment of resonances were supplemented by $^{1}H–^{1}H$ COSY, $^{13}C\{^{1}H\}$ APT, and $^{1}H–^{13}C\{^{1}H\}$ HSQC/HMBC experiments.

Elemental analyses (%CHN) were conducted at the University of Lethbridge on an Elementar Americas Vario MicroCube Analyzer (C, H, N, O, S capabilities) using bulk recrystallized compounds. "Universal Combustion Additive", purchased from Elemental Microanalysis, was added to all standards, blanks, and samples. Infrared spectroscopy was conducted with a Bruker Tensor 37 FT spectrometer (0.6 cm^{-1} resolution) using bulk recrystallized compounds (vs = very sharp, s = sharp, w = wide).

Synthesis and Characterization of New Compounds

***κ*^{2}-*L*(CO)Rh(Si(H)Mes) (6)**. Recrystallized **1** (25 mg, 0.036 mmol) was dissolved in 5 mL of toluene and cooled to –30 °C. In a separate flask, excess H_3SiMes (27 mg, 0.18 mmol) was dissolved in 3 mL of toluene and then added dropwise to the **1** solution dropwise over approximately one minute. The mixture was transferred into a sealed vessel and heated at 45 °C for 5 hours. After removal of the solvent under reduced pressure, the product was washed with 3 × 0.5 mL of pentane. The crude solid was recrystallized over 3 days from 5 mL of Et_2O at –30 °C to yield 16.5 mg (50% yield) of **2** as light yellow crystals. The compound co-crystallized with one equivalent of Et_2O. Anal Calcd for $C_{44}H_{64}N_3O_2P_2RhSi•C_4H_{10}O$: C, 62.80; H, 8.12; N, 4.58. Found: C, 62.42; H, 8.14; N, 4.41. **^{1}H NMR (benzene-*d*$_6$, 23 °C):** δ 7.56 (d, $^{3}J_{HH}$ = 7.6 Hz, 2H, Pipp Ar *H*); 7.20 (br d, $^{3}J_{HH}$ = 8.0 Hz, 1H, Pipp Ar *H*); 7.10 (d, $^{3}J_{HH}$ = 7.6 Hz, 2H, Pipp Ar *H*); 7.00 (br d, $^{3}J_{HH}$ = 8.0 Hz, 1H, Pipp Ar *H*); 6.95 (s, 1H, Mes Ar *H*); 6.62 (s, 1H, Mes Ar *H*); 6.58 (br d, $^{3}J_{HH}$ = 8.0 Hz, Pipp Ar *H*); 6.59 (ov m, 1H, 3,4-pyrrole C*H*; 1H, Pipp Ar *H*, 1H Si–*H*); 6.43 (ov dd, $^{3}J_{PH}$ = $^{3}J_{PH}$ = 3.6 Hz, 3,4-pyrrole C*H*); 3.25 (ov s, 3H, Mes CH_3); 2.75 (sp, $^{3}J_{HH}$ = 6.9 Hz, 1H, Pipp

ArC*H*$(CH_3)_2$); 2.57 (sp, $^3J_{HH}$ = 6.9 Hz, 1H, Pipp ArC*H*$(CH_3)_2$); 2.38 (m, 1H, PC*H*$(CH_3)_2$); 2.24-2.16 (ov m, 2H, PC*H*$(CH_3)_2$; 3H, Mes C*H*$_3$); 2.15 (s, 3H, Mes C*H*$_3$); 2.02 (dsp, $^2J_{HP}$ = 14.4 Hz, $^3J_{HH}$ = 7.2 Hz, 1H, PC*H*$(CH_3)_2$); 1.87 (dd, $^3J_{HP}$ = 16.2 Hz, $^3J_{HH}$ = 7.2 Hz, 3H, PCH(C*H*$_3)_2$); 1.22 (dd, $^3J_{HP}$ = 15.5 Hz, $^3J_{HH}$ = 7.2 Hz, 3H, PCH(C*H*$_3)_2$); 1.13 (dd, $^3J_{HP}$ = 18.1 Hz, $^3J_{HH}$ = 7.2 Hz, 3H, PCH(C*H*$_3)_2$); 1.10 (dd, $^3J_{HP}$ = 16.6 Hz, $^3J_{HH}$ = 7.2 Hz, 3H, PCH(C*H*$_3)_2$); 1.05 (ov d, $^3J_{HH}$ = 6.9 Hz, 3H, Pipp ArCH(C*H*$_3)_2$); 1.03 (ov d, $^3J_{HH}$ = 6.9 Hz, 3H, Pipp ArCH(C*H*$_3)_2$); 1.00 (dd, $^3J_{HP}$ = 15.3 Hz, $^3J_{HH}$ = 7.2 Hz, 3H, PCH(C*H*$_3)_2$); 0.94 (dd, $^3J_{HP}$ = 15.1 Hz, $^3J_{HH}$ = 7.2 Hz, 3H, PCH(C*H*$_3)_2$); 0.50 (dd, $^3J_{HP}$ = 17.8 Hz, $^3J_{HH}$ = 7.2 Hz, 3H, PCH(C*H*$_3)_2$); 0.13 (dd, $^3J_{HP}$ = 14.7 Hz, $^3J_{HH}$ = 7.24 Hz, 3H, PCH(C*H*$_3)_2$). **^{13}C{^{1}H} NMR (benzene-*d*$_6$, 23 °C):** δ 193.44 (d, $^1J_{CRh}$ = 76.8 Hz, Rh–*C*O); 151.25 (s, Ar *C*); 146.94 (s, Ar *C*); 144.57 (s, Mes Ar *C*); 143.02 (s, Mes Ar *C*); 141.70 (s, Ar *C*); 140.82 (d, $^2J_{CP}$ = 2.2 Hz, Ar *C*); 139.12 (br m, Mes Ar *C*); 138.24 (ov d, $^1J_{CP}$ = 144.4 Hz, 2,5-pyrrole *C*); 138.14 (ov d, $^1J_{CP}$ = 144.4 Hz, 2,5-pyrrole *C*); 136.85 (s, Mes Ar *C*); 131.72 (d, J_{CP} = 5.6 Hz, Ar *C*H); 128.93 (s, Mes Ar *C*H); 128.50 (s, Mes Ar *C*H); 126.94 (s, Ar *C*H); 126.80 (d, J_{CP} = 8.2 Hz, Ar *C*H); 126.46 (s, Ar *C*H); 126.33 (s, Ar *C*H); 120.25 (dd, $^2J_{CP}$ = 25.3 Hz, $^3J_{CP}$ = 10.6 Hz, 3,4-pyrrole *C*H); 114.49 (dd, $^2J_{CP}$ = 24.6 Hz, $^3J_{CP}$ = 11.4 Hz, 3,4-pyrrole *C*H); 33.80 (s, Ar*C*H$(CH_3)_2$); 33.72 (s, Ar*C*H$(CH_3)_2$); 28.18 (d, $^1J_{CP}$ = 56.4 Hz, P*C*H$(CH_3)_2$); 27.44 (d, $^1J_{CP}$ = 52.0 Hz, P*C*H$(CH_3)_2$); 27.02 (d, $^1J_{CP}$ = 52.0 Hz, P*C*H$(CH_3)_2$); 25.82 (s, Mes *C*H$_3$); 24.64 (s, Mes *C*H$_3$); 24.51 (s, ArCH(*C*H$_3)_2$); 24.21 (d, $^1J_{CP}$ = 61.9 Hz, *C*H$(CH_3)_2$); 24.15 (s, ArCH(*C*H$_3)_2$); 21.40 (s, Mes *C*H$_3$); 18.04 (d, $^2J_{CP}$ = 3.3 Hz, PCH(*C*H$_3)_2$); 16.88 (s, PCH(*C*H$_3)_2$); 16.60 (d, $^2J_{CP}$ = 1.9 Hz, PCH(*C*H$_3)_2$); 16.55 (d, $^2J_{CP}$ = 2.4 Hz, PCH(*C*H$_3)_2$); 16.26 (d, $^2J_{CP}$ = 2.4 Hz, PCH(*C*H$_3)_2$); 16.16 (d, $^2J_{CP}$ = 2.4 Hz, PCH(*C*H$_3)_2$); 15.93 (d, $^2J_{CP}$ = 3.7 Hz, PCH(*C*H$_3)_2$); 14.75 (d, $^2J_{CP}$ = 3.4 Hz, PCH(*C*H$_3)_2$). **^{31}P{^{1}H} NMR (benzene-*d*$_6$, 23 °C):** δ 50.2 (s, 1P, *P*–N–Rh); 41.1 (s, 1P, *P*–N–Si). **^{29}Si{^{1}H} NMR (benzene-*d*$_6$, 23 °C):** δ 38.0 (ddd, $^3J_{SiP}$ = 2.0 Hz, $^2J_{SiP}$ = 9.3 Hz, $^1J_{SiRh}$ = 52.6 Hz). **IR (cm^{-1}):** 1920 (s, CO stretch).

κ^2-*L*(CO)Rh(^{meta}XylBH$_2$) (7). κ^2-*L*(CO)Rh(^{meta}XylBH$_2$) was prepared according to the following modified literature procedure.[4] Recrystallized **1** (15 mg, 0.022 mmol) was dissolved in a minimum quantity of toluene (~0.25 mL). In a separate flask, ^{meta}XylBH$_2$ (2.6 mg, 0.022 mmol) was also dissolved in a minimum amount of toluene (~0.1 mL) and added to the stirring solution of **1**. Immediately after addition of borane, the solvent was removed *in vacuo* to yield 17 mg of **7** as an off-white residue (97% yield). Compound **7** rapidly begins to convert to compound **8** in solution, and all isolated samples of **7** contain trace amounts of compounds **1** and **8** as indicated by ^{31}P and ^{1}H NMR spectroscopy. Thus, elemental analysis and ^{13}C NMR spectroscopic data are not included. **^{1}H NMR (benzene-d_6, 23 °C):** δ 7.47 (ov d, $^{3}J_{HH}$ = 8.2 Hz, 2H, Pipp Ar *H*); 7.46 (ov d, $^{3}J_{HH}$ = 8.2 Hz, 2H, Pipp Ar *H*); 7.26 (s, 2H, *ortho*-Xyl Ar *H*); 7.02 (d, $^{3}J_{HH}$ = 8.2 Hz, 2H, Pipp Ar *H*); 6.87 (d, $^{3}J_{HH}$ = 8.2 Hz, 2H, Pipp Ar *H*); 6.74 (s, 1H, *para*-Xyl Ar *H*); 6.49 (m, 2H, 3,4-pyrrole C*H*); 2.71 (sp, $^{3}J_{HH}$ = 6.9 Hz, 1H, ArC*H*(CH$_3$)$_2$); 2.61 (sp, $^{3}J_{HH}$ = 6.9 Hz, 1H, ArC*H*(CH$_3$)$_2$); 2.37 (m, 4H, PC*H*(CH$_3$)$_2$); 2.25 (s, 6H, Xyl C*H*$_3$); 1.14 (ov d, $^{3}J_{HH}$ = 6.9 Hz, 6H, ArCH(C*H*$_3$)$_2$); 1.13 (ov dd, $^{3}J_{HH}$ = 7.2 Hz, 6H, PCH(C*H*$_3$)$_2$); 1.06 (ov d, $^{3}J_{HH}$ = 6.9 Hz, 6H, ArCH(C*H*$_3$)$_2$); 1.02 (dd, $^{3}J_{HP}$ = 16.0 Hz, $^{3}J_{HH}$ = 6.9 Hz, 6H, PCH(C*H*$_3$)$_2$); 0.97 (dd, $^{3}J_{HP}$ = 15.7 Hz, $^{3}J_{HH}$ = 7.2 Hz, 6H, PCH(C*H*$_3$)$_2$); 0.86 (ov dd, $^{3}J_{HH}$ = 7.1 Hz, 3H, PCH(C*H*$_3$)$_2$); –3.10 (br s, 2H, B*H*$_2$).). **^{31}P{^{1}H} NMR (benzene-d_6, 23 °C):** δ 49.0 (s, 1P, *P*–N–Rh); 46.8 (s, 1P, *P*–N–B). **^{11}B{^{1}H} NMR (benzene-d_6, 23 °C):** δ –9.3 (br s, B).

(κ^2-NN'-2,5-[^{i}Pr$_2$P=N(4-^{i}PrC$_6$H$_4$)]$_2$-N'(C$_4$H$_2$)$^-$)B(H)^{meta}Xyl (8). κ^2-*L*(CO)Rh(^{meta}XylBH$_2$) (10 mg, 0.012 mmol) was allowed to sit as a quiescent toluene solution at ambient temperature for 12 hours. The solution was filtered through a pad of Celite, followed by removal of the solvent *in vacuo*. The crude residue was washed with 0.5 mL of pentane and dried under vacuum to yield 6.9 mg of compound **4** as an off-white solid (95% yield). Compound **8** can also be synthesized independently by adding a 1 mL toluene solution of HL (20 mg, 0.035 mmol) to a 1 mL toluene solution of ^{meta}XylBH$_2$ (4.2 mg, 0.035 mmol), resulting in immediate effervescence. Removal of solvent *in vacuo*, followed by washing the residue with 3 × 5 mL of pentane yielded 15 mg of the product as

an off-white solid (98% yield). In both cases, the product is contaminated with small amounts of a Lewis acid-base byproduct wherein a second moiety of ^{meta}XylBH$_2$ is bound to the free phosphinimine donor of the ligand, rendering it impossible to obtain an analytically pure sample. **^{1}H NMR (benzene-d_6, 23 °C):** δ 7.62 (m, 1H, 3,4-pyrrole C*H*); 7.35 (d, $^3J_{HH}$ = 8.4 Hz, 2H, Pipp Ar *H*); 7.05-7.15 (ov m, 2H, *ortho*-Xyl C*H*; ov d, $^3J_{HH}$ = 7.5 Hz, 2H, Pipp Ar *H*; ov d, 2H, Pipp Ar *H*); 6.96 (d, $^3J_{HH}$ = 8.4 Hz, 2H, Pipp Ar *H*); 6.74 (s, 1H, *para*-Xyl C*H*); 6.35 (dd, $^3J_{HH}$ = 3.6 Hz, $^3J_{HP}$ = 0.4 Hz, 1H, 3,4-pyrrole C*H*); 4.72 (br s, 1H, B*H*); 3.01 (m, 1H, PC*H*(CH$_3$)$_2$); 2.85 (sp, $^3J_{HH}$ = 6.9 Hz, 1H, ArC*H*(CH$_3$)$_2$); 2.62 (sp, $^3J_{HH}$ = 6.9 Hz, 1H, ArC*H*(CH$_3$)$_2$); 2.19 (s, 6H, 3,5-Xyl C*H*$_3$); 1.91 (m, 2H, PC*H*(CH$_3$)$_2$); 1.51 (dd, $^3J_{HP}$ = 16.5 Hz, $^3J_{HH}$ = 7.2 Hz, 3H, PCH(C*H*$_3$)$_2$); 1.35 (dd, $^3J_{HP}$ = 15.2 Hz, $^3J_{HH}$ = 7.0 Hz, 3H, PCH(C*H*$_3$)$_2$); 1.28 (d, $^3J_{HH}$ = 6.9 Hz, 6H, ArCH(C*H*$_3$)$_2$); 1.15 (m, 1H, PC*H*(CH$_3$)$_2$); 1.06 (dd, $^3J_{HH}$ = 6.9 Hz, *J* = 1.3 Hz, 6H, ArCH(C*H*$_3$)$_2$); 0.97 (dd, $^3J_{HP}$ = 16.6 Hz, $^3J_{HH}$ = 6.8 Hz, 3H, PCH(C*H*$_3$)$_2$); 0.92 (ov dd, $^3J_{HP}$ = 17.2 Hz, $^3J_{HH}$ = 7.2 Hz, 3H, PCH(C*H*$_3$)$_2$); 0.86-0.90 (ov m, 6H, PCH(C*H*$_3$)$_2$); 0.70 (dd, $^3J_{HP}$ = 17.6 Hz, $^3J_{HH}$ = 7.1 Hz, 3H, PCH(C*H*$_3$)$_2$); 0.59 (dd, $^3J_{HP}$ = 16.9 Hz, $^3J_{HH}$ = 7.2 Hz, 3H, PCH(C*H*$_3$)$_2$). **^{13}C{^{1}H} NMR (benzene-d_6, 23 °C):** δ 151.62 (d, $^2J_{CP}$ = 2.9 Hz, Pipp Ar *C*); 143.36 (s, Pipp Ar *C*); 141.26 (s, Pipp Ar *C*); 136.07 (s, Xyl Ar *C*); 135.99 (s, Pipp Ar *C*); 133.91 (d, *J* = 77.8 Hz, 2,5-pyrrole *C*); 132.71 (s, Xyl Ar *C*H); 128.66 (dd, *J* = 14.6, 11.1 Hz, 3,4-pyrrole C*H*); 128.35 (ov s, Xyl Ar *C*H); 128.08 (ov s, Xyl *C*); 127.19 (s, Pipp Ar *C*H); 126.60 (s, Pipp Ar *C*H); 124.77 (d, $^3J_{CP}$ = 15.5 Hz, Pipp Ar *C*H); 124.53 (d, $^3J_{CP}$ = 5.4 Hz, Pipp Ar *C*H); 117.33 (dd, *J* = 128.7, 7.4 Hz, 2,5-pyrrole *C*); 113.92 (dd, *J* = 19.1, 9.2 Hz, 3,4-pyrrole *C*H); 33.88 (s, Pipp Ar*C*H(CH$_3$)$_2$); 33.62 (s, Pipp Ar*C*H(CH$_3$)$_2$); 29.13 (d, $^1J_{CP}$ = 64.8 Hz, P*C*H(CH$_3$)$_2$); 28.06 (d, $^1J_{CP}$ = 82.0 Hz, P*C*H(CH$_3$)$_2$); 27.38 (d, $^1J_{CP}$ = 52.5 Hz, P*C*H(CH$_3$)$_2$); 26.46 (d, $^1J_{CP}$ = 55.0 Hz, P*C*H(CH$_3$)$_2$); 24.88 (s, Pipp ArCH(*C*H$_3$)$_2$); 24.19 (s, Pipp ArCH(*C*H$_3$)$_2$); 24.03 (s, Pipp ArCH(*C*H$_3$)$_2$); 21.61 (s, Xyl Ar(*C*H$_3$)); 19.91 (d, $^2J_{CP}$ = 2.6 Hz, PCH(*C*H$_3$)$_2$); 19.12 (d, $^2J_{CP}$ = 4.3 Hz, PCH(*C*H$_3$)$_2$); 16.92-16.98 (ov d, 2 x PCH(*C*H$_3$)$_2$); 16.74 (s, PCH(*C*H$_3$)$_2$); 16.33 (d, $^2J_{CP}$ = 3.1 Hz, PCH(*C*H$_3$)$_2$); 15.51-15.54 (ov m, 2 x PCH(*C*H$_3$)$_2$). **^{31}P{^{1}H} NMR (benzene-d_6, 23 °C):** δ 51.0 (s, 1P, *P*–N–B); 13.4 (s, 1P, *P*=N). **^{11}B{^{1}H} NMR (benzene-d_6, 23 °C):** δ 2.5 (br s, B).

***κ*²-*L*(CO)Rh(SiEt₂) (9)**. Recrystallized **1** (15 mg, 0.022 mmol) was dissolved in 5 mL toluene. In a separate vial, excess H_2SiEt_2 (10 mg, 0.11 mmol) was dissolved in 3 mL toluene then added dropwise to the solution of **1** over approximately one minute. The solution was stirred at 45 °C for one hour. Upon cooling to ambient temperature, the solution was clear and dark yellow in colour. After removal of the solvent under reduced pressure, the residue was washed with 3 × 0.5 mL of pentane, and the crude solid recrystallized from Et_2O at –30 °C over 2 days to yield 13.5 mg (81% yield) of **9** as a light yellow crystals. Anal Calcd for $C_{39}H_{62}N_3OP_2RhSi$: C, 59.91; H, 7.99; N, 5.37. Found: C, 59.80; H, 7.98; N, 5.19. **^{1}H NMR (benzene-*d*₆, 23 °C):** δ 7.64 (d, $^3J_{HH}$ = 7.1 Hz, 2H, Pipp Ar *H*); 7.14-7.17 (ov m, 4H, Pipp Ar *H*); 6.96 (d, $^3J_{HH}$ = 8.2 Hz, 2H, Pipp Ar *H*); 6.51 (ov dd, $^3J_{HH}$ = $^3J_{PH}$ = 3.5 Hz, 1H, 3,4-pyrrole C*H*); 6.42 (ov dd, $^3J_{HH}$ = $^3J_{PH}$ = 3.5 Hz, 1H, 3,4-pyrrole C*H*); 2.80 (sp, $^3J_{HH}$ = 6.9 Hz, 1H, ArC*H*$(CH_3)_2$); 2.68 (sp, $^3J_{HH}$ = 6.9 Hz, 1H, ArC*H*$(CH_3)_2$); 2.33 (m, 2H, PC*H*$(CH_3)_2$); 2.23 (m, 2H, PC*H*$(CH_3)_2$); 1.45 (t, $^3J_{HH}$ = 7.7 Hz, 6H, $SiCH_2CH_3$); 1.22 (d, $^3J_{HH}$ = 6.9 Hz, 6H, ArCH(C*H*$_3)_2$); 1.15 (dd, $^3J_{HP}$ = 15.3 Hz, $^3J_{HH}$ = 7.2 Hz, 6H, PCH(C*H*$_3)_2$); 1.11 (d, $^3J_{HH}$ = 6.9 Hz, 6H, ArCH(C*H*$_3)_2$); 1.05 (dd, $^3J_{HP}$ = 15.7 Hz, $^3J_{HH}$ = 7.2 Hz, 6H, PCH(C*H*$_3)_2$); 1.01-0.91 (ov m, 4H, $SiCH_2CH_3$); 0.94 (ov dd, $^3J_{HP}$ = 15.3 Hz, $^3J_{HH}$ = 7.2 Hz, 6H, PCH(C*H*$_3)_2$); 0.83 (dd, $^3J_{HP}$ = 16.7 Hz, $^3J_{HH}$ = 7.2 Hz, 6H, PCH(C*H*$_3)_2$). **^{13}C{^{1}H} NMR (benzene-*d*₆, 23 °C):** δ 195.75 (d, $^1J_{CRh}$ = 78.3 Hz, Rh–*C*O); 151.25 (s, Ar *C*); 146.97 (s, Ar *C*); 140.27 (s, Ar *C*); 139.19 (s, Ar *C*); 138.09 (d, $^1J_{CP}$ = 16.3 Hz, 2,5-pyrrole *C*); 137.27 (d, $^1J_{CP}$ = 16.2 Hz, 2,5-pyrrole *C*); 130.42 (d, $^3J_{CP}$ = 3.97 Hz, Ar *C*H); 126.95 (s, Ar *C*H); 126.49 (s, Ar *C*H); 126.36 (d, $^3J_{CP}$ = 9.2 Hz, Ar *C*H); 119.64 (dd, $^2J_{CP}$ = 25.0 Hz, $^3J_{CP}$ = 10.24 Hz, 3,4-pyrrole *C*H); 114.53 (dd, $^2J_{CP}$ = 24.4 Hz, $^3J_{CP}$ = 11.1 Hz, 3,4-pyrrole *C*H); 33.81 (s, Ar*C*H$(CH_3)_2$); 33.78 (s, Ar*C*H$(CH_3)_2$); 26.82 (d, $^1J_{CP}$ = 51.7 Hz, P*C*H$(CH_3)_2$); 26.00 (d, $^1J_{CP}$ = 59.9 Hz, P*C*H$(CH_3)_2$); 24.53 (s, ArCH(*C*H$_3)_2$); 24.13 (s, ArCH(*C*H$_3)_2$); 16.77-16.68 (ov d, 2x PCH(*C*H$_3)_2$); 16.57-16.50 (ov d, 2x PCH(*C*H$_3)_2$); 15.07 (s, Si*C*H_2CH_3); 10.31 (s, $SiCH_2$*C*H_3). **^{31}P{^{1}H} NMR (benzene-*d*₆, 23 °C):** δ 49.5 (s, 1P, *P*–N–Rh); 39.9 (s, 1P, *P*–N–Si). **^{29}Si{^{1}H} NMR (benzene-*d*₆, 23 °C):** δ 67.5 (ddd, $^3J_{SiP}$ = 1.6 Hz, $^2J_{SiP}$ = 6.5 Hz, $^1J_{SiRh}$ = 57.1 Hz). **IR (cm^{-1}):** 1900 (s, CO stretch)

***κ*²-*L*(CO)Rh(GePh₂) (10)**. Crystalline **1** (25 mg, 0.036 mmol) was dissolved in 5 mL of toluene. In a separate flask, excess H_2GePh_2 (41 mg, 0.18 mmol) was dissolved in 3 mL of toluene and then added dropwise to the solution of **1** over approximately a minute. The solution was heated to 50 °C, stirred for three hours, then allowed to cool to ambient temperature, resulting in a bright yellow solution. Solvent was removed under vacuum and the crude solid recrystallized from 3 mL of pentane over 24 hours to afford 20.1 mg (61% yield) of **10** as light orange blocks. Anal Calcd for $C_{47}H_{62}N_3OP_2RhGe$: C, 61.19; H, 6.77; N, 4.58. Found: C, 60.91; H, 6.81; N, 4.41. **^{1}H NMR (benzene-*d*₆, 23 °C):** δ 7.83 (m, 4H, GePh *H*); 7.59 (m, 2H, Pipp Ar *H*); 7.18-7.11 (ov m, 6H, GePh *H*; 2H, 4-iPr-C_6H_4); 6.65-6.60 (ov m, 1H, 3,4-pyrrole; 2H, 4-iPr-C_6H_4); 6.56 (d, $^3J_{HH}$ = 8.3 Hz, 2H, 4-iPr-C_6H_4); 6.44 (ov dd, $^3J_{HP}$ = $^3J_{HH}$ = 3.5 Hz, 1H, 3,4-pyrrole); 2.78 (sp, $^3J_{HH}$ = 6.9 Hz, 1H, ArC*H*$(CH_3)_2$); 2.53 (sp, $^3J_{HH}$ = 6.9 Hz, 1H, ArC*H*$(CH_3)_2$); 2.32 (m, 2H, PC*H*$(CH_3)_2$); 2.15 (m, 2H, PC*H*$(CH_3)_2$); 1.19 (d, $^3J_{HH}$ = 6.9 Hz, 6H, ArCH(C*H*$_3)_2$); 1.08-1.02 (ov m, 12H PC*H*$(CH_3)_2$); 0.99 (dd, $^3J_{HP}$ = 15.8 Hz, $^3J_{HH}$ = 6.9 Hz, 6H, PCH(C*H*$_3)_2$); 0.92 (dd, $^3J_{HP}$ = 16.4 Hz, $^3J_{HH}$ = 6.9 Hz 6H, PCH(C*H*$_3)_2$). **^{13}C{^{1}H} NMR (benzene-*d*₆, 23 °C):** δ 193.42 (d, $^1J_{CRh}$ = 71.7 Hz, Rh–*C*O); 151.54 (s, Ar *C*); 148.47 (s, GePh *C*); 146.15 (s, Ar *C*); 141.78 (s, Ar *C*); 141.48 (s, Ar *C*); 137.68 (br m, 2,5-pyrrole *C*); 136.33 (s, GePh *C*H); 130.55 (d, $^3J_{CP}$ = 5.0 Hz, Ar *C*H); 127.72 (s, GePh *C*H); 127.70 (s, GePh *C*H); 127.11 (s, Ar *C*H); 127.06 (s, Ar *C*H); 126.88 (br s, Ar *C*H); 123.70 (br m, 2,5-pyrrole *C*); 120.22 (br m, 3,4-pyrrole *C*H); 114.81 (br m, 3,4-pyrrole *C*H); 34.17 (s, Ar*C*H$(CH_3)_2$); 34.11 (s, Ar*C*H$(CH_3)_2$); 26.99 (d, $^1J_{CP}$ = 52.0 Hz, P*C*H$(CH_3)_2$); 26.66 (d, $^1J_{CP}$ = 59.4 Hz, P*C*H$(CH_3)_2$); 24.80 (s, Ar CH(*C*H$_3)_2$); 24.60 (s, Ar CH(*C*H$_3)_2$); 17.43 (d, $^2J_{CP}$ = 3.0 Hz, PCH(*C*H$_3)_2$); 17.10 (d, $^2J_{CP}$ = 1.9 Hz, PCH(*C*H$_3)_2$); 16.98 (d, $^2J_{CP}$ = 2.5 Hz, PCH(*C*H$_3)_2$); 16.82 (d, $^2J_{CP}$ = 2.1 Hz, PCH(*C*H$_3)_2$). **^{31}P{^{1}H} NMR (benzene-*d*₆, 23 °C):** δ 47.6 (s, 1P, *P*–N–Rh); 43.8 (s, 1P, *P*–N–Ge). **IR (cm^{-1}):** 1914 (s, CO stretch).

***L*GeH₂Mes (11)**. Recrystallized **1** (25 mg, 0.036 mmol) was dissolved in 5 mL of toluene. In a separate vial, excess H_3GeMes (29.2 mg, 0.150 mmol) was dissolved in 3 mL of toluene and the

resultant solution was added dropwise to the stirring solution of **1** over approximately one minute. The initially homogenous orange-yellow solution separated into an orange residue and clear colorless supernatant over the course of 2 hours of stirring at ambient temperature. The residue was only sparingly soluble in conventional non-halogenated solvents (*e.g.*, Et_2O, toluene, pentane). Multinuclear NMR spectroscopy revealed **11** as the major product, though it was contaminated with intractable impurities. **^{1}H NMR (benzene-d_6, 23 °C):** δ 7.52 (d, $^3J_{HH}$ = 8.2 Hz, 4H, Pipp Ar *H*); 7.10 (d, $^3J_{HH}$ = 8.2 Hz, 4H, Pipp Ar *H*); 6.73 (s, 2H, Mes C*H*); 6.62 (s, 2H, 3,4-pyrrole C*H*); 4.21 (s, 2H, GeH_2); 2.57 (sp, $^3J_{HH}$ = 6.8 Hz, 2H, ArC*H*$(CH_3)_2$); 2.26 (s, 6H, Mes CH_3); 2.10 (s, 3H, Mes CH_3); 2.08 (m, 4H, PC*H*$(CH_3)_2$); 1.20 (sp, $^3J_{HH}$ = 6.8 Hz, 2H, ArC*H*$(CH_3)_2$); 0.95 (ov dd, $^3J_{HP}$ = 16.7 Hz, $^3J_{HH}$ = 7.0 Hz, 12H, PCH(CH_3)$_2$); 0.92 (ov dd, $^3J_{HP}$ = 16.7 Hz, $^3J_{HH}$ = 7.0 Hz, 12H, PCH(CH_3)$_2$). **^{31}P{^{1}H} NMR (benzene-d_6, 23 °C):** δ 34.4 (s).

***κ*^{2}-*L*(CO)Rh(Ge(H)^{t}Bu) (12)**. Recrystallized **1** (25 mg, 0.036 mmol) was dissolved in 5 mL of toluene. In a separate vial, excess H_3Ge^tBu (24 mg, 0.18 mmol) was dissolved in 3 mL of toluene then added dropwise to the stirring solution of **1** over approximately one minute. The stirring solution was heated to 50 °C for 5 hours resulting in a yellow-orange solution. The solvent was removed *in vacuo* and 2 mL of pentane was added, dissolving the residue. Upon cooling to –35 °C, crystals rapidly formed leading to 14 mg (47% yield) of **12** as light orange-yellow crystals. Anal Calcd for $C_{39}H_{62}N_3OP_2RhGe$: C, 56.68; H, 7.56; N, 5.08. Found: C, 55.98; H, 7.57; N, 4.99. **^{1}H NMR (benzene-d_6, 23 °C):** δ 7.66 (d, $^3J_{HH}$ = 7.81 Hz, 2H, Pipp Ar *H*); 7.43 (d, $^3J_{HH}$ = 7.13 Hz, 2H, Pipp Ar *H*); 7.17 (ov d, 2H, Pipp Ar *H*); 7.01 (d, $^3J_{HH}$ = 7.81 Hz, 2H, Pipp Ar *H*); 6.56 (ov dd, $^3J_{HH}$ = $^3J_{HP}$ = 3.14 Hz, 1H, 3,4-pyrrole); 6.38 (ov dd, $^3J_{HH}$ = $^3J_{HP}$ = 3.14 Hz, 1H, 3,4-pyrrole); 5.90 (t, $^3J_{HP}$ = $^2J_{HRh}$ = 10.62, 1H, Ge–*H*); 2.80 (sp, $^3J_{HH}$ = 6.80 Hz, 1H, ArC*H*$(CH_3)_2$); 2.70 (sp, $^3J_{HH}$ = 6.97 Hz, 1H, ArC*H*$(CH_3)_2$); 2.28 (m, 2H, PC*H*$(CH_3)_2$); 2.17 (m, 2H, PC*H*$(CH_3)_2$); 1.70 (dd, $^3J_{HP}$ = 15.61 Hz, $^3J_{HH}$ = 6.80 Hz, 3H, PCH(CH_3)$_2$); 1.39 (s, 9H, GeCCH_3); 1.40-1.20 (ov m, 12H, ArCH(CH_3)$_2$; PCH(CH_3)$_2$); 1.14-1.09 (ov m, 9H, ArCH(CH_3)$_2$; PCH(CH_3)$_2$); 0.93 (dd, $^3J_{HP}$ = 15.33 Hz, $^3J_{HH}$ =

7.04 Hz, 3H, PCH(CH_3)$_2$); 0.87 (dd, $^3J_{HP}$ = 14.93 Hz, $^3J_{HH}$ = 7.33 Hz, 3H, PCH(CH_3)$_2$); 0.56 (dd, $^3J_{HP}$ = 14.99 Hz, $^3J_{HH}$ = 7.27 Hz, 3H, PCH(CH_3)$_2$); 0.47 (dd, $^3J_{HP}$ = 17.07 Hz, $^3J_{HH}$ = 6.80 Hz, 3H, PCH(CH_3)$_2$). **^{13}C{^{1}H} NMR (benzene-d_6, 23 °C):** δ 194.13 (d, $^1J_{CRh}$ = 74.62 Hz, Rh–*C*O); 151.23 (s, Ar *C*); 145.91 (s, Ar *C*); 145.60 (s, Ar *C*); 140.59 (s, Ar *C*); 136.65 (d, $^1J_{CP}$ = 15.5 Hz, 2,5-pyrrole *C*); 135.83 (d, $^1J_{CP}$ = 16.0 Hz, 2,5-pyrrole *C*); 130.70 (d, J_{CP} = 4.2 Hz, Ar *C*H); 126.98 (s, Ar *C*H); 126.50 (s, Ar *C*H); 126.16 (d, J_{CP} = 9.4 Hz, Ar *C*H); 120.39 (dd, $^2J_{CP}$ = 23.9, $^3J_{CP}$ = 10.4 Hz, 3,4-pyrrole *C*H); 114.85 (dd, $^2J_{CP}$ = 24.6, $^3J_{CP}$ = 10.9 Hz, 3,4-pyrrole *C*H); 33.83 (s, Ar *C*HCH$_3$); 33.78 (s, Ar *C*HCH$_3$); 31.19 (d, *J* = 2.3 Hz, Ge *C*(CH$_3$)$_3$); 29.83 (s, Ge C(*C*H$_3$)$_3$); 27.44 (d, $^1J_{CP}$ = 52.2 Hz, P*C*H(CH$_3$)$_2$); 26.26 (d, $^1J_{CP}$ = 51.5 Hz, P*C*H(CH$_3$)$_2$); 26.01 (d, $^1J_{CP}$ = 57.3 Hz, P*C*H(CH$_3$)$_2$); 24.19 (d, $^1J_{CP}$ = 46.8 Hz, P*C*H(CH$_3$)$_2$); 24.61 (s, Ar CH(*C*H$_3$)$_2$); 24.43 (s, Ar CH(*C*H$_3$)$_2$); 24.18 (d, $^2J_{CP}$ = 4.1 Hz, PCH(*C*H$_3$)$_2$); 19.30 (d, $^2J_{CP}$ = 3.3 Hz, PCH(*C*H$_3$)$_2$); 17.14 (d, $^2J_{CP}$ = 2.5 Hz, PCH(*C*H$_3$)$_2$); 17.08 (d, $^2J_{CP}$ = 3.3 Hz, PCH(*C*H$_3$)$_2$); 17.03 (d, $^2J_{CP}$ = 1.9 Hz, PCH(*C*H$_3$)$_2$); 17.0 (s, Ar CH(*C*H$_3$)$_2$); 16.51 (d, $^2J_{CP}$ = 2.5 Hz, PCH(*C*H$_3$)$_2$); 16.22 (d, $^2J_{CP}$ = 2.3 Hz, PCH(*C*H$_3$)$_2$); 15.37 (d, $^2J_{CP}$ = 3.1 Hz, PCH(*C*H$_3$)$_2$). **^{31}P{^{1}H} NMR (benzene-d_6, 23 °C):** δ 47.4 (s, 1P, *P*–N–Rh); 43.5 (s, 1P, *P*–N–Ge). **IR (cm^{-1}):** 1898 (s, CO stretch).

Reaction of 1 with Ph_2SnH_2. Recrystallized **1** (15 mg, 0.022 mmol) was dissolved in 5 mL of toluene and the mixture cooled to –30 °C. Under the occlusion of light, Ph_2SnH_2 (5.9 mg, 0.022 mmol) was dissolved in 3 mL of toluene and added dropwise to the stirring solution of complex **1** over approximately one minute. Upon addition of Ph_2SnH_2 the solution immediately changed from bright orange to dark red in color. The solution was stirred for 2 hours. Removal of solvent *in vacuo* resulted in a yellow-red oily residue containing multiple unidentified products. Extraction of the oil with Et_2O resulted in a less complicated mixture wherein the major product is hypothesized to be a transmetalated product similar to **11.**

General Procedures for Dehydrogenative Coupling

Reaction between complex **1**, R_2EH_2, and pinacol: A PTFE-sealed NMR tube was charged with approximately 0.5 mL of a benzene-d_6 solution of 1:1 R_2EH_2 and pinacol. Complex **1** (10% catalyst loading) was dissolved in approximately 0.5 mL of benzene-d_6 and added to the NMR tube. Immediate effervescence was observed. Formation of $PinER_2$ was monitored by ^1H and $^{13}C\{^1H\}$ NMR spectroscopy. The spectra for $PinSiPh_2$ matched literature values as the model substrate.[19]

Control reactions between κ^2-*L*(CO)Rh($SiPh_2$), complex **1** or HL and the 1:1 Ph_2SiH_2/pinacol mixture followed similar procedures described above and also used a 10% loading of metal complex or ligand. For κ^2-*L*Rh(CO)($SiPh_2$), conversion to complex **1** was estimated by integration of diagnostic resonances in the ^{31}P NMR spectra. The reaction was followed by NMR spectroscopy by acquiring spectra every 30 minutes for a period of 5 hours. For HL, no reaction was observed *via* NMR spectroscopy, even after heating the mixture at 80 °C for 24 hours.

Stoichiometric reaction between κ^2-*L*(CO)Rh($SiPh_2$) and pinacol: A PTFE-sealed NMR tube was charged with κ^2-*L*(CO)Rh($SiPh_2$) (10 mg, 0.011 mmol) and pinacol (1.3 mg, 0.011 mmol), and dissolved in 1 mL of benzene-d_6. No effervescence was observed. The NMR tube was heated at 80 °C and monitored by NMR spectroscopy. After 32 hours, 90%+ was converted to complex **1** and Ph_2SiPin as established by relative integrations of signals in the ^1H and ^{31}P NMR spectra.

3.5. References

[1] a) Z.-L. Wang, H.-S. Hu, L. von Szentpály, H. Stoll, S. Fritzsche, P. Pyykkö, W. H. E. Schwarz, J. Li, *Chem. Eur. J.* **2020**, *26*, 15558-15564; b) R. West, *Polyhedron* **2002**, *21*, 467-472; c) G. Balázs, L. J. Gregoriades, M. Scheer, *Organometallics* **2007**, *26*, 3058-3075.

[2] a) R. Waterman, P. G. Hayes, T. D. Tilley, *Acc. Chem. Res.* **2007**, *40*, 712-719; b) M. Okazaki, H. Tobita, H. Ogino, *Dalton Trans.* **2003**, 493-506.

[3] a) D. Seyferth, *Organometallics* **2001**, *20*, 4978-4992; b) B. Pachaly, J. Weis, in *Organosilicon Chemistry Set*, **2005**, pp. 478-483.

[4] a) K. E. Litz, J. E. Bender Iv, J. W. Kampf, M. M. B. Holl, *Angew. Chem. Int. Ed.* **1997**, *36*, 496-498; b) P. G. Hayes, C. W. Gribble, R. Waterman, T. D. Tilley, *J. Am. Chem. Soc.* **2009**, *131*, 4606-4607; c) A. Shinohara, J. McBee, T. D. Tilley, *Inorg. Chem.* **2009**, *48*, 8081-8083; d) K. K. Pandey, P. P. Power, *Organometallics* **2011**, *30*, 3353-3361; e) R. Waterman, R. C. Handford, T. D. Tilley, *Organometallics* **2019**, *38*, 2053-2061.

[5] C. S. MacNeil, P. G. Hayes, *Chem. Eur. J.* **2019**, *25*, 8203-8207.

[6] C. S. MacNeil, S.-J. Hsiang, P. G. Hayes, *Chem. Commun.* **2020**, *56*, 12323-12326.

[7] J. D. Feldman, J. C. Peters, T. D. Tilley, *Organometallics* **2002**, *21*, 4065-4075.

[8] C. Lenczyk, D. K. Roy, J. Nitsch, K. Radacki, F. Rauch, R. D. Dewhurst, F. M. Bickelhaupt, T. B. Marder, H. Braunschweig, *Chem. Eur. J.* **2019**, *25*, 13566-13571.

[9] K. Nagata, H. Omura, M. Matsuoka, H. Tobita, H. Hashimoto, *Organometallics* **2023**, *42*, 1131-1138.

[10] a) J. D. Feldman, G. P. Mitchell, J.-O. Nolte, T. D. Tilley, *J. Am. Chem. Soc.* **1998**, *120*, 11184-11185; b) C. Zybill, G. Müller, *Angew. Chem. Int. Ed.* **1987**, *26*, 669-670.

[11] R. J. P. Corriu, J. J. E. Moreau, *J. Organomet. Chem* **1976**, *120*, 337-346.

[12] a) R. L. Melen, *Chem. Soc. Rev.* **2016**, *45*, 775-788; b) A. A. Toutov, K. N. Betz, M. C. Haibach, A. M. Romine, R. H. Grubbs, *Org. Lett.* **2016**, *18*, 5776-5779.

[13] L. Yang, D. R. Powell, R. P. Houser, *Dalton Trans.* **2007**, 955-964.

[14] P. G. Hayes, R. Waterman, P. B. Glaser, T. D. Tilley, *Organometallics* **2009**, *28*, 5082-5089.

[15] S. Bajo, M. M. Alcaide, J. López-Serrano, J. Campos, *Chem. Eur. J.* **2021**, *27*, 16422-16428.

[16] T. P. Dhungana, H. Hashimoto, M. Ray, H. Tobita, *Organometallics* **2020**, *39*, 4350-4361.

[17] O. Minge, S. Nogai, H. Schmidbaur, *Z. Naturforsch. B* **2004**, *59*, 153-160.

[18] C. Zeppek, J. Pichler, A. Torvisco, M. Flock, F. Uhlig, *J. Organomet. Chem.* **2013**, *740*, 41-49.

[19] D. Mukherjee, R. R. Thompson, A. Ellern, A. D. Sadow, *ACS Catal.* **2011**, *1*, 698-702.

Chapter 4. Rhodium-mediated Assembly of New Heterocycles: From Borylenes to Oxaboroles

Abstract and Preface

Base-stabilized rhodium borylene complex κ^2-*L*(CO)Rh(BMes), **3**; κ^2-*L* = κ^2-NN'-Rh,κ^1-N-B-(2,5-[^{i}Pr$_2$P=N(4-^{i}PrC$_6$H$_4$)]$_2$-N'(C$_4$H$_2$)$^-$); Mes = mesityl, reacts with a series of alkynes (PhC≡C—R; R = Ph, Me, CO_2Et, H) to yield unique structures whereby the alkyne has regioselectively added across boron and the carbon atom of a CO ligand. The resulting complexes, *L*Rh[C(O)C(Ph)C(R)B(Mes)], **13^R**, react with additional CO to afford cycle-containing products, *L*(CO)Rh($\overline{\text{PhCCR=BMesOC}}$), **15^R**, that ultimately release highly functionalized organic heterocycles of the form $\overline{\text{PhC=CRBMesOC}}$=NPipp (Pipp = 4-^{i}PrC$_6H_4$), **16**. These oxaboroles, which were assembled from a primary hydroborane, CO, an alkyne, and an azide-generated NPipp, are structurally analogous to two of the five boron-containing therapeutics approved by the FDA.

This chapter serves as a climax to the work detailed thus far in this thesis. Moving away from the dehydrogenative coupling experiments with pinacol, reaction of borylene complex **3** with a series of alkynes presented brand new reactivity that showcases the potential applications of borylene transfer. The precedent for organometallic species to generate functionalized heterocycles also demonstrates the stunning potential of metal-ligand cooperative processes.

This chapter is reproduced from "Hsiang, S.J.; Hayes, P.G.*, Rhodium-mediated Assembly of New Heterocycles: From Borylenes to Oxaboroles. *Angewandte Chemie International Edition.* **2025**, e202421302." The citation style follows that of *Angewandte Chemie International Edition*, published by Wiley. Experimental Information including synthetic procedures, characterization details, X-Ray crystallographic details, computational details, and additional NMR spectra are provided in Appendix III.

4.1. Introduction

Transition metal (TM) assisted assembly of value-added products from simple molecular building blocks is essential for meeting the demand of the high throughput chemical industry, and the ever-increasing growth of green chemistry initiatives which aim for high levels of atom economy. The ubiquity of carbonyl (C=O) functional groups in pharmaceutically-relevant molecules, which play key roles in orienting the drug molecule against active sites and participating in intermolecular interactions, is well documented.[1] Carbon monoxide, the most simple multiply bonded carbon–oxygen moiety, is therefore an appealing C1 substrate for the efficient synthesis of carbonyl-containing compounds. Given that the CO ligand is one of the most common donors in coordination chemistry, TM complexes that can activate, and subsequently install, CO into complicated architectures are attractive.[2] Accordingly, the scientific literature is replete with examples of TM assisted activation of carbon monoxide in processes akin to industrially important Fischer–Tropsch, Pauson-Khand and hydroformylation reactions.[3] Even so, the preparation of structurally complex "fine chemicals" *via* the selective combination of CO and multiple other small molecules remains synthetically challenging.[3a] A notable recent achievement is the catalytic carbonylation of alkynes to form retinoid esters, using a one-pot methodology that employs acetylenes, alcohols, and carbon monoxide (Scheme 4.1a).[3a, 4] Kawatsura reported another elegant example wherein the [2+2+1] cycloaddition of carbon monoxide and disubstituted internal alkynes afforded highly functionalized heterocycles (Scheme 4.1b).[3a, 5] More recently, Kobayashi presented Suzuki–Miyaura cross-coupling reactions in the presence of CO gas to yield diaryl ketones (Scheme 4.1c).[3a, 6]

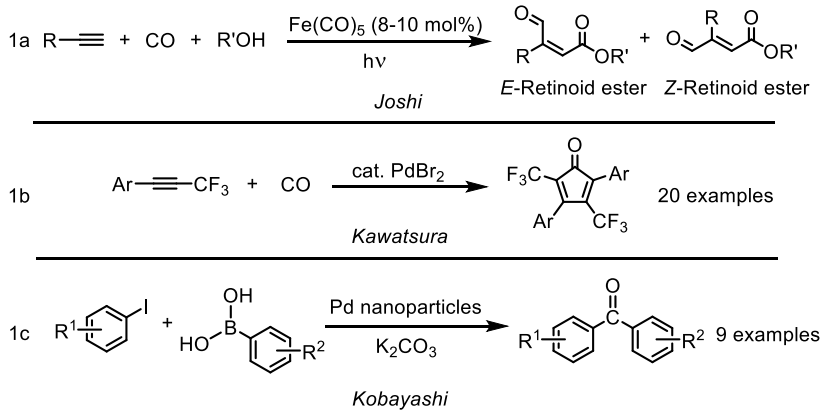

Scheme 4.1. Recent examples of direct CO incorporation into highly functionalized molecules.

Boron containing molecules are perhaps best known for their use in Suzuki-Miyaura cross-coupling processes, wherein the boron atom is discarded during the C–C bond forming reaction.[7] In recent decades, however, the development of technologies that capitalize upon the unique properties of boron has increased dramatically. Transition metal free catalysis, for example, often leverages the Lewis acidic properties of boron for bond activation purposes, *in lieu* of formal redox processes prevalent in traditional metal-mediated pathways.[8] On the pharmaceutical side, since the anti-cancer capabilities of bortezomib were discovered in 2003, four additional boron-containing drugs, all of which feature a boron heterocycle, have received FDA-approval.[9]

Previously, we disclosed that a rhodium carbonyl complex supported by a κ^3-*NNN* pincer ligand, *L*RhCO (**1**; *L* = κ^3-*NNN'* = 2,5-[^{i}Pr$_2$P=N(4-^{i}PrC$_6$H$_4$)]$_2$-N'(C$_4$H$_2$)$^-$), is able to dehydrogenate group 13 and 14 molecules.[10] In particular, the reaction between **1** and H$_2$BMes (Mes = mesityl), releases H$_2$ gas and generates the base-stabilized rhodium borylene complex κ^2-*L*(CO)Rh(BMes) (**3**; κ^2-*L* = κ^2-NN'-Rh,κ^1-N-B).[10c] The activation of primary boranes, and subsequent use of the resultant species as :BR synthons, is an appealing alternative to hydroboration for the synthesis of structurally complex boranes. Such compounds may then be used further downstream as high value substrates in cross-coupling reactions, as standalone reagents, or as pharmaceutical precursors. For example, borylene transfer to alkynes generally produces three membered borirene heterocycles, as demonstrated by Braunschweig *et al*. with their [(OC)$_5$M=B=N(SiMe$_3$)$_2$] (M = Cr, Mo)

complexes (Scheme 4.2a).[11] The same group also reported stepwise borylene metathesis that proceeds through an isolable [2 + 2] cycloaddition intermediate that contains a Mn–B(^{t}Bu)–O–C(Ph)$_2$ heterocycle, exhibiting the non-innocence of the benzophenone carbonyl group (Scheme 4.2b).[12]

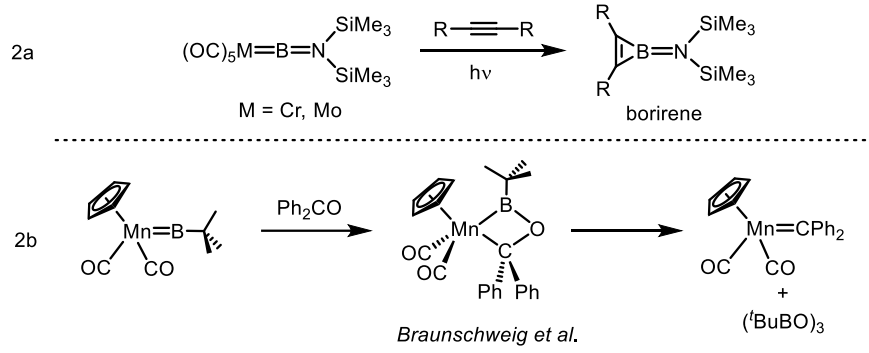

Scheme 4.2. a) Transfer of a terminal aminoborylene to alkynes; b) Borylene metathesis with benzophenone.

As our rhodium borylene compounds are Lewis-base stabilized, we sought to investigate their reactivity with alkynes, in contrast to work previously published on terminal borylenes and aminoborylenes. Remarkably, reaction of complex **2** with diphenylacetylene did not undergo elimination of the anticipated borirene product, but instead generated an isolable species that features formal alkyne addition across boron and the carbon atom of the CO ligand (Scheme 4.3). Herein we detail our studies into the generality of this chemistry, as well as the subsequent release of novel five-membered oxaborole species, uniquely assembled from CO, BMes, NPipp (Pipp = 4-^{i}PrC$_6$H$_4$), and PhC≡CR. To the best of our knowledge, this class of molecule, which boasts a remarkable degree of built-in functionality sourced from simple substrates, is unprecedented.

4.2. Results and Discussion

4.2.1. Reaction of Complex 2 with Alkynes

Starting from κ^2-*L*Rh(BMes), complex **3**, reaction with diphenylacetylene was attempted in an effort to establish if formal borylene transfer is possible. Surprisingly, the ^{31}P NMR spectrum,

recorded after heating at 50 °C for 2 hours in benzene-d_6, revealed two new resonances in a 1:1 ratio (δ 51.8 and 44.7), as opposed to the anticipated regeneration of monocarbonyl **1** (δ 58.4) and concomitant release of 1-mesityl-2,3-diphenyl-1*H*-borirene (Scheme 4.3). Close examination of the corresponding ^{1}H and ^{13}C NMR spectra indicated two sets of aromatic and aliphatic resonances for the acetylene moiety, suggesting an unsymmetric product. Additionally, free rotation about the B–$C_{mesityl}$ bond is restricted on the NMR timescale, resulting in three distinct CH_3 resonances in the ^{1}H NMR spectrum. These spectroscopic signatures contradicted the formation of a simple alkyne coordination product, prompting further investigation into the identity of the complex. Gratifyingly, an X-ray crystal structure obtained from a moderately diffracting single crystal elucidated the compound's connectivity, wherein the alkyne has formally added across the Rh carbonyl and borylene functionalities, affording κ^2-*L*Rh[C(O)C(Ph)C(Ph)B(Mes)], **13^{Ph}** (Figure 4.1, top left, *vide infra*).

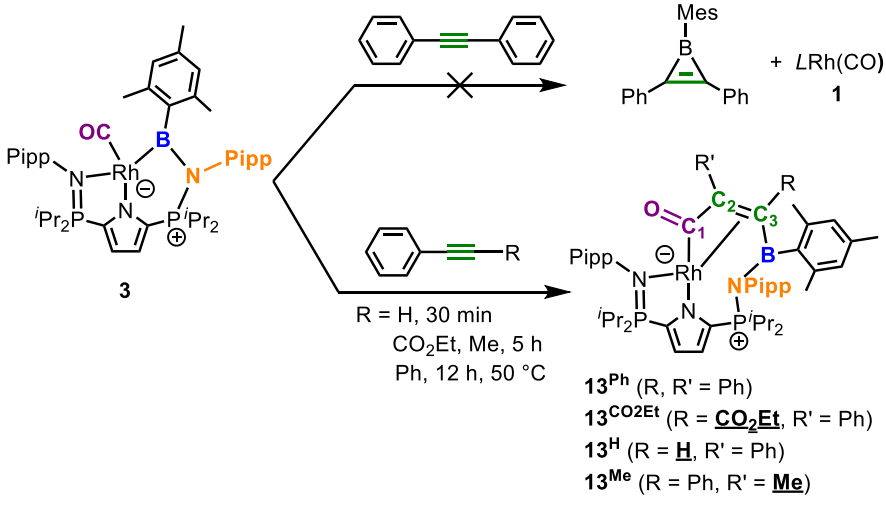

Scheme 4.3 Reaction of complex **3** with a series of alkynes (Ph-C≡C-R, R = Ph, Me, CO_2Et, H) to yield complexes **13**.

When considering the structure of **13^{Ph}**, the newly formed C1(O)–C2(Ph)–C3(Ph)–B(Mes) framework, and its interaction with rhodium, is worthy of discussion. The ^{13}C NMR resonances for C2 and C3, at δ 140.0 and 84.0, respectively (assigned in relation to other complexes in the series,

vide infra), indicate prominent polarization in the C2–C3 bond compared to δ 90.2 in symmetrical diphenylacetylene. The upfield shift in the C3 resonance, despite the proximity of C3 to the Lewis acidic boron atom, suggests a decrease in the C2–C3 bond order. Meanwhile, the downfield shifted C2 resonance is consistent with its proximity to the newly formed carbonyl functionality (C1=O). A downfield shift was also observed for the ^{31}P NMR resonance assigned to the phosphorus atom in the phosphinimine bound to boron (δ 44.7, *c.f.* δ 37.8 in complex **3**), suggesting increased polarization in the $^{\delta+}$P–$^{\delta-}$N bond, which is well documented to possess substantial ylidic character.[10a,13] Unfortunately, the low quality of the X-ray crystal data for complex **13^{Ph}** prevents a detailed discussion of the metrical parameters; nonetheless, it is clear that C1, C2, and C3 each exhibit trigonal planar geometry that is consistent with formal sp^2 hybridization (Figure 4.1, top left). Notably, C2 and C3 are approximately equidistant from rhodium, implying η^2-coordination of the alkene. The geometry at boron is only slightly distorted from trigonal planar (Σ_{angles} = 353.6°), arguing against substantial Rh–B bonding. At 1734 cm^{-1} the ν_{CO} stretching frequency is higher than related neutral rhodium acyl species, but is comparable to anionic $[AsPh_4]_2[(EtCO)Rh(CO)I_3]_2$ (1768 cm^{-1}).[14] Anionic rhenium acyl complexes have also been documented to exhibit higher ν_{CO} wavelengths than their neutral counterparts.[15] Given this information, we consider the most appropriate canonical structure to bear formal charges on rhodium and phosphorus, which maintains a metal oxidation state of +1 and an electron count of 16 at the metal center.

In order to garner a better understanding of the reaction between **3** and diphenylacetylene (PhC≡CPh), as well as the unusual bonding within the product, three additional alkynes, each with different steric and/or electronic properties, were selected to probe the generality of this chemistry. Reaction of complex **3** with an excess of ethyl-3-phenylpropiolate (PhC≡CO_2Et) in toluene, either at ambient temperature for five hours, or at 50 °C for one hour, led to isolation of *κ*^{2}-*L*Rh[C(O)C(Ph)C(C$\underline{O_2}$Et)B(Mes)], **13^{CO2Et}**. Reaction of complex **3** with excess phenyl acetylene (PhC≡CH), for 30 minutes at ambient temperature afforded *κ*^{2}-*L*Rh[C(O)C(Ph)C($\underline{H}$)B(Mes)], **13^{H}**,

whereas 1-phenyl-1-propyne (PhC≡CMe), required more judicious conditions to give the addition product κ^2-*L*Rh[C(O)C(Me)C(Ph)B(Mes)], **13^{Me}**, in 42% yield (Scheme 4.3). While slow conversion to **13^{Me}** was observed when the reaction was conducted over five hours at ambient temperature, prolonged heating led to darkening of the solution and the appearance of multiple new unidentified resonances in the ^{31}P and ^{1}H NMR spectra.

Remarkably, multinuclear NMR spectroscopy and X-ray crystallography confirmed that reactions with ethyl-3-phenylpropiolate and phenyl acetylene proceeded regio-specifically, wherein the phenyl substituent is adjacent (C2) to the carbonyl group (as opposed to boron) in the products (Figure 4.1, top right, bottom left). Conversely, reaction between **3** and 1-phenyl-1-propyne is predominantly (>85% by NMR spectroscopy) regioselective for the other isomer, placing the phenyl group at C3 (Figure 4.1, bottom right). Careful examination of the ^{31}P NMR spectrum of **13^{Me}** revealed prominent resonances at δ 51.7 and 42.9 in a 1:1 ratio, as well as a lower intensity set at δ 50.7 and 43.2, postulated to be the minor regioisomer.

In all three unsymmetric alkyne addition products, **13^{H}**, **13^{CO2Et}**, and **13^{Me}**, free rotation about the B–$C_{mesityl}$ bond is once again restricted on the ^{1}H NMR timescale. 2-Dimensional-^{1}H-^{13}C HMBC and HSQC NMR experiments confirmed that the C2 and C3 resonances in **13^{H}** and **13^{CO2Et}** are downfield and upfield shifted, respectively, compared to free alkyne. Meanwhile, the different regioselectivity in **13^{Me}** led to both C2 and C3 being downfield shifted compared to 1-phenyl-1-propyne (δ 144.1 and 93.1, *c.f.* δ 86.2 and 80.5 in PhC≡CMe). Given that there is a preference for electron donating groups adjacent to the rhodium carbonyl (Me > Ph > H >> CO_2Et), it is likely that there is positive charge buildup on C2 in the transition state, though it is unclear if the reaction proceeds in a concerted or stepwise fashion (Scheme 4.3, *vide supra*).

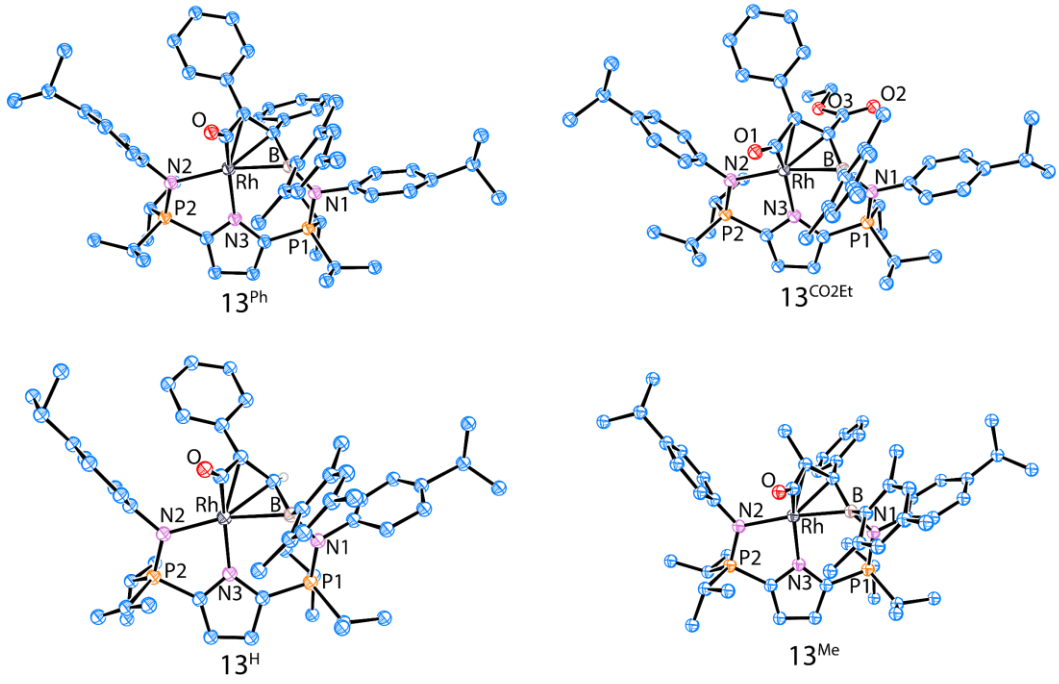

Figure 4.1. Connectivity structures of **13^{Ph}**, **13^{CO2Et}**, **13^{H}**, and **13^{Me}** depicted with no thermal ellipsoid probabilities shown. Hydrogen atoms, apart from the C3 bound H in **13^{H}**, disorder models, and co-crystallized solvent moieties have been removed for clarity.

Unfortunately, this class of compound crystallizes in low diffracting clusters, and despite exhaustive efforts, we were unable to obtain high quality, solid-state data suitable for metrical discussions (See Appendix Table III.1).

4.2.2. Reaction of Complexes 13 with CO

With a series of alkyne insertion products in hand, it was postulated that addition of CO gas might release a functionally rich organic molecule, along with concomitant generation of monocarbonyl **1**. To this end, complex **13^{CO2Et}**, which possesses a diagnostic C3-bound ester group, was selected for probing experiments. One atmosphere of CO gas was added to a *J*-Young NMR tube charged with a degassed benzene-d_6 solution of **13^{CO2Et}**. Progress of reaction was monitored *via* ^{31}P NMR spectroscopy and within two hours at ambient temperature signals for **13^{CO2Et}** were

completely supplanted by two equal intensity resonances at δ 58.3 and –0.8. Upon careful scrutiny it was established that conversion to this unidentified species proceeded through a transient intermediate (**15**^{CO2Et}, *vide infra*) which gives rise to peaks at δ 56.4 and 46.7. Notably, the chemical shift of the signal at δ –0.8 is too far upfield for a phosphinimine bound to a metal center, but is consistent with either a free phosphinimine or reduced P(III) nucleus.[10a,16] An X-ray diffraction study of single crystals corroborated the NMR spectroscopic evidence. Specifically, the NPipp group was excised by P–N bond cleavage, yielding the dicarbonyl rhodium complex $L^2Rh(CO)_2$ (L^2 = κ^2-[2-^{i}Pr$_2$P=N(4-^{i}PrC$_6$H$_4$)-5-P^{i}Pr$_2$]-N'(C$_4$H$_2$)$^-$), **14**, (Figure 4.2) as the sole metal-containing product. Inspection of the ^{1}H NMR spectrum revealed a new set of resonances attributed to the phenyl and ester moieties of the former alkyne, the liberated NPipp, and the boron-bound mesityl group. The substantially different chemical shifts indicate distinct chemical environments from complex **13**^{CO2Et}, and coupled with their matching relative integrations, suggest formation of a single new organic compound.

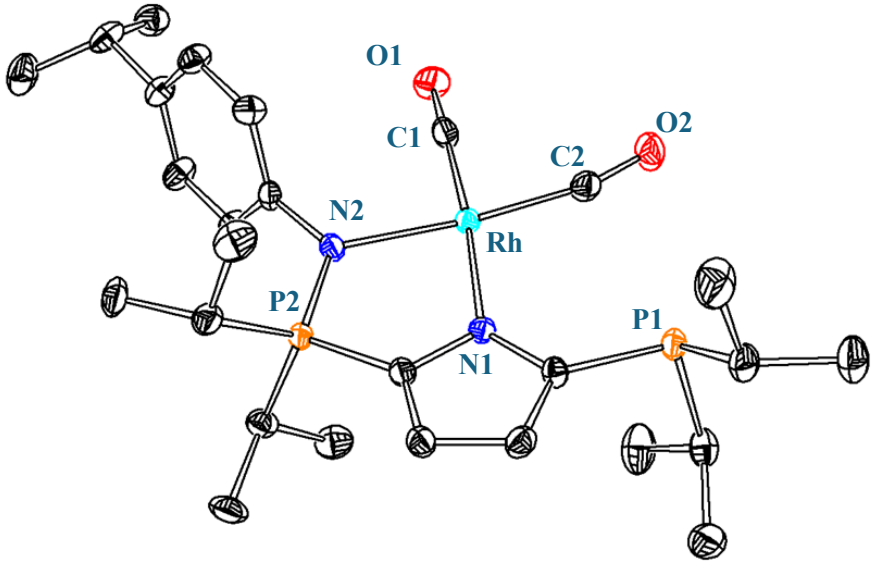

Figure 4.2. X-ray crystal structure of complex **14** with thermal ellipsoids represented at 50% probability. Hydrogen atoms removed for clarity. Selected bond distances (Å) and angles [°]: C1–O1 1.130(5), C2–O2 1.134(5), Rh–N2 2.086(3), Rh–N1 2.079(3), N1–Rh–N2 84.1(1).

Exposure of **13^{Ph}** to CO for 14 hours at 45 °C in benzene solvent also afforded complex **14**, though in this case no evidence for intermediates was observed by either ^{31}P or ^{13}C NMR spectroscopy. Conversely, reaction of **13^{H}**, which lacks a C1 substituent, with 1 atm of CO, permitted isolation of κ^2-*L*(CO)Rh(PhCCH=BMesOC), **15^{H}**, (^{31}P: δ 54.7 and 45.1). Complex **15^{H}** forms rapidly (<10 minutes) at ambient temperature. Removal of residual CO prevents conversion to complex **14**, thereby allowing for complete characterization by NMR spectroscopy (Scheme 4.4, top). Free rotation about the B–$C_{mesityl}$ bond, as indicated by a single resonance for the *ortho*-CH_3 groups, implies less steric hindrance at boron in **15^{H}**, compared to **13^{H}**. A 2D-HSQC experiment allowed a broad singlet in the ^{13}C NMR spectrum (δ 119.0) to be attributed to C3, which is downfield shifted from δ 70.3 in **13^{H}**. The substantial change in chemical shift is expected because of electron delocalization throughout the ring, as well as proximity to the adjacent Lewis acidic boron atom. Likewise, the ^{1}H NMR signal for the C3-bound hydrogen moved from δ 4.85 in **13^{H}** to δ 6.15 in **15^{H}**. Carbon 2, which exhibits weak coupling to ^{103}Rh ($^{1}J_{C–Rh}$ = 12 Hz), was established by 2D-HMBC experiments to resonate at δ 175.1. Finally, C1, which originated from the activated CO ligand, appears as a doublet of doublets centered at δ 105.7 ($^{1}J_{C–Rh}$ = 41 Hz, $^{2}J_{C–P}$ = 10 Hz). Coupling to phosphorus supports interaction between C1 and the phosphinimine nitrogen, as required for generation of the new C1–C2–C3–B–O ring (Scheme 4.4). A new ^{13}C resonance at δ 196.4, with a $^{1}J_{C–Rh}$ coupling constant of 83 Hz, is attributed to a newly coordinated CO ligand. Addition of an atmosphere of CO gas, under ambient conditions, to compound **15^{H}** resulted in exclusive conversion to dicarbonyl **14**, along with release of the cyclic organic product PhC=CHBMesOC=NPipp, **16^{H}**. Given the identity of **14** (Figure 4.2) and **15^{Me}**, as confirmed by X-ray crystallography (*vide infra,* Figure 4.3), it is reasonable to assume that release of compounds **16** (from **15**) involves cleavage of the P–N bond closest to C1 (Scheme 4.4, bottom).

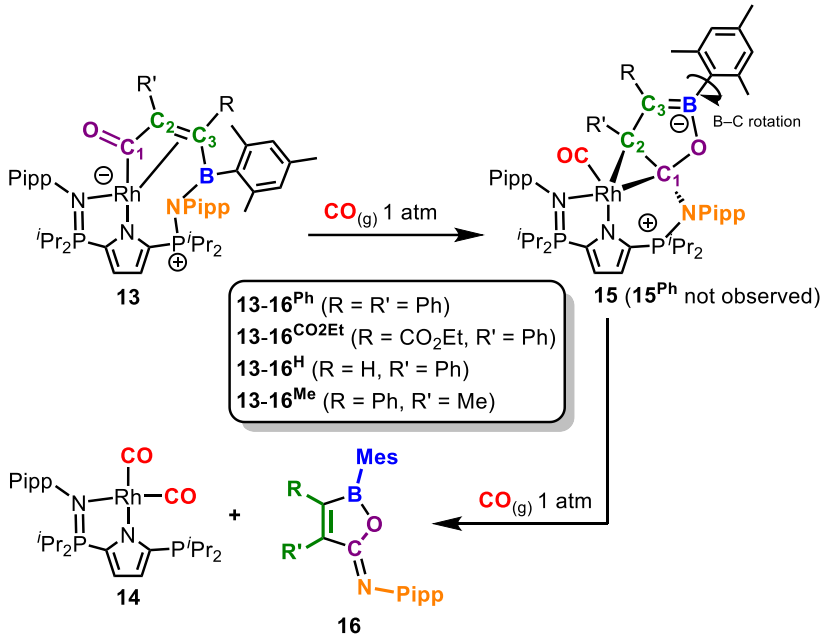

Scheme 4.4. Top: Reaction between complexes **13** with $CO_{(g)}$ to form cyclic intermediates $\mathbf{15}^{\mathbf{CO2Et}}$, $\mathbf{15}^{\mathbf{H}}$ and $\mathbf{15}^{\mathbf{Me}}$, respectively. $\mathbf{13}^{\mathbf{Ph}}$ is presumed to proceed through the analogous intermediate, but $\mathbf{15}^{\mathbf{Ph}}$ was not observed spectroscopically. Bottom: Reaction of complexes **15** with additional $CO_{(g)}$ to yield complexes **14** and cyclic oxaboroles **16**.

When excess CO was introduced to a benzene-d_6 solution of $\mathbf{13}^{\mathbf{Me}}$, two ^{31}P NMR resonances similar to those observed for both $\mathbf{15}^{\mathbf{H}}$ and $\mathbf{15}^{\mathbf{CO2Et}}$, appeared at δ 54.4 and 45.1. These signals were quickly replaced by those corresponding to complex **14**. As previously mentioned, excessive heating during the preparation of $\mathbf{13}^{\mathbf{Me}}$ darkened the solution and generated numerous unidentified signals in the ^{31}P NMR spectrum. Single crystals suitable for an X-ray diffraction study were grown from this reaction mixture and established to be $\mathbf{15}^{\mathbf{Me}}$ (Figure 4.3). Although $\mathbf{15}^{\mathbf{Me}}$ is presumably a minor by-product, likely arising from intermolecular CO transfer from one molecule of $\mathbf{13}^{\mathbf{Me}}$ to another, its solid-state structure and spectroscopic signatures corroborate the proposed structures for $\mathbf{15}^{\mathbf{Ph}}$, $\mathbf{15}^{\mathbf{H}}$ and $\mathbf{15}^{\mathbf{CO2Et}}$. While the low quality of the structure limits detailed discussion, notable metrics include C1–C2 and C2–C3 bond lengths of 1.52(2) Å and 1.55(2) Å, respectively, as well as a short B–C3 distance (1.35(2) Å), the combination of which led to the proposed canonical structure shown

in Scheme 4.4 and Scheme 4.5. Boron maintains a trigonal planar geometry (Σ_{angles} = 360°), while C1 and C2 deviate slightly from planarity (Σ_{angles} = 355° and 347°, respectively).

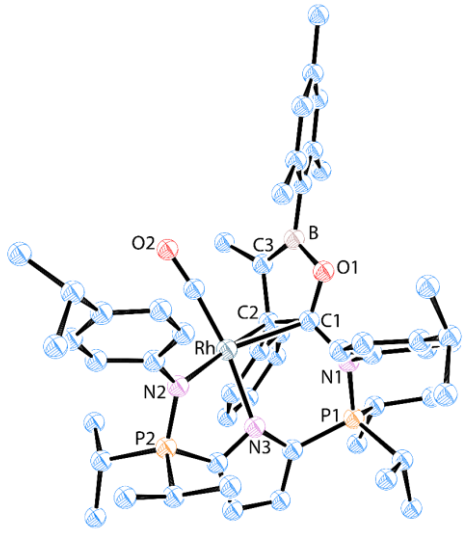

Figure 4.3. Connectivity structure of compound **15^{Me}** with no thermal ellipsoid probabilities shown. Hydrogen atoms, as well as disorder models removed for clarity.

In an effort to lend credence to the possibility of intermolecular CO transfer from one rhodium complex to another, κ^2-*L*Rh(CO)$_2$, a synthetic precursor to monocarbonyl **1**, was selected as a convenient stoichiometric source of CO, particularly on a milligram scale.[16] Heating a 1:1 mixture of **13^H** and κ^2-*L*Rh(CO)$_2$ in benzene-d_6 at 50 degrees for 10 hours led to complete consumption of both species, and exclusive formation of complexes **1** and **15^H** (Scheme 4.5).

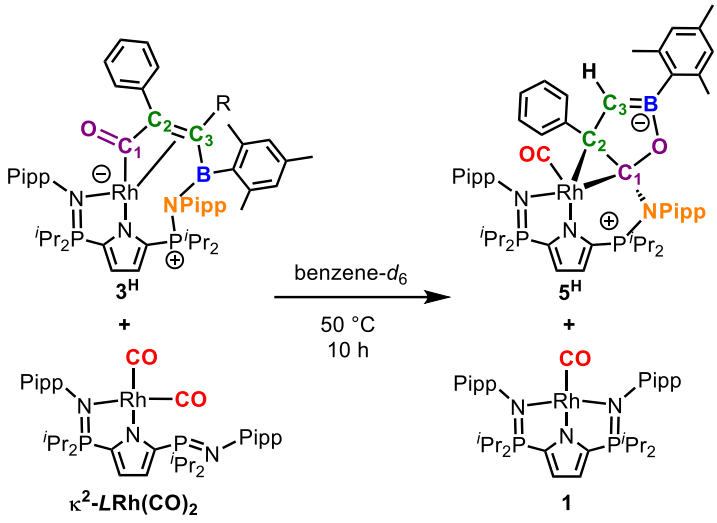

Scheme 4.5 Reaction of complex $\mathbf{13^H}$ with κ^2-*L*Rh(CO)$_2$ to afford $\mathbf{15^H}$ and monocarbonyl **1** *via* CO transfer from κ^2-*L*Rh(CO)$_2$.

High resolution mass spectrometric experiments using a direct injection orbitrap instrument unambiguously gave rise to peaks for the parent ions (M^+ or M+H) of each of the organic products $\mathbf{16^{Ph}}$, $\mathbf{16^{CO2Et}}$, $\mathbf{16^H}$, and $\mathbf{16^{Me}}$. Furthermore, spectra obtained from gas chromatography-mass spectrometry (GC-MS) experiments performed on a lower resolution instrument indicated fragmentation patterns consistent with that expected for compounds **16** (See Appendix III. III). To the best of our knowledge, this highly functionalized heterocycle is unprecedented. The unsaturated C2–C3 bond, as well as the C1 bound imine, offer platforms for a wide range of future organic transformations. In addition, incorporation of an ester on C3 in $\mathbf{16^{CO2Et}}$, which is also ideal for subsequent derivation, is pharmaceutically relevant. Notably, benzoxaborole-containing tavaborole (Kerydin) and crisaborole (Eucrisa) represent two of the five boron-containing drugs that are currently FDA approved (Figure 4.4, left).[9a] Accordingly, related 3-substituted-2(*5H*)-oxaboroles and their derivatives have prompted numerous studies over the past five years that explore their utility as antimicrobial therapeutics and agrochemical solutions.[17]

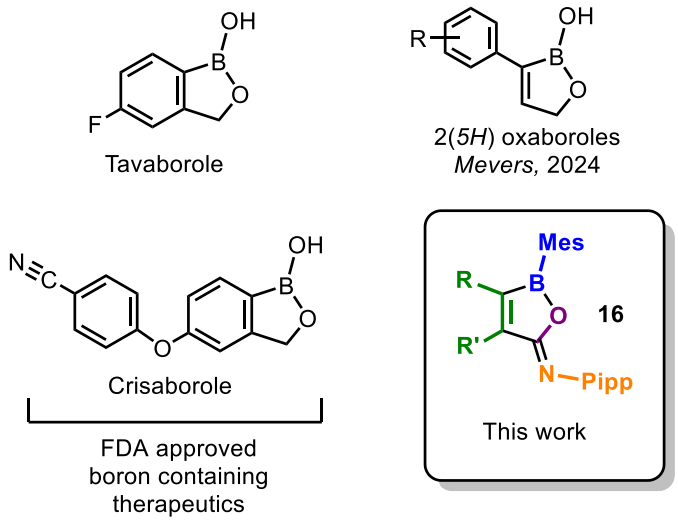

Figure 4.4. Structural comparison between FDA approved topical anti-fungal therapeutics tavaborole and crisaborole, 2(*5H*)oxaboroles studied by Mevers *et al.* as antimicrobial therapeutics,[17a] and oxaboroles **16.**

4.2.3. ^{13}C NMR Labelling Studies

In order to unambiguously follow the carbonyl carbon (C1) throughout this unusual series of reactions, ^{13}C labelling studies were undertaken. ^{13}CO labelled borylene complex **[^{13}C]-3** was prepared, and as expected, exhibited a prominent doublet centered at δ 196.6 ($^{1}J_{C–Rh}$ = 88 Hz). The four alkyne addition products gave rise to downfield shifted C1 ^{13}C signals that ranged from δ 201.4 in **[^{13}C]-13^{CO2Et}** to δ 206.4 in **[^{13}C]-13^{Me}** (Table 4.1). The minor regioisomer of **[^{13}C]-13^{Me}** exhibited a low intensity labelled resonance at δ 203.3. When complexes **[^{13}C]-15** were synthesized *via* addition of natural abundance CO gas to complexes **[^{13}C]-13**, the labelled C1 resonances shifted dramatically upfield to δ 105.7-108.9 and appeared as doublets of doublets with distinct coupling to both rhodium ($^{1}J_{C–Rh}$ = 36-42 Hz) and the nearby phosphorus atom ($^{2}J_{C–P}$ = 10-11 Hz). The chemical shift can be rationalized by substantial electronic donation from the phosphinimine nitrogen, as well as a marked decrease in C–O multiple bond character. Finally, the isotopically enriched ^{13}C resonances in the extruded organic products (**[^{13}C]-16**) were observed between δ 157.4 and δ 176.9. Release from the organometallic complex to yield compounds **[^{13}C]-16** was corroborated by the fact that these signals exhibited no coupling whatsoever to either ^{31}P or ^{103}Rh.

Furthermore, no signals consistent with isotopically enriched ^{13}C were observed bound to rhodium, indicating that the ^{13}C label in complexes **[^{13}C]-13** and **[^{13}C]-15** is not susceptible to exchange, nor is the reaction that yields **13** from **3** reversible under these conditions. This finding is additionally supported by the fact that no obvious decrease in labeled ^{13}C signal intensity was apparent even when the reaction mixture was exposed to a vast excess of natural isotopic abundant CO gas for a prolonged period. By contrast, the control reaction between isotopically enriched **[^{13}C]-3** and an atmosphere of unlabelled CO gas resulted in gradual decrease in signal intensity over an hour at ambient temperature. Finally, an excess of isotopically enriched ^{13}CO gas was added to **13^{H}**, ultimately affording diagnostic ^{13}C resonances for **14** at δ 186.2 (dd, $^{1}J_{C–Rh}$ = 69 Hz, $^{3}J_{C–P}$ = 10 Hz) and 183.2 (dd, $^{1}J_{C–Rh}$ = 70 Hz, $^{3}J_{C–P}$ = 10 Hz). No incorporation of ^{13}CO into oxaborole **16^{H}** was observed.

Table 4.1. Selected NMR resonances observed while monitoring the reaction between isotopically enriched **[^{13}C]-3** and various alkynes

	^{31}P (P=N–Rh) (δ)	**^{31}P (δ)**	**C1 ^{13}C ($^{1}J_{CRh}$, $^{2}J_{CP}$) (δ, Hz, Hz)**
[^{13}C]-3 + diphenylacetylene			
[^{13}C]-13^{Ph}	51.8	44.7	203.7 (d, 22)
Intermediate	Not observed		
Organic Product (**16^{Ph}**)	–	–	176.9
[^{13}C]-3 + ethyl-3-phenylpropiolate			
[^{13}C]-13^{CO2Et}	51.6	45.6	201.4 (d, 22)
Intermediate (**[^{13}C]-15^{CO2Et}**)	56.4	46.7	108.9 (dd, 11, 36)
Organic Product (**[^{13}C]-16^{CO2Et}**)	–	–	157.4
[^{13}C]-3 + phenylacetylene			
[^{13}C]-13^{H}	48.2	45.1	206.1 (d, 21)
Intermediate (**[^{13}C]-15^{H}**)	54.7	45.1	105.7 (dd, 10, 41)
Organic Product (**[^{13}C]-16^{H}**)	–	–	157.9
[^{13}C]-3 + 1-phenyl-1-propyne			
[^{13}C]-13^{Me}	51.7	42.9	206.4 (d, 22)
Intermediate (**[^{13}C]-15^{Me}**)	54.4	45.1	108.0 (dd, 11, 42)
Organic Product (**[^{13}C]-16^{Me}**)	–	–	160.3

When dicarbonyl **14** remains in the reaction mixture, gradual transition to a new product with ^{31}P NMR resonances at δ 54.3 and 38.9 was observed. Notably, the signal at δ 38.9 is a broad doublet with a large coupling constant ($^{1}J_{P–Rh}$ = 147 Hz), reminiscent of coupling exhibited by rhodium triphenylphosphine complexes. Diagnostic peaks pertaining to the unsymmetric L^2 ligand exist in the ^{1}H NMR spectrum, while the ^{13}C NMR spectrum displays no intense signals attributable to isotopically enriched ^{13}CO. This product is postulated to be dinuclear, resulting from coordination of the newly generated phosphine to rhodium in another molecule of **14**.

4.2.4. Computational Studies

The lack of high-quality X-ray data, as well as the novel bonding modes within this series of compounds, prompted us to explore computational methods to further our understanding. The idealized solution-phase geometries were calculated using density functional theory (DFT) at the def2SVP level of theory using Truhlar and co-workers' SMD model (solvent = toluene).[18] All optimized structures matched closely with metrics obtained by X-ray diffraction analysis for the alkyne insertion products **13** (Rh–C1, Rh–C2, Rh–C3, N–B, bond distances all matched within 0.05, 0.02, 0.02 and 0.03 Å respectively). In all four optimized structures, C2 and C3 are equidistant from rhodium, and C1, C2, C3, and boron all exhibit trigonal planar geometry, supporting the previously described bonding motif (See Appendix Table III.3). The calculated and experimental bond lengths for the borane-bound iminophosphorane P–N support single bond character; it is elongated compared to its rhodium coordinated counterpart. Examination of the localized natural bonding orbitals (NBOs) in these four complexes (with regard to the N–B interaction) revealed a formal σ-bonding NBO between the two atoms that is occupied by approximately two electrons (*e.g.* 1.939 in $\mathbf{13^{Ph}}$). Conversely, the C2–C3 π-bonding NBOs are only partially occupied (1.261-1.590), suggesting extensive electron delocalization and/or donation to the rhodium metal center. Second order perturbation analysis corroborated this interpretation, whereby a moderate ($E^{(2)}$: 41.82 kcal mol^{-1} in $\mathbf{13^{Ph}}$) donor-acceptor interaction was established between the C2–C3 π-bonding NBO and the vacant lp* orbital on rhodium. A stronger ($E^{(2)}$: 113.73 kcal mol^{-1} in $\mathbf{13^{Ph}}$) interaction was noted between the same C2–C3 π-bonding NBO and the Rh–C1 anti-bonding orbital. The p-orbital on boron appears to have little interaction with the C2–C3 π-system, and is instead involved in a strong ($E^{(2)}$: 29.13 kcal mol^{-1} in $\mathbf{13^{Ph}}$) donor-acceptor interaction with the lone pair on nitrogen N(lp)→B(p).

A hypothesized reaction intermediate between complexes **13** and **15**, wherein an equivalent of CO is coordinated to rhodium prior to cyclization, was modelled in an attempt to glean additional

information about the reaction mechanism (Figure 4.5). Coordination of CO to the metal center appears to distort the geometry of the system so as to promote cyclization. Namely, in all four examples, the Rh–C1–C2–C3 torsion angle increases by approximately 10°, while C1–C2–C3–B decreases by a similar amount, bringing the carbonyl group closer in proximity to the boron atom. In all cases, the Rh–C2 and Rh–C3 distances elongate and the C2–C3 bond contracts (*e.g.* 2.251, 2.308, 1.407 Å *c.f.* 2.127, 2.144, 1.452 Å in **13**^{Ph}). NBO analysis suggests an increase in orbital occupancy in the C2–C3 p-bonding NBOs. The natural charge distribution calculated for the boron atom (0.918) and C1 (0.615) revealed that they bear the highest localized positive charges in the system, aside from the phosphorus atoms, rendering them susceptible to nucleophilic attack.

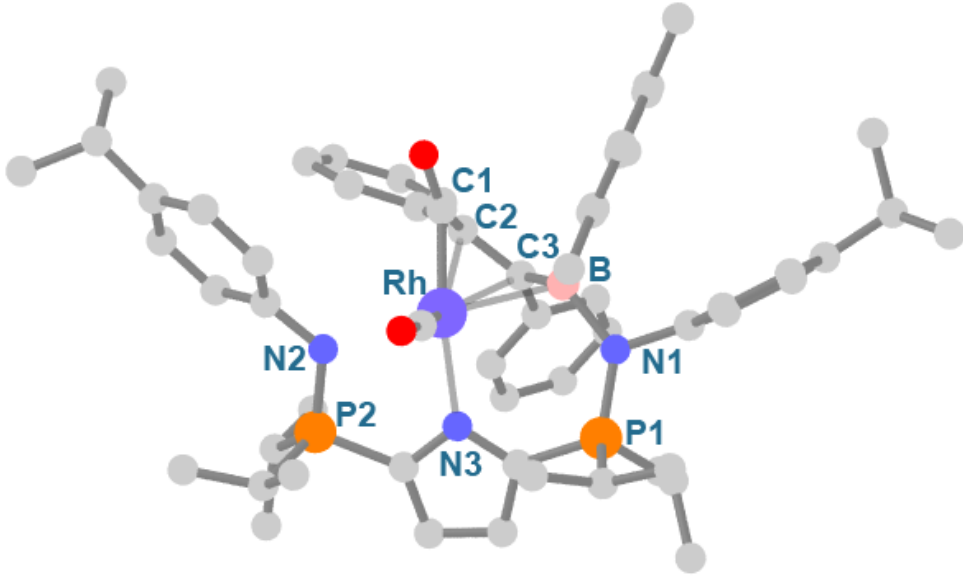

Figure 4.5. Optimized structure of a hypothesized reaction intermediate between complexes **13**^{Ph} and **15**^{Ph} wherein an equivalent of CO has coordinated to **13**^{Ph} prior to cyclization of the organic framework. Selected calculated bond distances (Å): Rh–C1 1.947, Rh–C2 2.251, Rh–C3 2.308, C2–C3 1.407.

4.3. Conclusions

Overall, a remarkable series of sequential transformations between rhodium complex **1**, a primary borane, an alkyne, an auxiliary CO ligand, and the pincer ligand's phosphinimine NPipp group, yielded a new class of boron-containing compound, one with great potential utility for organic, organometallic, and pharmaceutical applications. The system is tolerant of a variety of alkynes, including terminal and ester substituted examples, and displays a high degree of regioselectivity when unsymmetric compounds are used. Isotopic labelling experiments unambiguously demonstrate that the carbonyl ligand in complex **3** is ultimately incorporated into the final oxaborole products.

Given the pharmaceutical relevance of the five-membered oxaborole structure, ongoing studies aim to further expand the substrate scope in this system and enhance our mechanistic understanding of the unique cyclization. Furthermore, we envision that sequential addition of $PippN_3$ and *L*Rh(COE) to complex **14** should spontaneously release N_2 and regenerate complex **1**, thereby completing the synthetic cycle.

4.4. References

[1] A. Renslo, in *The Organic Chemistry of Medicinal Agents* (Ed.: A. Renslo), McGraw-Hill Education, New York, NY, **2016**.

[2] B. F. Straub, *Angew. Chem., Int. Ed.* **2010**, *49*, 7622-7622.

[3] a) R. M. B. Carrilho, M. J. F. Calvete, G. Mikle, L. Kollár, M. M. Pereira, *Chin. J. Chem* . **2024**, *42*, 199-221; b) K. M. Brummond, J. L. Kent, *Tetrahedron* **2000**, *56*, 3263-3283.

[4] R. K. Joshi, N. Satrawala, *Tetrahedron Lett.* **2017**, *58*, 2931-2935.

[5] S. Murakami, T. Sonehara, K. Iwakami, H. Tsuji, M. Kawatsura, *Tetrahedron Lett.* **2019**, *60*, 598-601.

[6] T. Yasukawa, Z. Zhu, Y. Yamashita, S. Kobayashi, *Synlett* **2021**, *32*, 502-504.

[7] J. P. G. Rygus, C. M. Crudden, *J. Am. Chem. Soc.* **2017**, *139*, 18124-18137.

[8] a) S. Mummadi, C. Krempner, *Molecules* **2023**, *28*, 1340; b) L. Schweighauser, H. A. Wegner, *Chem. Eur. J.* **2016**, *22*, 14094-14103; c) V. Nori, F. Pesciaioli, A. Sinibaldi, G. Giorgianni, A. Carlone, *Catalysts* **2022**, *12*, 5.

[9] a) K. Messner, B. Vuong, G. K. Tranmer, *Pharmaceuticals* **2022**, *15*, 264; b) B. J. Wang, M. P. Groziak, in *Adv. Heterocycl. Chem., Vol. 118* (Eds.: E. F. V. Scriven, C. A. Ramsden), Academic Press, **2016**, pp. 47-90.

[10] a) S.-J. Hsiang, P. G. Hayes, *Chem. Eur. J.* **2024**, *30*, e202304302; b) C. S. MacNeil, P. G. Hayes, *Chem. Eur. J.* **2019**, *25*, 8203-8207; c) C. S. MacNeil, S.-J. Hsiang, P. G. Hayes, *Chem. Commun.* **2020**, *56*, 12323-12326.

[11] a) H. Braunschweig, T. Herbst, D. Rais, F. Seeler, *Angew. Chem. Int. Ed.* **2005**, *44*, 7461-7463; b) C. E. Anderson, H. Braunschweig, R. D. Dewhurst, *Organometallics* **2008**, *27*, 6381-6389.

[12] H. Braunschweig, M. Burzler, K. Radacki, F. Seeler, *Angew. Chem. Int. Ed.* **2007**, *46*, 8071-8073.

[13] a) K. Dehnicke, F. Weller, *Coord. Chem. Rev.* **1997**, *158*, 103-169; b) J. L. Lortie, M. Davies, P. D. Boyle, M. Karttunen, P. J. Ragogna, *Inorg. Chem.* **2024**, *63*, 6335-6345; c) I. M. Marin, A. Auffrant, *Eur. J. Inorg. Chem.* **2018**, *2018*, 1634-1644; d) W. W. Schoeller, T. Busch, E. Niecke, *Chem. Ber.* **1990**, *123*, 1653-1654.

[14] a) M. Bassetti, A. Capone, L. Mastrofrancesco, M. Salamone, *Organometallics* **2003**, *22*, 2535-2538; b) Y. Chen, D. Liu, Y. Yu, *RCS Adv.* **2017**, *7*, 49875-49882; c) J. Conradie, J. C. Swarts, *Organometallics* **2009**, *28*, 1018-1026; d) P. Das, M. Sharma, N. Kumari, D. Konwar, D. K. Dutta, *Appl. Organomet. Chem.* **2002**, *16*, 302-306; e) L. A. Howe, E. E. Bunel, *Polyhedron* **1995**, *14*, 167-173; f) B. D. Panthi, S. L. Gipson, A. Franken, *Inorg. Chim. Acta* **2015**, *425*, 176-181; g) S. I. Vdovenko, I. I. Gerus, V. P. Kukhar, *Spectrochim. Acta A.* **2008**, *71*, 779-785.

[15] A. C. Filippou, B. Lungwitz, G. Kociok-Ko¨hn, I. Hinz, *J. Organomet. Chem.* **1996**, *524*, 133-146.

[16] C. S. MacNeil, K. E. Glynn, P. G. Hayes, *Organometallics* **2018**, *37*, 3248-3252.

[17] a) R. Campbell, N. W. Buchbinder, C. Szwetkowski, Y. Zhu, K. Piedl, M. Truong, J. B. Matson, W. L. Santos, E. Mevers, *ACS Med. Chem. Lett.* **2024**, *15*, 349-354; b) Z. He, D.-C. Huang, D. Guo, F. Deng, Q. Sha, M.-Z. Zhang, W.-H. Zhang, Y.-C. Gu, *Adv. Agrochem* **2023**, *2*, 185-195; c) K. Nowicki, J. Krajewska, T. M. Stępniewski, M. Wielechowska, P. Wińska, A. Kaczmarczyk, J. Korpowska, J. Selent, P. H. Marek-Urban, K. Durka, K.

Woźniak, A. E. Laudy, S. Luliński, *RSC Med. Chem.* **2024**, *15*, 1751-1772; d) A. L. Walker, A. Denis, R. P. Bingham, A. Bouillot, E. V. Edgar, A. Ferrie, D. S. Holmes, A. Laroze, J. Liddle, M.-H. Fouchet, A. Moquette, P. Nassau, A. C. Pearce, O. Polyakova, K. J. Smith, P. Thomas, J. H. Thorpe, L. Trottet, Y. Wang, A. Hovnanian, *Bioorg. Med. Chem. Lett.* **2019**, *29*, 126675.

[18] a) A. V. Marenich, C. J. Cramer, D. G. Truhlar, *J. Phys. Chem. B.* **2009**, *113*, 6378-6396; b) F. Weigend, *Phys. Chem. Chem. Phys.* **2006**, *8*, 1057-1065; c) F. Weigend, R. Ahlrichs, *Phys. Chem. Chem. Phys.* **2005**, *7*, 3297-3305.

Chapter 5. Synthesis and Reaction Chemistry of a Rhodium Silylyne Complex

Abstract and Preface

Base-stabilized rhodium silylene complex κ^2-*L*(CO)Rh(Si(H)Mes), **6^{Mes}**; (κ^2-*L* = κ^2-NN'-Rh,κ^1-N-Si-(2,5-[^{i}Pr$_2$P=N(4-^{i}PrC$_6$H$_4$)]$_2$-N'(C$_4$H$_2$)$^-$); Mes = mesityl, reacts with hydride abstracting agent B(C$_6$F$_5$)$_3$ to yield an unprecedented example of a group 9 coordinated silylyne species [κ^2-*L*(CO)Rh≡SiMes][HB(C$_6$F$_5$)$_3$], **17^{Mes}**. Reaction with more sterically accessible κ^2-*L*(CO)Rh(Si(H)Ph), **2^{Ph}**, on the other hand, results in transmetalation. Silylyne **17^{Mes}** was reacted with phenyl acetylene, yielding a [2+2] addition product.

The chapter details an introductory foray into the synthesis of transition metal – silicon triple bonds. Markedly, this account fills a noticeable gap in the literature towards Group 9 silylyne species and demonstrates a synthetic route starting from a primary silane starting material. The work also serves as a good branching point for this research project, extending the methodology towards a related sub-set of complexes.

This chapter is reproduced from a manuscript submitted to a special issue of the *Canadian Journal of Chemistry* dedicated to the memory of Prof. Stephen A. Westcott, that is currently under peer review. Complex **2** and **6** are redefined as **2^{Ph}** and **6^{Mes}**, respectively, to stay consistent with the pre-existing text. The citation style follows that of the *Journal of American Chemistry*, published by the American Chemistry Society. Experimental details including experimental procedure and characterization details are included in the body of the text. Supplementary NMR spectra are included in Appendix IV.

5.1. Introduction

While the electronic structure and reactivity patterns of transition metal–carbon triple bonds are fairly well understood, the synthesis of heavier group 14 homologues (M≡E; M = transition metal, E = Si, Ge, Sn, Pb) remain relatively elusive.[1-3] Filippou *et al*. have made substantial contributions to this area, reporting a variety of complexes that feature triple bonds between Nb, Cr, Mo, W, Mn, Re, Ni, Pt and group 14 elements (E = Si, Ge, Sn, Pb).[4,5] Particularly noteworthy examples from the Hashimoto and Tobita[6,7], Tilley[8,9], and Powers[10] research groups feature early to mid (groups 6-8) transition metals, marked by their lower number of valent *d* electrons compared to later transition metals. To the best of our knowledge, Widemann and co-workers were the first to report group 9 tetrylyne homologues, specifically, species that feature Rh≡Sn and Rh≡Pb functionalities (Scheme 5.1).[11] The synthetic protocol for these tetrylyne species can be largely split between whether the main group starting material exists in the divalent E(II) or tetravalent E(IV) states, with all examples of late transition metal tetrylynes being synthesized using the former method.[1] This rationalizes the lack of Si and Ge examples from the Widemann group, as sources of stable divalent silicon and germanium materials bearing a hydrogen substituent are incredibly rare.

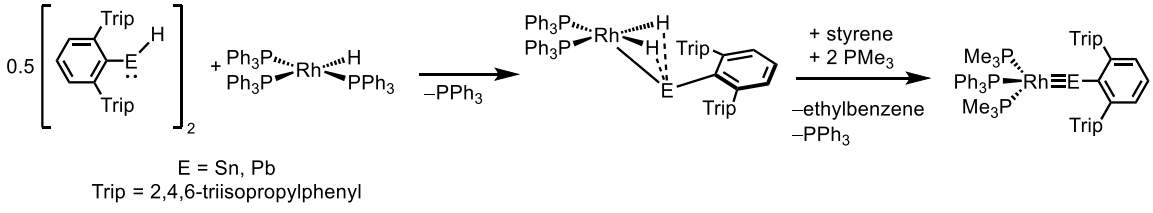

Scheme 5.1. First reported example (2021) of a rhodium tetrylyne complex by Widemann

In transition metal carbyne complexes a general trend in electronic structure has been observed moving from early (triplet, Schrock carbynes, electrophilic at M), to late transition metals (singlet, Fischer carbynes, electrophilic at C). In comparison, the vast majority of known transition metal tetrylyne complexes appear to exist in the singlet state, with the M–E bond polarized towards the

metal ($M^{\delta-}$—$E^{\delta+}$).[1,2,3] This is corroborated by the linear structure of these compounds, even when group 9 and 10 elements are incorporated.[5,11,12] Tilley *et al*., however, have previously demonstrated the isolation of an osmium silylyne complex with a formal Os≡Si linear linkage, as well as a related metallostannylene species, which is best described as having a single bond between osmium and a tin atom that bears a stereochemically active lone pair, leading to a presumed bent geometry (Figure 5.1).[8,13] Although interconversion between these two species was not observed (the metallostannylene was generated by H-migration from an osmium stannylene complex), the previous example of a rhodium tetrylyne reported by Widemann indeed forms *via* an isolable metallotetrylene intermediate that features the predicted bent geometry. Filippou and co-workers have also computationally juxtaposed the linear versus bent geometry of late transition metal tetrylyne complexes, concluding that the bent metallotetrylene description is more accurate when group 10 metals are paired with heavy group 14 elements, such as Sn and Pb.[5] These findings necessarily generate numerous questions regarding the bonding, structure and reaction chemistry within this class of complex, and a noticeable gap can be found in the lack of group 9 complexes featuring M≡Si bonds.

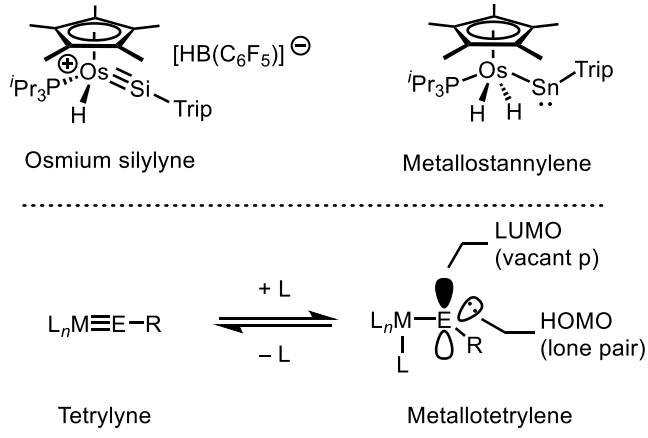

Figure 5.1. Top: Osmium silylyne and metallostannylene compounds reported by Tilley *et al*. Bottom: Relationship between triple bonded tetrylyne and single bonded metallotetrylene compounds (L = 2 electron donor ligand)[1]

Previously, we disclosed the generation of base-stabilized rhodium tetrylene complexes (E = Si, Ge) utilizing a dehydrogenative approach that is facilitated by metal-ligand cooperation.[14,15] Notably, this process allows for the isolation of neutral species that feature H-substitution at silicon and germanium; no evidence for E–H migration or interaction with rhodium was observed (Scheme 5.2).

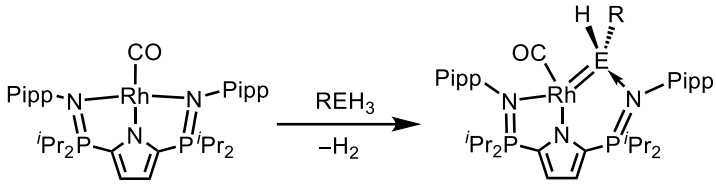

E = Si, R = Mes, Ph; E = Ge, R = ^{t}Bu

Previous Work

Scheme 5.2. Dehydrogenative synthesis of a base-stabilized silylene and germylene complexes which feature H-substitution at the main group element.

Formation of M≡E triple bonds by abstraction of an Si or Ge substituent has been documented, with examples from both the Tilley and Hashimoto groups that form cationic and neutral tetrylynes, respectively, using halide and hydride abstracting agents (Scheme 5.3).[6,8,9,16] Taking an analogous approach, we sought to react our base-stabilized rhodium silylene complexes, κ^2-*L*(CO)Rh=Si(H)R (R = Ph, Mesityl; κ^2-*L* = κ^2-NN'-Rh,κ^1-N-Si, 2,5-[^{i}Pr$_2$P=N(4-^{i}PrC$_6$H$_4$)]$_2$-N'(C$_4$H$_2$)$^-$), **2^{Ph}** and **6^{Mes}**, with the Lewis acid B(C$_6$F$_5$)$_3$ to remove the Si bound hydride and form the first example of a rhodium silylyne complex**.** Herein we report the synthesis and characterization of a base-stabilized silylyne complex, as well as attempts at conventional [2+2] cycloaddition reactions, which are known for other transition metal silylyne systems.[1-3,17]

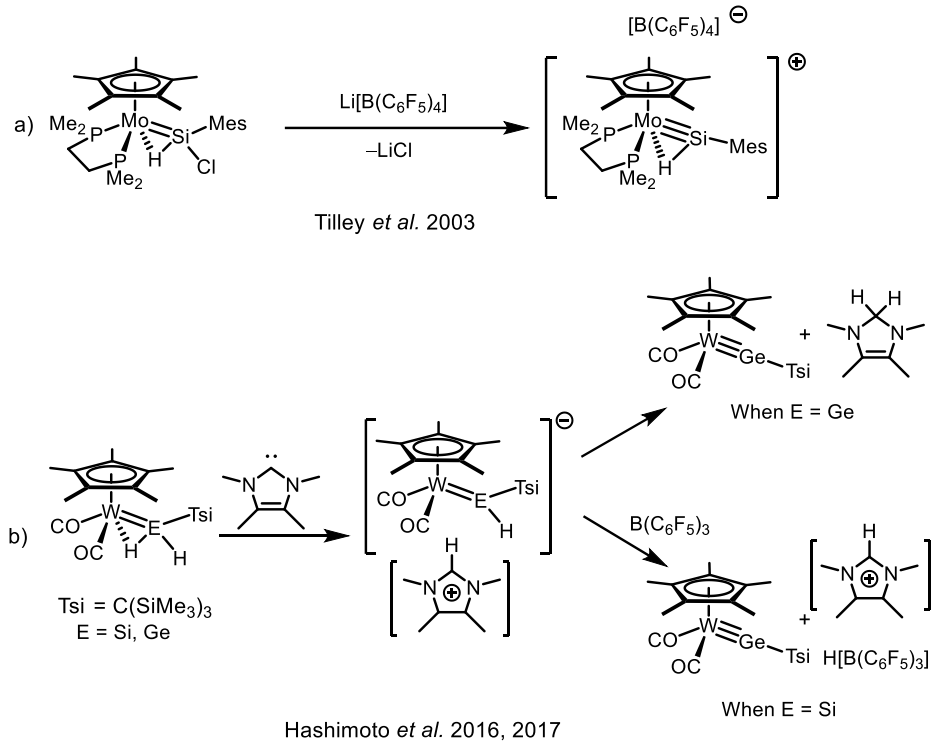

Scheme 5.3. a) Halide abstraction from a neutral silylene to yield cationic silylyne complexes by *Tilley et al.*[9] b) Sequential deprotonation and hydride abstraction from a germylene to afford a neutral germylyne and silylyne complexes by Hashimoto *et al.*[16,17]

5.2. Results and Discussion

In contrast to silylene complexes presented by Tilley and Hashimoto (Scheme 5.3, *vide supra*), our rhodium examples are free of metal-bound hydrides and there is no indication of a Rh–H–Si interaction on the ^{1}H NMR timescale. Rather, the complexes κ^2-*L*(CO)Rh=SiH(Mes), **6^{Mes}** and κ^2-*L*(CO)Rh=SiH(Ph), **2^{Ph}**, are base-stabilized by a strong N→Si donation which results in significantly reduced double bond character between the metal and silicon (Scheme 5.4). Nonetheless, the silicon bound hydrogen atom remains as an appealing target for hydride abstraction. Accordingly, the Lewis acid $B(C_6F_5)_3$ was selected as a suitable reagent that would afford the weakly-coordinating anion $[HB(C_6F_5)_3]^-$, which exhibits diagnostic ^{11}B and ^{19}F NMR signals.

Combination of stoichiometric quantities of $B(C_6F_5)_3$ and complex **6^{Mes}** in benzene-d_6 at ambient temperature generated a dark brown reaction mixture (no evidence for the formation of precipitate or insoluble oils was observed). ^{11}B and ^{19}F NMR spectra recorded at t = 5 mins revealed formation of the putative $[HB(C_6F_5)_3]^-$ anion as the sole boron and fluorine containing species in solution: ^{11}B δ –24.5 (*c.f.* δ 61.3 in $B(C_6F_5)_3$), ^{19}F δ –132.3, –163.9, –166.7 (*c.f.* δ –128.8, –141.5, –159.9 in $B(C_6F_5)_3$).[8] The ^{31}P NMR spectrum exhibited two resonances at δ 55.4 and 44.7 (*c.f.* δ 50.2, 41.1 in **6^{Mes}**), suggesting an unsymmetric complex consistent with the base-stabilized silylyne complex [κ^2-*L*(CO)Rh≡SiMes][$HB(C_6F_5)_3$], **17^{Mes}** (Scheme 5.4). The slight downfield shift in both ^{31}P NMR signals can likely be attributed to an increase in N→Rh and N→Si donation, resulting from the cationic nature of the complex. Notably, a minor impurity (5-15% by relative integration) gave rise to a ^{31}P NMR resonance at δ 42.8, which appears in varying amounts across independent syntheses. The resonance in the ^1H NMR spectrum attributed to the silicon bound H in **6^{Mes}** was absent, while a broad multiplet centered at δ 4.65 that sharpened to a singlet when decoupled from ^{11}B, was observed, suggesting successful hydride abstraction by $B(C_6F_5)_3$. While all three mesityl CH_3 resonances in complex **6^{Mes}** were distinct on the NMR timescale, a much more pronounced separation between the *ortho* substituents' resonances is apparent in the new product: δ 2.62, 2.18, 1.67 (*c.f.* δ 3.25, 2.18, 2.15 in **6^{Mes}**). The resonances attributed to the 3,4-pyrrole protons are shifted substantially downfield to δ 7.07 and 6.90 (*c.f.* 6.52 and 6.43 in **6^{Mes}**), suggesting an increase in electron donation from the pyrrole-nitrogen to rhodium. Intriguingly, the ^{29}Si NMR spectrum exhibits a new broad signal at δ 41.2 (d, $^1J_{Si\text{-}Rh}$ = 100.9 Hz) that is only slightly downfield shifted relative to the doublet of doublets centered at δ 38.0 ($^2J_{Si\text{-}P}$ = 9.3 Hz, $^1J_{Si\text{-}Rh}$ = 52.4 Hz) in **6^{Mes}**, despite the removal of a substituent from silicon**.** Although only a limited number of examples exist for comparison, Hashimoto *et al*. reported the neutral group 6 silylyne species $Cp^*(CO)_2Mo{\equiv}SiAr$ (Ar = 1,1,3,3,5,5,7,7-octaethyl-*s*-hydrindacen-4-yl), which exhibits a ^{29}Si resonance at δ 302.1 that is only 40.3 ppm downfield of the precursor silylene $Cp^*(CO)_2(H)Mo{=}Si(H)Ar$ (δ 261.8).[6] A more closely related cationic silylyne from the Tilley group, [$Cp^*(^iPr_3P)(H)Os{\equiv}Si$(2,6-

$^{i}Pr_2C_6H_3$)][$HB(C_6F_5)_3$], was also prepared by hydride abstraction from an H-bearing silylene ($Cp^*(^{i}Pr_3P)(H)Os{=}Si(\mathbf{H})(2,6\text{-}^{i}Pr_2C_6H_3)$), though in that case a difference in chemical shift of 91 ppm was observed (δ 321 vs. δ 230, respectively).[8,13] It is apparent that base-stabilization in our system results in upfield ^{29}Si resonances for both silylene and silylyne species, compared to these examples, and may have a dampening effect on the change expected upon conversion between the two. The greater Si–Rh coupling constant in $\mathbf{2}^{\mathbf{Mes}}$ ($^{1}J_{Si\text{-}Rh}$ = 100.9 Hz) compared to $\mathbf{1}^{\mathbf{Mes}}$ ($^{1}J_{Si\text{-}Rh}$ = 52.4 Hz) also corroborates the abstraction of the Si–*H* leading to a postulated trigonal planar geometry about silicon. It is established that valence electron spin-spin coupling constants for group 14 elements are strongly governed by the "Fermi contact" term which is in turn related to hybridization (amount of *s*-character) of the atom participating in the bond.[19, 20] Assuming a relatively static geometry about rhodium, the increase in coupling constant can therefore be related to a change in hybridization about silicon from sp^3 to sp^2, as depicted in the resonance structure below (Scheme 5.4, top right).

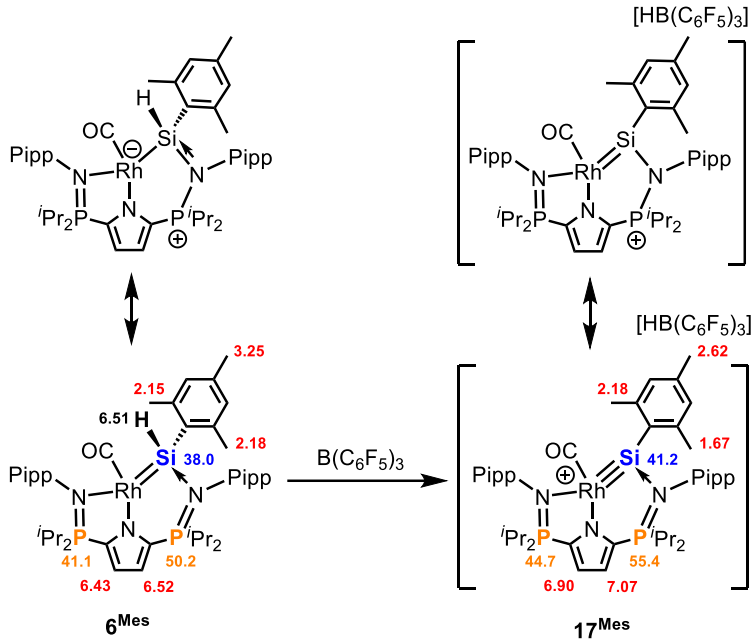

Scheme 5.4. Reaction between $\mathbf{6}^{\mathbf{Mes}}$ and $B(C_6F_5)_3$ to yield $\mathbf{17}^{\mathbf{Mes}}$. Canonical resonance structures that more accurately depict the influence of base-stabilization are shown, along with selected NMR chemical shifts (benzene-d_6, ppm, black = ^{1}H, blue = ^{29}Si, orange = ^{31}P).

Since the unidentified minor impurity was postulated to be due to a competing reaction pathway, the synthesis of $\mathbf{17}^{\mathbf{Mes}}$ was repeated in toluene solution at –35 °C, with slow addition (over 10 min) of the $B(C_6F_5)_3$ solution. Gratifyingly, this synthetic strategy selectively generated the base-stabilized silylyne species [κ^2-*L*(CO)Rh≡SiMes][HBCF], $\mathbf{17}^{\mathbf{Mes}}$ in analytical purity as confirmed by NMR spectroscopy (Figure 5.2 and Figure 5.3) and combustion analysis.

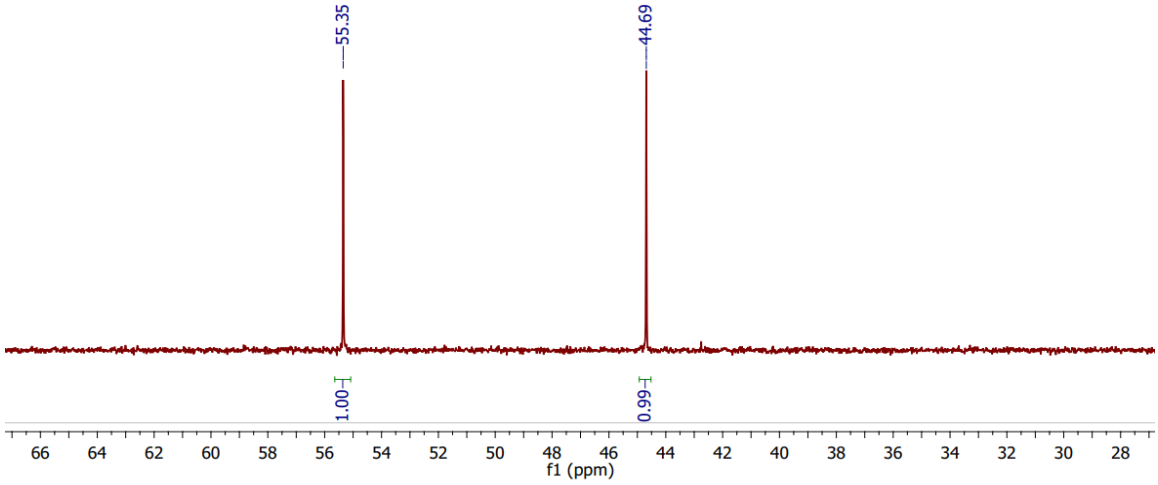

Figure 5.2. $^{31}P\{^{1}H\}$ NMR (283.5 MHz) spectrum of complex **17**$^{\mathbf{Mes}}$ in benzene-d_6 at 22 °C

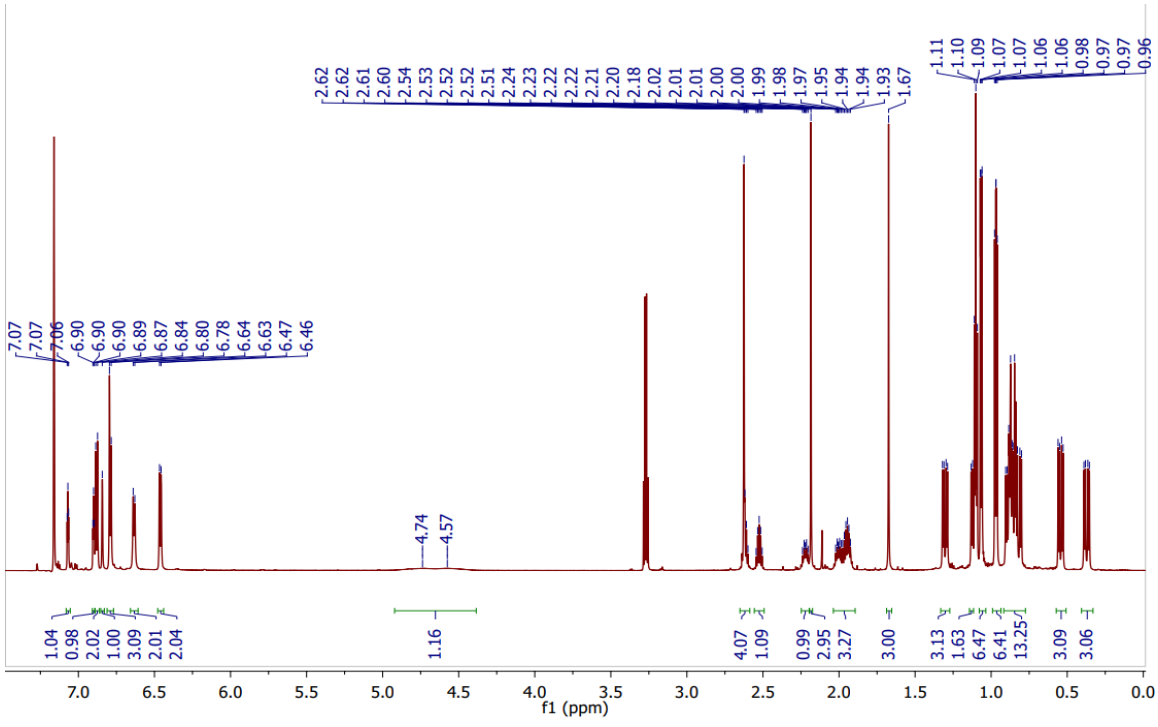

Figure 5.3. ^{1}H NMR (700 MHz) spectrum of complex **17**$^{\mathbf{Mes}}$ in benzene-d_6 at 22 °C.

Given the limited solubility of many ionic species in non-polar solvents, the aforementioned experiment was repeated in bromobenzene-d_5 solvent. Surprisingly, only low intensity resonances (<10% of total integrated) assigned to **17**$^{\mathbf{Mes}}$ were observed in the ^{31}P NMR spectrum (δ 55.1, 44.4

in C_6D_5Br *c.f.* δ 55.4, 44.7 in benzene-d_6). In addition, several other unidentified phosphorus-containing species were prominent, and the mixture rapidly became more complicated once the solution was warmed to ambient temperature. When portions of a sample of **17^{Mes}** prepared in toluene were dissolved in cold bromobenzene-d_5, major resonances attributed to **17^{Mes}** were initially visible but rapidly decomposed into multiple species similar to that described above within 30 minutes at ambient temperatures. Notably, when the remaining portion of the **17^{Mes}** sample was reconstituted in benzene-d_6, **17^{Mes}** was exclusively observed *via* multinuclear NMR spectroscopy. Since both solvents were rigorously dried and purified (See Experimental section for procedures) it is assumed that the observed decomposition in bromobenzene-d_5 is due to reaction with Br^- or Br•, or possibly self-annihilation facilitated by the enhanced polarity of the solvent.

Following the isolation of pure **17^{Mes}**, we turned our attention to the structurally related **2^{Ph}** in hope of demonstrating generality. Thus, silylene **2^{Ph}** was first allowed to react with $B(C_6F_5)_3$ at ambient temperature in benzene-d_6. Rather than the two 1:1 signals that would be anticipated for the formation of an unsymmetric silylyne analogous to **17^{Mes}**, the ^{31}P NMR spectrum exhibited a dominant resonance centered about δ 44.7 (*c.f.* δ 53.0, 43.5 in **2^{Ph}**), indicative of one C_{2v} or C_S-symmetric species. Given the similar ^{31}P NMR chemical shift, it is possible the identity of this species is related to the minor impurity observed in the synthesis of **17^{Mes}**. Interestingly, the ^{11}B and ^{19}F NMR spectra maintained diagnostic resonances for the $[HB(C_6F_5)_3]^-$ anion. Even more noteworthy is the fact that the ^1H NMR spectrum contains a triplet at δ 5.77 (J = 9.3 Hz, $^1J_{H\text{-}Si}$ = 300 Hz; *c.f.* δ 5.90, dd, $^2J_{H\text{-}Rh}$ = 11.1 Hz, $^3J_{H\text{-}P}$ = 5.4 Hz, $^1J_{H\text{-}si}$ = 183 Hz for **2^{Ph}**) attributed to a silicon bound hydrogen. The presence of an SiH seems to contradict the complete consumption of $B(C_6F_5)_3$, as well as the presence of a $[HB(C_6F_5)_3]^-$ anion, which is further corroborated by the broad ^1H signal centered at δ 4.63. Finally, the ^{29}Si NMR spectrum exhibits a single peak at δ –82.6, more than 100 ppm upfield of **2^{Ph}** (δ 54.6). The lone ^{31}P resonance, combined with the ^{29}Si chemical shift, are reminiscent of spectral signatures observed for previously observed transmetalation products

by our group, suggesting the *NNN*-pincer ligand has transferred from rhodium to silicon (Scheme 5.5, top).[14] This proposal is further supported by the lack of a discernable ^{13}C NMR signal for a rhodium carbonyl moiety, even when the reaction was performed using ^{13}C-labeled (κ^2-*L*(^{13}CO)Rh=Si(H)Ph), **^{13}C-2^{Ph}**.

While no direct comparisons in terms of structure and synthetic route were found in the literature, upfield ^{29}Si chemical shifts for base stabilized silylium cations have been reported. For example, Boudjouk *et al*. previously disclosed cationic hexacoordinate silicon (IV) species stabilized by neutral pentamethyldiethylenetriamine donors. Those compounds give rise to ^{29}Si chemical shifts between δ –108.7 and –130.2 with similarly large Si–H coupling constants ($^1J_{Si\text{-}H}$ = 358-380 Hz) (Scheme 5.5, bottom left).[21] Divalent [Cp*Si][HB(C_6F_5)$_3$] also exhibits a remarkably upfield ^{29}Si NMR shift of δ –398.8 (Scheme 5.5, bottom right).[22] Finally, it is well established within the field that significantly upfield resonances are expected for silicon atoms bearing high coordination numbers.[19] Unfortunately, the unbalanced stoichiometry, coupled with difficulties in unambiguously establishing connectivity using X-ray crystallography or NMR spectroscopy, render it impossible to be 100% confident of our assignment.

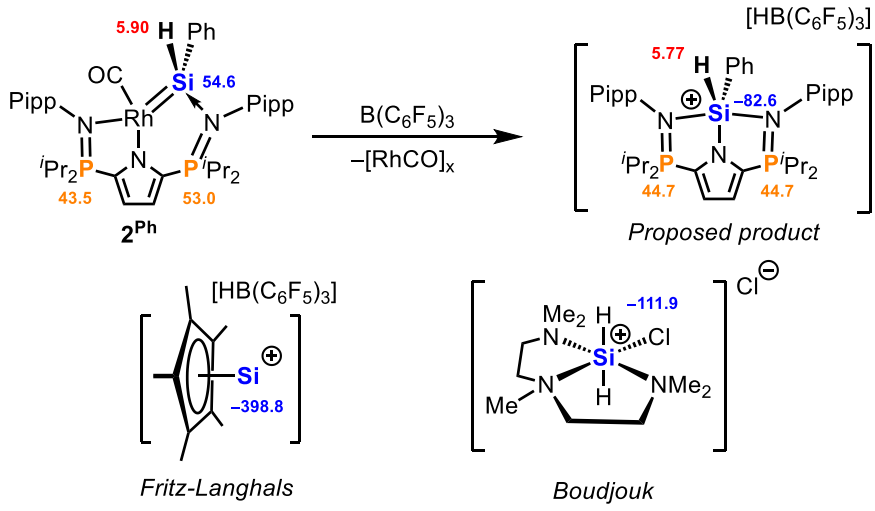

Scheme 5.5. Top: Proposed reaction between $\mathbf{2^{Ph}}$ and $B(C_6F_5)_3$, generating the transmetalated product κ^3-*L*Si(H)Ph. Selected NMR chemical shifts included for comparison (benzene-d_6, ppm, black = ^{1}H, blue = ^{29}Si, orange = ^{31}P). Bottom: Related structures by Fritz-Langhals and Boudjouk included for comparison of ^{29}Si NMR chemical shifts.

Since the oily nature of $\mathbf{17^{Mes}}$ precluded the growth of X-ray quality crystals, we sought to provide additional evidence for its identity by probing its reaction chemistry. Because [2+2] cycloaddition of alkynes and silylyne complexes has been well documented,[2] one equivalent of phenylacetylene (PhC≡CH) was added to silylyne $\mathbf{17^{Mes}}$ in benzene-d_6 solution at ambient temperature. Monitoring the reaction by NMR spectroscopy revealed rapid conversion to a new species with ^{31}P NMR resonances at δ 57.6 and 55.4 in a 1:1 ratio. Intriguingly, a small quantity of the same impurity observed during the formation of $\mathbf{17^{Mes}}$ at ambient temperature was found in the spectrum (δ 42.8). The ^{11}B NMR spectrum exhibited a signal at δ –15.2, as well as one at the expected chemical shift of δ –24.5. The ratio between these resonances varied across multiple syntheses (from approximately 1:1 to 1:8 by relative integration), as well as within the same sample at different times. The ^{1}H NMR spectrum retained key resonances attributed to the ligand, the mesityl group, and the alkyne phenyl; the alkyne C*H* resonance shifted characteristically downfield from δ 2.73 to 6.63. The carbonyl ^{13}C resonance was retained and appeared as a doublet at δ 185.2 ($^1J_{C\text{-}Rh}$ = 70.0

Hz). While the overlap of many unsaturated signals makes unambiguous assignment of the Rh–*C*(Ph)=*C*(H)–Si carbons difficult, no alkynyl peaks were observed between δ 50 and 100 (phenylacetylene resonates at δ 83.9 and 77.9). Finally, a single ^{29}Si NMR resonance was observed as a broad doublet centered at δ –52.9 (J = 13.6), consistent with what we propose to be the [2+2] cycloaddition product [κ^2-*L*(CO)Rh=Si(Mes)C(Ph)=C(H)][HB(C$_6$F$_5$)$_3$], **18^{Mes}** (Scheme 5.6a). It should be noted that the absolute regioselectivity of complex **3^{Mes}** is tentatively assigned in line with literature examples from Hashimoto, as well as the known electrophilicity of the silicon atom in these systems, due to the lack of a solid state structure.

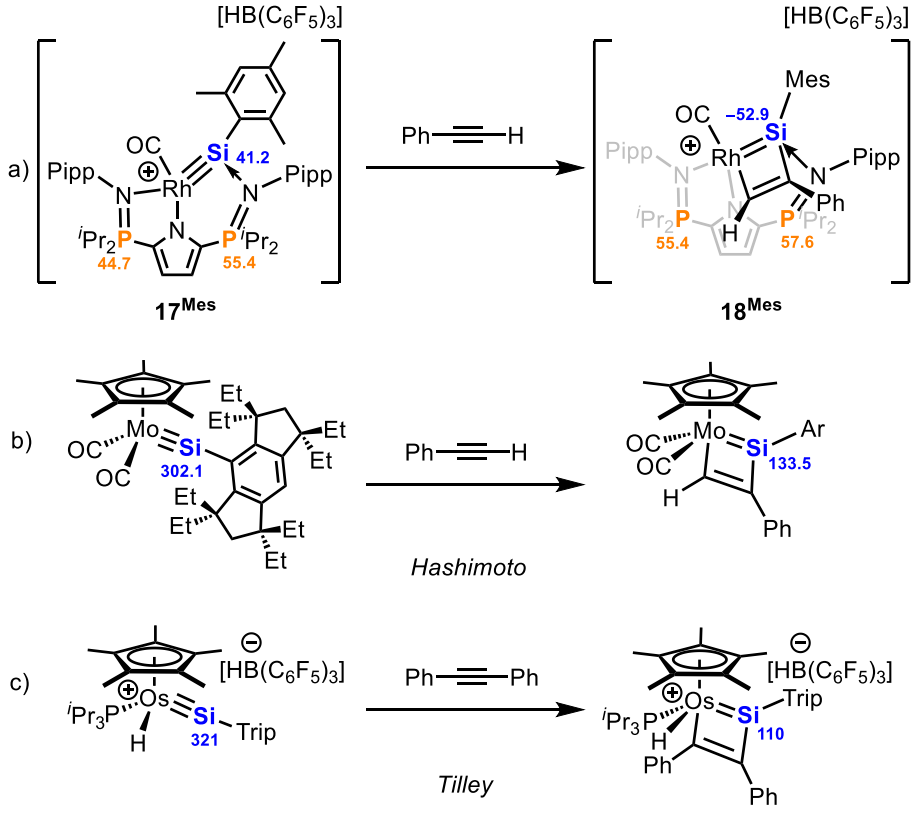

Scheme 5.6. a) Reaction of **17^{Mes}** and phenylacetylene to yield the [2+2] addition product **18^{Mes}**. Selected NMR data are included for comparison (benzene-d_6, ppm, blue = ^{29}Si, orange = ^{31}P). b) Work by Hashimoto *et al*. demonstrating [2+2] cycloaddition of phenylacetylene across Mo≡Si. c) [2+2] cycloaddition of diphenylacetylene across the Os≡Si bond of a cationic silylyne complex, reported by Tilley *et al*.

The change in the ^{29}Si NMR chemical shift between **17^{Mes}** and **18^{Mes}** ($\Delta\delta$ = 90.9) is less dramatic, but nonetheless, comparable to that observed ($\Delta\delta$ = 168.6) between Cp*(CO)$_2$Mo=Si(Ar)C(Ph)=CH (δ 133.5) and Cp*(CO)$_2$Mo≡Si(Ar) (δ 302.1) by Hashimoto *et al*. (Scheme 5.6b).[6] In comparison to the fast reaction between **17^{Mes}** and phenylacetylene (t < 10 min), Hashimoto's group 6 complexes require hours to days, depending on the identity of the metal centre (Mo >> W).[6,18] Rationalization for the difference in reaction time was attributed to Mo≡Si having greater polarization, and consequently, Si electrophilicity, than W≡Si. Given the cationic nature of complex **17^{Mes}**, and higher Pauli electronegativity of Rh compared to Mo (both 4d metals), a larger polarization, and hence, more electrophilic silicon, may explain the rapid reaction time.

Tilley reported that terminal alkynes can add C–H across the Os≡Si triple bond of [Cp*(^{i}Pr$_3$P)(H)Os≡SiTrip][HB(C$_6$F$_5$)$_3$], using deuterium labelling experiments to prove that oxidative addition at the metal center was not the first step in the process.[8] While no ^{13}C nor ^{29}Si NMR resonances were reported, reaction with internal alkynes yielded analytically pure [2+2] addition products which were fully characterized by multinuclear NMR spectroscopy. Notably, reaction of [Cp*(^{i}Pr$_3$P)(H)Os≡SiTrip][HB(C$_6$F$_5$)$_3$] (δ 321) with diphenylacetylene afforded [Cp*(^{i}Pr$_3$P)(H)Os=Si(Trip)C(Ph)=C(Ph)][HB(C$_6$F$_5$)$_3$] which exhibited a ^{29}Si signal 211 ppm upfield of the silylyne starting material (δ 110; $\Delta\delta$ = 211) (Scheme 5.6c).

When the **18^{Mes}** solution was left at ambient temperature for two days, the relative integration of the impurity observed *via* ^{31}P NMR spectroscopy (δ 42.8) grew relative to the major product. In an attempt to push conversion, the solution was heated at 50 °C for five days. While minor resonances attributed to **6^{Mes}** were still visible in the ^{31}P spectrum, new signals attributed to silylyne complex **17^{Mes}** were also observed, implying that the postulated [2+2] cycloaddition may be reversible. Currently, the identity of the vexatious impurity remains unknown, and the potential non-innocence of the [*H*B(C$_6$F$_5$)$_3$]$^-$ hydride is being investigated.

5.3. Conclusions

In summary, we have prepared the first example of a group 9 silylyne complex, **17^{Mes}**. While the base-stabilization of this species results in upfield shifted ^{29}Si resonances compared to terminal examples by Hashimoto and Tilley, similar trends (substantial downfield shift from silylene to silylyne, upfield shift from silylyne to cycloaddition product) were observed. Hence, this silylyne serves as a unique point of comparison to known group 6 and 8 examples and fills an important gap in the series of rhodium complexes established by Widemann *et al*.

5.4. Experimental

General Considerations

All air- and moisture-sensitive manipulations were carried out using vacuum line, Schlenk and cannula techniques, or in an MBraun inert atmosphere (argon) glove box unless otherwise noted. All glassware was stored in a pre-heated (110 °C) oven or flame-dried prior to use. Solvents used for air-sensitive procedures were purified using an MBraun solvent purification system (SPS), dried in PTFE-sealed glass vessels over sodium benzophenone ketyl (THF, diethylether, pentane, and toluene), and distilled in small batches over 4 Å molecular sieves in PTFE-sealed glass vessels for use in the glove box. Benzene-d_6 was dried over sodium benzophenone ketyl, degassed with three freeze-pump-thaw cycles, distilled *in vacuo* and stored over 4 Å molecular sieves in PTFE-sealed glass vessels under argon. Bromobenzene-d_5 was dried over CaH_2, degassed with three freeze-pump-thaw cycles, distilled *in vacuo* and stored over 4 Å molecular sieves in PTFE-sealed glass vessels under argon. $MesSiH_3$ was prepared according to literature procedures.[14] Phenyl acetylene was purchased from Sigma Aldrich, dried over 4 Å molecular sieves and degassed by three freeze pump thaw cycles before being stored in an inert atmosphere glove box in vials with Teflon lined caps. Complexes $\mathbf{2^{Ph}}$ and $\mathbf{6^{Mes}}$ were synthesized according to previous literature procedures.[14,15] Unless otherwise noted, all NMR spectra were recorded at ambient temperature with a Bruker Avance III NMR spectrometer (700.44 MHz for ^{1}H, 224.63 MHz for ^{11}B, 176.13 MHz for ^{13}C, 139.10 MHz for ^{29}Si, and 283.54 MHz for ^{31}P) or a Bruker Avance II (300.13 MHz for ^{1}H, 96.25 MHz for ^{11}B, 282.43 MHz for ^{19}F). All ^{1}H, ^{29}Si, and ^{13}C NMR chemical shifts are reported in ppm relative to $SiMe_4$ using the residual ^{1}H (benzene-d_6: 7.16 ppm) and ^{13}C (benzene-d_6: 128.06 ppm) chemical shifts of the solvent as reference. ^{11}B NMR chemical shifts were referenced externally to $BF_3{\cdot}Et_2O$ (δ 0.0). ^{31}P NMR chemical shifts were referenced to external 85% H_3PO_4 in H_2O (δ 0.0). NMR data are reported as follows: chemical shift, multiplicity (s = singlet, d = doublet, t = triplet, q = quartet, quin = quintet, sp = septet, m = multiplet, br = broad,

ov = overlapping), coupling constant(s) (Hz), integration (for ^{1}H, ^{19}F, and ^{31}P), assignment. Assignment of resonances was supplemented by ^{1}H–^{1}H COSY, ^{13}C{^{1}H} APT, and ^{1}H–^{13}C{^{1}H} HSQC/HMBC experiments.

Elemental analyses (%CHN) were conducted at the University of Lethbridge on an Elementar Americas Vario MicroCube Analyzer (C, H, N, O, S capabilities) using bulk recrystallized compounds. "Universal Combustion Additive", purchased from Elemental Microanalysis, was added to all standards, blanks, and samples.

Synthesis and Characterization of New Compounds

Preparation of [κ^2-*L*(CO)Rh≡SiMes][HB(C$_6$F$_5$)$_3$], 17^{Mes}. Recrystallized **6^{Mes}** (50.0 mg, 0.059 mmol) was dissolved in 5 mL of toluene and placed in a –35 °C freezer for 30 minutes. In a separate flask, tris(pentafluorophenyl)borane (BCF) (30.3 mg, 0.060 mmol) was dissolved in 2 mL of toluene and then added to a stirring solution of cold **6^{Mes}** dropwise over 5 minutes. The mixture was stirred for an additional 5 minutes, changing from a light orange to dark brown in color. After removal of the solvent under reduced pressure, the product was washed with 3 × 0.5 mL of pentane during which the oily paste gradually transitioned into a chunky solid (70.7 mg, 88.1% yield). Anal Calcd. for $C_{62}H_{64}BF_{15}N_3OP_2RhSi$: C, 54.92; H, 4.76; N, 3.10. Found: C, 55.38; H, 4.65; N, 3.72.

^{1}H NMR (benzene-*d*$_6$, 23 °C): δ 7.07 (ov dd, $^{3}J_{HH}$ = $^{3}J_{HP}$ = 3.35 Hz, 1H, 3,4-pyrrole C*H*); 6.90 (ov dd, $^{3}J_{HH}$ = $^{3}J_{HP}$ = 3.31 Hz, 1H, 3,4-pyrrole C*H*); 6.88 (d, $^{3}J_{HH}$ = 8.31 Hz, 2H, Pipp Ar *H*); 6.84 (s, 1H, Mes Ar *H*); 6.79 (ov s, 1H, Mes Ar *H*); 6.79 (ov d, $^{3}J_{HH}$ = 8.31 Hz, 2H, Pipp Ar *H*); 6.63 (d, $^{3}J_{HH}$ = 7.48 Hz, 2H, Pipp Ar *H*); 6.46 (d, $^{3}J_{HH}$ = 7.14 Hz, 2H, Pipp Ar *H*); 4.65 (br m, 1H, *H*BCF); 2.62 (ov s, 3H, Mes C*H*$_3$); 2.62 (ov sp, $^{3}J_{HH}$ = 6.92 Hz, 1H, Pipp C*H*(CH$_3$)$_2$); 2.22 (m, 1H, PC*H*(CH$_3$)$_2$); 2.18 (s, 3H, Mes C*H*$_3$); 2.00 (m, 1H, PC*H*(CH$_3$)$_2$); 1.95 (ov sp, 2H, PC*H*(CH$_3$)$_2$); 1.67 (s, 3H, Mes C*H*$_3$); 1.30 (dd, $^{3}J_{HH}$ = 6.97, $^{3}J_{HP}$ = 16.62 Hz, 3H, PCH(C*H*$_3$)$_2$); 1.11 (ov dd, $^{3}J_{HH}$ = 7.13 Hz, 3H, PCH(C*H*$_3$)$_2$); 1.07 (dd, *J* = 1.43 Hz, $^{3}J_{HH}$ = 6.92, 6H Hz, Pipp CH(C*H*$_3$)$_2$); 0.97 (dd, *J* = 5.40 Hz, $^{3}J_{HH}$ = 6.90 Hz, Pipp CH(C*H*$_3$)$_2$); 0.90-0.80 (ov m, 12 H, PCH(C*H*$_3$)$_2$); 0.54 (dd, $^{3}J_{HH}$ =

6.98, $^{3}J_{HP}$ = 16.36 Hz, 3H, PCH(CH_3)$_2$); 0.37 (dd, $^{3}J_{HH}$ = 7.09, $^{3}J_{HP}$ = 18.09 Hz, 3H, PCH(CH_3)$_2$). **^{13}C{^{1}H} NMR (benzene-d_6, 23 ºC):** δ 189.9 (d, $^{1}J_{C\text{-}Rh}$ = 81.8 Hz, Rh–*C*O); 150.0 (br s, HBCF Ar *C*); 149.6 (s, Pipp Ar *C*); 148.7 (br s, HBCF Ar *C*); 146.5 (s, Mes Ar *C*); 144.4 (s, Pipp Ar *C*); 143.0 (s, Pipp Ar *C*); 141.0 (s, Mes Ar *C*); 140.0 (s, Mes Ar *C*); 139.2 (br s, HBCF Ar *C*); 137.9 (br s, HBCF Ar *C*); 136.6 (br s, HBCF Ar *C*); 133.9 (d, *J* = 5.2 Hz, Mes Ar *C*); 132.9 (s, Pipp Ar *C*); 130.8 (s, Mes Ar *C*H); 130.6 (s, Mes Ar *C*H); 130.3 (d, *J* = 2.9 Hz, Pipp Ar *C*H); 128.8 (ov dd, *J* =6.1 Hz, 2,5-pyrrole *C*); 127.7 (s, Pipp Ar *C*H); 127.6 (d, *J* = 6.5 Hz, Pipp Ar *C*H); 127.3 (s, Pipp Ar *C*H); 125.8 (dd, $^{2}J_{CP}$ = 15.7 Hz, $^{3}J_{CP}$ = 4.8 Hz, 3,4-pyrrole *C*H); 122.3 (dd, $^{2}J_{CP}$ = 16.4 Hz, $^{3}J_{CP}$ = 11.6 Hz, 3,4-pyrrole *C*H); 118.7 (dd, $^{1}J_{CP}$ = 116.4 Hz, $^{4}J_{CP}$ = 7.4 Hz, 2,5-pyrrole *C*); 33.8 (s, Pipp *C*H(CH$_3$)$_2$); 33.6 (s, Pipp *C*H(CH$_3$)$_2$); 30.5 (d, $^{1}J_{CP}$ = 60.4 Hz, P*C*H(CH$_3$)$_2$); 29.0 (s, Mes *C*H$_3$); 26.9 (d, $^{1}J_{CP}$ = 51.3 Hz, P*C*H(CH$_3$)$_2$); 26.8 (d, $^{1}J_{CP}$ = 53.2 Hz, P*C*H(CH$_3$)$_2$); 24.1 (d, *J* = 10.4 Hz, Pipp CH(*C*H$_3$)$_2$); 23.8 (d, *J* = 2.0 Hz, Pipp CH(*C*H$_3$)$_2$); 22.7 (d, $^{1}J_{CP}$ = 54.0 Hz, P*C*H(CH$_3$)$_2$); 21.5 (s, Mes *C*H$_3$); 21.1 (s, Mes *C*H$_3$); 16.7 (d, $^{2}J_{CP}$ = 4.4 Hz, PCH(*C*H$_3$)$_2$); 16.6 (br s, PCH(*C*H$_3$)$_2$); 15.9 (br s, PCH(*C*H$_3$)$_2$); 15.8 (d, $^{2}J_{CP}$ = 3.9 Hz, PCH(*C*H$_3$)$_2$); 15.0 (d, $^{2}J_{CP}$ = 3.3 Hz, PCH(*C*H$_3$)$_2$); 14.9 (br s, PCH(*C*H$_3$)$_2$). **^{31}P{^{1}H} NMR (283.42 MHz, benzene-d_6, 23 ºC):** δ 55.4 (s, 1P, *P*–N–Rh); 44.7 (s, 1P, *P*–N–B). **^{11}B{^{1}H} NMR (224.63 MHz, benzene-d_6, 23 °C):** δ –25.5 (br s). **^{19}F{^{1}H} NMR (282.43 MHz, benzene-d_6, 23 °C):** δ –132.3 (d, $^{3}J_{FF}$ = 20.1 Hz, 2F, *ortho*-B(C$_6$*F*$_5$)); –163.9 (t, $^{3}J_{FF}$ = 20.1 Hz, 1F, *para*-B(C$_6$*F*$_5$)), –166.7 (ov dd, 2F, *meta*-B(C$_6$*F*$_5$)). **^{29}Si{^{1}H} NMR (139.10 MHz, benzene-d_6, 23 °C):** δ 41.2 (d, $^{1}J_{Si\text{-}Rh}$ = 100.76 Hz, Rh–*Si*–N).

Preparation of [κ^2-L(CO)Rh=Si(Mes)C(Ph)=C(H)][HB(C$_6$F$_5$)$_3$], Compound 18^{Mes}. Recrystallized **6^{Mes}** (50.0 mg, 0.059 mmol) was dissolved in 5 mL of toluene and placed in a –35 °C freezer for 30 minutes. In a separate flask, tris(pentafluorophenyl)borane (B(C$_6$F$_5$)$_3$) (30.3 mg, 0.060 mmol) was dissolved in 2 mL of toluene and then added to a stirring solution of cold **6^{Mes}** dropwise over 5 minutes. The mixture was stirred for an additional 5 minutes, changing from a light orange to dark brown in color. Phenylacetylene (6.0 mg, 0.060 mmol) was then dissolved in

a separate 2 mL of toluene and added dropwise to the *in situ* generated **17^{Mes}** solution over a period of 5 minutes. After addition of phenylacetylene was completed, the solution was quickly placed under reduced pressure to remove solvent. The resulting residue was quickly washed with 3 × 1 mL of pentane, resulting in rapid solidification to a light brown solid that could be manipulated into 63 mg of a fine, beige powder (Yield: 78.4%) of **18^{Mes}**.

^{1}H NMR (benzene-d_6, 23 °C): δ 7.47 (d, $^{3}J_{HH}$ = 7.4 Hz, 1H, Pipp Ar *H*); 7.27 (d, *J* = 5.33 Hz, 1H, Pipp Ar *H*); 7.15-7.09 (ov m, 4H, Ph Ar *H*, Pipp Ar *H*); 7.04 (dd, *J* = 7.6, 1.7 Hz, 2H, Pipp Ar *H*); 6.96 (dd, *J* = 7.8, 1.7 Hz, 2H, Pipp Ar *H*); 6.94-6.90 (ov m, 3H, Ph Ar *H*, Pipp Ar *H*); 6.81 (t, $^{3}J_{HP}$ = $^{3}J_{HH}$ = 3.6 Hz, 1H, 3,4-pyrrole C*H*); 6.73 (s, 1H, Mes C*H*); 6.69 (t, $^{3}J_{HP}$ = $^{3}J_{HH}$ = 3.6 Hz, 1H, 3,4-pyrrole C*H*); 6.63 (s, 1H, C≡C*H*); 6.36 (s, 1H, Mes C*H*); 4.60 (br m, 1H, *H*B(C_6F_5)$_3$); 3.15 (s, 3H, Mes CH_3); 2.62 (sp, $^{3}J_{HH}$ = 6.8 Hz, 1H, Pipp C*H*(CH_3)$_2$); 2.55 (sp, $^{3}J_{HH}$ = 6.8 Hz, 1H, Pipp C*H*(CH_3)$_2$); 2.41 (ov m, 1H, PC*H*(CH_3)$_2$); 2.16-2.05 (ov m, 3H, PC*H*(CH_3)$_2$); 1.98 (s, 3H, Mes CH_3); 1.95 (s, 3H, Mes CH_3); 1.06 (dd, $^{3}J_{HH}$ = 6.9 Hz, *J* = 3.4 Hz, 6H, Pipp CH(CH_3)$_2$); 1.01 (ov dd, $^{3}J_{HH}$ = 6.9 Hz, *J* = 2.3 Hz, 6H, Pipp CH(CH_3)$_2$); 1.01 (ov dd, $^{3}J_{HH}$ = 7.12 Hz, 3H, PCH(CH_3)$_2$); 0.98 (dd, $^{3}J_{HH}$ = 7.12 Hz, $^{3}J_{HP}$ = 17.4 Hz, 3H, PCH(CH_3)$_2$); 0.90 (dd, $^{3}J_{HH}$ = 7.33 Hz, $^{3}J_{HP}$ = 18.0 Hz, 3H, PCH(CH_3)$_2$); 0.84-0.75 (ov m, 9H, PCH(CH_3)$_2$); 0.68 (dd, $^{3}J_{HH}$ = 7.2 Hz, $^{3}J_{HP}$ = 16.0 Hz, 3H, PC*H*(CH_3)$_2$); 0.52 (dd, $^{3}J_{HH}$ = 7.09 Hz, $^{3}J_{HP}$ = 16.8 Hz, 3H, PC*H*(CH_3)$_2$). **^{31}P{^{1}H} NMR (283.42 MHz, benzene-d_6, 23 ºC):** δ 57.6 (s, 1P, *P*–N–Rh); 55.4 (s, 1P, *P*–N–Si). **^{11}B{^{1}H} NMR (224.63 MHz, benzene-d_6, 23 °C):** δ –15.3 (br s); –25.5 (br s). **^{19}F{^{1}H} NMR (282.43 MHz, benzene-d_6, 23 °C):** δ –132.5 (d, $^{3}J_{FF}$ = 20.1 Hz, 2F, *ortho*-B(C_6F_5)); –164.2 (t, $^{3}J_{FF}$ = 20.1 Hz, 1F, *para*-B(C_6F_5)), –166.7 (ov dd, 2F, *meta*-B(C_6F_5)). **^{29}Si{^{1}H} NMR (139.10 MHz, benzene-d_6, 23 °C):** δ –52.9 (br d, $^{1}J_{Si\text{-}Rh}$ = 12.7 Hz, Rh–*Si*–N).

5.5. References

(1) Hashimoto, H.; Nagata, K. Transition-metal Complexes with Triple Bonds to Si, Ge, Sn, and Pb and Relevant Complexes. *Chem. Lett.* **2021**, *50*, 778-787. DOI: 10.1246/cl.200872.

(2) Hashimoto, H.; Tobita, H. Recent advances in the chemistry of transition metal–silicon/germanium triple-bonded complexes. *Coord. Chem. Rev.* **2018**, *355*, 362-379. DOI: 10.1016/j.ccr.2017.09.023.

(3) (a) Saini, S.; Agarwal, A.; Bose, S. K. Transition metal chemistry of heavier group 14 congener triple-bonded complexes: syntheses and reactivity. *Dalton Trans.* **2020**, *49*, 17055-17075. DOI: 10.1039/D0DT03378; (b) B. Balázs, G.; Gregoriades, L. J.; Scheer, M. Triple Bonds between Transition Metals and the Heavier Elements of Groups 14 and 15. *Organometallics* **2007**, *26*, 3058-3075. DOI: 10.1021/om070108o.

(4) (a) Filippou, A. C.; Baars, B.; Chernov, O.; Lebedev, Y. N.; Schnakenburg, G. Silicon–Oxygen Double Bonds: A Stable Silanone with a Trigonal-Planar Coordinated Silicon Center. *Angew. Chem. Int. Ed.* **2014**, *53*, 565-570. DOI: 10.1002/anie.201308433; (b) Filippou, A. C.; Ghana, P.; Chakraborty, U.; Schnakenburg, G. Manganese–Tin Triple Bonds: A New Synthetic Route to the Manganese Stannylidyne Complex Cation *trans*-$[H(dmpe)_2Mn{\equiv}Sn(C_6H_3\text{-}2,6\text{-}Mes_2)]^+$ (dmpe = $Me_2PCH_2CH_2PMe_2$, Mes = 2,4,6-Trimethylphenyl). *J. Am. Chem. Soc.* **2013**, *135*, 11525-11528. DOI: 10.1021/ja406290t; (c) Filippou, A. C.; Hoffmann, D.; Schnakenburg, G. Triple bonds of niobium with silicon, germaniun and tin: the tetrylidyne complexes $[(\kappa^3\text{-tmps})(CO)_2Nb{\equiv}E–R]$ (E = Si, Ge, Sn; tmps = $MeSi(CH_2PMe_2)_3$; R = aryl). *Chem. Sci. J.* **2017**, *8*, 6290-6299. DOI: 10.1039/C7SC02708G; (d) Ghana, P.; Arz, M. I.; Chakraborty, U.; Schnakenburg, G.; Filippou, A. C. Linearly Two-Coordinated Silicon: Transition Metal Complexes with the Functional Groups M≡Si—M and M═Si═M. *J. Am. Chem. Soc.* **2018**, *140*, 7187-7198. DOI: 10.1021/jacs.8b02902.

(5) Maurer, L. R.; Rump, J.; Filippou, A. C. The Electronic Nature of Cationic Group 10 Ylidyne Complexes. *Inorganics* **2023**, *11*, 129. DOI:10.3390/inorganics11030129

(6) Hashimoto, H.; Watanabe, K.; Yoshimoto, T.; Hayakawa, N.; Matsuo, T.; Tobita, H. Neutral Silylyne Complex of Molybdenum: Synthesis, Properties, and Access to Silaiminoacyl Complexes via [2+3] Cycloaddition. *Chem. Eur. J.* **2023**, *29*, e202302470. DOI: 10.1002/chem.202302470.

(7) (a) Matsuoka, M.; Nagata, K.; Ohno, R.; Matsuo, T.; Tobita, H.; Hashimoto, H. Neutral Chromium Complex with a Cr≡Si Triple Bond: Synthesis and Photoinduced H−H and Benzene C−H Bond Activation. *Chem. Eur. J.* **2024**, *30*, e202303765. DOI: 10.1002/chem.202303765; (b) Nagata, K.; Omura, H.; Hashimoto, H. Π-Character of Chromium Germylyne Complex in the Reactions with Enone, Butadiene, and Alkynes: Formation of Germacycles through [2+4] Cycloaddition with Conjugated Molecules. *Chem.: Asian J.* **2023**, *18*, e202300801. DOI: 10.1002/asia.202300801.

(8) Hayes, P. G.; Xu, Z.; Beddie, C.; Keith, J. M.; Hall, M. B.; Tilley, T. D. The Osmium–Silicon Triple Bond: Synthesis, Characterization, and Reactivity of an Osmium Silylyne Complex. *J. Am. Chem. Soc.* **2013**, *135*, 11780-11783. DOI: 10.1021/ja406799y.

(9) Mork, B. V.; Tilley, T. D. Multiple Bonding Between Silicon and Molybdenum: A Transition-Metal Complex with Considerable Silylyne Character. *Angew. Chem. Int. Ed.* **2003**, *42*, 357-360. DOI: 10.1002/anie.200390116.

(10) Queen, J. D.; Phung, A. C.; Caputo, C. A.; Fettinger, J. C.; Power, P. P. Metathetical Exchange between Metal–Metal Triple Bonds. *J. Am. Chem. Soc.* **2020**, *142*, 2233-2237. DOI: 10.1021/jacs.9b13604. Simons, R. S.; Power, P. P. $(\eta^5\text{-}C_5H_5)(CO)_2MoGeC_6H_3\text{-}2,6\text{-}Mes_2$: A Transition-Metal Germylyne Complex. *J. Am. Chem. Soc.* **1996**, *118*, 11966-11967. DOI: 10.1021/ja963132u.

(11) Widemann, M.; Eichele, K.; Schubert, H.; Sindlinger, C. P.; Klenner, S.; Pöttgen, R.; Wesemann, L. Synthesis and Hydrogenation of Heavy Homologues of Rhodium Carbynes: $[(Me_3P)_2(Ph_3P)Rh{\equiv}E\text{-}Ar^*]$ (E=Sn, Pb). *Angew. Chem. Int. Ed.* **2021**, *60*, 5882-5889. DOI: 10.1002/anie.202015725.

(12) Keil, P. M.; Hadlington, T. J. Accessing cationic tetrylene-nickel(0) systems featuring donor–acceptor E–Ni triple bonds (E = Ge, Sn). *Chem. Commun.* **2022**, *58*, 3011-3014. DOI: 10.1039/D2CC00422D.

(13) Hayes, P. G.; Gribble, C. W.; Waterman, R.; Tilley, T. D. A Hydrogen-Substituted Osmium Stannylene Complex: Isomerization to a Metallostannylene Complex via an Unusual α-Hydrogen Migration from Tin to Osmium. *J. Am. Chem. Soc.* **2009**, *131*, 4606-4607. DOI: 10.1021/ja901050m.

(14) Hsiang, S.-J.; Hayes, P. G. Rhodium-Mediated Dehydrogenation of Hydroboranes and Group 14 Compounds: Base-Stabilized Silylene and Germylene Complexes vs. Transmetalation. *Chem. Eur. J.* **2024**, *30*, e202302925. DOI: https://doi.org/10.1002/chem.202302925.

(15) MacNeil, C. S.; Hayes, P. G. An H-Substituted Rhodium Silylene. *Chem. Eur. J.* **2019**, *25*, 8203-8207. DOI: 10.1002/chem.201901882.

(16) Fukuda, T.; Hashimoto, H.; Tobita, H. NHC-induced conversion of a W–Ge double bond into the triple bond through formation of W–Ge single and double bonded intermediates. *J. Organomet. Chem.* **2017**, *848*, 89-94. DOI: 10.1016/j.jorganchem.2017.07.027.

(17) Fukuda, T.; Yoshimoto, T.; Hashimoto, H.; Tobita, H. Synthesis of a Tungsten–Silylyne Complex via Stepwise Proton and Hydride Abstraction from a Hydrido Hydrosilylene Complex. *Organometallics* **2016**, *35* (7), 921-924. DOI: 10.1021/acs.organomet.6b00095.

(18) Yoshimoto, T.; Hashimoto, H.; Ray, M.; Hayakawa, N.; Matsuo, T.; Chakrabarti, J.; Tobita, H. Products of [2+2] Cycloaddition between a W≡Si Triple-bonded Complex and Alkynes: Isolation, Structure, and Non-classical Bonding Interaction. *Chem. Lett.* **2020**, *49*, 311-314. DOI: 10.1246/cl.190952.

(19) Marsmann, H. C. NMR Spectroscopy, 29Si. In *Encyclopedia of Spectroscopy and Spectrometry (Third Edition)*, Lindon, J. C., Tranter, G. E., Koppenaal, D. W. Eds.; Academic Press, **2017**; pp 284-293.

(20) Pettinari, C. NMR Spectroscopy, Heteronuclei, Ge, Sn, Pb. In *Encyclopedia of Spectroscopy and Spectrometry (Third Edition)*, Lindon, J. C., Tranter, G. E., Koppenaal, D. W. Eds.; Academic Press, **2017**; pp 330-341.

(21) Kim, B.-K.; Choi, S.-B.; Kloos, S. D.; Boudjouk, P. Synthesis and Characterization of New Cationic Hexacoordinate Silanes. *Inorg. Chem.* **2000**, *39*, 728-731. DOI: 10.1021/ic990415p.

(22) Fritz-Langhals, E. Silicon(II) Cation $Cp^*Si:^+ X^-$: A New Class of Efficient Catalysts in Organosilicon Chemistry. *Org. Process Res. Dev.* **2019**, *23*, 2369-2377. DOI: 10.1021/acs.oprd.9b00260.

Chapter 6. Conclusions and Future Work

6.1. Conclusions

The dehydrogenation of group 13 and 14 substrates has been demonstrated using a metal-ligand cooperative approach by pairing electron rich rhodium (I) and an *NNN*-pincer ligand featuring strongly σ- and π-donating phosphinimine groups. This thesis expanded upon previous work by Dr. Connor MacNeil that juxtaposed the reactivity of *L*Rh(CO) and *L*Rh(COE) with primary and secondary silanes which led to dehydrogenation *vs.* oxidative addition. An expanded substrate scope for the dehydrogenation methodology was established while also presenting rich reaction chemistry with the resulting silylene and borylene complexes.

In Chapter 2, the ligand-assisted dehydrogenation of primary aryl boranes was described. With respect to substrate scope, this work complements existing publications, supporting the hypothesis that only *ortho*-substituted aryl boranes have sufficient steric bulk to induce borylene formation.[1] A key intermediate, κ^2-*L*(CO)Rh(^{meta}Xyl^{F}BH$_2$), compound **4**, was identified whereby the primary borane was captured by the Lewis basic phosphinimine donor of the pincer ligand in a manner comparable to Lewis acid/base adduct formation. This finding provides additional evidence that participation of the pincer ligand in our dehydrogenative process is not limited to merely coordination/dissociation steps analogous to common phosphine ligands, but rather, ligand-substrate interaction, and ultimately, activation. Weak interaction between the rhodium center and the MesB*H*$_2$ hydrogens was suggested by the ^{1}H NMR signal attributed to them collapsing into two separate resonances at low temperatures (δ 3.9 (B–*H*); δ –9.8 (Rh–*H*–B)), which supports that oxidative addition of the B–H bond is an operative step in our dehydrogenation pathway. Finally, this first foray into group 13 substrates also included reaction chemistry with pinacol, a proof of concept demonstration of formal borylene transfer to yield dehydrogenative coupling products of the form MesBPin. As a whole, this chapter and the publication it was based on, serves to provide

an alternative route to transition metal borylene species.[2] The details on substrate scope, as well as the isolation of key intermediates, substantiated by computations, provided a better understanding of the electronic structure and formation of these relatively under-investigated compounds. The base-stabilized borylene complex **3**, κ^2-*L*(CO)Rh(BMes), also serves as a thermally stable platform from which rich reactivity was demonstrated in later chapters.

In Chapter 3, attention was turned toward the heavier group 14 congeners of transition metal carbene complexes. While the literature is evidently replete with examples of carbon engaging in multiple-bonding interactions with various transition metals, it is well established that silicon, germanium, and tin are much more reluctant to participate in similar bonding modes. This publication serves to provide a more comprehensive investigation into the substate scope of our dehydrogenation platform reported in the initial communication from Dr. Connor MacNeil, which focused on phenylsilane ($PhSiH_3$) and diphenylsilane (Ph_2SiH_2).[3] Notably, rare examples of transition metal silylene and germylene species bearing alkyl substituents were isolated and characterized which we propose to only be possible due to the stabilization provided by our internal Lewis base. This added advantage may guide others in their experimental design, either through similar incorporation of internal Lewis bases, or use of external Lewis bases like 4-dimethylaminopyridine (DMAP) to aid the isolation of alkyl-substituted silylene/germylene species. As a follow-up to Chapter 2, additional details regarding the reaction of monocarbonyl rhodium complex **1**, *L*Rh(CO), and *meta*-substituted aryl boranes was provided, describing a transmetalation process that occurs when dehydrogenation is not favorable. Specifically, a solid-state structure, as well as independent synthesis of the transmetalated product, κ^2-*L*B(H)Mes, compound **8**, confirmed migration of the *NNN*-pincer ligand from rhodium to boron. Spectroscopic parallels can be drawn to the products observed *in situ* when reacting **1** with mesityl germane ($MesGeH_3$) and diphenyl tin (Ph_2SnH_2) wherein dehydrogenation did not occur. Lastly, use of the silylene and germylene complexes as main group $:SiR_2$/$:GeR_2$ synthons was demonstrated once

more by reaction with pinacol. In this case, however, catalytic release of the dehydrogenative coupling products was able to be presented, showing commercial utility for transition metal tetrylenes.

While preliminary reactions with pinacol provided a fundamental starting point for probing the reaction chemistry of these multiply bonded complexes, pinacol boranes, silanes, and germanes can be synthesized using less expensive and more straightforward processes.[4] In order to demonstrate higher impact applications, Chapter 4 presented a pointed investigation into the reaction between base-stabilized borylene complex **3** and a series of alkynes. Compared to terminal and aminoborylene examples from Braunschweig *et al*. that generated [1 + 2] cycloaddition products (borirenes) of the form [(RC═CR′)(μ-BAr)],[5] a unique series of step-wise transformations led to elimination of oxaborole species bearing structural similarities to boron-containing therapeutics recently approved by the FDA.[6] This chemistry serves as a climax to the work presented in this thesis document, pushing the envelope one step further from the development of methodology and showcasing real world applications (Scheme 6.1).

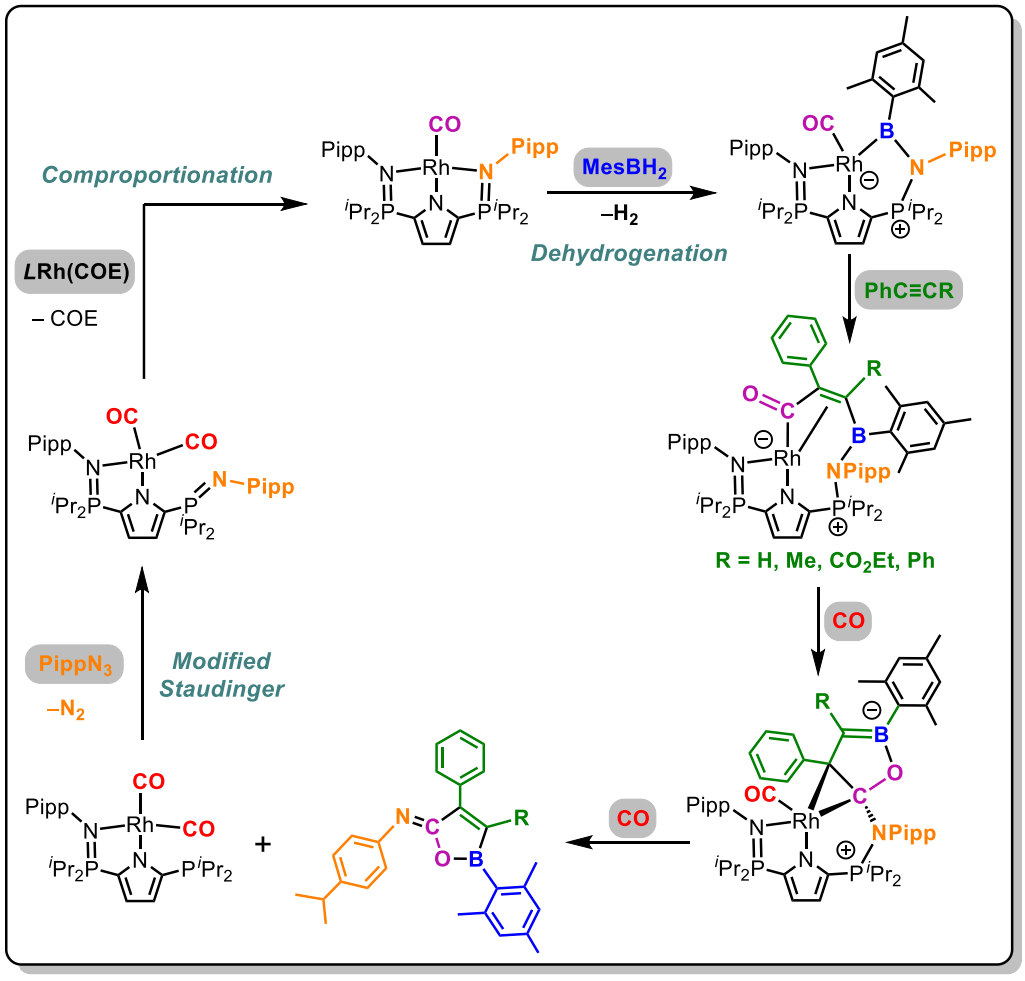

Scheme 6.1. Stepwise synthesis of oxaborole products starting from monocarbonyl rhodium complex **1**

In addition to these boron containing products being highly functionalized, they are also non-trivial to make, emphasizing the importance and elegance of transition metal mediated processes. Since even terminal aminoborylene complexes bearing carbonyl ligands, such as $(CO)_5Cr{=}B{=}N(SiMe_3)_2$, react with alkynes to yield only borirene products,[5b] our borylene complex **3** appears to strike a delicate balance between the choice of late transition metal, steric proximity of the boron and carbonyl carbon atoms, and the degree of N → B donor interaction, to achieve divergent reactivity.

Given the success of reacting borylene complex **3** with alkynes, it was hypothesized that an iso-structural silylyne complex might display similar reaction chemistry and yield high impact products with alkynes. Silylyne functionalities are exceedingly rare in the literature, with no

examples previously known for group 9 metals.[7] In Chapter 5, the H-substituted rhodium silylene complexes detailed in Chapter 3 were identified as ideal candidates for hydride abstraction methodologies established by Tilley and Hashimoto to generate terminal silylyne species. Starting from κ^2-*L*(CO)Rh(Si(H)Mes), complex **6**, where the silylene silicon atom bears mesityl and hydrogen substitutents, tris(pentafluorophenyl)borane was employed as a hydride abstracting agent to generate the base-stabilized silylyne [κ^2-*L*(CO)Rh≡SiMes][HBCF], **17**. Although no solid-state evidence was acquired, comprehensive NMR data indicated exclusive conversion to the expected silylyne. As is the case for most known silylyne complexes, the silicon atom can be considered electrophilic, being stabilized by donation from the phosphinimine's nitrogen lone pair. Analogies can therefore be drawn between **17** and borylene complex **3**, as both species contain a three-coordinate, electrophilic, main group element connected to a mesityl group, rhodium, and the phosphinimine nitrogen of the ligand. Reaction with phenylacetylene leads to the [2+2] cycloaddition product [κ^2-*L*(CO)Rh=Si(Mes)C(Ph)=C(H)][HB(C_6F_5)$_3$], **18**, resulting in similar upfield chemical shifts in the ^{29}Si NMR spectrum to those reported by Hashimoto.[8] Altogether this chapter showed a new avenue of potential research, extending our scope from metal-main group double bonds to triple bonds. By presenting the first example of a group 9 silylyne species, we also fill an important gap in the literature, allowing for comparisons to be made to stannylene species presented by Widemann, as well as early transition metal silylynes.[9]

6.2. Future Work

6.2.1. Preface

In order to properly present the chemistry below, a short preface is included here to introduce a postulated mechanism behind the dehydrogenation of group 13/14 substrates within our rhodium platform. In line with extrusion processes proposed by Tilley *et al*.,[10] we propose that monocarbonyl rhodium complex *L*Rh(CO), **1**, first reacts with R_nEH_2 substrates (n = 1 or 2; R = alkyl, aryl, or H; E = B, Si, or Ge) *via* oxidative addition of the E–H bond. Whether the donor

serves to activate the substrate is currently unknown, although reaction with aryl boranes has shown that formation of Lewis acid/base adducts is possible (See Chapter 2). Lewis base activation in the dehydrogenative coupling of silanes resulting in transient five coordinate species has been documented, where attack of the base weakens the Si–H bond.[4] Oxidative addition is presumably followed by Rh–*H* deprotonation by the phosphinimine nitrogen, inducing 1,2 H-migration from E to the metal centre. Finally, coupling of the Rh–H hydride and the N–H proton eliminates H_2 and allows for isolation of the intended Rh=E(R_n)←N functionality (Scheme 6.2). Deprotonation by the phosphinimine nitrogen is supported by spectral evidence of κ^2-*NN'*-(H-*N*)*L*(CO)Rh($SiPh_3$) which was generated *in situ* when **1** was reacted with Ph_3SiH.[3]

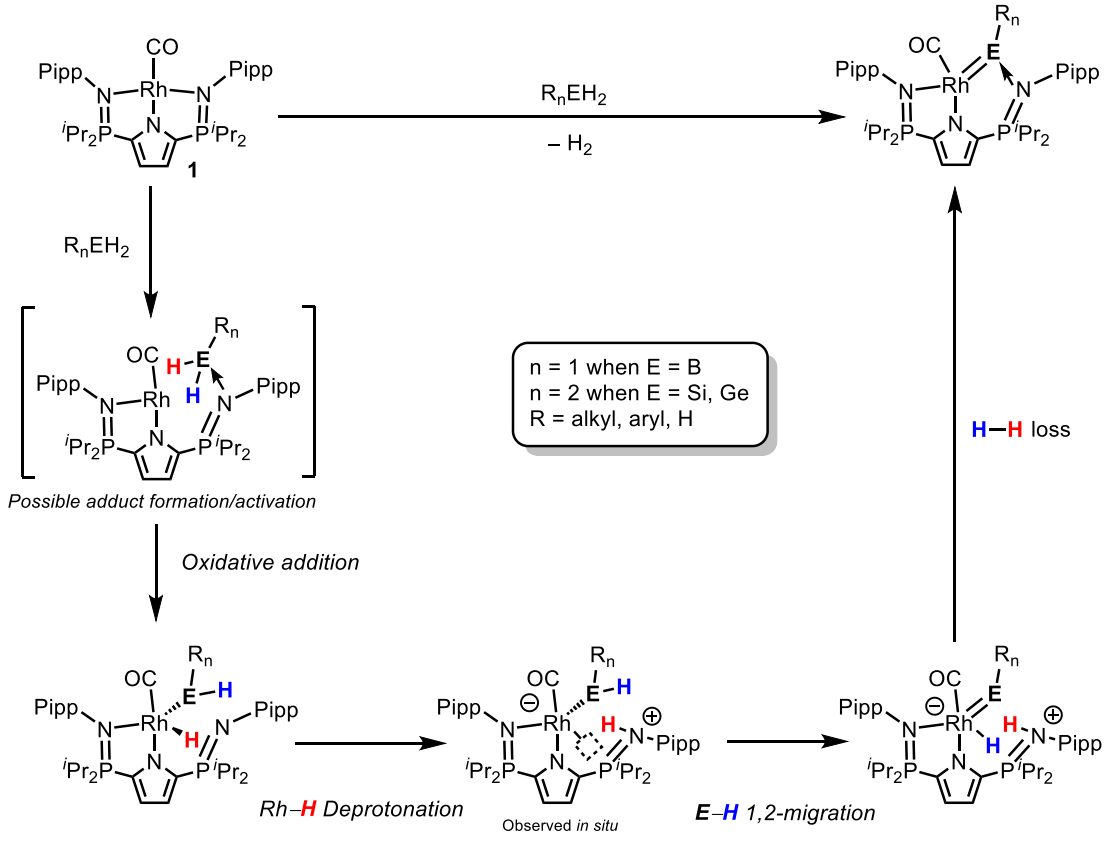

Scheme 6.2. Proposed mechanism for substrate dehydrogenation

While substantial evidence has been accumulated that is consistent with this proposed mechanism, a comprehensive investigation has yet to be conducted. The future work illustrated below has been

designed in part to probe various aspects of this pathway, and obtain a fuller understanding of the chemistry at play.

6.2.2. Ligand modifications

All work presented thus far has ultimately arisen from complex **1**, which features a rhodium (I) metal center stabilized by a carbonyl ligand and one specific iteration of the *NNN*-pincer ligand used in the Hayes lab: $L = \kappa^3$-NNN' = 2,5-[^{i}Pr$_2$P=N(4-^{i}PrC$_6$H$_4$)]$_2$-N'(C$_4$H$_2$)$^-$). Previous students have demonstrated that alterations to the substitutents on the phosphinimine phosphorus and nitrogen atoms are facile, either by using a different chlorophosphine ClPR$_2$ (R = alkyl or aryl) or azide (Scheme 6.3).[11] Specifically, the incorporation of groups such as 2,6-dimesitylphenyl (dmp), would significantly increase the steric bulk about the metal center. Demonstrated in Chapters 2 and 3, dehydrogenation of Group 13/14 reagents appears to be affected by steric influences. Increasing steric interactions between rhodium and the phosphinimine nitrogen may permit expansion of dehydrogenation substrate scope to include non-*ortho* substituted aryl boranes, or substrates like mesityl germane that previously led only to transmetalation.

Polarization of the P$^{\delta+}$–N$^{\delta-}$ bond is well documented and is a key rationale for the strongly donating ability of the phosphinimine group. In the context of metal-ligand cooperation, being able to fine-tune the donor strength of the ligand arm should shift the dissociation equilibrium, while simultaneously affecting the extent of ligand-substrate interactions. Initial results have shown that aryl groups bearing electron-withdrawing nitro- and bromo- substituents can be installed on the R$_2$P=N<u>Ar</u> nitrogen atom (Scheme 6.3), potentially decreasing its donor strength. In a similar vein, groups bearing electron-donating substituents should increase donor ability.

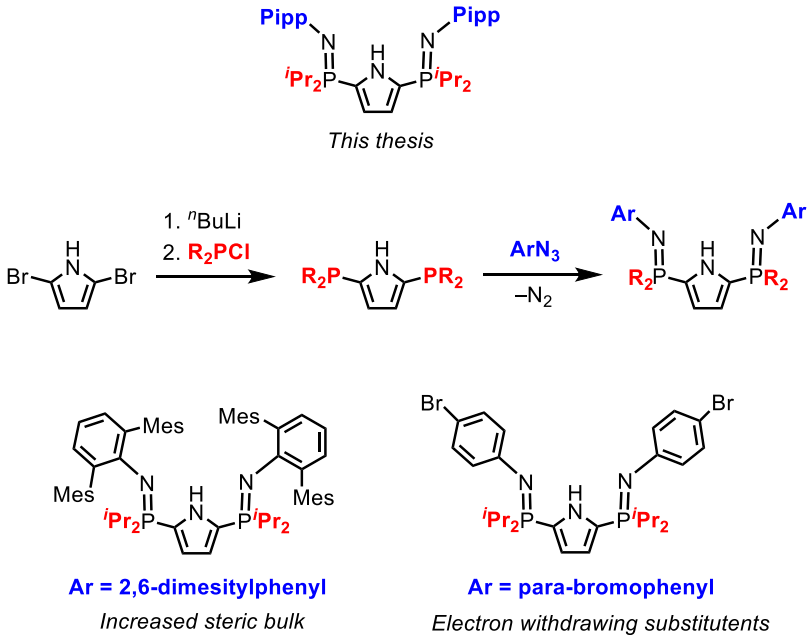

Scheme 6.3. Methodology to adjust the groups on phosphorus and nitrogen in the NNN-pincer ligand system, as well as select examples.

A potential future project involves the exploration of reaction kinetics with regard to this platform, as dissociated 14-electron Rh species can be trapped by reaction with carbon monoxide, yielding κ^2-*L*Rh(CO)$_2$ (Scheme 6.4, top). Whether the carbonyl moiety coordinates prior to or after phosphinimine dissociation is a question that will provide context for the mechanism behind E–H bond activation (E = main group element). Careful kinetic experiments whereby [CO] is varied during the synthesis of κ^2-*L*Rh(CO)$_2$ can provide evidence for whether the reaction rate is dependent upon the concentration of CO. If not, the reaction may be dissociative, indicating that the phosphinimine donor dissociates prior to CO coordination and is rate determining.

Mentioned in Chapter 1 of this document, the multidentate nature of pincer ligands renders them more difficult to displace fully, a phenomenon known more generally as the chelate effect. Throughout this thesis, however, irreversible loss of the *NNN*-pincer ligand occasionally prevailed. In order to combat this problem while maintaining sufficient hemilability for metal-ligand cooperation, unsymmetric ligand scaffolds should be targeted. Preliminary experiments have

established that reaction of the disubstituted phosphinopyrrole, 2,5-(^{i}Pr$_2$P)-C$_4$H$_2$N*H,* with one equivalent of *para*-bromo- or *para*-nitro- substituted aryl azide affords selective phosphinimine formation at only one side of the pyrrole backbone (Scheme 6.4, bottom). While electron-donating groups should be targeted in order to increase donor strength, and a stronger resulting ligand→rhodium binding affinity, these preliminary tests show that there is potential for unsymmetric ligands wherein one side exhibits hemilability and the other is more tightly bound. Along these lines, a mixed imine (σ-donating but π-accepting)/phosphinimine system could be targeted; the π-accepting imine functionality would bind even more tightly to rhodium.

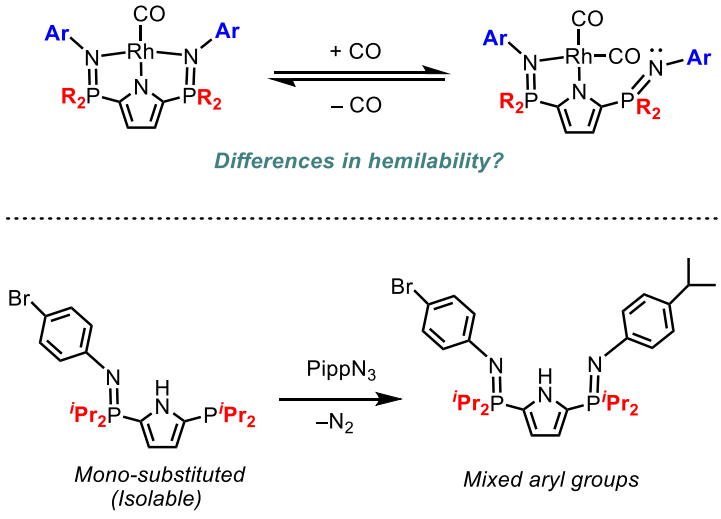

Scheme 6.4. Top) Dissociation of phosphinimine donor induced by addition of CO. Bottom) Installation of mixed aryl groups to the NNN-pincer ligand

6.2.3. Replacing CO with Tertiary Phosphines

Preliminary efforts have also been undertaken to replace the auxiliary carbonyl ligand with a different neutral donor. Starting with *L*Rh(COE), addition of triphenyl phosphine exclusively affords *L*Rh(PPh$_3$), compound **19**, as the only phosphorus-containing product. Tertiary phosphines are appealing because they have similar back-bonding capabilities as CO, but also due to the large library of examples available through decades of organometallic research. From the perspective of practicality, phosphines exist mostly in the solid or liquid phase, circumventing the technical

challenges of adding a highly toxic gas, such as carbon monoxide. When **19** was reacted with diphenylsilane, however, very slow oxidative addition, rather than dehydrogenation was observed, along with concurrent release of the phosphine donor (Scheme 6.5). This is evidenced by the growth of a diagnostic signal for triphenylphosphine (δ = –5.4), as well as a new resonance at δ 64.5 in the ^{31}P NMR spectrum. Furthermore, diagnostic upfield resonances were observed in the ^{1}H NMR spectrum (δ –13.7, dd) matching previous accounts.[3] Fortunately, the steric profile and electronic properties of phosphines can be easily fine-tuned, and the employment of a more π-accepting phosphine, such as (PhO)PH_2 or (C_6F_5)PH_2 may lead to the desired reactivity.

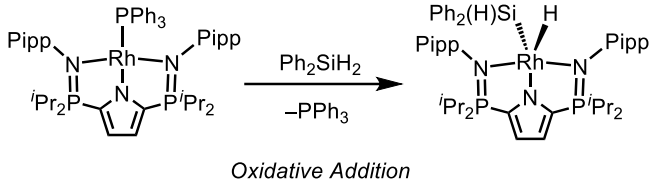

Scheme 6.5. Reaction between complex 19 and diphenylsilane

The use of phosphine ligands opens doors for direct comparison of our systems to FLP chemistry, with respect to borylene formation and alkyne activation. While phosphine ligands are usually regarded as spectator ligands, using the unexpected CO activation described in Chapter 4 as a basis, a rare instance of phosphine activation may be pursued, especially if a phosphine substituted analogue to complex **3** could be isolated (Scheme 6.6, top). P–C bond cleavage has been recognized as a common deactivation pathway for homogeneous catalysis, and P–C/X exchange has also been observed in a number of cases.[12] By generating highly reactive species in the vicinity of carefully selected phosphine groups, addition of an alkyne across the phosphorus and boron atoms may yield value-added products, or "activated" species poised for further derivatization.

As mentioned in Chapter 1, incorporation of metal centers, whether in homogenous or heterogeneous catalysis, usually serves to guide/change the reactivity and/or selectivity of otherwise unwieldly processes. It has been demonstrated that "free" FLP systems involving

phosphorus and boron are selective for the *trans*-substitution of alkynes, while only systems where the phosphorus and boron atoms are tethered in close proximity with an organic linker are capable of forming cyclic *cis*-substituted alkenes (Scheme 6.6, middle).[13] Since alkyne coordination to the rhodium center can be proposed as a logical first step in our systems, selectivity for the *cis*-substituted alkene product may be envisioned without tethering the Lewis basic and acidic atoms together. Furthermore, reaction with terminal alkynes may circumvent the deprotonation of the acidic alkynyl hydrogen, common for FLP systems, as such substrates were tolerated in the formation of compounds **13** (*vide supra*). Elimination of the organic product may be straightforward upon addition of an alcohol to yield *cis*-substituted phospinoboronate products (Scheme 6.6, bottom). In comparison, Westcott *et al*. discovered that direct phospinoboration of terminal alkynes, such as phenylacetylene (PhC≡CH), with the adduct $Ph_2P\rightarrow BPin$ in the presence of $[RhCl(PPh_3)_3]$ resulted in 1,2-substitution; adding both phosphorus and boron to the same vinylic carbon in the form of $(Ph)(H)C=C(BPin)(PPh_2)$.[14]

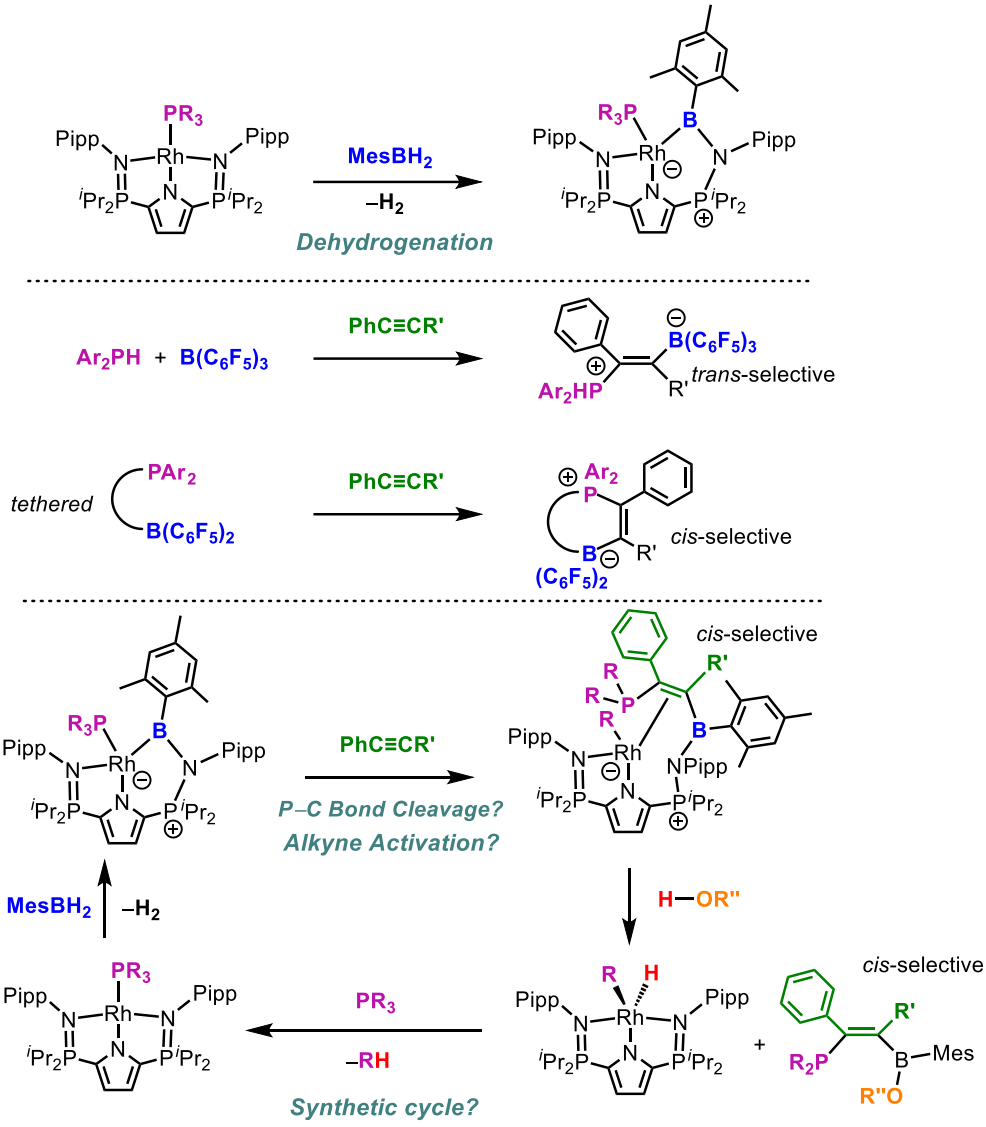

Scheme 6.6. Top) Potential dehydrogenation of primary boranes starting from PR3 substituted rhodium complexes analogous to 3. Middle) trans- vs cis- selective activation of alkynes by FLP systems. Bottom) Proposed activation and release of cis-substituted products.

6.2.4. Considerations Towards the Activation of C–H, N–H, and P–H Bonds

While the dehydrogenation of heavier group 14 elements and boron have been synthetically rewarding goals of this project, activation of C–H, N–H, and P–H bonds are better positioned towards targeting biologically and industrially relevant molecules. While the incorporation of carbon into fine molecules perhaps needs no introduction, amines are similarly

ubiquitous in biological systems and find industrial use in solvents, additives for pharmaceuticals, bactericides, flotation auxiliaries, anti-foam agents, corrosion inhibitors, detergents and dyes.[15] The anti-Markovnikov addition of N–H bonds across a C=C unsaturation was also lauded as one of the "ten challenges of catalysis" in previous decades, and still remains a synthetic challenge despite the heavy use of hydroamination catalysis in industrial settings.[15-16] Phosphorus also plays a critical role in the structural framework of DNA and RNA, and organo-phosphorus molecules find roles in the pharmaceutical industry as nucleotide analogues, prodrugs, and transition state inhibitors, usually in the form of phosphonates ($R–P(O)(OR')_2$).[17] Outside of pharmaceuticals, phosphines are widely used as ligands in organometallic chemistry and as substrates in materials chemistry, making the activation of P–H bonds in favor of P–C bonds similarly important. Classical methods involving Grignard and Michaelis–Arbuzov reactions are usually employed, yet have limited selectivity, as well as poor atom economy.[18] Transition metal catalyzed hydrophosphination ($H–PR_2$) and hydrophosphinylation ($H–P(O)(R')_2$) have therefore been posited as efficient and atom economical alternatives to synthesizing a wide array of both pharmaceutically relevant products and ligands for transition metal catalysis.[18] Oxidative addition of P–H bonds by precious metal catalysts, such as Pd, Pt, and Rh, demonstrated in catalytic hydrophosphination, is generally considered to proceed through a concerted mechanism similar to that established for H–H and Si–H oxidative addition of H_2 and silanes, respectively, due to the highly covalent and non-polar nature of the bond.[18a] As the first step in our dehydrogenation mechanism has been proposed to be oxidative addition of E–H bonds, our methodology can potentially be applied to simple substrates of the form R_2CH_2, RNH_2, and RPH_2; where the resulting carbene, imine, and phosphinidene complexes may serve as $\{CR_2\}$, $\{NR\}$, and $\{PR\}$ synthons for direct transfer to more complicated organic architectures.

Recognizing that C–H bond activation is an incredibly powerful tool in the synthesis of complex organic molecules, numerous studies and reviews have been published on the subject of C–H

oxidative addition. A 2004 Crabtree review commented on the propensity for organic C–H as well as B–H and Si–H bonds to form σ-bonding interactions with the metal center as a first step to activation. Here, the σ-bonding interaction is proposed to play a key role in acidification of the C–H bond, allowing for loss of the proton.[19] This is functionally similar to the description of concerted oxidative addition pathways, where similar σ-complexes are proposed. It should be noted here that the terms "reactive" or "inert" are very loosely defined for CH activation and depends on the activation mechanism. Compounds that have acidic protons as defined by low pKa values, may be homolytically strong as defined by their bond dissociation energies, hindering concerted oxidative addition pathways, and vice versa.[20] The C(sp^3)–H bond of 1-propene, for example, has a relatively high pKa value of 44 compared to the C(sp^3)–H bond of acetaldehyde (16.7), yet it features a lower bond dissociation energy (BDE) of 369 kJ mol^{-1} compared to 395 kJ mol^{-1}.[20] From a thermodynamic perspective, a recent 2021 tutorial from Chirik *et al*. postulates that in determining site selectivity for aryl C(sp^2)–H oxidative addition, formation of the stronger M–C bond is preferred over breaking the weaker C–H bond, and may be an interesting point of consideration when selecting substrates.[21] While the mechanism for oxidative addition in our system is likely concerted, both bond dissociation energies and pKa values are considered in the activation of substrates.

Despite the slightly higher bond dissociation energy for P–H (343 kJ mol^{-1} *c.f.* 330 kJ mol^{-1} in B–H, 321.3 in Ge–H, and 298.5 in Si–H), experimental pKa values for PhPH_2 (24.5 in THF) are much lower than that of Ph_2SiH_2 (33.9 in THF), suggesting that dehydrogenation of primary phosphines may be viable.[22] Amines present as interesting substrates as the bond dissociation energy of RNH_2 substrates are fairly high (~430 kJ mol^{-1} for alkyl, ~340 kJ mol^{-1} for aryl), yet primary aryl amines can exhibit low pKa values, such as 4.6 in phenylamine.[22] Specific C–H bonds such as those in Ph_2CH_2 (pka = 33.2, BDE = 340 kJ mol^{-1}) or cyclopentadiene (pka = 16, BDE = 358 kJ mol^{-1}), may also be amenable to dehydrogenation.[23] In the dehydrogenation of

boranes, silanes, and germanes, the newly formed M=E bond has always been electrophilic at the main group element, allowing for a Lewis acid/base interaction with the phosphinimine nitrogen of the ligand. Given the general Lewis basicity of trivalent phosphines and amines, the extent of P←N and N←N interaction would be of substantial interest, especially considering the pre-existing $P^{\delta+}$–$N^{\delta-}$ polarization of the phosphinimine bond.

6.2.5. Transition Metal Phosphinidenes

Generation of metal phosphorus double bonds through base-assisted dehydrohalogenation or deamination of phosphine ligands has been known since the early 1980's, drawing many parallels to strategies employed in silylene and germylene extrusion from Tilley and Hashimoto (Scheme 6.7, top).[24] Despite their relatively early discovery, transition metal phosphinidenes are still considered highly elusive in their synthesis, with the few existing examples being classified as either Fischer or Schrock varieties similar to transition metal carbenes.[24] Electrophilic Fischer-type phosphinidenes are generally considered to be highly reactive transient species that react with alkene and alkyne substrates, while nucleophilic Schrock-type phosphinidenes are much more well behaved and easier to isolate.[24] Similar to transition metal carbenes, the nucleophilicity vs. electrophilicity of the phosphorus atom depends largely on the identity of the metal and the ligands attached to it. For example, while Cp_2W=PMes, which bears π-donating ligands, is isolable and nucleophilic at phosphorus, $(CO)_5W$=PR species that contain π-accepting ligands can only be generated *in situ* and are employed as highly reactive electrophilic reagents.[24] These electrophilic species react rapidly with olefins, transferring the ":PR" group to yield three membered heterocycles (Scheme 6.7, middle) akin to the borirene examples from Braunschweig briefly described above and in Chapter 5.[24c]

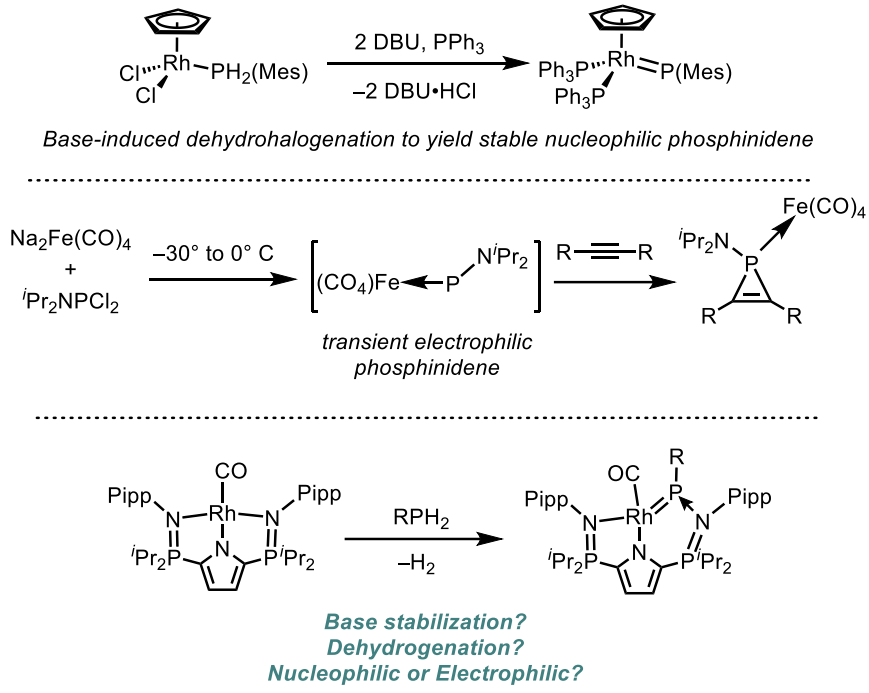

Scheme 6.7. Top) Base-induced dehydrohalogenation of rhodium phosphine complexes. Middle) Synthesis of transient Fischer-type phosphinidenes. Bottom) Proposed dehydrogenation of primary phosphines.

Given that the phosphinimine side arm of the *NNN*-pincer ligand is strongly σ- and π- donating, and the carbonyl ligand in monocarbonyl rhodium complex **1** is π-accepting, the nucleophilicity of a hypothesized phosphinidene species is ambiguous on paper (Scheme 6.7, bottom). The base-stabilization mentioned throughout this thesis, however, would likely assist in the isolation of electrophilic phosphinidene complexes, which may allow for more careful examination of their reactivity with various substrates, filling in a unique gap in the literature.

Unfortunately, an initial probing experiment involving complex **1** and the primary phenyl phosphine ($PhPH_2$) resulted in rapid color change of the solution, and complete consumption of **1**, but only proteo ligand was observed spectroscopically. It is possible that the greater acidity of the phosphine, compared to other main group substrates, resulted in protonation of the pyrrole nitrogen, in turn causing irreversible de-coordination of the ligand. Nonetheless, scission of the P–H bond is a good first step to have observed, and adjustments to the substituent on phosphorus and/or reaction

conditions may provide access to phosphinidenes. For example, inductively donating alkyl substituents, rather than aryl groups could be used, increasing the pKa from 22.4 in $PhPH_2$ to 29.8 in $^tBuPH_2$ given the precedent for dehydrogenation in our systems with $^tBuGeH_3$.[22c] As each unit increase of pKa represents a ten fold decrease in acidity, $^tBuPH_2$ can be considered substantially ($10^{7.4}$) less acidic than $PhPH_2$, and is more closely aligned with demonstrated substrates presented in this document.

6.2.6. Transition Metal Imido Complexes

Oxidative addition of N–H bonds at group 9 metal centers is well documented, and iridium catalyzed dehydrogenation of primary amines to nitriles can be accomplished with PCP pincer ligands (Scheme 6.8, top).[25] Generation of transition metal imido functionalities from amido-ligands has similarly been demonstrated through α-hydrogen abstraction strategies, although the amido-ligand is generally installed *via* salt-metathesis with lithium salts (Scheme 6.8, middle).[26] In particular, imido-trapping has been demonstrated with zirconocene species using THF as an external Lewis base. Finally, synthesis of transition metal imides through direct reaction with primary amines has been demonstrated through imido-deoxygenation reactions with early to mid transition metal oxides (Scheme 6.8, bottom).[27] Altogether, these literature precedents suggest that dehydrogenation of primary amines is a plausible route towards rhodium imido complexes. The acidic nature of these substrates, however, may lead to similar ligand protonation to $PhPH_2$, and base-stabilization by the phosphinimine nitrogen donor may be discouraged by the Lewis basicity of nitrogen.

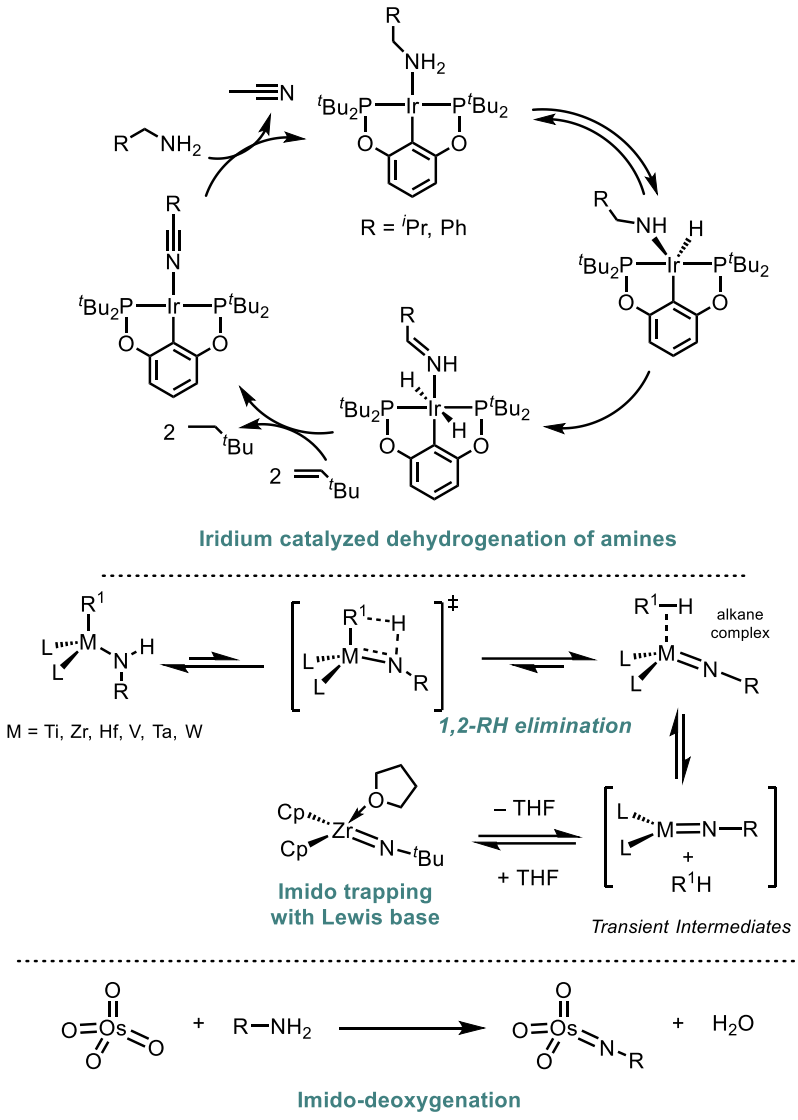

Scheme 6.8. Top) Iridium catalyzed dehydrogenation of amines to imines. Middle) 1,2-migration in the formation of imido-complexes. Bottom) Deoxygenation routes towards imido-complexes.

6.2.7. Alternative Bond Activations

The vast majority of examples involving MLC follow the activation of E–H bonds (See Chapter 1 Section 1.3). Given the analogies that can be drawn to FLP chemistry, however, it can be postulated that other polarizable bonds are viable targets. For example, Lewis acid/base adducts of the transition metal complex $Na[Fe(CO)_3(PMe_3)_2]$ with the weakly coordinating borate anion

$[B(C_6F_5)_4]^-$, has been demonstrated by the Young group to activate aliphatic C–X (X = F, Cl, Br, I), as well as carbon–triflate and carbon–mesylate bonds in an FLP-type manner.[28]

Previously, a colleague in the Hayes group demonstrated that H_2 oxidative addition to *NNN*-pincer supported iridium complexes is possible, yielding transient iridium dihydride species [*L*Ir(H)$_2$].[29] As H_2 activation by frustrated Lewis pairs was the landmark discovery that jump-started an entire field of chemistry, ligand assisted scission of the H_2 bond, and subsequent transfer, could be an alternative to conventional H_2 oxidative addition (Scheme 6.9). While previous Hayes lab alumni have already looked at the use of the rhodium cylcooctene complex L^{Ph}Rh(COE) (L^{Ph} = 2,5-[**Ph**$_2$P=N(4-^{i}PrC$_6$H$_4$)]$_2$-N**'**(C$_4$H$_2$)$^-$; COE = cyclooctene) as a hydrogenation catalyst with H_2, no such experimental work has been attempted with *L*Rh(CO), complex **1**.[11c]

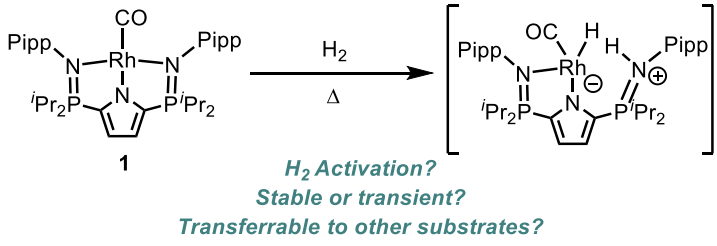

Scheme 6.9. Proposed H2 activation by complex 1 in an FLP type manner.

Rather than C–H or Si–H bond activation, C–Br or Si–Br bonds may be worth targeting in order to probe the scope of this methodology. C–Br bonds (280 kJ mol^{-1}) are noticeably weaker than typical C–H bonds (337.2 kJ mol^{-1}), and may be easier substrates to activate.[22b] Bromine is proposed here instead of the lighter halogens due to the difference in atomic orbital energies, as well as larger atom size, both of which lead to weaker bonds with first and second row main group elements. Considering Pauling electronegativity, both silicon (1.8) and boron (2.0) have lower electronegativities than hydrogen (2.1), resulting in a small $E^{\delta+}$–$H^{\delta-}$ polarization. Currently, it is unknown as to whether or not this weak polarization is necessary in our systems for MLC-assisted dehydrogenation, but the dramatic change from hydrogen to bromine may offer insight on this front.

Given that carbon (2.5) has a higher Pauling electronegativity than hydrogen, transitioning to C–Br bonds (Br = 2.8) may also aid the activation of carbon-based substrates should such polarization be necessary. Considering the proposed mechanism for dehydrogenation posited in Section 6.2.1 above, substrates of the form $R_2E(H)Br$ would likely be required (E = Si, C; materials are commercially available). The main detractor for this methodology is whether or not 1,2-migration from E–Br to rhodium is possible (Scheme 6.10). Loss of HBr could be encouraged by addition of DBU (1,8-Diazabicyclo[5.4.0]undec-7-ene) as a classic promotor of dehydrohalogenation.

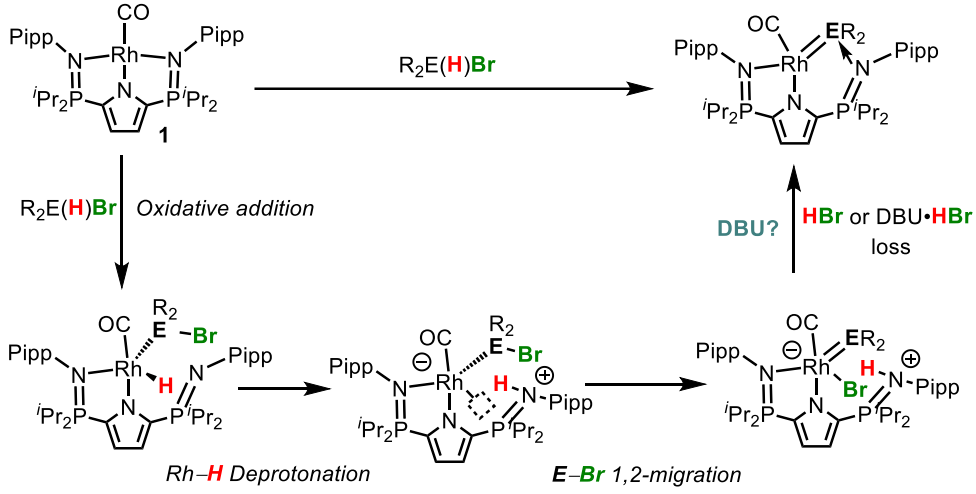

Scheme 6.10. Proposed dehydrohalogenation route towards metal–group 14 multiple bonds.

6.3. References

[1] C. Lenczyk, D. K. Roy, J. Nitsch, K. Radacki, F. Rauch, R. D. Dewhurst, F. M. Bickelhaupt, T. B. Marder, H. Braunschweig, *Chem. Eur. J.* **2019**, *25*, 13566-13571.

[2] C. S. MacNeil, S.-J. Hsiang, P. G. Hayes, *Chem. Commun.* **2020**, *56*, 12323-12326.

[3] C. S. MacNeil, P. G. Hayes, *Chem. Eur. J.* **2019**, *25*, 8203-8207.

[4] A. A. Toutov, K. N. Betz, M. C. Haibach, A. M. Romine, R. H. Grubbs, *Org. Lett.* **2016**, *18*, 5776-5779.

[5] a) H. Braunschweig, *Angew. Chem. Int. Ed.* **2012**, *51*, 7839-7842; b) H. Braunschweig, T. Herbst, D. Rais, F. Seeler, *Angew. Chem. Int. Ed.* **2005**, *44*, 7461-7463.

[6] a) R. Campbell, N. W. Buchbinder, C. Szwetkowski, Y. Zhu, K. Piedl, M. Truong, J. B. Matson, W. L. Santos, E. Mevers, *ACS Med. Chem. Lett.* **2024**, *15*, 349-354; b) Z. He, D.-C. Huang, D. Guo, F. Deng, Q. Sha, M.-Z. Zhang, W.-H. Zhang, Y.-C. Gu, *Adv. Agrochem* **2023**, *2*, 185-195; c) K. Nowicki, J. Krajewska, T. M. Stępniewski, M. Wielechowska, P. Wińska, A. Kaczmarczyk, J. Korpowska, J. Selent, P. H. Marek-Urban, K. Durka, K. Woźniak, A. E. Laudy, S. Luliński, *RSC Med. Chem.* **2024**, *15*, 1751-1772.

[7] H. Hashimoto, H. Tobita, *Coord. Chem. Rev.* **2018**, *355*, 362-379.

[8] H. Hashimoto, K. Watanabe, T. Yoshimoto, N. Hayakawa, T. Matsuo, H. Tobita, *Chem. Eur. J.* **2023**, *29*, e202302470.

[9] M. Widemann, K. Eichele, H. Schubert, C. P. Sindlinger, S. Klenner, R. Pöttgen, L. Wesemann, *Angew. Chem. Int. Ed.* **2021**, *60*, 5882-5889.

[10] R. Waterman, P. G. Hayes, T. D. Tilley, *Acc. Chem. Res.* **2007**, *40*, 712-719.

[11] a) D. T. Chisholm, P. G. Hayes, *New J. Chem.* **2021**, *45*, 15043-15052; b) T. K. K. Dickie, A. A. Aborawi, P. G. Hayes, *Organometallics* **2020**, *39*, 2047-2052; c) M. M. Hänninen, M. T. Zamora, C. S. MacNeil, J. P. Knott, P. G. Hayes, *ChemComm* **2016**, *52*, 586-589.

[12] S. A. Macgregor, *Chem. Soc. Rev.* **2007**, *36*, 67-76.

[13] a) J. Guo, M. Yan, D. W. Stephan, *Org. Chem. Front.* **2024**, *11*, 2375-2396; b) D. W. Stephan, *Science* **2016**, *354*, aaf7229.

[14] E. N. Daley, C. M. Vogels, S. J. Geier, A. Decken, S. Doherty, S. A. Westcott, *Angew. Chem. Int. Ed.* **2015**, *54*, 2121-2125.

[15] K. C. Hultzsch, *Adv. Synth. Catal.* **2005**, *347*, 367-391.

[16] a) K. D. Hesp, M. Stradiotto, *ChemCatChem* **2010**, *2*, 1192-1207; b) T. E. Müller, K. C. Hultzsch, M. Yus, F. Foubelo, M. Tada, *Chem. Rev.* **2008**, *108*, 3795-3892.

[17] J. B. Rodriguez, C. Gallo-Rodriguez, *ChemMedChem* **2019**, *14*, 190-216.

[18] a) D. S. Glueck, *J. Org. Chem.* **2020**, *85*, 14276-14285; b) M. Tanaka, in *New Aspects in Phosphorus Chemistry IV* (Ed.: J.-P. Majoral), Springer Berlin Heidelberg, Berlin, Heidelberg, **2004**, pp. 25-54.

[19] R. H. Crabtree, *J. Organomet. Chem.* **2004**, *689*, 4083-4091.

[20] Y. Qin, L. Zhu, S. Luo, *Chem. Rev.* **2017**, *117*, 9433-9520.

[21] T. P. Pabst, P. J. Chirik, *Organometallics* **2021**, *40*, 813-831.

[22] a) Y. Fu, L. Liu, R.-Q. Li, R. Liu, Q.-X. Guo, *J. Am. Chem. Soc.* **2004**, *126*, 814-822; b) J. A. Kerr, *Chem. Rev.* **1966**, *66*, 465-500; c) J.-N. Li, L. Liu, Y. Fu, Q.-X. Guo, *Tetrahedron* **2006**, *62*, 4453-4462; d) E. Buncel, T. K. Venkatachalam, *J. Organomet. Chem.* **2000**, *604*, 208-210.

[23] W. S. Matthews, J. E. Bares, J. E. Bartmess, F. G. Bordwell, F. J. Cornforth, G. E. Drucker, Z. Margolin, R. J. McCallum, G. J. McCollum, N. R. Vanier, *J. Am. Chem. Soc.* **1975**, *97*, 7006-7014.

[24] a) H. Aktaş, J. C. Slootweg, K. Lammertsma, *Angew. Chem. Int. Ed.* **2010**, *49*, 2102-2113; b) E. Gross, K. Jörg, K. Fiederling, A. Göttlein, W. Malisch, R. Boese, *Angew. Chem. Int. Ed.* **1984**, *23*, 738-739; c) K. Lammertsma, in *New Aspects in Phosphorus Chemistry III* (Ed.: J.-P. Majoral), Springer Berlin Heidelberg, Berlin, Heidelberg, **2003**, pp. 95-119; d) K. Lammertsma, Mark J. M. Vlaar, *Eur. J. Org. Chem.* **2002**, *2002*, 1127-1138.

[25] M. Albrecht, M. M. Lindner, *Dalton Trans.* **2011**, *40*, 8733-8744.

[26] a) D. J. Mindiola, *Acc. Chem. Res.* **2006**, *39*, 813-821; b) P. T. Wolczanski, *Organometallics* **2018**, *37*, 505-516.

[27] D. N. Zarubin, A. U. Nikolai, *Russ. Chem. Rev.* **2006**, *75*, 671.

[28] a) K. Lye, R. D. Young, *Chem. Sci. J.* **2024**, *15*, 2712-2724; b) H. Tinnermann, S. Sung, D. Csókás, Z. H. Toh, C. Fraser, R. D. Young, *J. Am. Chem. Soc.* **2021**, *143*, 10700-10708.

[29] S. L. Drescher, A. University of Lethbridge. Faculty of, Science, Lethbridge, Alberta. : University of Lethbridge, Dept. of Chemistry and Biochemistry **2023**.

Appendix I. Supporting information for Chapter 2

Reformatted from the published electronic supporting information associated with "MacNeil, C.S.; Hsiang, S.J.; Hayes, P.G.*, Dehydrogenation of a Primary Borane: A Source of :BR for Group Transfer Reactions. *Chemical Communications.* **2020**, *56*, 12323-12326."

Table of Contents

Appendix I. I General Experimental Considerations

All air- and moisture-sensitive manipulations were carried out using vacuum line, Schlenk and cannula techniques or in an MBraun inert atmosphere (argon) dry box unless otherwise noted. All glassware was stored in a pre-heated (110 ºC) oven or flame-dried prior to use. The solvents used for air- and moisture-sensitive manipulations were dried and deoxygenated using literature procedures and stored over 4 Å molecular sieves under argon.[1] Aryldihydroboranes H_2BMes and H_2BArF, and **1** where prepared according to literature procedures.[2,3] Pinacol, $B(OMe)_3$, 2-bromomesitylene, and $BH_3{\bullet}SMe_2$ were purchased from Sigma-Aldrich and used without further purification. 1,3-bis(trifluoromethyl)-5-bromobenzene was purchased from Alfa Aesar and used as received.

Unless otherwise noted all NMR spectra were recorded at ambient temperature with a Bruker Avance II NMR spectrometer (300.13 MHz for ^{1}H, 96.29 MHz for ^{11}B, 75.47 MHz for ^{13}C, 282.40 MHz for ^{19}F and 121.48 MHz for ^{31}P) or Avance III NMR spectrometer (700.44 MHz for ^{1}H, 224.63 MHz for ^{11}B, 176.13 MHz for ^{13}C, 658.78 MHz for ^{19}F and 283.54 MHz for ^{31}P) NMR spectrometer. All ^{1}H and ^{13}C NMR chemical shifts are reported in ppm relative to $SiMe_4$ using the ^{1}H (benzene-d_6: 7.16 ppm) and ^{13}C (benzene-d_6: 128.06 ppm) chemical shifts of the solvent as a standard.[4] ^{11}B NMR chemical shifts were referenced externally to $BF_3{\cdot}Et_2O$ (δ 0.0). ^{19}F NMR chemical shifts were referenced externally to C_6H_5F (δ –113.11 in benzene-d_6).[5] ^{31}P NMR chemical shifts were reference to external 85% H_3PO_4 in H_2O (δ 0.0). ^{1}H NMR data for diamagnetic compounds are reported as follows: chemical shift, multiplicity (s = singlet, d = doublet, t = triplet, q = quartet, p = pentet, br = broad, m = multiplet, app = apparent, obsc = obscured, ov = overlapping), coupling constants (Hz), integration, assignment. ^{13}C NMR data for diamagnetic compounds are reported as follows: chemical shift, assignment. Assignment of resonances were supplemented by ^{1}H–^{1}H COSY, $^{13}C\{^{1}H\}$ APT, ^{1}H–$^{13}C\{^{1}H\}$, and HSQC/HMBC experiments.

Elemental analysis (%CHN) was conducted at the University of Lethbridge on an Elementar Americas Vario MicroCube Analyzer (C, H, N, O, S capabilities) using bulk recrystallized compounds. Infrared spectroscopy was conducted on a Thermo-Nicolet iS10 FT-IR spectrometer using bulk recrystallized compounds.

Appendix I. II Preparation of Organoboranes and Rhodium Complexes

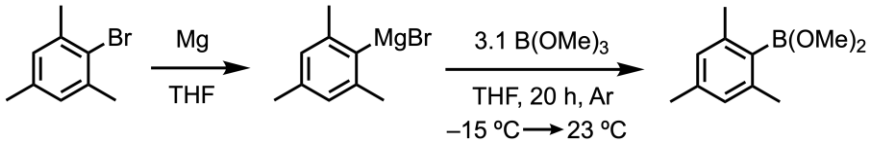

$(OMe)_2$BMes. Adapting from a literature procedure, an oven-dried 250 mL 3-neck round-bottom flask was charged with a stir bar, 2.803 g of magnesium turnings, and a small crystal of iodine (I_2). The flask was evacuated on a double-manifold vacuum line and cooled to –78 ºC with a mixture of dry-ice and acetone. Approximately 15 mL of THF was transferred under reduced pressure to wet the Mg turnings. A separate flask was charged with 18.2 g (91.3 mmol) of mesityl bromide, degassed by repeated freeze-pump-thaw cycles, and dissolved in 70 mL of THF. The THF solution was transferred *via* canula needle into a 100 mL dropping funnel outfitted to the side arm of the 250 mL flask containing the magnesium turnings. The mesityl bromide solution was added dropwise over 45 minutes resulted in gentle bubbling and warming of the mixture. The dropping funnel was removed, and reaction mixture was heated to reflux for 18 hours at which point the solution was grey and opaque. The Grignard reagent was transferred *via* syringe to a 250 mL 2-neck round-bottom flask containing 3.1 equivalents (283 mmol, 0.035 L) of $B(OMe)_3$ dissolved in 15 mL of cold (–15 ºC) diethylether. The reaction mixture became cloudy with a dense white precipitate that formed after several minutes. The mixture was warmed to ambient temperatures, stirred for 20 hours and then diluted with 150 mL of pentane. The supernatant was transferred *via* canula into a 500 mL Teflon-sealable thick-walled flask. Volatiles were removed under reduced pressure affording dimethoxymesitylborane as a colorless oil (10.5 g, 60% yield). NMR data (^{1}H, ^{11}B) agreed well with literature data.[2]

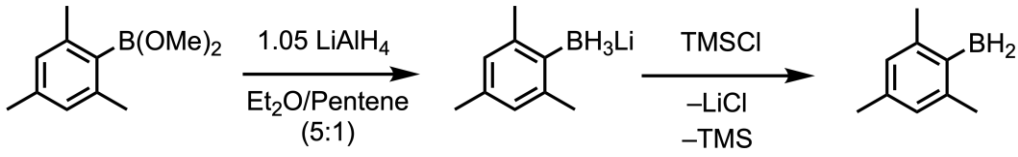

H_2BMes. A 100 mL round-bottom flask was charged with a stir bar and 2.00 g (0.010 mol) of distilled $(OMe)_2$BMes dissolved in 60 mL of a 5:1 mixture of diethylether and pentane. The mixture was then cooled to 0 ºC. In a separate 50 mL round-bottomed flask 1.05 equivalents of $LiAlH_4$ (0.415 g) was suspended in diethylether (20 mL). The $LiAlH_4$ slurry was added dropwise to the cold (0 ºC) stirring $(OMe)_2$BMes solution over 2 minutes. The mixture was allowed to gradually warm to ambient temperature whereupon it was stirred for 3 hours. The product was filtered through a pad of Celite and washed with a 1:1 mixture of pentane and diethylether (3 × 5 mL). Volatiles were removed under reduced pressure to afford Li[H_3BMes] as a white solid (0.408 g, 28% yield). NMR data (^{1}H, ^{11}B) agreed well with literature data.[2] One equivalent of Me_3SiCl (0.232 g, 0.002 mol) was added to a diethylether solution of Li[H_3BMes] (0.302 g, 0.002 mol) at ambient temperature. The reaction mixture was rapidly stirred for 3 hours during which a white precipitate formed. The solvent was removed under vacuum and the residue extracted with pentane (3 × 5 mL) to yield H_2BMes as a crystalline white solid (0.358 g, 95% yield from Li[H_3BMes]). NMR data (^{1}H, ^{11}B) agreed well with literature data.[2] Note: It is not necessary to isolate Li[H_3BMes]. It can be generated and used in situ.

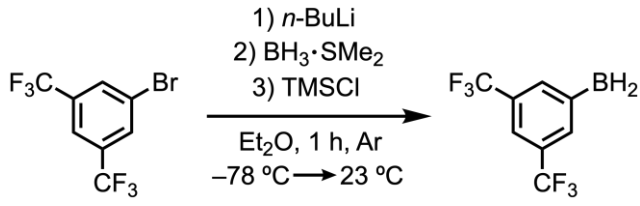

H_2BAr^F. Following a literature procedure,[2b] 150 mL Teflon-sealed thick-walled flask was charged with 3,5-bis(trifluoromethyl)bromobenzene (1.07 g, 3.62 mmol) and 20 mL of diethylether. The solution was degassed by three freeze–pump–thaw cycles and cooled to –78 ºC. Under an atmosphere of argon, 1.45 mL (1 equivalent, 3.62 mmol) of *n*-butyl lithium (2.5 M in hexanes) was added dropwise via syringe over 10 minutes. The solution turned from colorless to yellow during 15 minutes of stirring. The mixture was quenched with 0.343 mL of BH_3•SMe_2 (1 equivalent, 3.62 mmol), added over 30 seconds via syringe. The reaction mixture was warmed to 23 ºC, becoming a pale-yellow color. After 1 hour at 23 ºC, Me_3SiCl (0.46 mL, 1 equivalent, 3.6 mmol) was added via syringe over 10 seconds, yielding H_2BAr^F as a pale-orange solution. Since the product decomposes upon removal of the solvent, H_2BAr^F was used as a diethylether solution of known concentration (e.g. 0.287 mol L^{-1}). ^{1}H NMR (300.13 MHz, benzene-d_6): δ 8.01 (s, 2H, m Ar H); 7.83 (s, 1H, *o*-Ar H); 2.85 (br s, 2H, BH_2). ^{11}B NMR (96.29 MHz, benzene-d_6): δ 9.6 (br s). ^{19}F NMR (282.23 MHz, benzene-d_6): δ –62.3 (s, 6F). NMR data (^{1}H, ^{11}B, ^{19}F) agreed well with literature data.[2b]

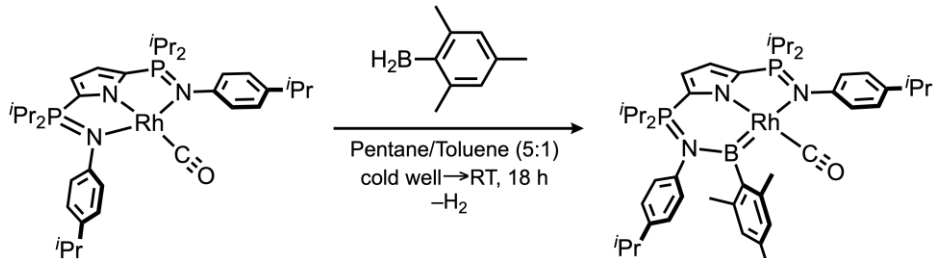

1 **3**

(^{iPr}NNN)(CO)Rh=B(2,4,6-(CH_3)$_3$$C_6H_2$) (3). A 20 mL scintillation vial was charged with 1-CO (0.045 g, 0.065 mmol), 1 equivalent of mesitylborane (9.1 mg, 0.066 mmol), and a Teflon-coated stir bar. The solids were dissolved in a mixture of pentane and toluene (5 mL, 5:1) giving a red-orange solution and the vial was placed in a cold well cooled with liquid nitrogen. The reaction mixture was rapidly stirred at low temperature for 1 h in the glove box with periodic sparging of the solution. The reaction solution became light-orange and was allowed to stand in the cold well for 18 h producing a dark yellow crystalline solid. The solid was washed with cold pentane (3 × 5 mL) to yield 0.028 g (53% yield) of **3** as a bright yellow powder. Anal. Calcd. for $C_{44}H_{63}BN_3OP_2Rh$: C, 64.01; H, 7.69; N, 5.09. Found: C, 63.83; H, 7.96; N, 4.65. (ν_{CO}): 1909 cm^{-1}. ^{1}H NMR (700.13 MHz, benzene-d_6, 23 ºC): δ 7.51 (d, $^3J_{HH}$ = 7.7 Hz, 2H, 4-iPr-C$_6H_4$); 7.06 (d, $^3J_{HH}$ = 7.9 Hz, 2H, 4-iPr-C$_6H_4$); 6.93 (d, $^3J_{HH}$ = 7.7 Hz, 2H, 4-iPr-C$_6H_4$); 6.67 (d, $^3J_{HH}$ = 7.9 Hz, 2H, 4-iPr-C$_6H_4$); 6.66 (obsc dd, $^3J_{HP}$ = $^3J_{HH}$ = 3.9 Hz, 1H, 3,4-pyrrole); 6.61 (s, 2H, Mes Ar *H*); 6.51 (dd, $^3J_{HP}$ = $^3J_{HH}$ = 3.9 Hz, 1H, 3,4-pyrrole); 3.26 (sp, $^3J_{HH}$ = 7.2 Hz, 2H, C*H*(CH$_3$)$_2$); 2.73 (sp, $^3J_{HH}$ = 6.9 Hz, 1H, C*H*(CH$_3$)$_2$); 2.72 (s, 6H, Mes C*H*$_3$); 2.43 (sp, $^3J_{HH}$ = 6.9 Hz, 1H, C*H*(CH$_3$)$_2$); 2.19 (ov m, 2H, C*H*(CH$_3$)$_2$); 2.09 (s, 3H, Mes C*H*$_3$); 1.16 (d, $^3J_{HH}$ = 6.9 Hz, 6H, CH(C*H*$_3$)$_2$); 1.11 (dd, $^3J_{HP}$ = 15.4 Hz, J_{HH} = 7.2 Hz, 6H, CH(C*H*$_3$)$_2$); 1.04 (dd, $^3J_{HP}$ = 15.7 Hz, J_{HH} = 6.9 Hz, 6H, CH(C*H*$_3$)$_2$); 0.97 (dd, $^3J_{HP}$ = 16.7 Hz, J_{HH} = 7.2 Hz, 6H, CH(C*H*$_3$)$_2$); 0.92 (d, $^3J_{HH}$ = 6.9 Hz, 6H, CH(C*H*$_3$)$_2$); 0.85 (dd, $^3J_{HP}$ = 16.2 Hz, J_{HH} = 7.2 Hz, 6H, CH(C*H*$_3$)$_2$). ^{13}C{^{1}H} NMR (75.46 MHz, benzene-d_6, 23 ºC): δ 196.6 (d, $^1J_{CRh}$ = 87.6 Hz, Rh–*C*O); 152.6 (br s, Ar *C*) 151.3 (s, Ar *C*); 147.1 (s, Ar *C*); 140.3 (s, Ar *C*); 140.1 (s, Ar *C*); 137.7 (dd, $^1J_{CP}$ = 145 Hz, $^3J_{CP}$ = 16.1 Hz, 2,5-pyrrole *C*); 133.6 (s, Ar *C*); 133.2 (s,

Ar *C*); 129.1 (s, Ar *C*H); 127.1 (s, Ar *C*H); 126.6 (s, Ar *C*H); 126.5 (s, Ar *C*H); 126.4 (s, Ar *C*H); 125.9 (s, Ar *C*H); 120.7 (ddd, $^{1}J_{CP}$ = 129 Hz, $^{3}J_{CP}$ = 13.5 Hz, $^{3}J_{CRh}$ = 3.4 Hz, 2,5-pyrrole *C*); 118.2 (dd, $^{2}J_{CP}$ = 24.6 Hz, $^{3}J_{CP}$ = 10.9 Hz, 3,4-pyrrole *C*H); 115.1 (dd, $^{2}J_{CP}$ = 24.8 Hz, $^{3}J_{CP}$ = 9.9 Hz, 3,4-pyrrole *C*H); 33.7 (s, *C*H(CH_3)$_2$); 33.6 (s, *C*H(CH_3)$_2$); 27.3 (s, CH(*C*H_3)$_2$); 26.6 (d, $^{n}J_{CP}$ = 8.4 Hz, *C*H(CH_3)$_2$); 24.1 (d, $^{n}J_{CP}$ = 54.9 Hz, CH(CH_3)$_2$); 23.9 (s, CH(CH_3)$_2$); 21.3 (s, CH(CH_3)$_2$); 16.7 (d, CH(CH_3)$_2$); 16.6 (d, CH(CH_3)$_2$); 16.5 (d, CH(CH_3)$_2$); 16.4 (d, CH(CH_3)$_2$). $^{31}P\{^{1}H\}$ NMR (283.42 MHz, benzene-d_6, 23 ºC): δ 52.6 (d, $^{2}J_{PRh}$ = 7.3 Hz, 1P, *P*–N–Rh); 37.8 (s, 1P, *P*–N–B). ^{11}B NMR (224.63 MHz, benzene-d_6, 23 ºC): δ 32.6 (br s, 1B).

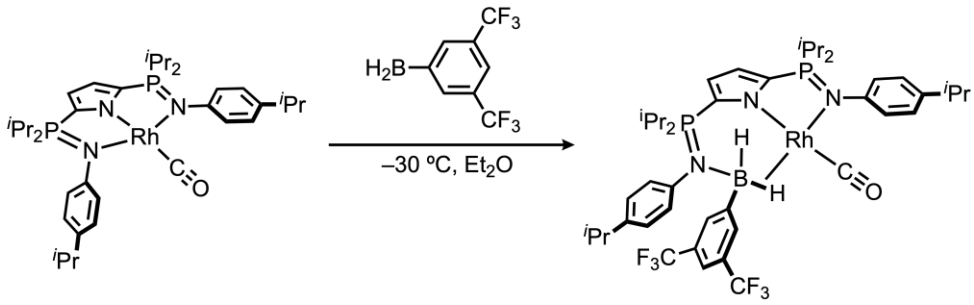

1 **4**

(^iPr^NNN)Rh(CO)H$_2$B(3,5-(CF$_3$)$_2$C$_6$H$_3$) (4). In a 20 mL scintillation vial, crystalline **1** (0.025 g, 35.9 mmol) was dissolved in 5 mL of Et_2O and chilled to –30 º C. A solution of $H_2B(3,5\text{-}(CF_3)_2C_6H_3)$ in Et_2O (0.125 mL, 37 mmol) was added via syringe over 10 seconds. The solution was stirred at –30 ºC for 2 hours becoming dark yellow in colour. The compound was dried under vacuum and washed with pentane (2 × 3 mL) giving 0.028 g of **4** as a bright yellow powder (84% yield). Anal. Calcd. for $C_{44}H_{60}BF_6N_3OP_2Rh$: C, 56.04; H, 6.23; N, 4.56. Found: C, 56.16; H, 6.16; N, 4.33. IR (ν_{CO}): 1950 cm^{-1}. ^{1}H NMR (700.13 MHz, benzene-d_6, 23 ºC): δ 8.04 (s, 2H, Ar *H*); 7.68 (s, 1H, Ar *H*); 7.29 (d, $^3J_{HH}$ = 7.85 Hz, 2H, 4-iPr-C$_6$*H*$_4$); 7.21 (d, $^3J_{HH}$ = 7.85 Hz, 2H, 4-iPr-C$_6$*H*$_4$); 7.05 (d, $^3J_{HH}$ = 8.15 Hz, 2H, 4-iPr-C$_6$*H*$_4$); 6.83 (d, $^3J_{HH}$ = 8.15 Hz, 2H, 4-iPr-C$_6$*H*$_4$); 6.47 (ov dd, $^3J_{HP}$ = $^3J_{HH}$ = 3.3 Hz, 1H, 3,4-pyrrole); 6.39 (ov dd, $^3J_{HP}$ = $^3J_{HH}$ = 3.3 Hz, 1H, 3,4-pyrrole); 2.70 (sp, $^3J_{HH}$ = 6.9 Hz, 1H, C*H*(CH$_3$)$_2$); 2.60 (sp, $^3J_{HH}$ = 6.9 Hz, 1H, C*H*(CH$_3$)$_2$); 2.23 (m, 2H, C*H*(CH$_3$)$_2$); 2.03 (m, 2H, C*H*(CH$_3$)$_2$); 1.13 (d, $^3J_{HH}$ = 6.9 Hz, CH(C*H*$_3$)$_2$); 1.06 (d, $^3J_{HH}$ = 6.9 Hz, CH(C*H*$_3$)$_2$); 0.99 dd, $^2J_{HP}$ = 15.5 Hz, $^3J_{HH}$ = 7.1 Hz, 6H, CH(C*H*$_3$)$_2$); 0.90 (ov m, 12H, CH(C*H*$_3$)$_2$); 0.84 (dd, $^2J_{HP}$ = 15.5 Hz, $^3J_{HH}$ = 7.1 Hz, 6H, CH(C*H*$_3$)$_2$); –3.10 (br s, 1H, B*H*). ^{13}C{^{1}H} NMR (176 MHz, benzene-d_6, 23 ºC): δ 190.63 (d, $^1J_{CRh}$ = 75.7 Hz, Rh–*C*O); 151.04 (s, Ar *C*); 146.87 (s, Ar *C*); 143.43 (s, Ar *C*); 142.90 (s, Ar *C*); 134.58 (br m, Ar *C*H); 129.87 (d, $^3J_{CF}$ = 4.0 Hz, Ar *C*H); 129.57 (d, $^2J_{CF}$ = 31.7 Hz); 127.67 (s, Ar *C*H); 127.49 (s, Ar *C*H); 127.22 (s, Ar *C*H); 127.15 (d, $^3J_{CF}$ = 7.0 Hz, Ar *C*H); 126.63 (s, Ar *C*H); 118.44 (dd, $^2J_{CP}$ = 23.0 Hz, $^3J_{CP}$ = 10.4 Hz, 3,4-pyrrole *C*H); 115.24 (dd, $^2J_{CP}$ = 24.6 Hz, $^3J_{CP}$ = 11.2 Hz, 3,4-pyrrole *C*H); 33.87 (s, *C*H(CH$_3$)$_2$); 33.73 (s, *C*H(CH$_3$)$_2$); 26.79 (d, $^1J_{CP}$ = 52.8 Hz, *C*H(CH$_3$)$_2$); 26.27 (d, $^1J_{CP}$ = 62.0 Hz, *C*H(CH$_3$)$_2$); 24.29 (s, CH(*C*H$_3$)$_2$); 24.06 (s,

CH(CH$_3$)$_2$); 16.97 (d, $^2J_{CP}$ = 2.68 Hz, CH(CH$_3$)$_2$); 16.40 (d, $^2J_{CP}$ = 2.38 Hz, CH(CH$_3$)$_2$); 16.20 (d, $^2J_{CP}$ = 2.73 Hz, CH(CH$_3$)$_2$); 16.15 (d, $^2J_{CP}$ = 1.91 Hz, CH(CH$_3$)$_2$); CF$_3$ signal could not be resolved from baseline. ^{31}P{^{1}H} NMR (283.42 MHz, benzene-d_6, 23 ºC): δ 51.25 (s, 1P, *P*–N–Rh); 48.82 (s, 1P, *P*–N–B). ^{19}F{^{1}H} NMR (282 MHz, benzene-d_6, 23 ºC): δ –62.07 (s, 6F, CF_3). ^{11}B NMR (224.63 MHz, benzene-d_6, 23 ºC): δ –5.92 (s, 1B).

Appendix I. III NMR Spectra

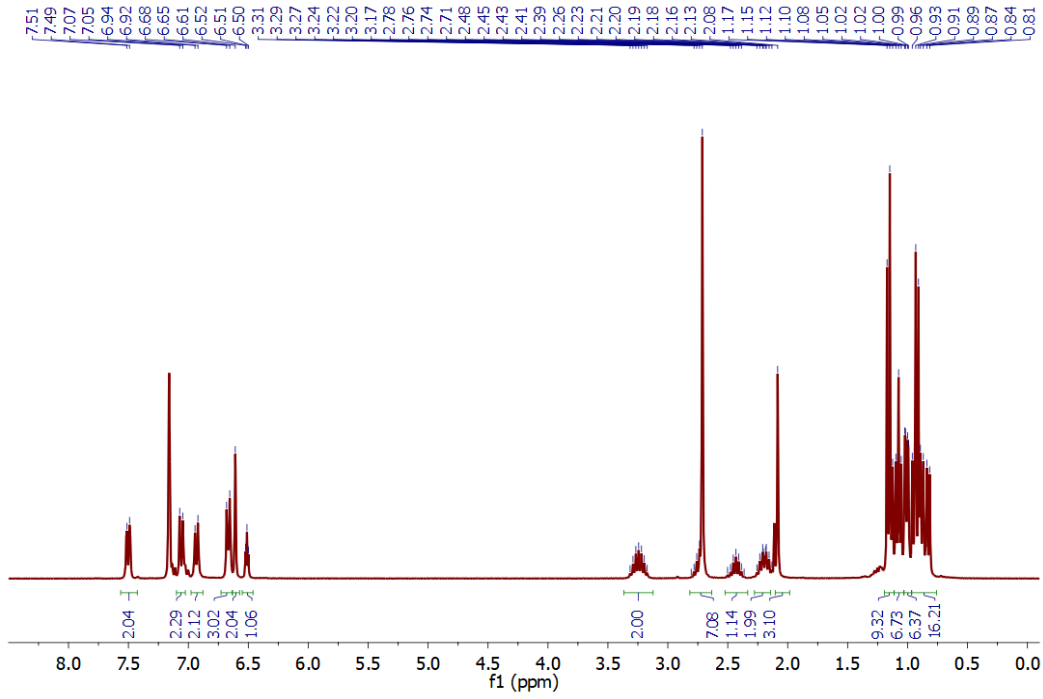

Appendix Figure I.1. ^{1}H NMR (300 MHz) spectrum of **3** in benzene-d_6 at 23 ºC.

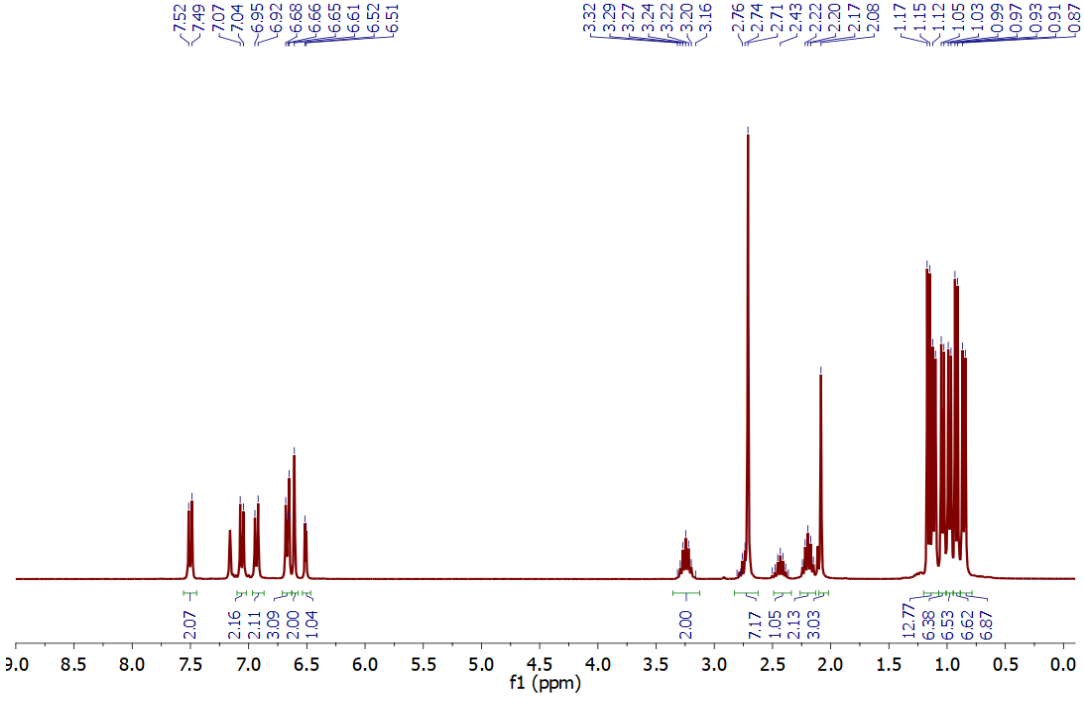

Appendix Figure I.2. ^{1}H{^{31}P} NMR (300 MHz) spectrum of **3** in benzene-d_6 at 23 ºC.

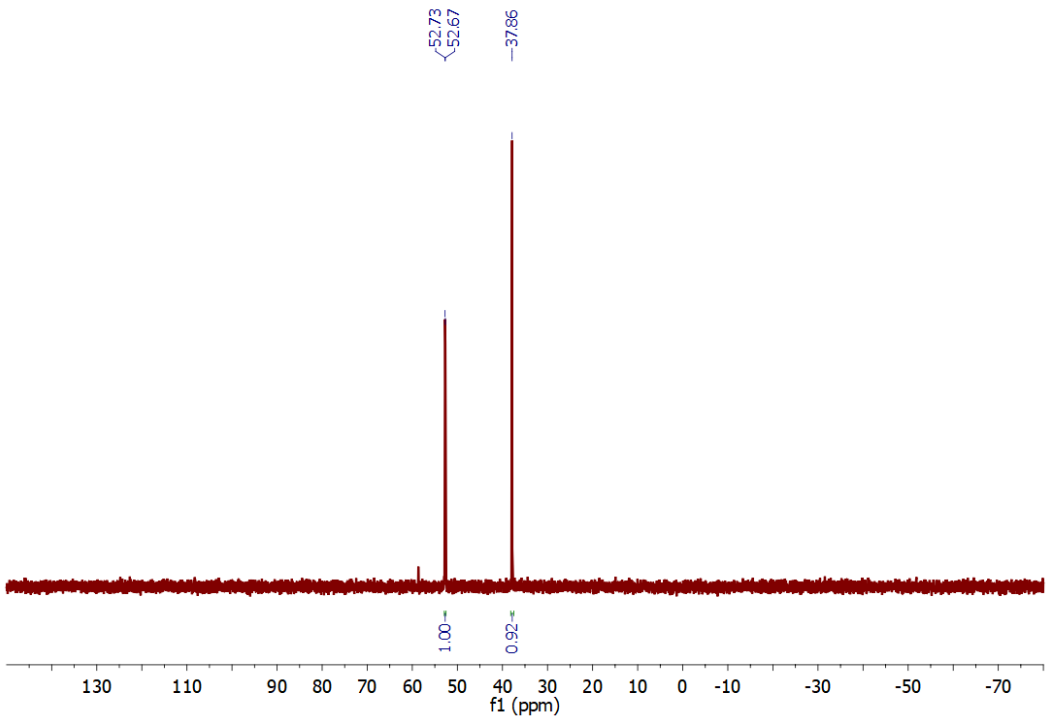

Appendix Figure I.3. $^{31}P\{^{1}H\}$ NMR (121 MHz) spectrum of **3** in benzene-d_6 at 23 ºC.

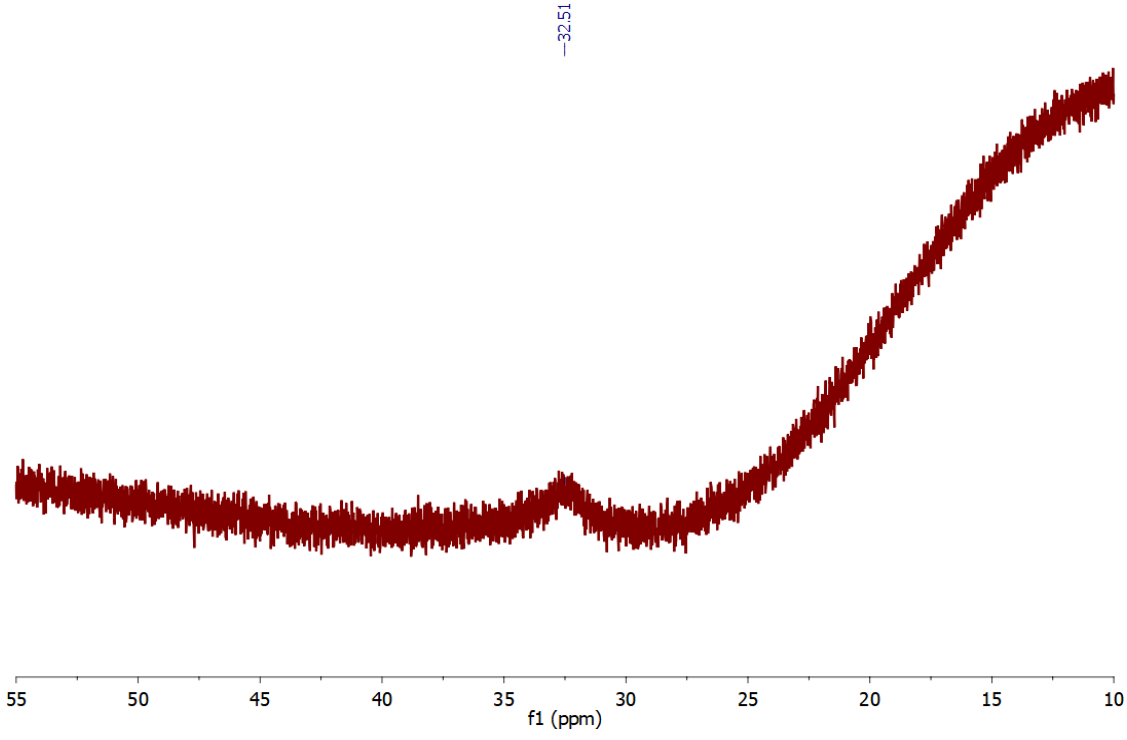

Appendix Figure I.4. $^{11}B\{^{1}H\}$ NMR (224 MHz) of **3** in benzene-d_6 at 23 ºC.

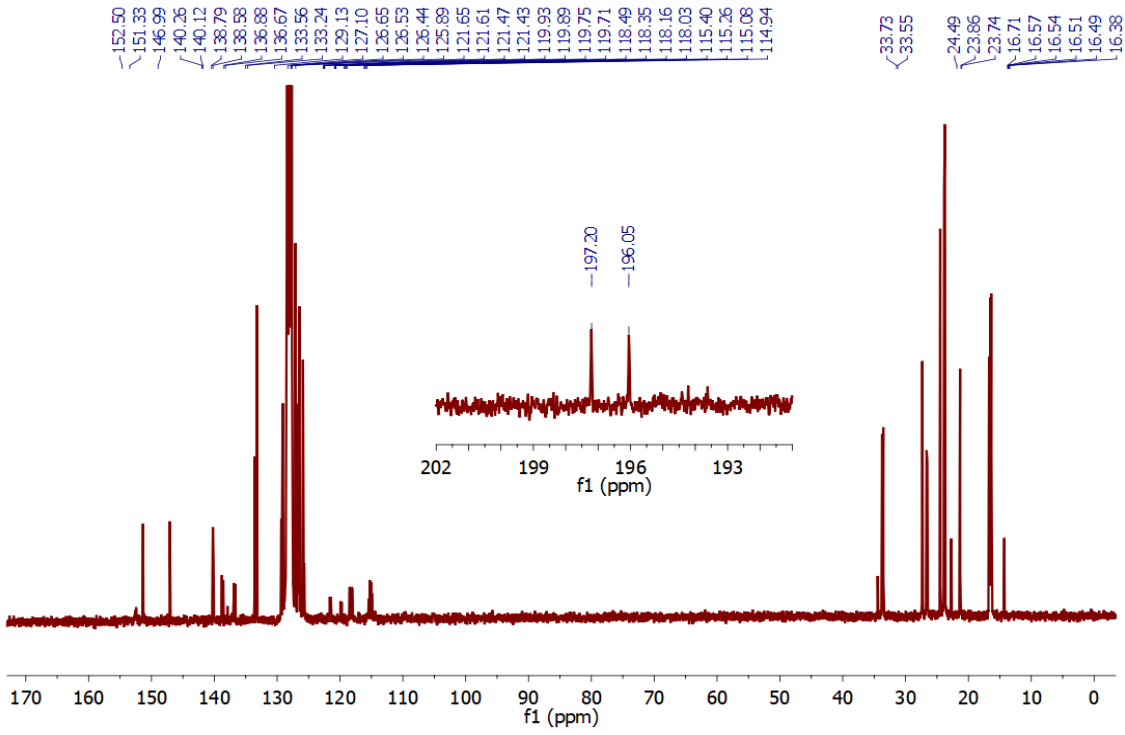

Appendix Figure I.5. $^{13}C\{^{1}H\}$ NMR (75 MHz) spectrum of **3** in benzene-d_6 at 23 ºC. Inset: Rh–*C*O resonance.

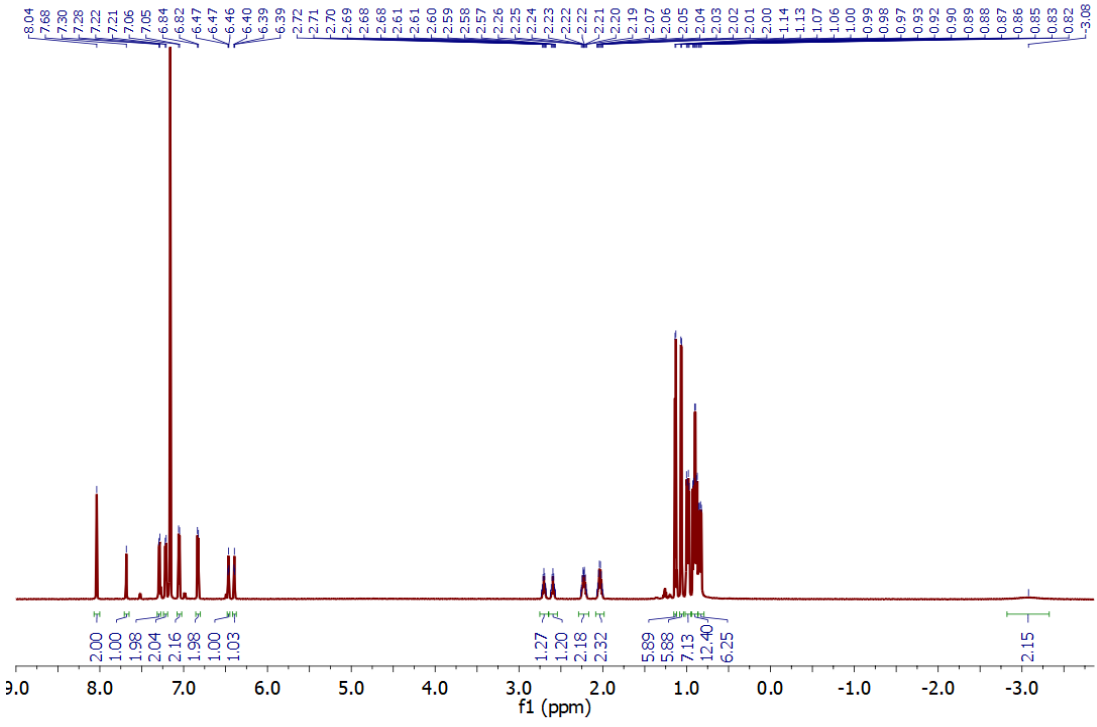

Appendix Figure I.6. ^{1}H NMR (700 MHz) spectrum of **4** in benzene-d_6 at 23 ºC.

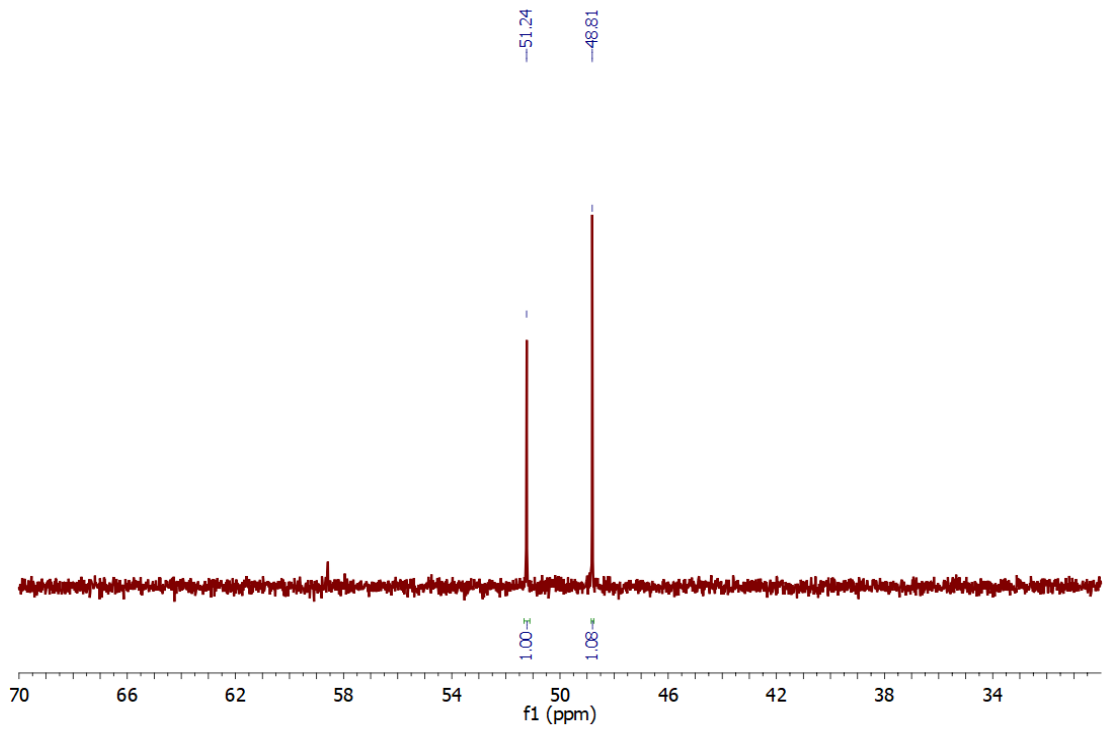

Appendix Figure I.7. $^{31}P\{^{1}H\}$ NMR (283 MHz) spectrum of **4** in benzene-d_6 at 23 ºC.

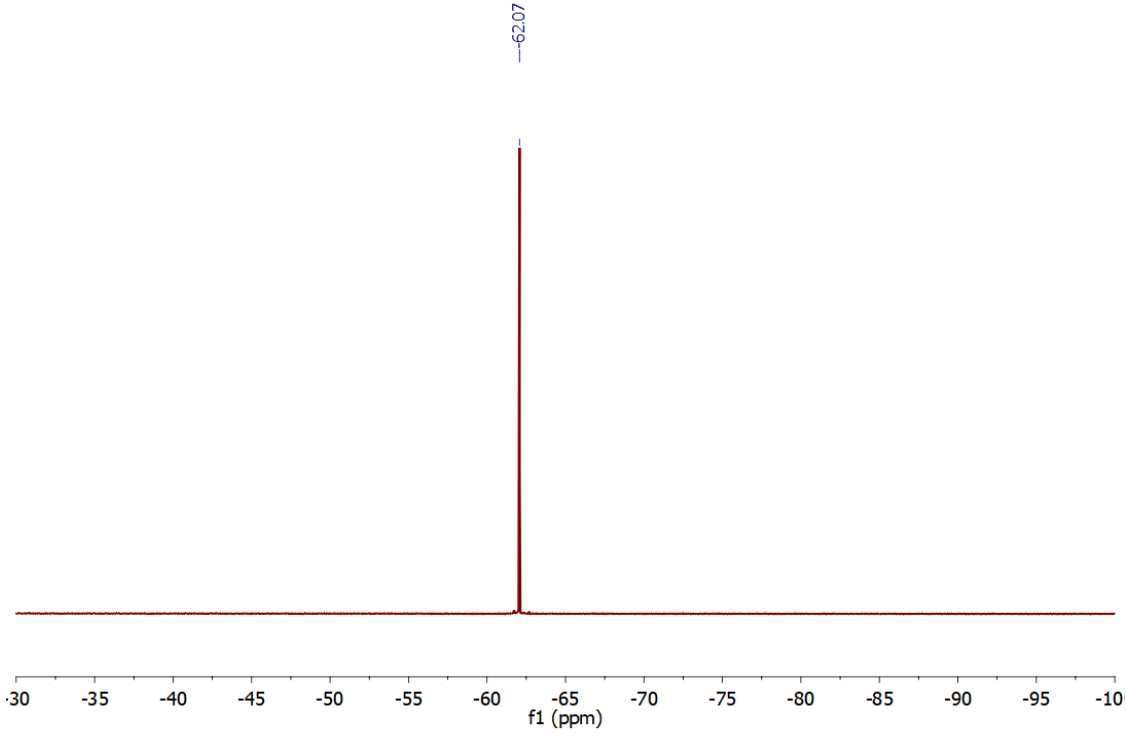

Appendix Figure I.8. $^{19}F\{^{1}H\}$ NMR (659 MHz) spectrum of **4** in benzene-d_6 at 23 ºC.

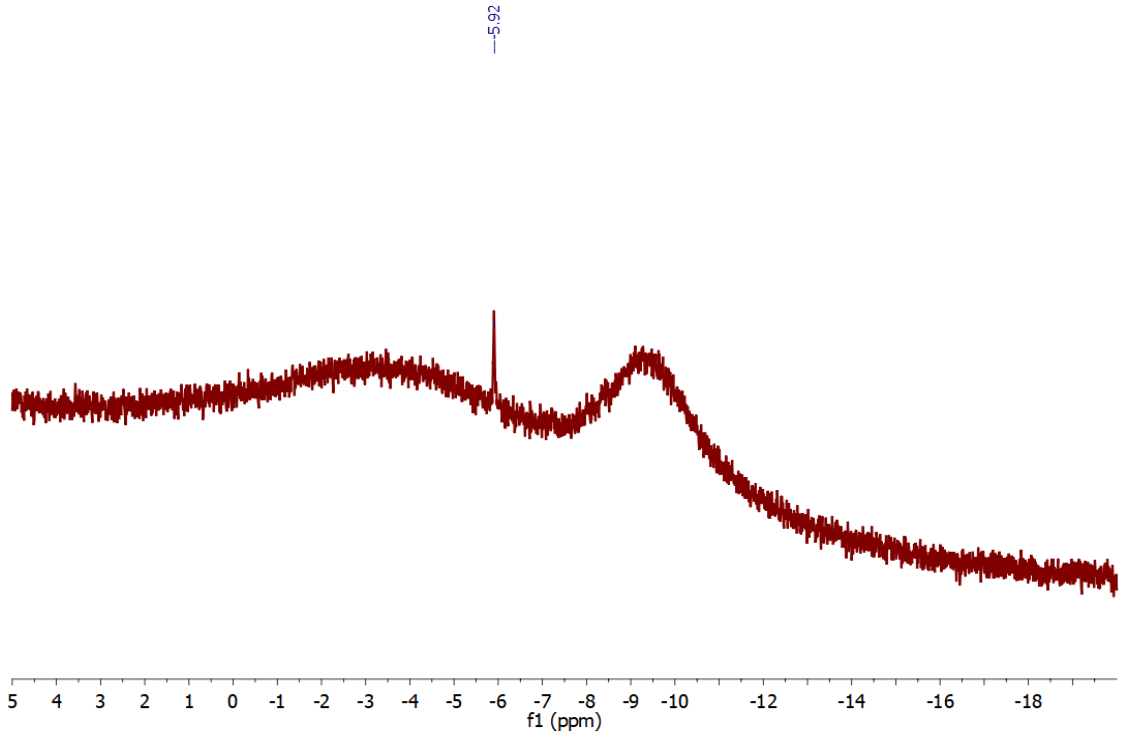

Appendix Figure I.9. $^{11}B\{^{1}H\}$ NMR (224 MHz) spectrum of **4** in benzene-*d*6 at 23 ºC.

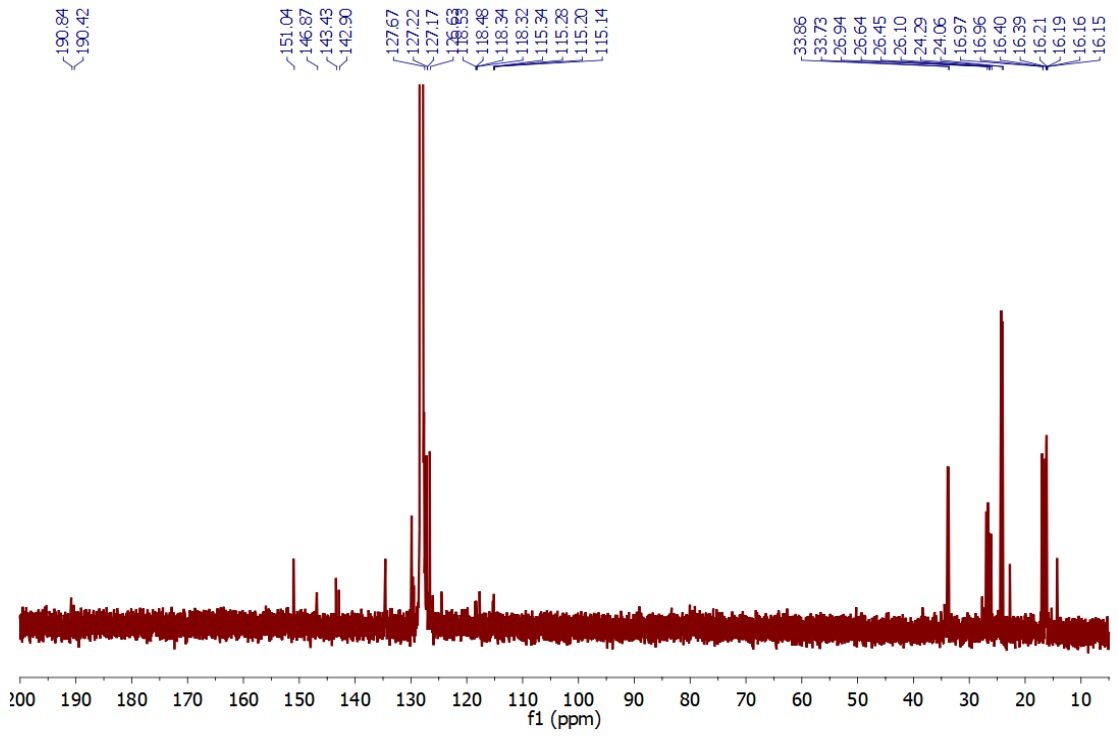

Appendix Figure I.10. $^{13}C\{^{1}H\}$ NMR (176 MHz) spectrum of **4** in benzene-d_6 at 23 ºC.

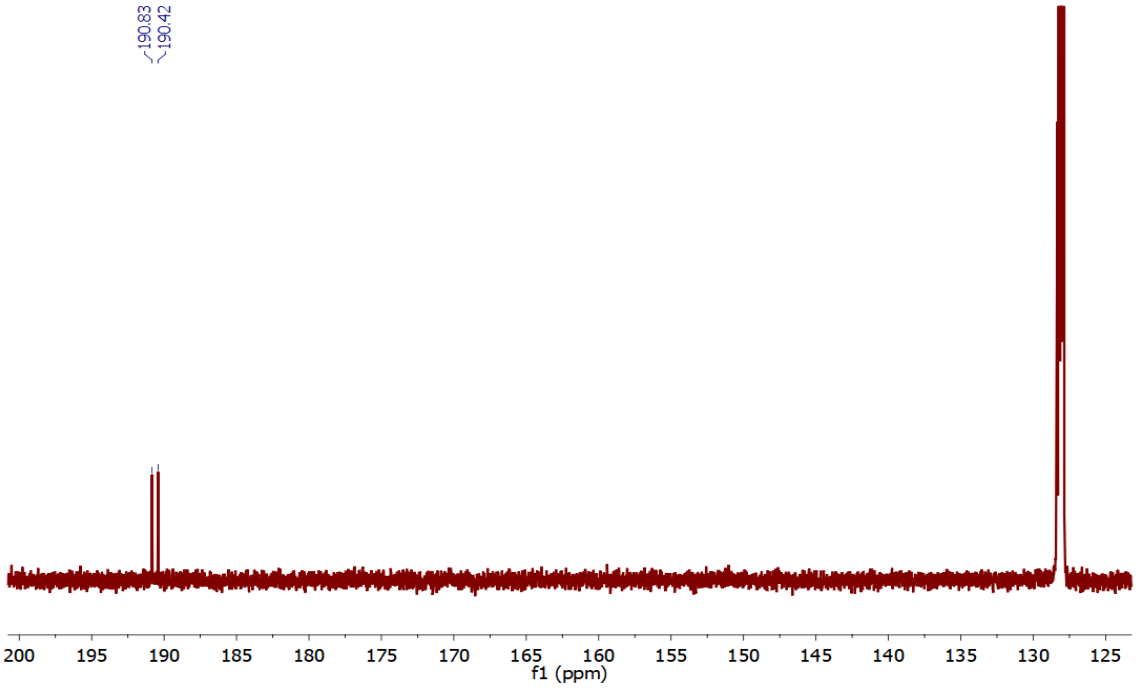

Appendix Figure I.11. $^{13}C\{^{1}H\}$ NMR (176 MHz, downfield region) spectrum of **^{13}CO-4** prepared with isotopically-enriched **^{13}CO-1** in benzene-d_6 at 23 ºC.

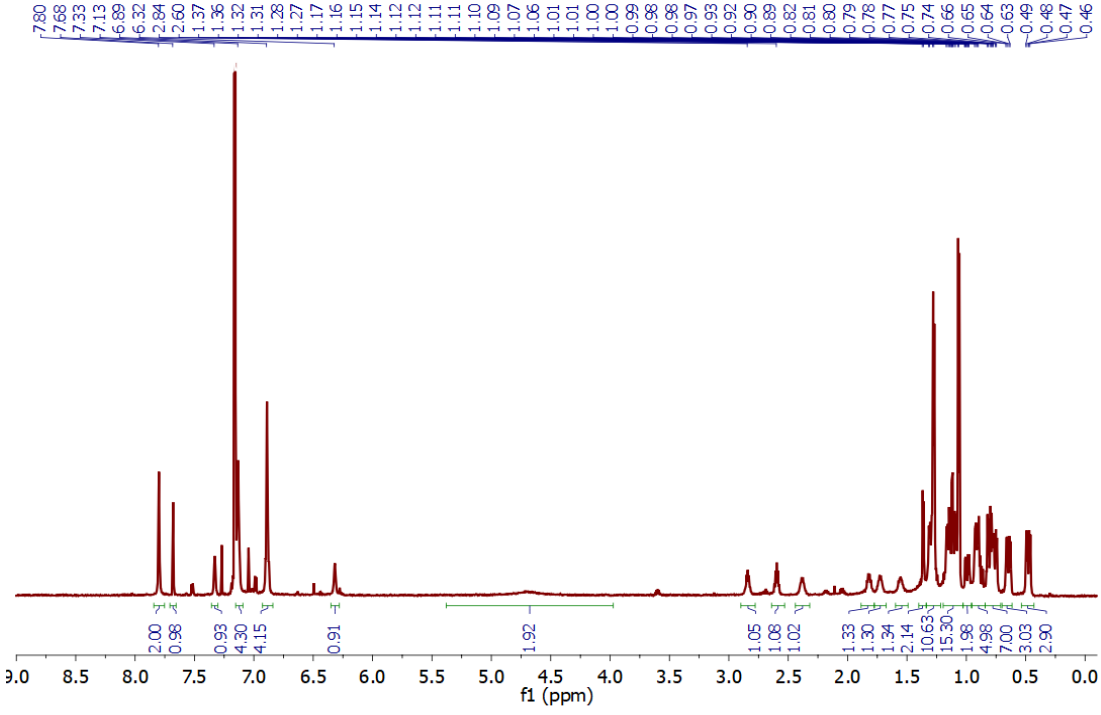

Appendix Figure I.12. ^{1}H NMR (700 MHz) spectrum of **5** in benzene-d_6 at 23 ºC.

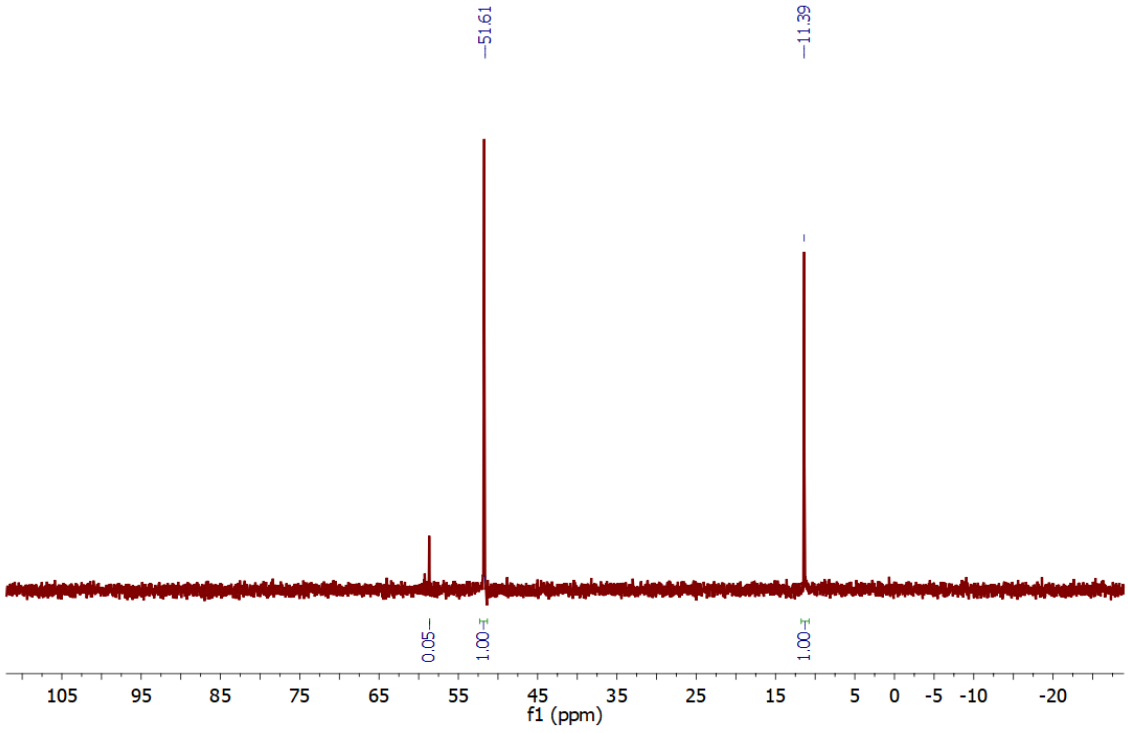

Appendix Figure I.13. $^{31}P\{^{1}H\}$ (283 MHz) NMR spectrum of **5** in benzene-d_6 at 23 ºC.

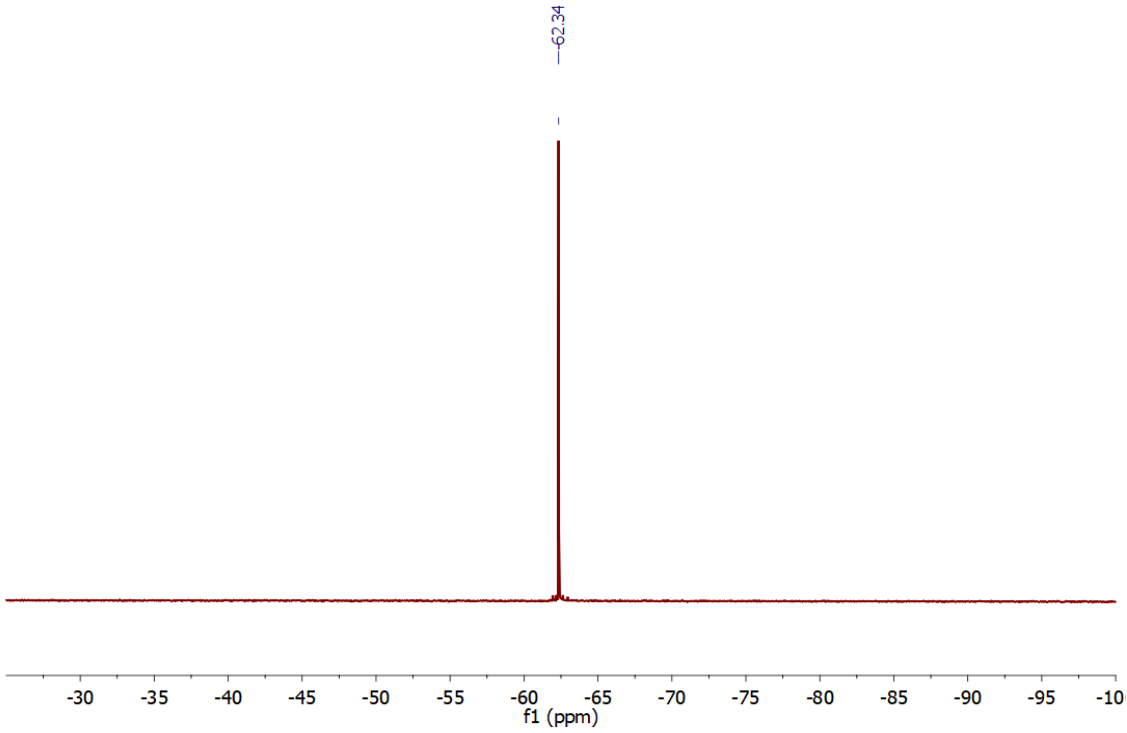

Appendix Figure I.14. $^{19}F\{^{1}H\}$ NMR (659 MHz) spectrum of **5** in benzene-d_6 at 23 ºC.

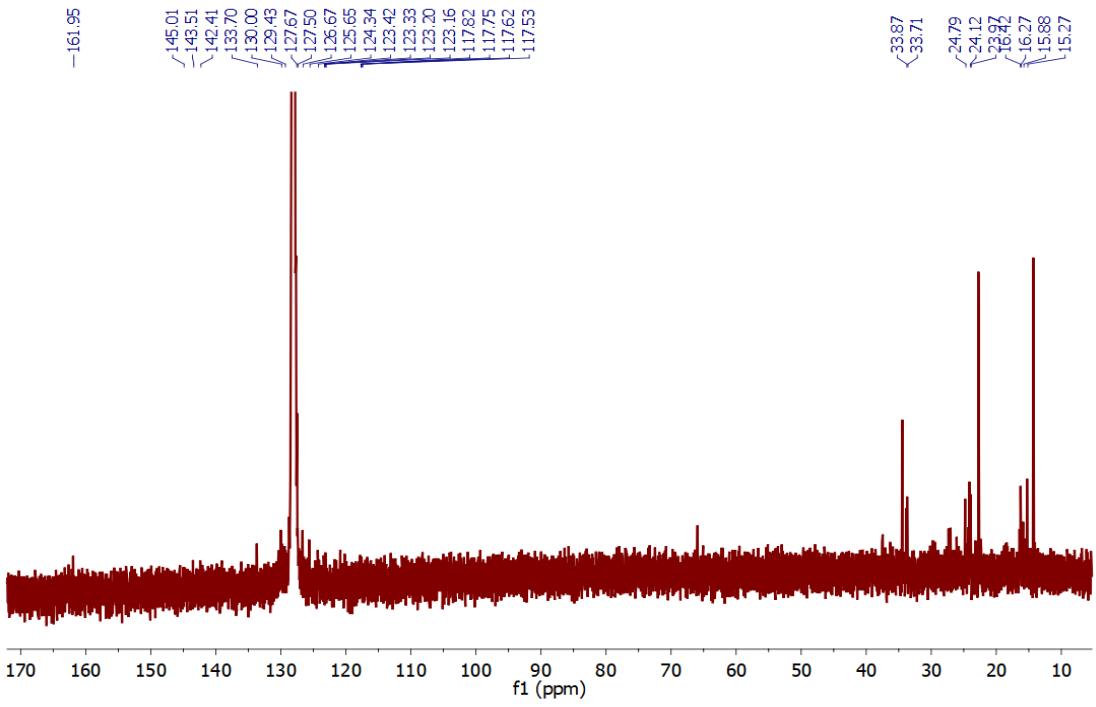

Appendix Figure I.15. $^{13}C\{^{1}H\}$ NMR (176 MHz) spectrum of **5** in benzene-d_6 at 23 ºC.

Reaction of **1** with 1:1 H_2BMes/D_2BMes

In a 20 mL scintillation vial, a benzene-d_6 solution of mesitylborane (0.002 g, 0.014 mmol, 0.5 equiv) and mesitylborane-d_2 (0.002 g, 0.014, 0.5 equiv) was combined with **1** (0.020 g, 0.029 mmol, 1 equiv). The mixture was briefly agitated and then transferred into J. Young NMR tube and sealed. The procedure was repeated without **1** and monitored. No HD gas was observed in the absence of a rhodium complex.

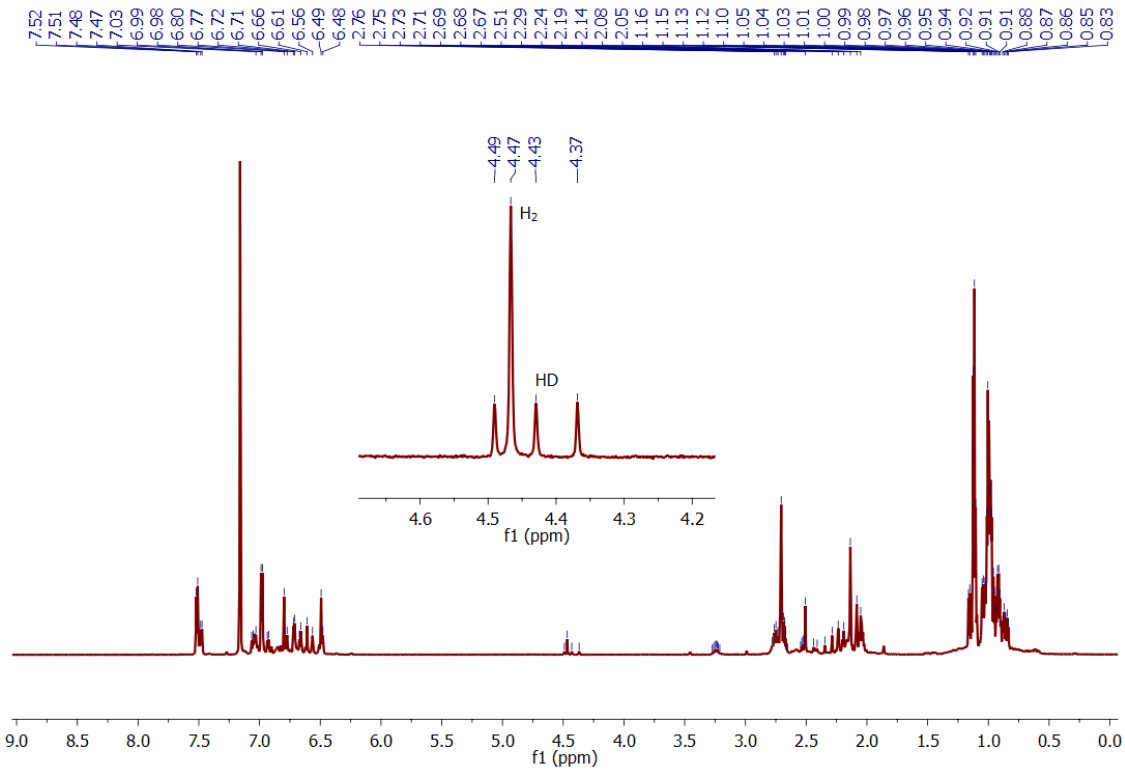

Appendix Figure I.16. ^{1}H NMR spectrum of **1** + 1:1 mixture of mesitylborane an mesitylborane-d_2. Inset: enlarged region showing H_2 and HD gas in benzene-d_6.

Variable Temperature NMR Data

A J. Young NMR tube was charged with 0.011 g of **4**, dissolved in 0.6 mL of toluene-d_8, and sealed. ^{1}H NMR spectra were first recorded at 22 ºC, and then at –80 ºC, rising in temperature to 22 ºC. The coalescence temperature T_{coal} was determined by careful inspection of the ^{1}H NMR spectra. At –25 ºC, the resonances assigned to Rh–*H* and B–*H* had disappeared into the baseline completely.

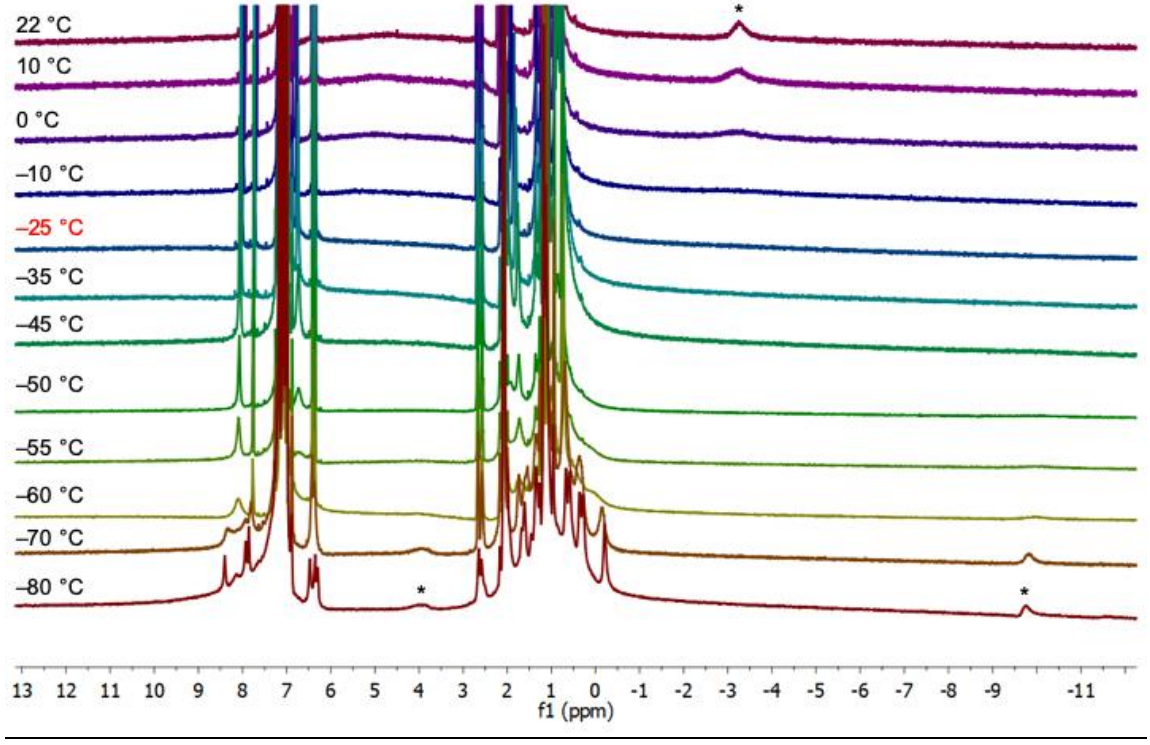

Appendix Figure I.17. Variable temperature ^{1}H NMR (700 MHz) spectra of **4** in toluene-d_8. The peaks corresponding to the borane B*H*$_2$ protons are marked with an asterisk (*) and the coalescence temperature (–25 ºC) is highlighted in red.

Determination of $\Delta G^{\ddagger}_{coal}$ from Variable Temperature NMR spectroscopy

The coalescence temperature (T_{coal}) was determined by careful inspection of the ^{1}H NMR spectra in toluene-d_8 at a range of temperatures. At –25 ºC, the peaks corresponding to the B–*H* and Rh–*H* protons vanished and the broad peak corresponding to the BH_2 moiety had not yet appeared. Here, Δν is the maximum peak separation in Hz. The $\Delta G^{\ddagger}$ was calculated according to the following equation (Eq. 1) at the coalescence temperature (–25 ºC) to be 9.9(4) kcal mol^{-1}.[6]

$$\Delta G^{\ddagger}_{coal}\,(\text{kcal mol}^{-1}) = \frac{1.914 \times 10^{-2}(T_{coal})[9.972+\log\frac{T_{coal}}{\Delta\nu}]}{4.184} \qquad \text{Eq. 1.}$$

T_{coal} = 248.15 K

Δν = 4078 Hz

Appendix I. IV Crystallographic Details

X-Ray Diffraction Techniques. All structures were collected on a Rigaku SuperNova diffractometer equipped with a Dectris Pilatus 3R 200K-A hybrid-pixel-array detector, a four-circle κ goniometer, sealed graphite-monochromated Mo Kα (λ = 0.71073 Å) and Cu Kα (λ = 1.54178 Å) X-ray sources, and an Oxford cryostream-cooling device fixed at 100 K. Single crystals suitable for X-ray diffraction studies were mounted on a MiTiGen cryo-loop using desiccated Paratone–*N* oil stored in the glovebox.

The structures were solved by the Intrinsic Phasing methods and refined by least-squares methods using SHELXT-2014 and SHELXL-2014 with the OLEX2 interface.[7-9] The program PLATON was employed to confirm the absence of higher symmetry space groups.[10] All non-H atoms were located in difference Fourier maps, and then refined anisotropically. Outlier reflections were omitted from refinement when appropriate. Hydrogen atoms on C atoms were placed at idealized positions and refined using a riding model. The isotropic displacement parameters of all hydrogen atoms were fixed to 1.2 times the atoms they are linked to (1.5 times for methyl groups). Crystallographic refinement details, including disorder modeling and software employed, have been delineated within in each crystallographic information file (*.cif). Molecular graphics were generated using ORTEP and Adobe Illustrator.

Further details on particular structures are noted below:

Complex 3. The unit cell contained two unique molecules oriented in a head-to-tail arrangement. A short contact (2.193 Å) was located between the carbonyl oxygen atom of one molecule and the pyrrole C–H atom of another.

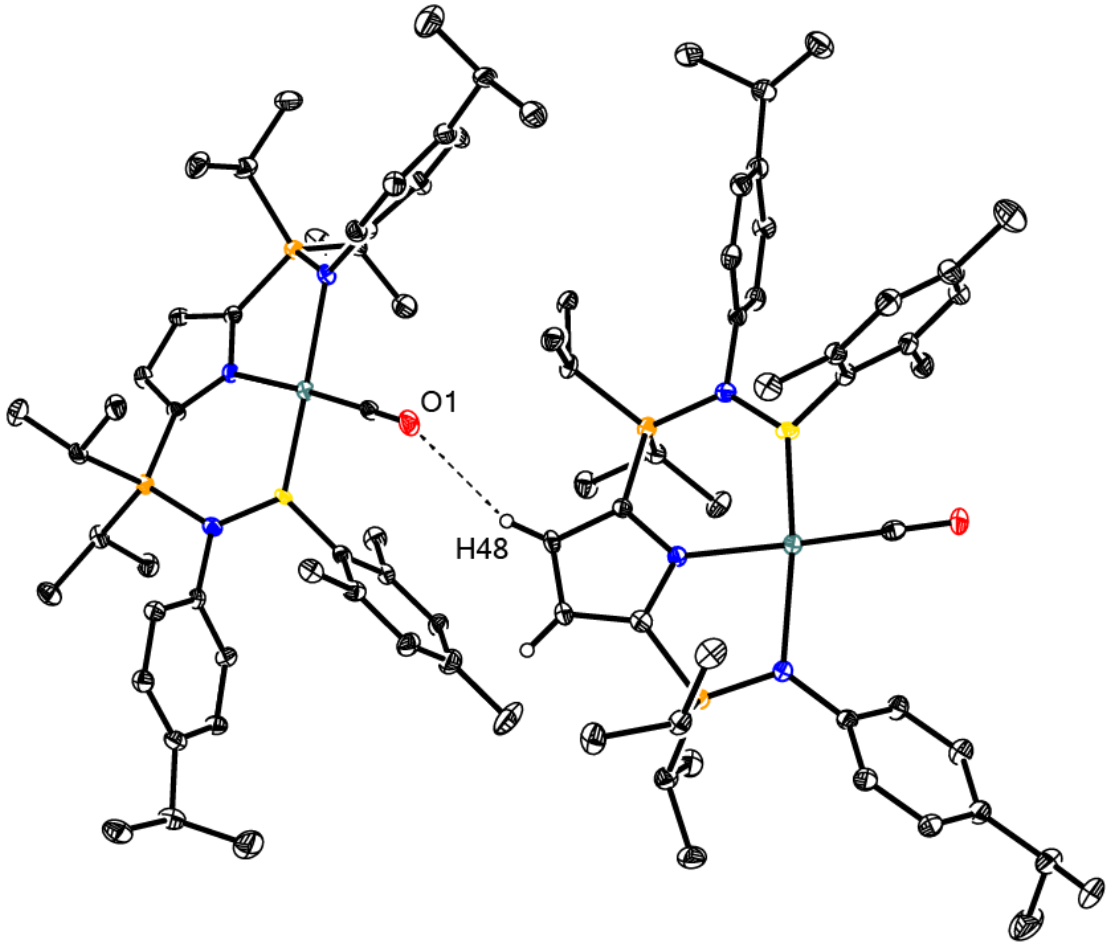

Appendix Figure I.18. Unit cell of **3** with 30% probability ellipsoids. Short contact (2.193 Å) between O1 and H48 is shown.

Appendix Table I.1. Single crystal X-ray diffraction details of reported complexes.

	3	**4**
CCDC Entry	198537	1985379
Crystal Size (mm)	0.20 × 0.10 × 0.05	0.25 × 0.25 × 0.25
Moiety Formula	$C_{44}H_{63}BN_3OP_2Rh$	$C_{43}H_{57}BF_6N_3OP_2Rh•C_6H_6$
Formula weight (g/mol)	825.63	999.68
l (nm)	1.54178	0.71073
T (K)	100(2)	100(2)
Crystal System	Triclinic	Monoclinic
Space group (*Z*)	P–1 (4)	*I*2/*a* (8)
a (Å)	14.5167(3)	28.3648(5)
b (Å)	18.5067(4)	12.2130(1)
c (Å)	19.7008(6)	32.5843(5)
α (deg)	65.627(2)	90
β (deg)	88.777(2)	111.394(2)
γ (deg)	77.349(2)	90
Volume ($Å^3$)	4689.8(2)	10510.0(3)
Calc. *r* ($g\ cm^{-3}$)	1.169	1.264
m (mm^{-1})	3.831	0.443
Reflections	18596	11658
Completeness (to 2θ)	0.960	0.995
C–C Bond Precision (Å)	0.0093	0.0025
R_1, wR_2 [$I > 2\sigma(I)$]	0.0759, 0.2131	0.0261, 0.0657
GooF	1.080	1.035

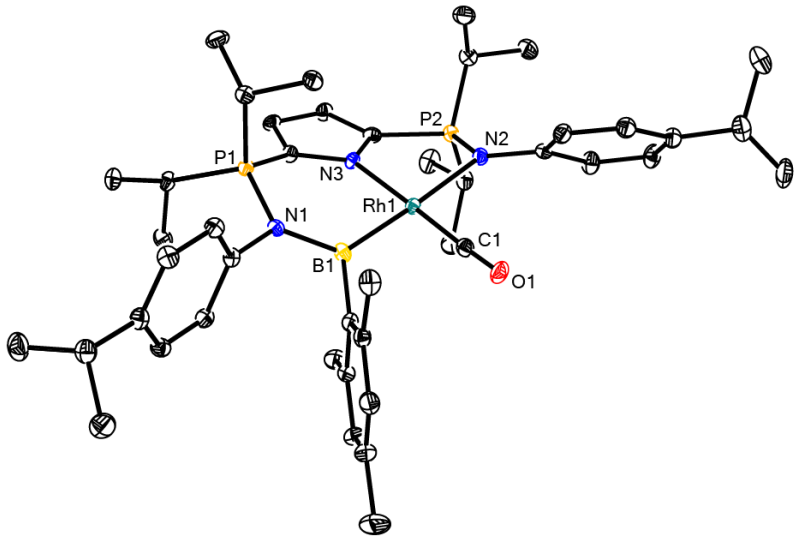

Appendix Figure I.19. Molecular structure of **3** with 30% probability ellipsoids. Hydrogen atoms omitted for clarity.

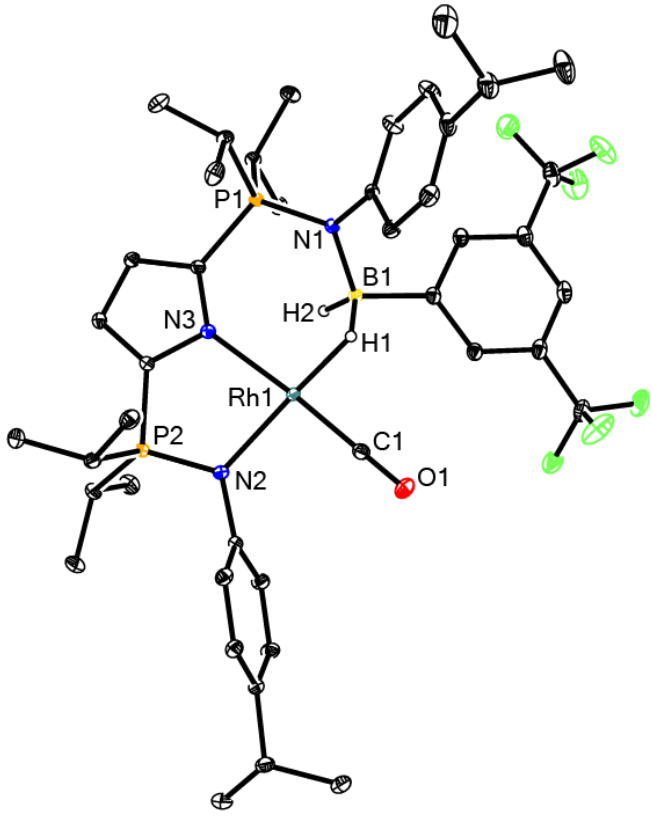

Appendix Figure I.20. Molecular structure of **4** with 30% probability ellipsoids. All hydrogen atoms except BH_2 and solvent molecules of recrystallization are omitted for clarity.

Appendix I. V Computational Details

Density Functional Theory (DFT) calculations were carried out on the unmodified structure of **3** using the Gaussian 16 (revision B.01) computational suite.[11] Cartesian coordinates were obtained from X-ray diffraction analysis. Gas-phase geometry optimization was performed using the B3LYP functional,[12] employing the aug-cc-pVDZ basis set with associated pseudopotentials (Rh) for non C, H atoms (cc-pVDZ).[13] Frequency calculations verified the absence of imaginary frequencies in all optimized structures. Visualization of optimized structures and rendering of molecular orbitals was performed using Gaussview.[14] Wiberg bond indices were determined using NBO 3.1,[15,16] also using the B3LYP/aug-cc-pVDZ level of theory.

Appendix Table I.2. Comparison of DFT-calculated (B3LYP/aug-cc-pVDZ) and experimental structural parameters in **3**.

Parameter	**Experimental**	**Calculated**	**% Difference**
d(Rh1–B1) (Å)	2.024(5)	2.031	0.34%
d(P1–N1) (Å)	1.658(6)	1.707	2.91%
d(N1–B1) (Å)	1.501(8)	1.518	1.12%
d(Rh1–C1) (Å)	1.797(6)	1.824	1.49%

Appendix Table I.3. Selected second-order interactions in **3**.

Donor	**Acceptor**	$E^{(2)}$ **(kcal mol^{-1})**	e_i-e_j	$F_{i,j}$
197. LP (4) Rh	209. LP* (2) B	1.89	0.21	0.018
202. LP (1) N	209. LP* (2) B	35.17	0.30	0.093
195. LP (2) Rh	209. LP* (2) B	10.35	0.21	0.044
196. LP (3) Rh	209. LP* (2) B	6.88	0.23	0.036

Appendix Table I.4. NBO-derived Wiberg Bond Indices (WBI) of selected bonds in **3** at the B3LYP/aug-cc-pVDZ level of theory.

Selected Bond	Wiberg Bond Index (WBI)
Rh1–B1	0.9308
N1–B1	0.7026
P1–N1	0.8570
P2–N2	1.0606

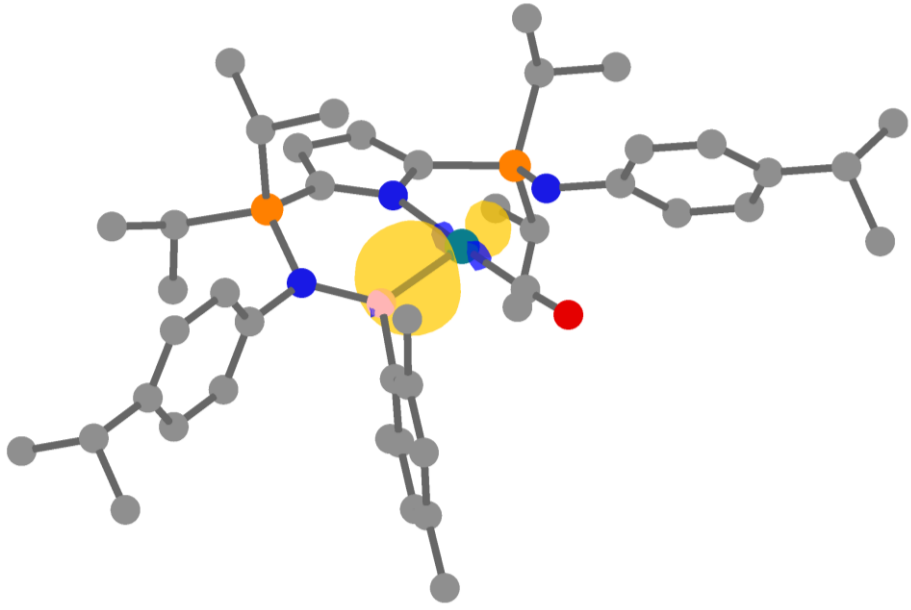

Appendix Figure I.21. NBO representation of the NBO-derived Rh–B bonding orbital (occupancy 1.807 electrons). Orbital surfaces are plotted with an isovalue of 0.08 using Gaussview.

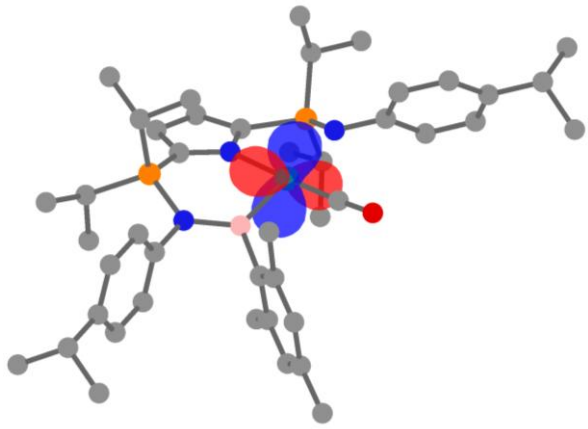

Appendix Figure I.22. NBO representation of the NBO-derived Rh d_{xz} orbital (occupancy 1.893 electrons). Orbital surfaces are plotted with an isovalue of 0.08 using Gaussview.

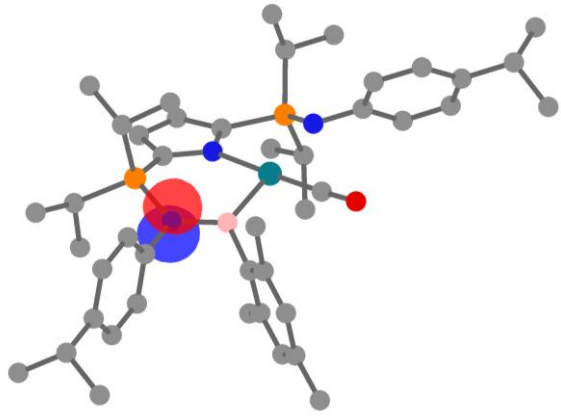

Appendix Figure I.23. NBO representation of the NBO-derived N LP donor orbital (occupancy 1.695 electrons). Orbital surfaces are plotted with an isovalue of 0.08 using Gaussview.

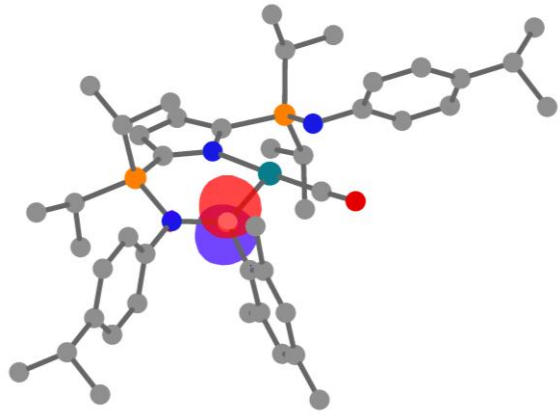

Appendix Figure I.24. NBO representation of the NBO-derived B LP* acceptor orbital (occupancy 0.271 electrons). Orbital surfaces are plotted with an isovalue of 0.08 using Gaussview.

Appendix I. VI References

1. A. B. Pangborn, M. A. Giardello, R. H. Grubbs, R. K. Rosen, F. J. Timmers, *Organometallics* **1996**, *15*, 1518–1520.
2. a) S. K. Mellerup, C. Li, J. Radtke, X. Wang, Q.-S. Li, S. Wang, *Angew. Chem. Int. Ed*. **2018**, *57*, 9634–9639. b) K. Samigullin, M. Bolte, H.-W. Lerner, M. Wagner, *Organometallics* **2014**, *33*, 3564–3569.
3. C. S. MacNeil, P. G. Hayes, *Chem. Eur. J.* **2019**, *25*, 8203–8207
4. G. R. Fulmer, A. J. M. Miller, N. H. Sherden, H. E. Gottlieb, A. Nudelman, B. M. Stoltz, J. E. Bercaw, K. I. Goldberg, *Organometallics* **2010**, *29*, 2176–2179.
5. C. P. Rosenau, B. J. Jelier, A. D. Gossert, A. Togni, *Angew. Chem. Int. Ed*. **2018**, *57*, 9528–9533.
6. J. Sandstrøm, Dynamic NMR Spectroscopy; Academic Press: New York, 1982.
7. G. M. Sheldrick, *Acta Crystallogr. Sect. A* **2015**, *71*, 3–8.
8. G. M. Sheldrick, *Acta Crystallogr. Sect. C* **2015**, *71*, 3–8.
9. O. V. Dolomanov, L. J. Bourhis, R. J. Gildea, J. A. K. Howard, H. Puschmann, *J. Appl. Crystallogr.* **2009**, *42*, 339–341.
10. A. Spek, *J. Appl. Crystallogr.* **2003**, *36*, 7–13.
11. Gaussian 16, Revision B.01, M. J. Frisch, G. W. Trucks, H. B. Schlegel, G. E. Scuseria, M. A. Robb, J. R. Cheeseman, G. Scalmani, V. Barone, G. A. Petersson, H. Nakatsuji, X. Li, M. Caricato, A. V. Marenich, J. Bloino, B. G. Janesko, R. Gomperts, B. Mennucci, H. P. Hratchian, J. V. Ortiz, A. F. Izmaylov, J. L. Sonnenberg, D. Williams-Young, F. Ding, F. Lipparini, F. Egidi, J. Goings, B. Peng, A. Petrone, T. Henderson, D. Ranasinghe, V. G. Zakrzewski, J. Gao, N. Rega, G. Zheng, W. Liang, M. Hada, M. Ehara, K. Toyota, R. Fukuda, J. Hasegawa, M. Ishida, T. Nakajima, Y. Honda, O. Kitao, H. Nakai, T. Vreven, K. Throssell, J. A. Montgomery, Jr., J. E. Peralta, F. Ogliaro, M. J. Bearpark, J. J. Heyd, E. N. Brothers, K. N. Kudin, V. N. Staroverov, T. A. Keith, R. Kobayashi, J. Normand, K. Raghavachari, A. P. Rendell, J. C.

Burant, S. S. Iyengar, J. Tomasi, M. Cossi, J. M. Millam, M. Klene, C. Adamo, R. Cammi, J. W. Ochterski, R. L. Martin, K. Morokuma, O. Farkas, J. B. Foresman, and D. J. Fox, Gaussian, Inc., Wallingford CT, 2016.

12. A. D. Becke, *J. Chem. Phys.* **1993**, *98*, 5648–5652.
13. D. Figgen, K. A. Peterson, M. Dolg, H. Stoll, *J. Chem. Phys.* **2009**, *130*, 164108.
14. GaussView, version 5.0 Gaussian, Inc., Wallingford, CT, **2016**.
15. NBO, version 6.0. E. D. Glendening, J. K. Badenhoop, A. E. Reed, J. E. Carpenter, J. A. Bohmann, C. M. Morales, C. R. Landis, F. Weinhold, Theoretical Chemistry Institute, University of Wisconsin, Madison, **2013**.
16. J. P. Foster, F. Weinhold, *J. Am. Chem. Soc.* **1980**, *102*, 7211–7218.

Appendix II. Supporting Information for Chapter 3

Reformatted from published supporting information associated with "Hsiang, S.J.; Hayes, P.G.*, Rhodium-mediated Dehydrogenation of Hydroboranes and Group 14 Compounds: Base-stabilized Silylene and Germylene Complexes vs. Transmetalation. *Chemistry – A European Journal.* **2023**, *30*, e202302925."

Table of Contents

Appendix II. I NMR Spectra

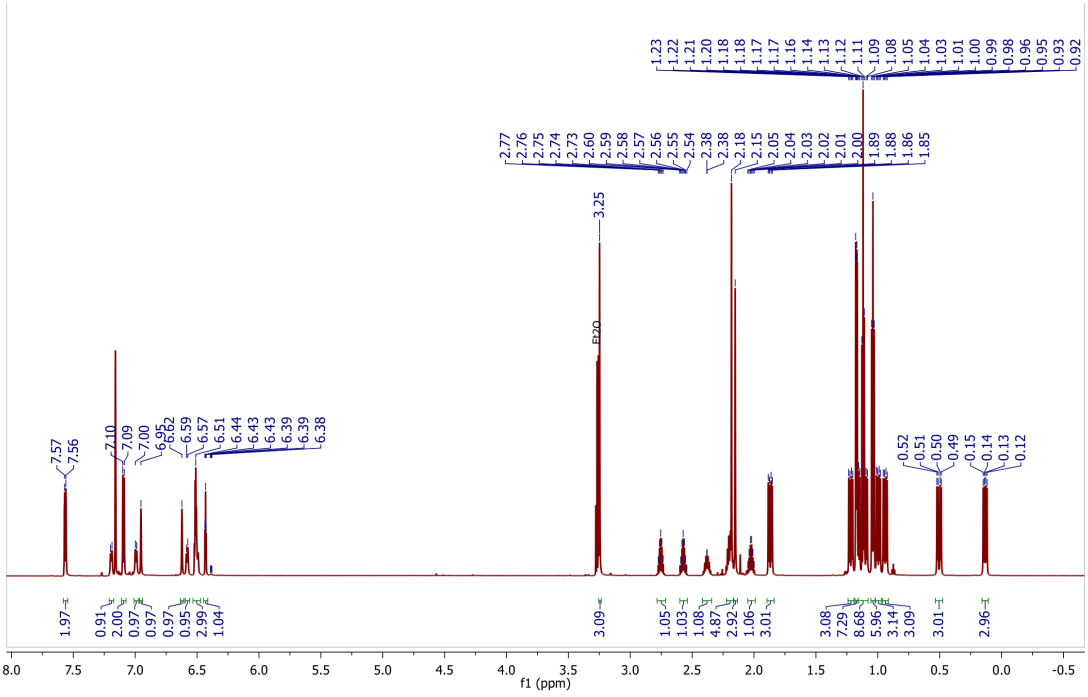

Appendix Figure II.1. ^{1}H NMR (700 MHz) spectrum of complex **6** in benzene-d_6 at 22 °C

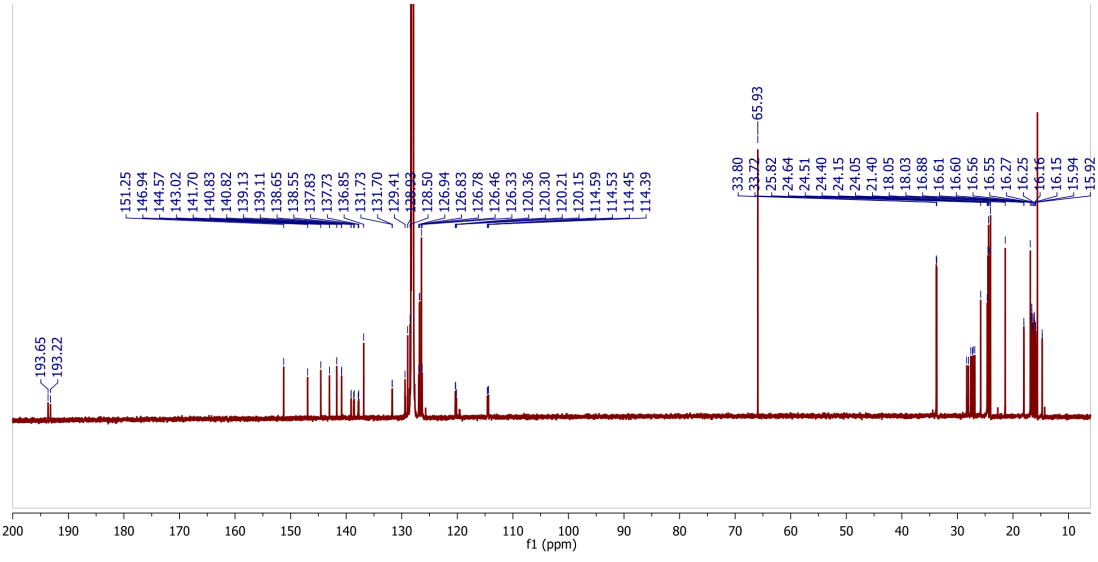

Appendix Figure II.2. ^{13}C{^{1}H} NMR (176 MHz) spectrum of complex **6** in benzene-d_6 at 22 °C

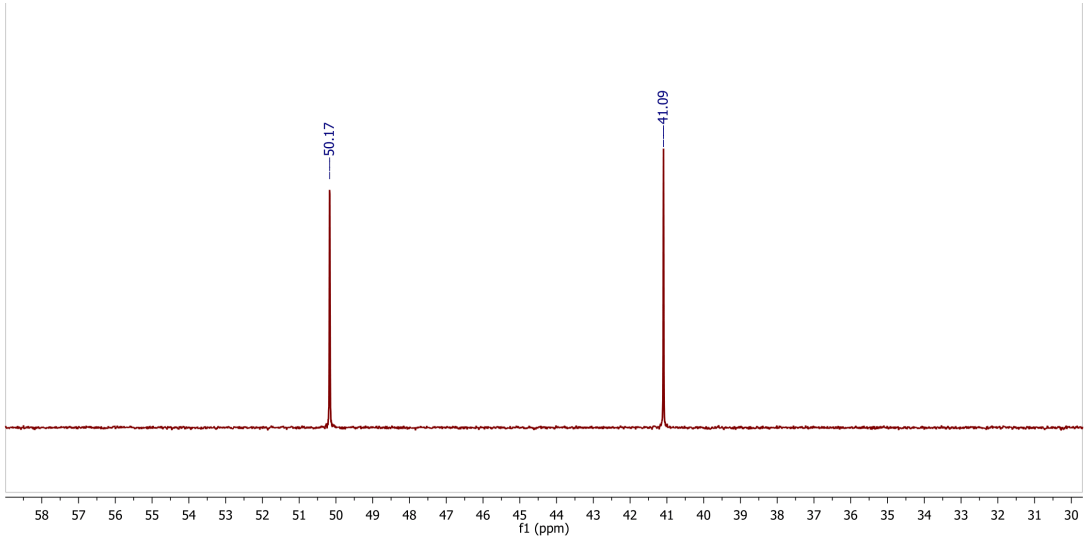

Appendix Figure II.3. $^{31}P\{^{1}H\}$ NMR (283.5 MHz) spectrum of complex **6** in benzene-d_6 at 22 °C

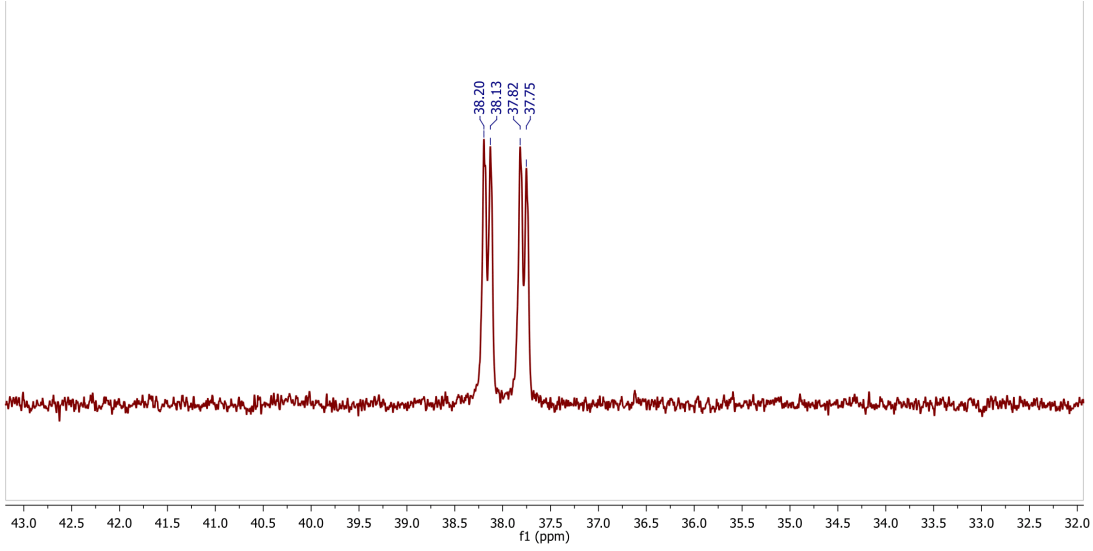

Appendix Figure II.4. $^{29}Si\{^{1}H\}$ NMR (139 MHz) spectrum of complex **6** in benzene-d_6 at 22 °C

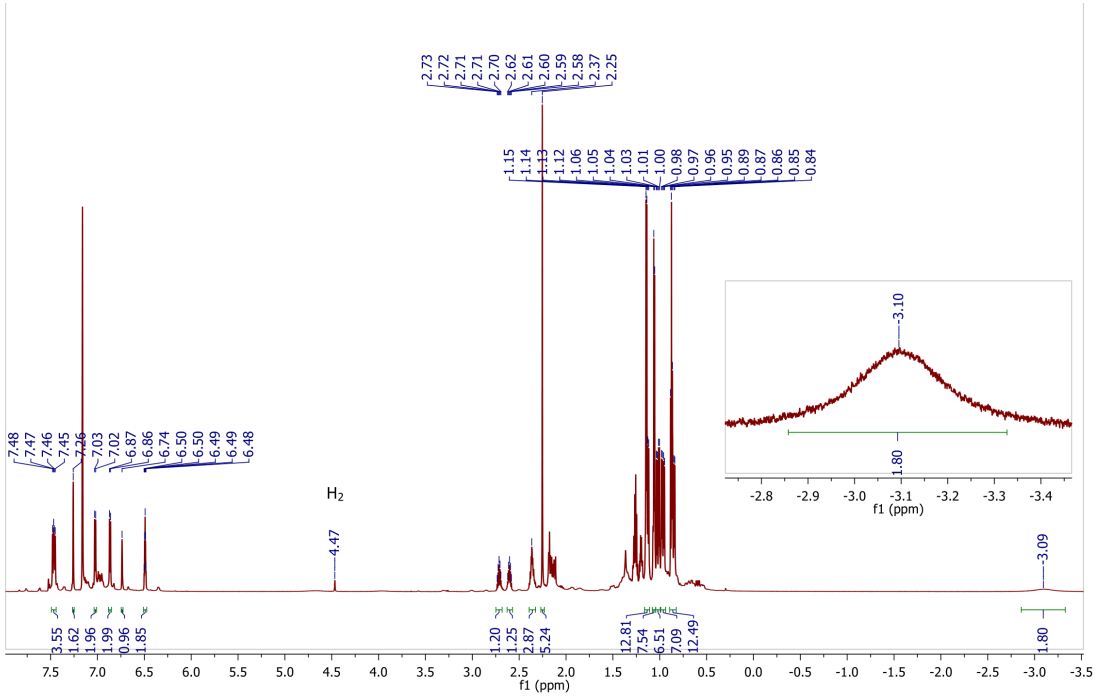

Appendix Figure II.5. ^{1}H NMR (700 MHz) spectrum of complex **7** in benzene-d_6 at 22 °C

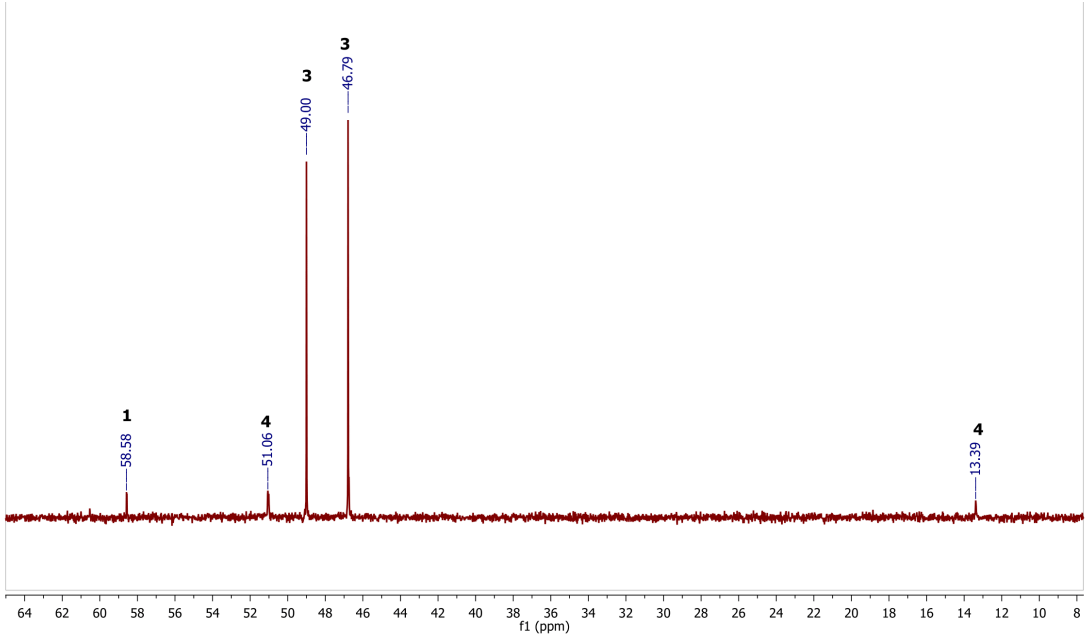

Appendix Figure II.6. ^{31}P{^{1}H} NMR (283.5 MHz) spectrum of complex **7** in benzene-d_6 at 22 °C

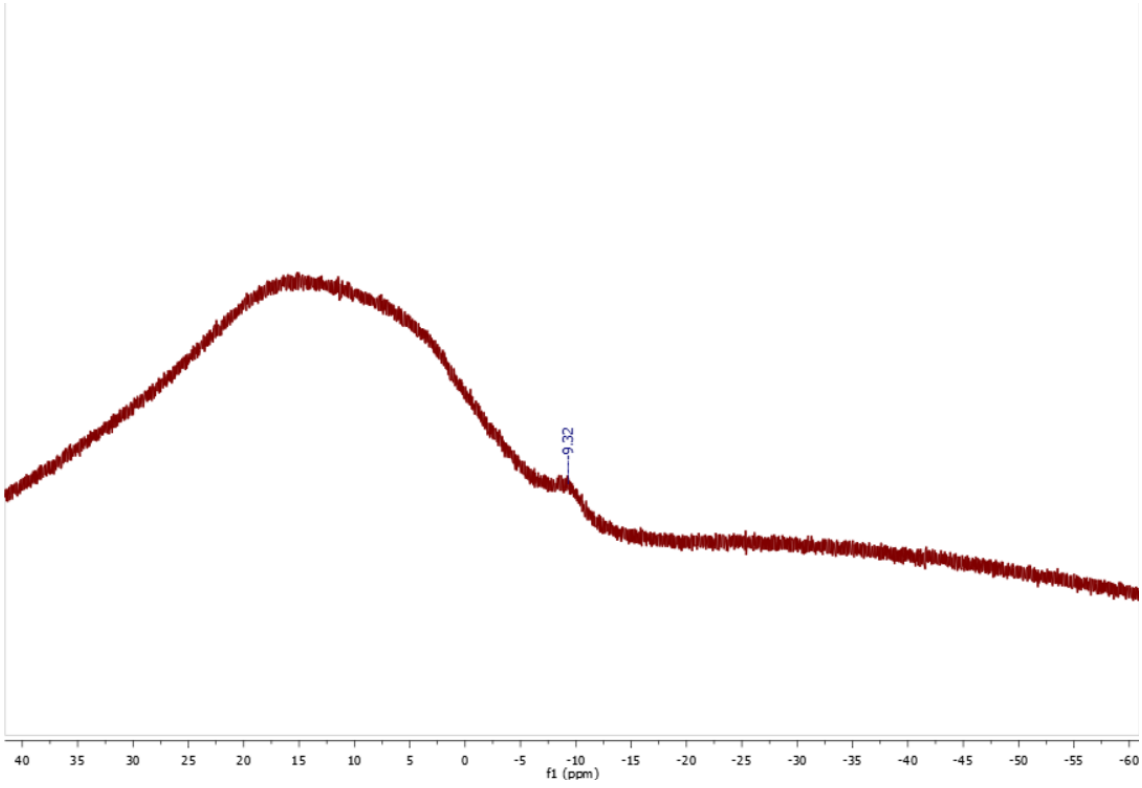

Appendix Figure II.7. $^{11}B\{^{1}H\}$ NMR (224.6 MHz) spectrum of complex **7** in benzene-d_6 at 22 °C

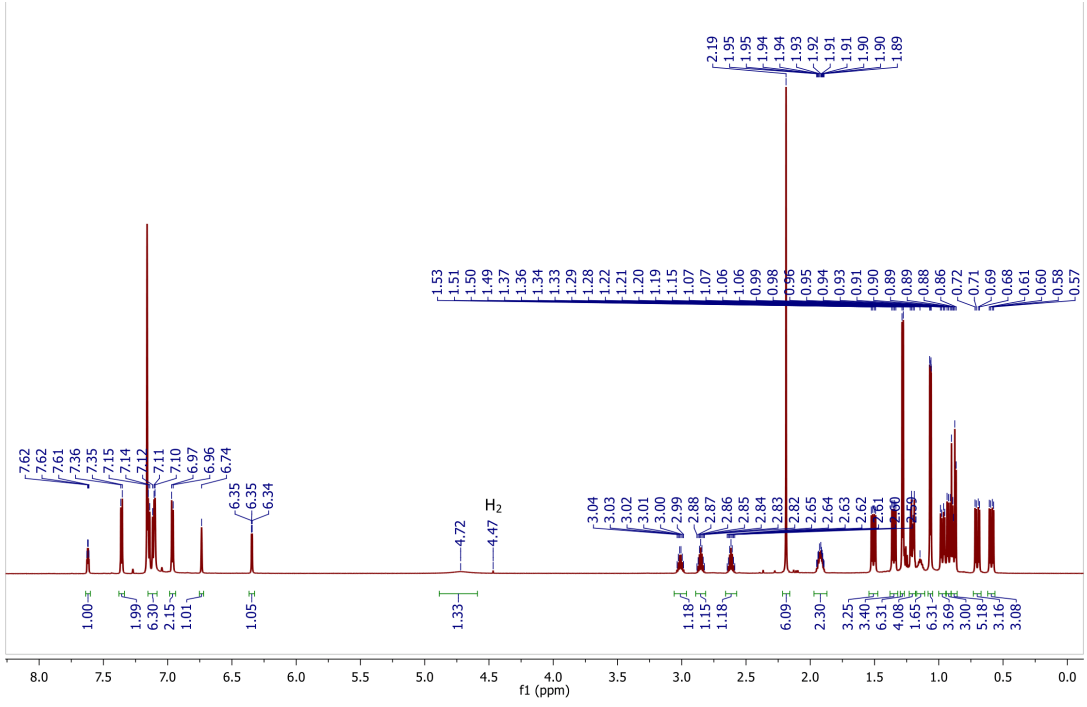

Appendix Figure II.8. ^{1}H NMR (700 MHz) spectrum of complex **8** in benzene-d_6 at 22 °C

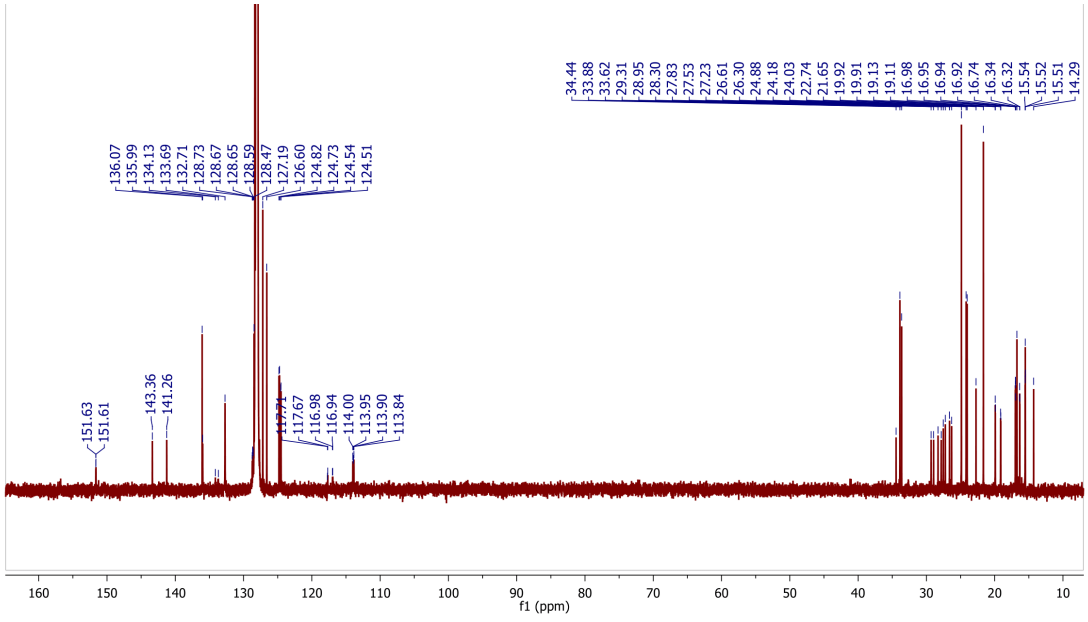

Appendix Figure II.9. $^{13}C\{^{1}H\}$ NMR (176 MHz) spectrum of complex **8** in benzene-d_6 at 22 °C

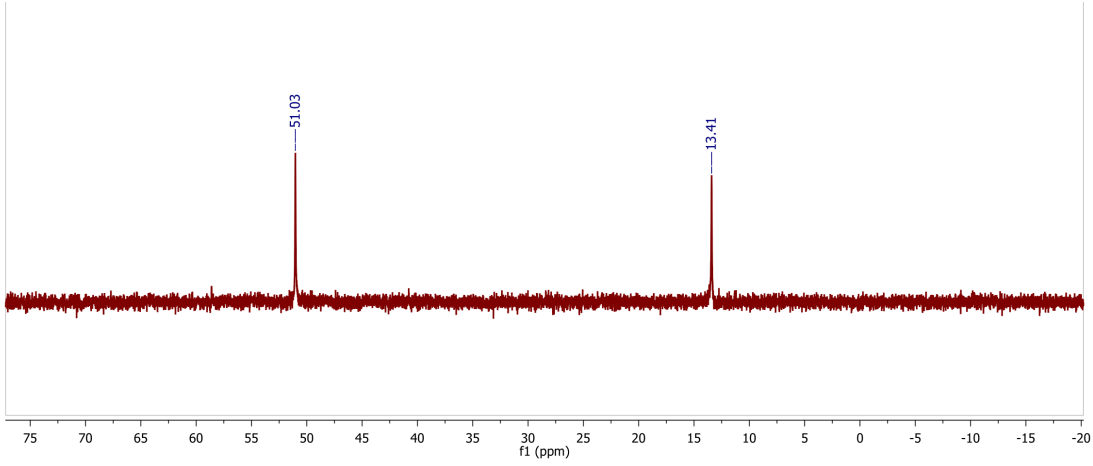

Appendix Figure II.10. $^{31}P\{^{1}H\}$ NMR (283.5 MHz) spectrum of complex **8** in benzene-d_6 at 22 °C

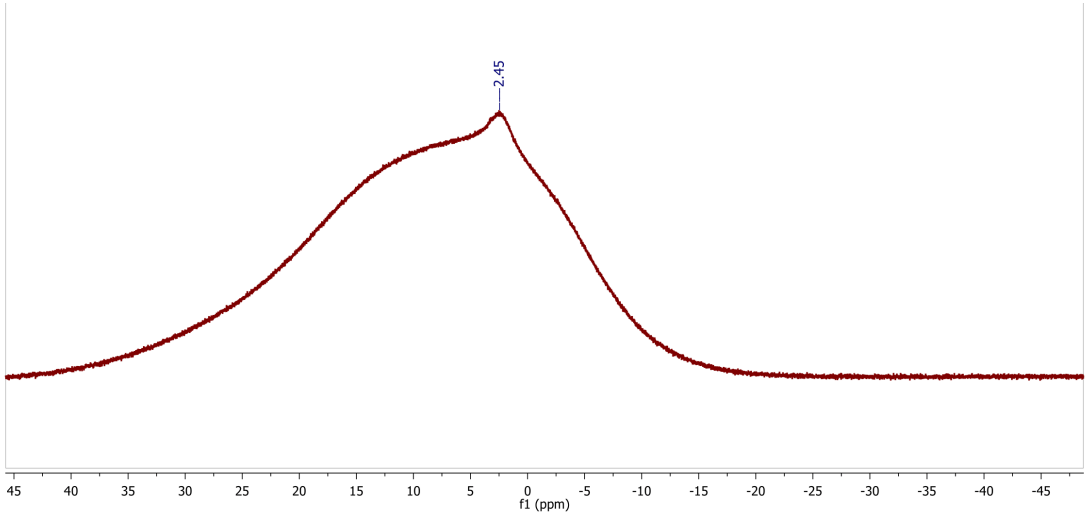

Appendix Figure II.11. $^{11}B\{^{1}H\}$ NMR (224.6 MHz) spectrum of complex **8** in benzene-d_6 at 22 °C

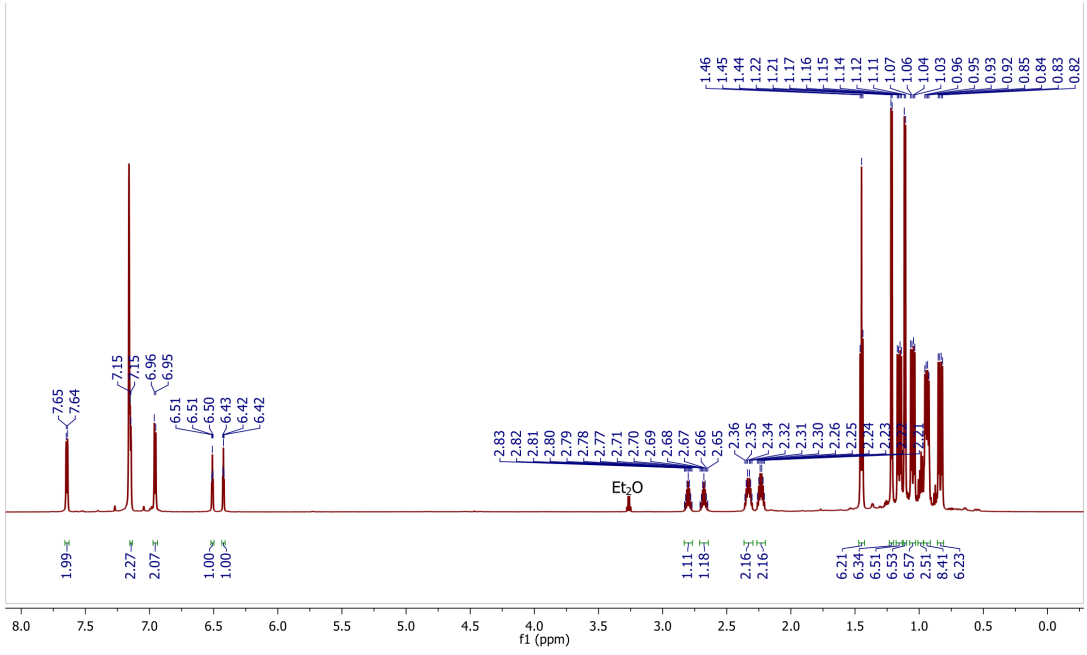

Appendix Figure II.12. ^{1}H NMR (700 MHz) spectrum of complex **9** in benzene-d_6 at 22 °C

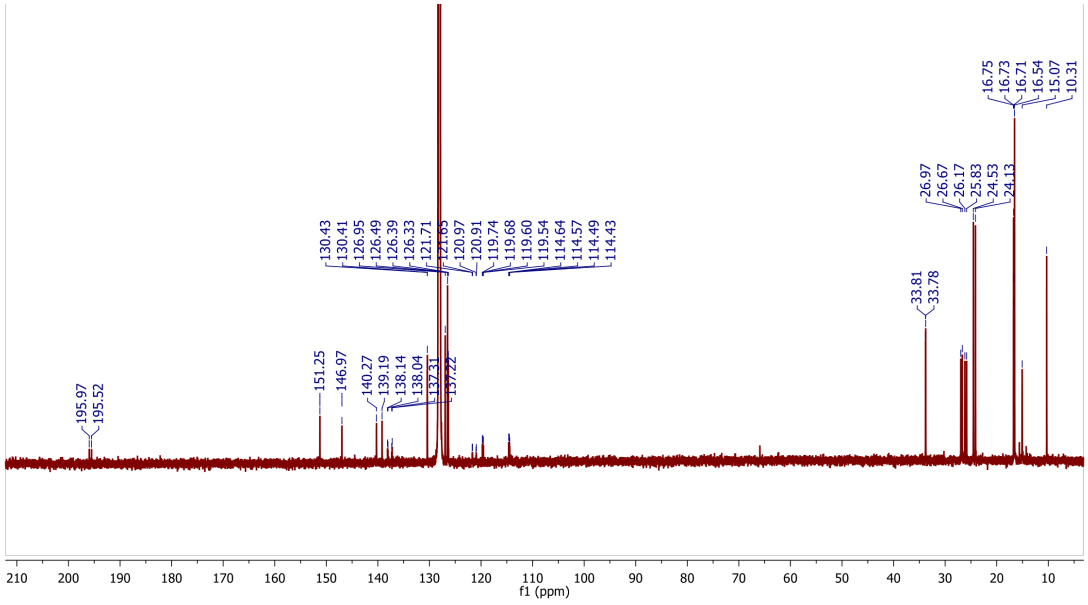

Appendix Figure II.13. $^{13}C\{^{1}H\}$ NMR (176 MHz) spectrum of complex **9** in benzene-d_6 at 22 °C

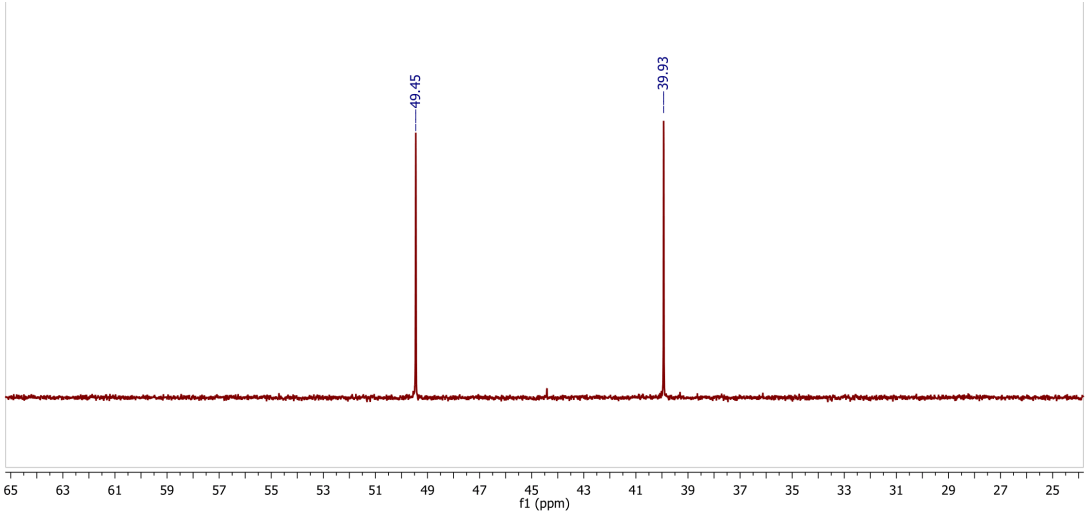

Appendix Figure II.14. $^{31}P\{^{1}H\}$ NMR (283.5 MHz) spectrum of complex **9** in benzene-d_6 at 22 °C

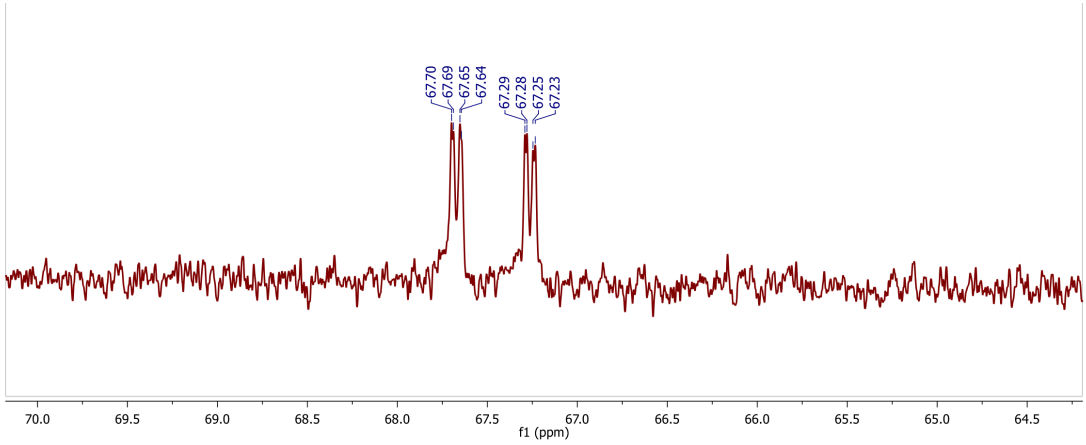

Appendix Figure II.15. $^{29}Si\{^{1}H\}$ NMR (139 MHz) spectrum of complex **9** in benzene-d_6 at 22 °C

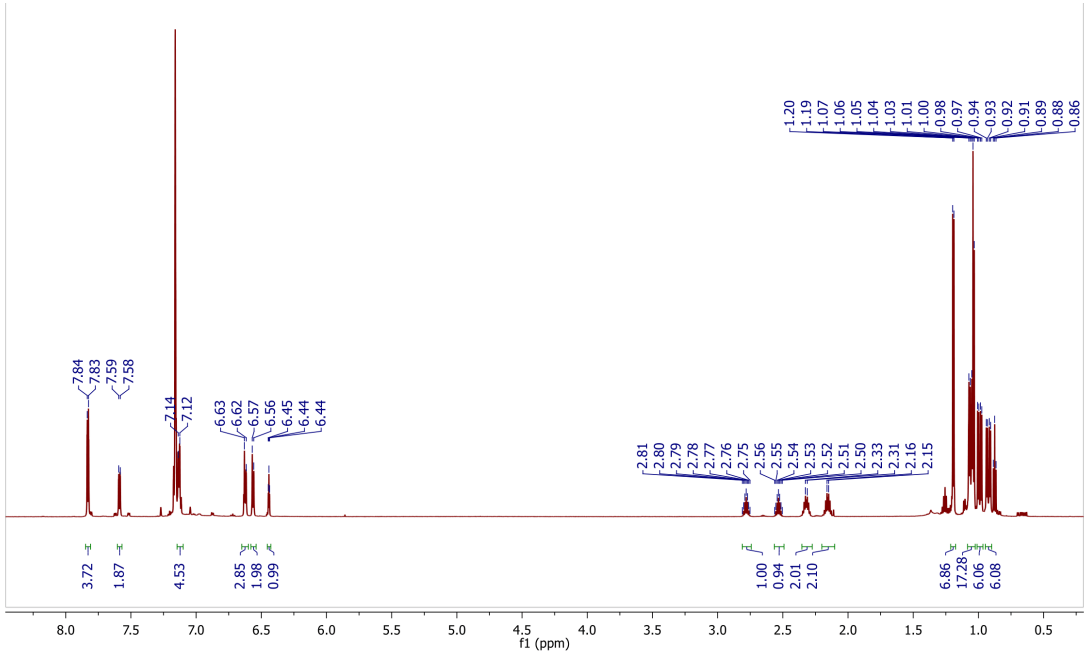

Appendix Figure II.16. ^{1}H NMR (700 MHz) spectrum of complex **10** in benzene-d_6 at 22 °C

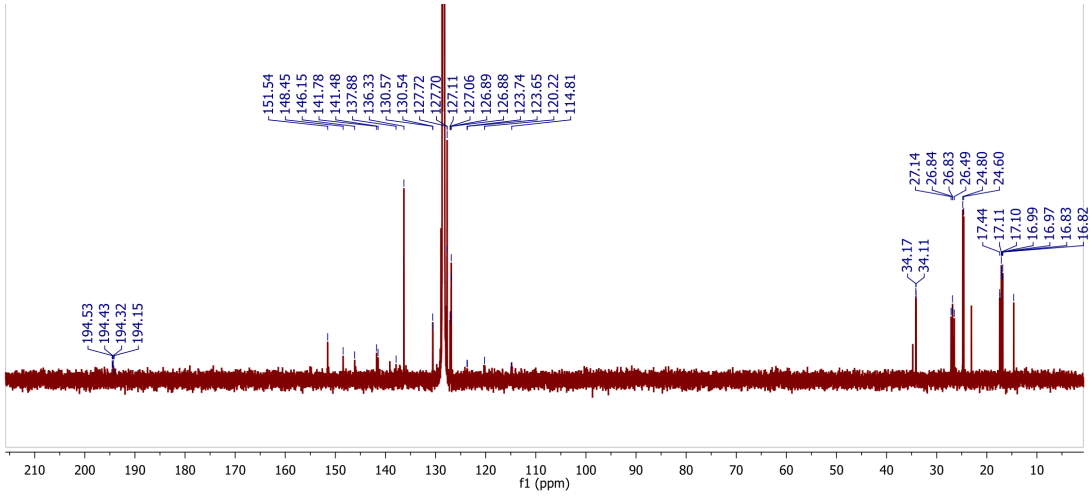

Appendix Figure II.17. $^{13}C\{^{1}H\}$ NMR (176 MHz) spectrum of complex **10** in benzene-d_6 at 22 °C

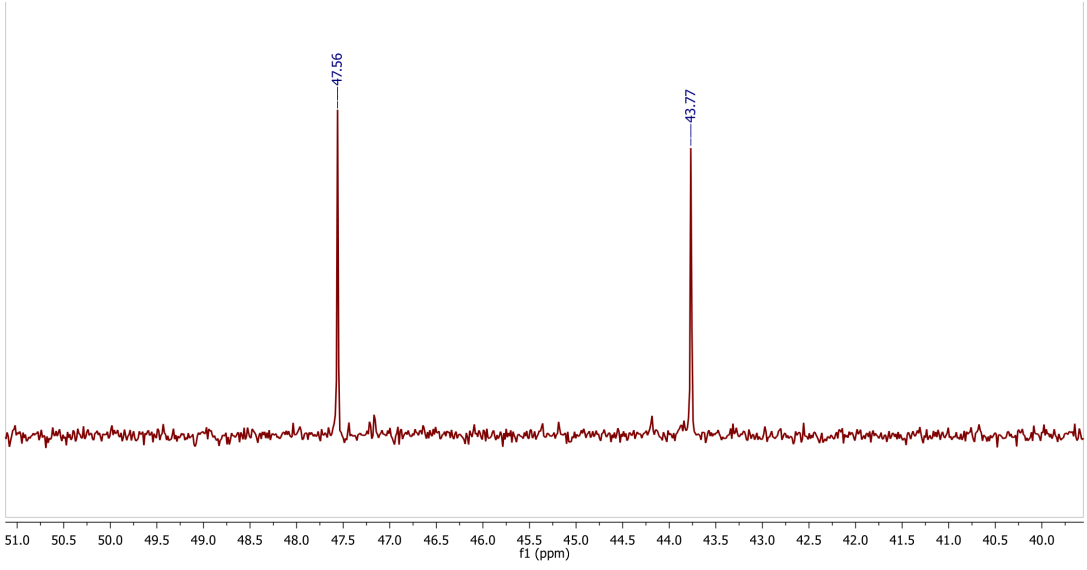

Appendix Figure II.18. $^{31}P\{^{1}H\}$ NMR (283.5 MHz) spectrum of complex **10** in benzene-d_6 at 22 °C

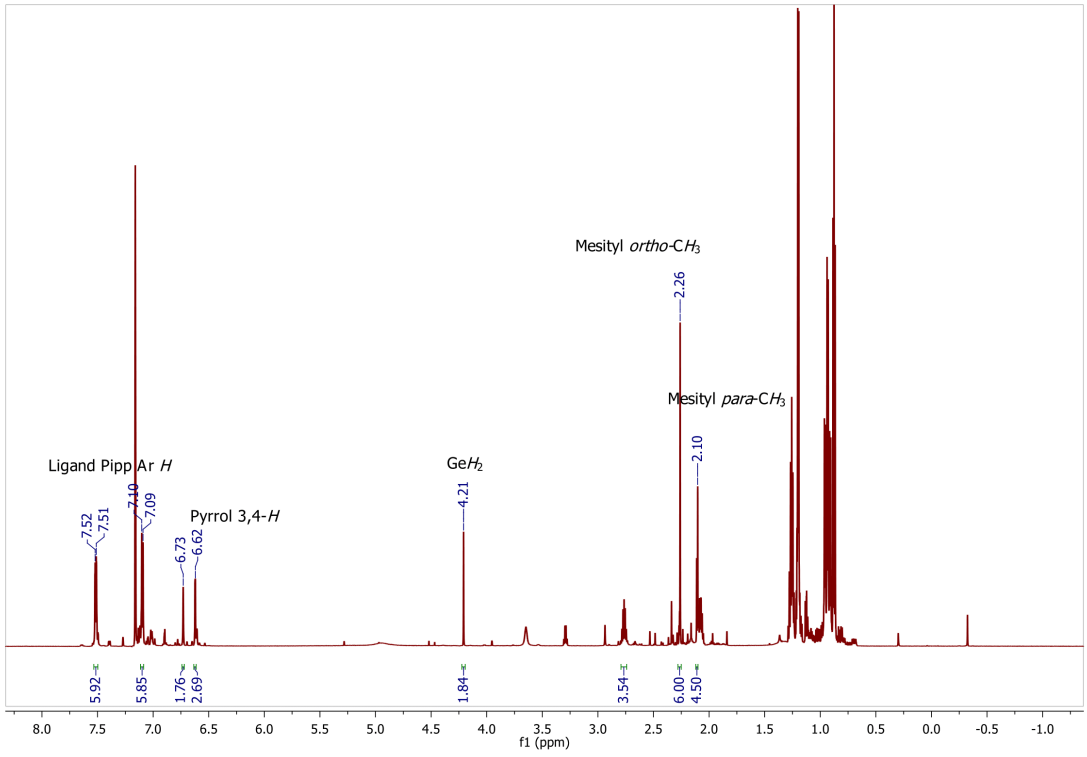

Appendix Figure II.19. ^{1}H NMR (300 MHz) spectrum of crude complex **11** in benzene-d_6 at 22 °C

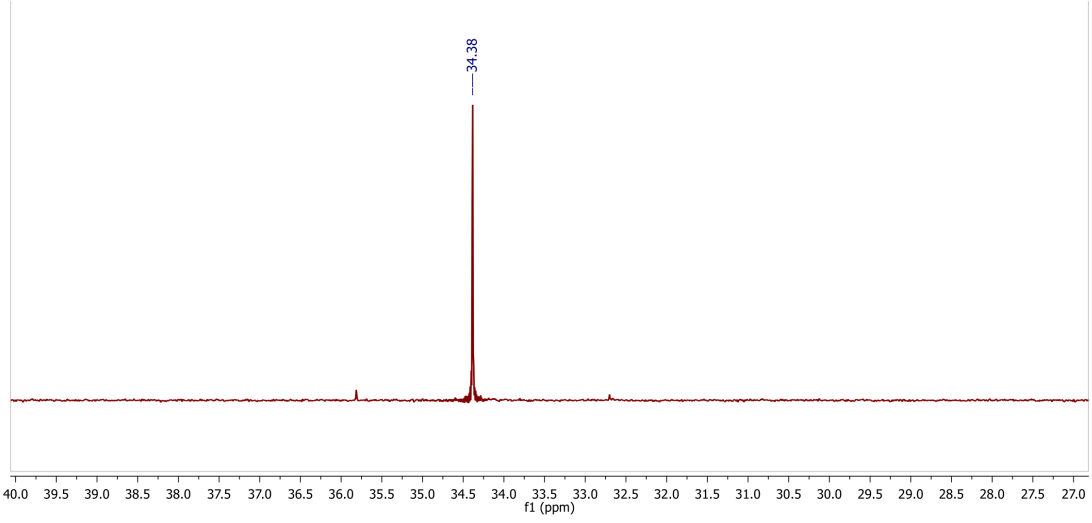

Appendix Figure II.20. ^{31}P{^{1}H} NMR (121.48 MHz) spectrum of crude complex **11** in benzene-d_6 at 22 °C

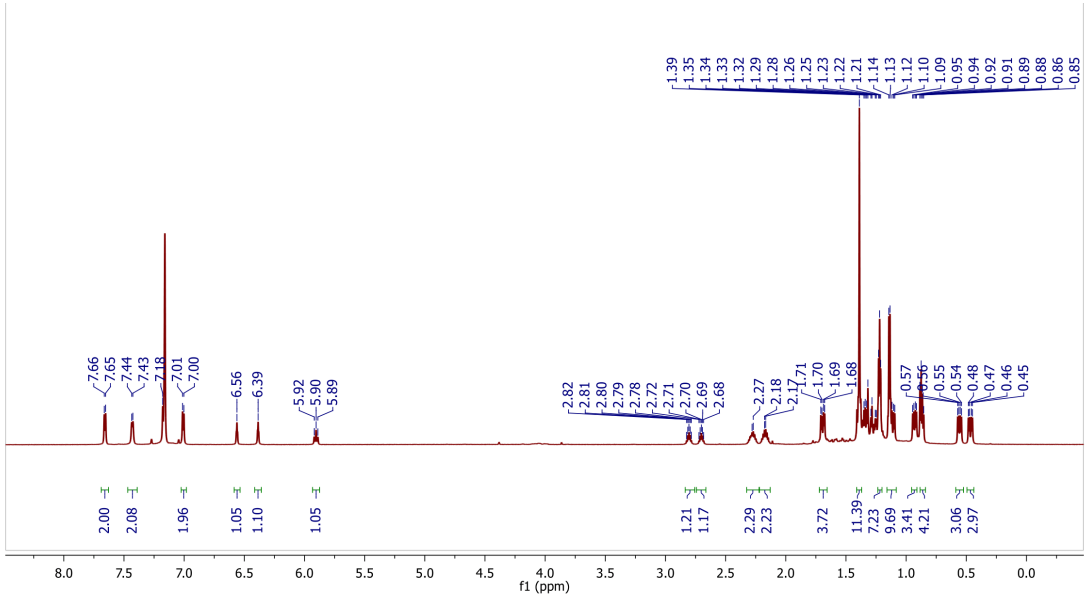

Appendix Figure II.21. ^{1}H NMR (700 MHz) spectrum of complex **12** in benzene-d_6 at 22 °C

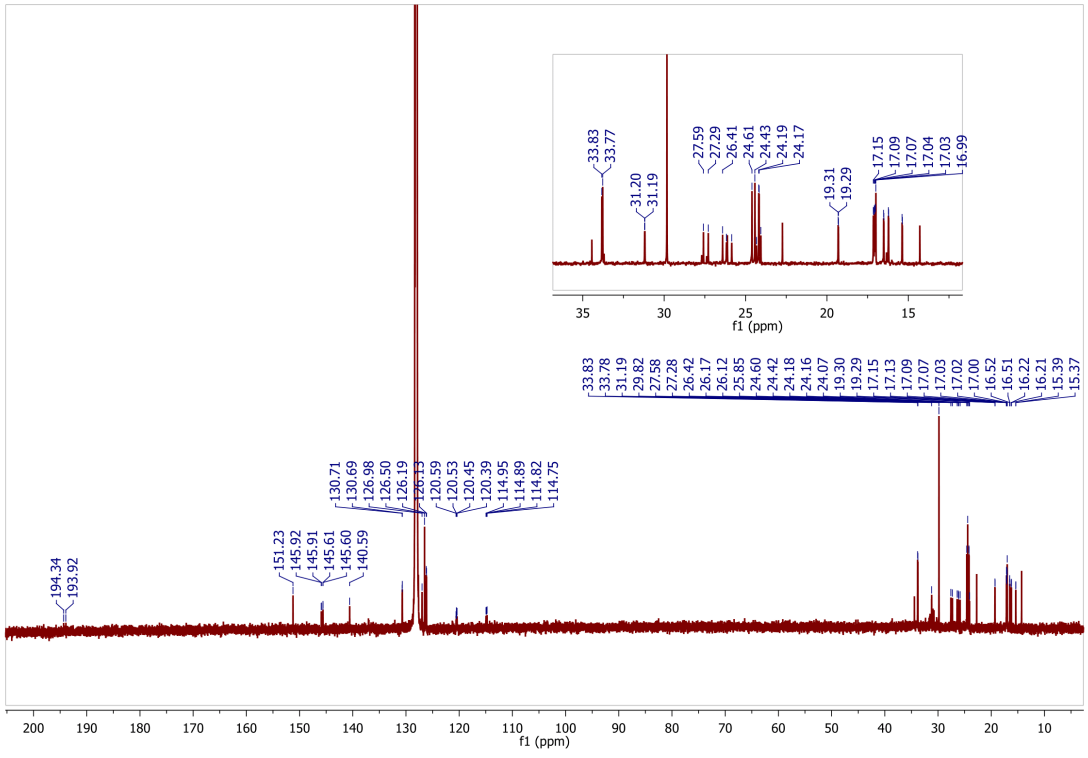

Appendix Figure II.22. ^{13}C{^{1}H} NMR (176 MHz) spectrum of complex **12** in benzene-d_6 at 22 °C

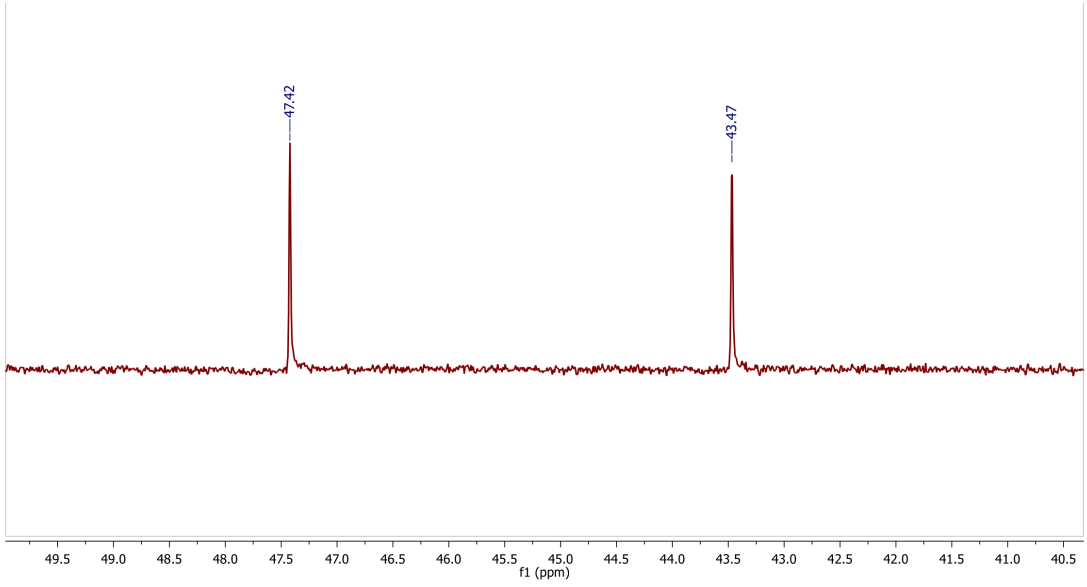

Appendix Figure II.23. $^{31}P\{^{1}H\}$ NMR (283.5 MHz) spectrum of complex **12** in benzene-d_6 at 22 °C

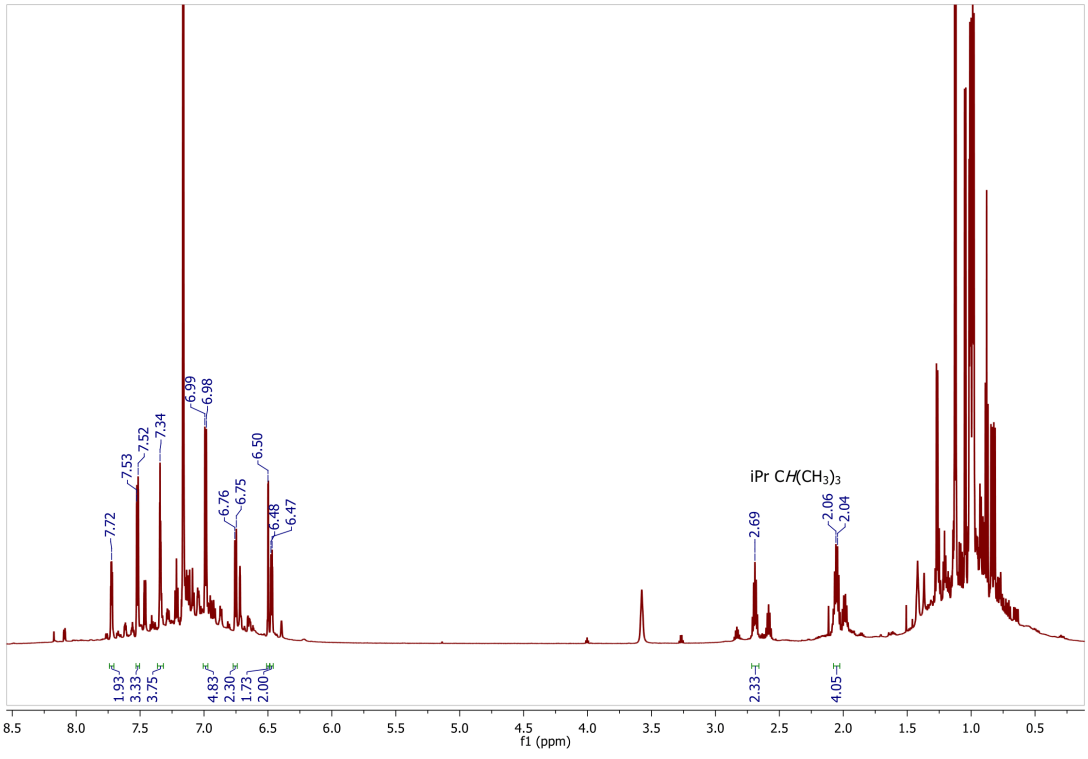

Appendix Figure II.24. ^{1}H NMR (700 MHz) spectrum of the reaction between **1** and Ph_2SnH_2 in benzene-d_6 at 22 °C

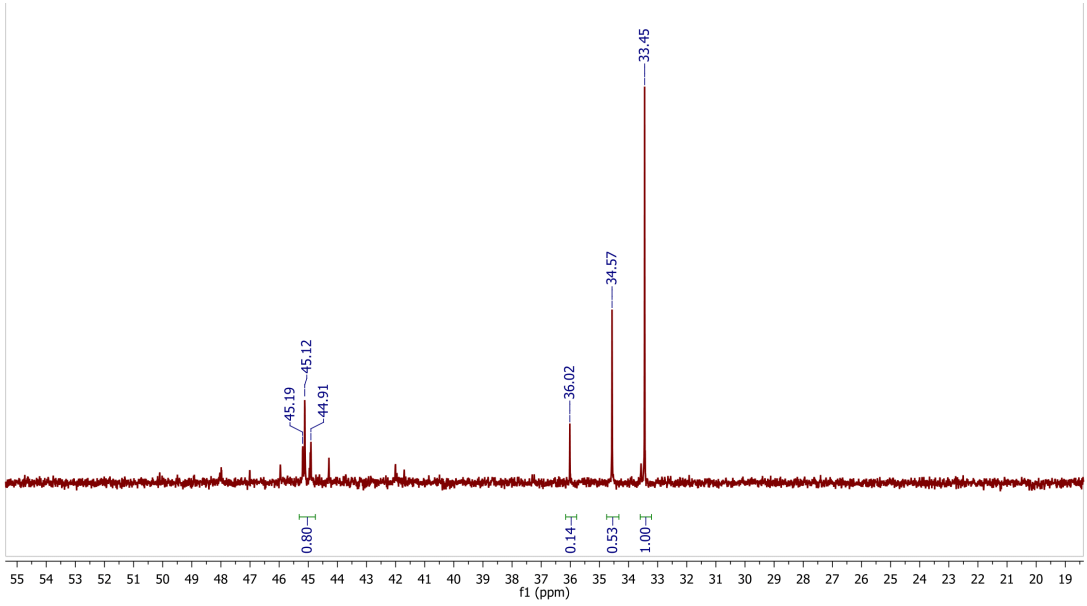

Appendix Figure II.25. $^{31}P\{^{1}H\}$ NMR (283.5 MHz) spectrum of the reaction between **1** and Ph_2SnH_2 in benzene-d_6 at 22 °C

Appendix II. II Crystallographic Details

X-Ray Diffraction Techniques. All structures were collected on a Rigaku SuperNova diffractometer equipped with a Dectris Pilatus 3R 200K-A hybrid-pixel-array detector, a four-circle κ goniometer, sealed graphite-monochromated Mo Kα (λ = 0.71073 Å) and Cu Kα (λ = 1.54178 Å) X-ray sources, and an Oxford cryostream-cooling device fixed at 100 K. Single crystals suitable for X-ray diffraction studies were mounted on a MiTiGen cryo-loop using desiccated Paratone–N oil stored in a glove box. The structures were solved by the Intrinsic Phasing methods and refined by least-squares methods using SHELXT-2014 and SHELXL-2014 with the OLEX2 interface.[6] All non-H atom were located in difference Fourier maps, and then refined anisotropically. Outlier reflections were omitted from refinement when appropriate. Hydrogen atoms on C atoms were placed at idealized positions and refined using a riding model. Hydrogen atoms on Si atoms were located in difference Fourier maps. Crystallographic refinement details, including disorder modeling and software employed, have been delineated within each crystallographic information file (*.cif) and are available via the CCDC database. Molecular graphics were generated using ORTEP and Adobe Illustrator.

Appendix Table II.1. X-ray Crystallographic Details for Reported Compounds

	κ^2-*L*(CO)Rh(Si(H)Mes)	κ^2-*L*(CO)Rh($SiEt_2$)	κ^2-*L*(CO)Rh($GePh_2$)
CCDC Entry ID	2284459	2284446	2284460
Crystal System	Triclinic	Triclinic	Monoclinic
Crystal size (mm)	0.218 × 0.07 × 0.049	0.2 × 0.08 × 0.05	0.17 × 0.04 × 0.03
Formula	$C_{44}H_{64}N_3O_2P_2RhSi$	$C_{39}H_{62}N_3OP_2RhSi$	$C_{47}H_{62}N_3OP_2RhGe$
Formula weight (g/mol)	859.93	781.87	922.51
Space Group	P-1	P-1	$P2_1/n$
a (Å)	10.4229(2)	10.26840(10)	11.80130(10)
b (Å)	14.7160(3)	15.1026(3)	20.9842(2)
c (Å)	16.8000(2)	28.1990(3)	18.6667(2)
α (deg)	97.4460(10)	99.1270(10)	90
β (deg)	100.3690(10)	91.4300(10)	103.8480(10)
γ (deg)	106.122(2)	108.302(2)	90
Z	2	4	4
V ($Å^3$)	2390.70(8)	4086.25(11)	4488.28(8)
Indep. Reflections	9689	17638	9063
R(int)	0.0484	0.0455	0.0352
R1(%)	4.30	4.87	2.62
wR2	0.1132	0.1410	0.0638
GoF	1.089	1.047	1.075

	κ^2-NN'B(H)Mes
CCDC Entry ID	2284461
Crystal System	Triclinic
Crystal size (mm)	0.16 × 0.1 × 0.06
Formula	$C_{43}H_{64}N_3P_2B$
Formula weight (g/mol)	695.74
Space Group	P-1
a (Å)	12.4456(5)
b (Å)	12.7936(6)
c (Å)	15.6046(7)
α (deg)	77.819(4)
β (deg)	71.043(4)
γ (deg)	61.781(4)
Z	2
V (Å^3)	2065.66(18)
Indep. Reflections	8253
R(int)	0.0607
R1(%)	5.67
wR2	0.1551
GoF	1.030

Appendix II. III References

[1] a) G. M. Sheldrick, *Acta Crystallogr., Sect. A: Found. Adv.* **2015**, *71*, 3-8; b) G. M. Sheldrick, *Acta Crystallogr., Sect. C: Struct. Chem.* **2015**, *71*, 3-8.

Appendix III. Supporting Information for Chapter 4

Reformatted from published supporting information association with “Hsiang, S.J.; Hayes, P.G.*, Rhodium-mediated Assembly of New Heterocycles: From Borylenes to Oxaboroles. *Angewandte Chemie International Edition.* **2025**, e202421302.”

Table of Contents

Appendix III. I Experimental Section

General Considerations

All air- and moisture-sensitive manipulations were carried out using vacuum line, Schlenk and cannula techniques, or in an MBraun inert atmosphere (argon) glove box unless otherwise noted. All glassware was stored in a pre-heated (110 °C) oven or flame-dried prior to use. Solvents used for air-sensitive procedures were purified using an MBraun solvent purification system (SPS), dried in PTFE-sealed glass vessels over sodium benzophenone ketyl (THF, diethylether, pentane, and toluene), and distilled in small batches over 4 Å molecular sieves in PTFE-sealed glass vessels for use in the glovebox. Benzene-d_6 was dried over sodium benzophenone ketyl, distilled *in vacuo* and stored over 4 Å molecular sieves in PTFE-sealed glass vessels under argon. $MesBH_2$ was prepared according to literature procedures.[1] Diphenylacetylene, ethyl-3-phenylpropiolate, 1-phenyl-1-propyne, and phenyl acetylene were purchased from Sigma Aldrich, and degassed through three freeze pump thaw cycles before being stored in an inert atmosphere glove box in vials with Teflon lined caps. Complexes **1** and **3** were synthesized according to previous literature procedures.[1] Unless otherwise noted, all NMR spectra were recorded at ambient temperature with a Bruker Avance III NMR spectrometer (700.44 MHz for ^{1}H, 224.63 MHz for ^{11}B, 176.13 MHz for ^{13}C, and 283.54 MHz for ^{31}P). All ^{1}H and ^{13}C NMR chemical shifts are reported in ppm relative to $SiMe_4$ using the ^{1}H (benzene-d_6: 7.16 ppm) and ^{13}C (benzene-d_6: 128.06 ppm) chemical shifts of the solvent as reference. ^{11}B NMR chemical shifts were referenced externally to BF3·Et2O (δ 0.0). ^{31}P NMR chemical shifts were referenced to external 85% H_3PO_4 in H_2O (δ 0.0). ^{1}H and ^{13}C NMR data are reported as follows: chemical shift, multiplicity (s = singlet, d = doublet, t = triplet, q = quartet, quin = quintet, sp = septet, m = multiplet, br = broad, ov = overlapping), coupling constant(s) (Hz), integration, assignment. Assignment of resonances were supplemented by ^{1}H–^{1}H COSY, $^{13}C\{^{1}H\}$ APT, and ^{1}H–$^{13}C\{^{1}H\}$ HSQC/HMBC experiments.

Elemental analyses (%CHN) were conducted at the University of Lethbridge on an Elementar Americas Vario MicroCube Analyzer (C, H, N, O, S capabilities) using bulk recrystallized compounds. "Universal Combustion Additive", purchased from Elemental Microanalysis, was added to all standards, blanks, and samples. Infrared spectroscopy was conducted on a Bruker Tensor 37 FT spectrometer (0.6 cm^{-1} resolution) using bulk recrystallized compounds (vs = very sharp, s = sharp, w = wide). High resolution mass spectroscopy was conducted by direct injection into Thermo Fisher Scientific Orbitrap Fusion instrument using electrospray ionization (ESI). Low resolution mass spectroscopy was obtained on Varian CP-3800 GC to Varian 4000 MS instrument using an electron impact (EI) ionization source.

Synthesis and Characterization of New Compounds

Preparation of κ^2-*L*Rh[C(O)C(Ph)C(Ph)B(Mes)], Compound 13^{Ph}. Recrystallized **3** (70 mg, 0.085 mmol) was dissolved in 5 mL of toluene. In a separate flask, diphenyl acetylene (17 mg, 0.091 mmol) was dissolved in 1 mL of toluene and then added to the solution of **3** in one portion. The mixture was stirred at 50 °C for 6 hours, going from a light yellow to darker orange in color. After removal of the solvent under reduced pressure, the product was washed with 3 × 0.5 mL of pentane. The crude solid was recrystallized over 3 days from 5 mL of Et_2O at –30 °C to yield 55 mg (65% yield) of **13^{Ph}** as light orange-yellow crystals. Anal Calcd. for $C_{58}H_{73}BN_3OP_2Rh$: C, 69.39; H, 7.33; N, 4.19. Found: C, 69.15; H, 7.41; N, 3.98.

^{1}H NMR (benzene-d_6, 23 °C): δ 8.39 (br s, 2H, Ph *H*); 7.67 (d, $^3J_{HH}$ = 7.0 Hz, 2H, Pipp Ar *H*); 7.54 (ov d, $^3J_{HH}$ = 8.24 Hz, 1H, Pipp Ar *H*); 7.52 (d, $^3J_{HH}$ = 6.70 Hz, 1H, *para*-Ph *H*); 7.14 (ov d, $^3J_{HH}$ = 7.89, 1H, Pipp Ar *H*); 7.12 (d, $^3J_{HH}$ = 7.84, 2H, Pipp Ar *H*); 7.02-6.96 (m, 2H, Ph *H*); 6.95 (s, Mes Ar *H*); 6.77 (ov m, 3H, Ph *H*); 6.64 (ov dd, $^3J_{HH}$ = $^3J_{HP}$ = 3.11 Hz, 1H, 3,4-pyrrole C*H*); 6.62 (ov d, 1H, Pipp Ar *H*); 6.57 (ov d, 2H, Ph *H*); 6.56 (ov d, 1H, Pipp Ar *H*); 6.51 (s, 1H, Mes Ar *H*); 6.48 (ov dd, $^3J_{HH}$ = $^3J_{HP}$ = 3.11 Hz, 1H, 3,4-pyrrole C*H*); 2.81 (ov s, 3H, Mes *para* CH_3); 2.81 (ov sp, $^3J_{HH}$ = 7.10, 1H, Pipp C*H*$(CH_3)_2$); 2.65 (sp, $^3J_{HH}$ = 6.88, 1H, Pipp C*H*$(CH_3)_2$); 2.39-2.32 (ov

m, 1H, PC*H*(CH_3)$_2$); 2.31 (ov s, 3H, Mes *ortho* C*H*$_3$); 2.26 (ov m, 1H, PC*H*(CH_3)$_2$); 2.18 (ov s, 3H, Mes *ortho* C*H*$_3$); 2.17-2.11 (ov m, 1H, PC*H*(CH_3)$_2$); 2.04 (m, 1H, PC*H*(CH_3)$_2$); 1.31 (dd, $^3J_{HH}$ = 7.09, $^3J_{HP}$ = 15.95 Hz, 3H, PCH(C*H*$_3$)$_2$); 1.28-1.23 (ov dd, $^3J_{HH}$ = 7.18, 3H, PCH(C*H*$_3$)$_2$); 1.26-1.22 (ov d, 6H, Pipp CH(C*H*$_3$)$_2$); 1.10 (dd, $^3J_{HH}$ = 6.80, $^4J_{HH}$ = 3.63, 6H, Pipp CH(C*H*$_3$)$_2$); 1.01 (dd, $^3J_{HH}$ = 7.09, $^3J_{HP}$ = 15.95 Hz, 3H, PCH(C*H*$_3$)$_2$); 0.86 (ov dd, $^3J_{HH}$ = 7.09, $^3J_{HP}$ = 15.01 Hz, 3H, PCH(C*H*$_3$)$_2$); 0.82 (ov dd, $^3J_{HH}$ = 7.01, $^3J_{HP}$ = 15.65 Hz, 3H, PCH(C*H*$_3$)$_2$); 0.58 (dd, $^3J_{HH}$ = 6.92, $^3J_{HP}$ = 16.66 Hz, 3H, PCH(C*H*$_3$)$_2$); 0.42 (br dd, $^3J_{HH}$ = 6.77, $^3J_{HP}$ = 14.16 Hz, 3H, PCH(C*H*$_3$)$_2$); 0.31 (dd, $^3J_{HH}$ = 7.13, $^3J_{HP}$ = 17.16 Hz, 3H, PCH(C*H*$_3$)$_2$). **^{13}C{^{1}H} NMR (benzene-d_6, 23 ºC):** δ 203.7 (d, $^1J_{CRh}$ = 21.5 Hz, Rh–*C*O); 149.3 (s, Pipp Ar *C*); 147.4 (s, Pipp Ar *C*); 146.1 (s, Ar *C*); 143.5 (s, Mes Ar *C*); 142.7 (s, Pipp Ar *C*); 140.9 (s, Mes Ar *C*); 140.0 (s, *C*(Ph)); 135.7 (s, Ph *C*); 135.6 (dd, $^1J_{CP}$ = 142.9 Hz, $^4J_{CP}$ = 15.4 Hz, 2,5-pyrrole *C*); 134.7 (s, Mes Ar *C*); 134.1 (d, J_{CP} = 4.0 Hz, Pipp Ar *C*H); 132.0 (s, Pipp Ar *C*H); 131.8 (s, Pipp Ar *C*H); 129.8 (s, Pipp Ar *C*H); 129.0 (s, Mes Ar *C*H); 128.7 (d, *J* = 6.0 Hz, Ph *C*H); 128.7 (s, Ar *C*H); 128.5 (s, Ar *C*H); 128.5 (s, Mes Ar *C*H); 128.4 (s, Pipp Ar *C*H); 128.3 (s, Ar *C*H); 128.1 (ov s, Ar *C*H); 127.3 (s, Pipp Ar *C*H); 127.0 (d, *J* = 2.2 Hz, Ph *C*H); 126.3 (s, Ar *C*H); 126.1 (s, Pipp Ar *C*H); 125.3 (s, Pipp Ar *C*H); 123.9 (s, Ar *C*H); 123.6 (s, Ph *C*H); 122.0 (dd, $^1J_{CP}$ = 130.4 Hz, $^4J_{CP}$ = 13.3 Hz, 2,5-pyrrole *C*); 120.8 (dd, $^2J_{CP}$ = 25.7 Hz, $^3J_{CP}$ = 10.2 Hz, 3,4-pyrrole *C*H); 114.8 (dd, $^2J_{CP}$ = 24.5 Hz, $^3J_{CP}$ = 10.3 Hz, 3,4-pyrrole *C*H); 84.0 (br s, *C*(Ph); 33.9 (ov s, 2x Pipp *C*H(CH_3)$_2$); 30.8 (d, $^1J_{CP}$ = 59.2 Hz, P*C*H(CH_3)$_2$); 26.7 (d, $^1J_{CP}$ = 53.3 Hz, P*C*H(CH_3)$_2$); 26.4 (d, $^1J_{CP}$ = 53.3 Hz, P*C*H(CH_3)$_2$); 25.6 (s, Mes *C*H$_3$); 25.4 (s, Mes *C*H$_3$); 24.9 (d, $^1J_{CP}$ = 58.8 Hz, P*C*H(CH_3)$_2$); 24.7 (s, Pipp CH(*C*H$_3$)$_2$); 24.6 (s, Pipp CH(*C*H$_3$)$_2$); 24.18 (s, Pipp CH(*C*H$_3$)$_2$); 23.1 (s, Pipp CH(*C*H$_3$)$_2$); 21.5 (s, Mes *C*H$_3$); 17.1 (s, PCH(*C*H$_3$)$_2$); 16.5 (br s, PCH(*C*H$_3$)$_2$); 16.4 (d, $^2J_{CP}$ = 1.9 Hz, PCH(*C*H$_3$)$_2$); 16.3 (d, $^2J_{CP}$ = 2.0 Hz, PCH(*C*H$_3$)$_2$); 16.1 (ov d, PCH(*C*H$_3$)$_2$); 16.1 (ov d, $^2J_{CP}$ = 2.1 Hz, PCH(*C*H$_3$)$_2$); 15.9 (d, $^2J_{CP}$ = 1.8 Hz, PCH(*C*H$_3$)$_2$); 15.8 (d, $^2J_{CP}$ = 2.6 Hz, PCH(*C*H$_3$)$_2$). **^{31}P{^{1}H} NMR (283.42 MHz, benzene-d_6, 23 ºC):** δ 51.8 (s, 1P, *P*–N–Rh); 44.7 (s, 1P, *P*–N–B). **^{11}B{^{1}H} NMR (224.63 MHz, benzene-d_6, 23 °C):** δ 13.4 (br s). **IR (cm^{-1}):** 1734 (s, C=O stretch).

Preparation of κ^2-*L*Rh[C(O)C(Ph)C(CO$_2$Et)B(Mes)], Compound 13^{CO2Et}. Recrystallized **3** (70 mg, 0.085 mmol) was dissolved in 5 mL of toluene. In a separate flask, ethyl phenylpropiolate (70 mg, 0.40 mmol) was dissolved in 1 mL of toluene and then added to the solution of **3** dropwise over a minute. The mixture was allowed to stir at ambient temperatures for 5 hours. After removal of the solvent under reduced pressure, the product was washed with 3 × 0.1 mL of pentane. The crude solid was recrystallized over 3 days from 5 mL of Et_2O at –30 °C to yield 63 mg (74% yield) of **13^{CO2Et}** as light yellow crystals. Anal Calcd. for $C_{55}H_{73}BN_3O_3P_2Rh$: C, 66.07; H, 7.36; N, 4.20. Found: C, 65.89; H, 7.37; N, 4.35.

^{1}H NMR (benzene-*d*$_6$, 23 °C): δ 8.22 (d, $^3J_{HH}$ = 7.9 Hz, 1H, Pipp Ar *H*); 7.46 (d, $^3J_{HH}$ = 7.6 Hz, 2H, Pipp Ar *H*); 7.20 (d, $^3J_{HH}$ = 7.9 Hz, 1H, Pipp Ar *H*); 6.99 (ov d, $^3J_{HH}$ = 7.7 Hz, 2H, Ph *ortho H*); 6.96 (ov d, $^3J_{HH}$ = 7.6 Hz, 2H, Pipp Ar *H*); 6.93 (m, 3H, Ph *meta, para H*); 6.87 (s, 1H, Mes *meta H*); 6.68 (br t, $^3J_{HH}$ = $^3J_{HP}$ = 3.6 Hz, 1H, 3,4-pyrrole C*H*); 6.62 (d, $^3J_{HH}$ = 7.9 Hz, 1H, Pipp Ar *H*); 6.52 (ov s, 1H, Mes *meta H*); 6.51 (ov, identified through ^{1}H–^{1}H COSY experiments, 1H, Pipp *Ar* H); 6.50 (br t, $^3J_{HH}$ = $^3J_{HP}$ = 3.6 Hz, 1H, 3,4-pyrrole C*H*); 4.09 (m, 2H, Et CH_2); 3.05 (br sp, $^3J_{HH}$ = 7.3 Hz, 1H, PC*H*(CH$_3$)$_2$); 2.75 (sp, $^3J_{HH}$ = 6.8 Hz, 1H, Pipp C*H*(CH$_3$)$_2$); 2.69 (s, 3H, Mes *para* CH_3); 2.63 (sp, $^3J_{HH}$ = 6.8 Hz, 1H, Pipp C*H*(CH$_3$)$_2$); 2.22 (ov d sp, 1H, PC*H*(CH$_3$)$_2$); 2.15 (s, 3H, Mes *ortho* CH_3); 2.13 (ov s, 3H, Mes *ortho* CH_3); 2.11 (ov sp, $^3J_{HH}$ = 8.4 Hz, 2H, PC*H*(CH$_3$)$_2$); 1.27 (m, 6H, PCH(CH_3)$_2$); 1.21 (ov d, $^3J_{HH}$ = 7.7, 3H, Pipp CH(CH_3)$_2$); 1.11 (ov m, 6H, PCH(CH_3)$_2$); 1.09 (ov d, $^3J_{HH}$ = 6.6 Hz, 6H, Pipp CH(CH_3)$_2$); 0.94 (dd, $^3J_{HH}$ = 6.81 Hz, $^3J_{HP}$ = 16.7 Hz, 3H, PCH(CH_3)$_2$); 0.85 (t, $^3J_{HH}$ = 7.1 Hz, Et CH_3); 0.80 (ov dd, $^3J_{HH}$ = 7.3 Hz, $^3J_{HP}$ = 14.7 Hz, 6H, PCH(CH_3)$_2$); 0.51 (dd, $^3J_{HH}$ = 6.8 Hz, $^3J_{HP}$ = 14.2 Hz, PCH(CH_3)$_2$). **^{13}C{^{1}H} NMR (benzene-*d*$_6$, 23 °C):** δ 201.4 (d, $^1J_{CRh}$ = 21.8 Hz, Rh–*C*O); 175.1 (s, *C*(O)OCH$_2$CH$_3$), 148.9 (s, Pipp Ar *C*); 147.5 (s, Pipp Ar *C*); 142.9 (s, Mes Ar *C*); 142.2 (s, Pipp Ar *C*); 141.8 (s, Mes Ar *C*); 141.8 (br s, *C*(Ph)); 139.0 (s, Pipp Ar *C*); 136.3 (s, Ph Ar *C*); 135.7 (dd, $^1J_{CP}$ = 143.1 Hz, $^4J_{CP}$ = 15.0 Hz, 2,5-pyrrole *C*); 134.9 (s, Mes Ar *C*); 133.6 (d, $^3J_{CP}$ = 3.6 Hz, Pipp Ar *C*H); 132.6 (d, $^3J_{CP}$ = 2.2 Hz, Pipp Ar *C*H);

128.9 (s, Ph *C*H); 128.3 (s, Mes Ar *C*H); 128.1 (ov s, identified through ^{13}C–^{1}H HSQC and HMBC experiments, Mes Ar *C*H); 128.0 (ov s, identified through ^{13}C–^{1}H HSQC and HMBC experiments, Pipp Ar *C*H); 127.6 (s, Ph *C*H); 126.6 (d, $^{3}J_{CP}$ = 1.6 Hz, Pipp Ar *C*H); 126.0 (s, Pipp Ar *C*H); 125.8 (s, Pipp Ar *C*H); 124.5 (s, Ph *C*H); 122.0 (dd, $^{1}J_{CP}$ = 130.6 Hz, $^{4}J_{CP}$ = 13.5 Hz, 2,5-pyrrole *C*); 120.5 (dd, $^{3}J_{CP}$ = 10.4 Hz, $^{2}J_{CP}$ = 25.2 Hz, 3,4-pyrrole *C*H); 114.9 (dd, $^{3}J_{CP}$ = 10.4 Hz, $^{2}J_{CP}$ = 25.2 Hz, 3,4-pyrrole *C*H); 76.2 (br s, *C*-C(O)OEt); 59.8 (s, C(O)O*C*H_2CH$_3$); 33.9 (s, Pipp *C*H(CH$_3$)$_2$); 33.8 (s, Pipp *C*H(CH$_3$)$_2$); 30.6 (d, $^{1}J_{CP}$ = 57.9 Hz, P*C*H(CH$_3$)$_2$); 27.1 (d, $^{1}J_{CP}$ = 53.6 Hz, P*C*H(CH$_3$)$_2$); 26.3 (d, $^{1}J_{CP}$ = 52.8 Hz, P*C*H(CH$_3$)$_2$); 25.1 (s, Mes *para* *C*H$_3$); 24.6 (s, Mes *ortho* *C*H$_3$); 24.5 (d, $^{1}J_{CP}$ = 20.2 Hz, P*C*H(CH$_3$)$_2$); 24.2 (s, Pipp CH(*C*H$_3$)$_2$); 24.1 (s, Pipp CH(*C*H$_3$)$_2$); 21.4 (s, Mes *ortho* *C*H$_3$); 17.7 (br s, PCH(C*H*$_3$)$_2$); 17.6 (d, $^{2}J_{CP}$ = 1.9 Hz, PCH(C*H*$_3$)$_2$); 16.5 (d, $^{2}J_{CP}$ = 2.3 Hz, PCH(C*H*$_3$)$_2$); 16.3 (d, $^{2}J_{CP}$ = 1.9 Hz, PCH(C*H*$_3$)$_2$); 16.2 (d, $^{2}J_{CP}$ = 3.5 Hz, PCH(C*H*$_3$)$_2$); 16.1 (d, $^{2}J_{CP}$ = 2.6 Hz, PCH(C*H*$_3$)$_2$); 15.9 (ov d, $^{2}J_{CP}$ = 2.3 Hz, PCH(C*H*$_3$)$_2$); 15.8 (ov d, $^{2}J_{CP}$ = 4.7 Hz, PCH(C*H*$_3$)$_2$); 14.0 (s, C(O)OCH$_2$*C*H$_3$). Boron-bound Mes *C* was unable to be resolved from baseline. **$^{31}P\{^{1}H\}$ NMR (283.42 MHz, benzene-d_6, 23 ºC):** δ 51.6 (s, 1P, *P*–N–Rh); 45.5 (s, 1P, *P*–N–B). **$^{11}B\{^{1}H\}$ NMR (224.63 MHz, benzene-d_6, 23 °C):** δ 12.3 (br s). **IR (cm^{-1}):** 1778 (m, Ester C=O stretch), 1698 (s, Rh–*C*=*O* stretch).

Preparation of κ^2-*L*Rh[C(O)C(Ph)C(H)B(Mes)], Compound 13^H. Recrystallized **3** (33 mg, 0.040 mmol) was dissolved in 5 mL of toluene. To this yellow solution, excess phenyl acetylene (20 mg, 0.20 mmol) was added in one straight portion and the reaction stirred for 20 minutes, resulting in gradual transition to an orange solution. The toluene was removed *in vacuo* followed by 2 washes with 1 mL pentane to isolate compound **13^H** (28 mg, 76% yield) as a pale yellow-orange solid. Anal Calcd. for $C_{52}H_{69}BN_3OP_2Rh$: C, 67.32; H, 7.50; N, 4.53. Found: C, 67.01; H, 7.65; N, 4.72.

^{1}H NMR (benzene-d_6, 23 °C): δ 7.57 (br s, 1H, Pipp Ar *H*); 7.44 (d, $^3J_{HH}$ = 7.44 Hz, 2H, *ortho*-Ph *H*); 7.12-7.04 (ov m, 3H, *meta/para*-Ph *H*; 4H, Pipp Ar *H*; 1H, Pipp Ar *H*); 6.91 (s, 1H, Mes Ar *H*); 6.64 (ov t, $^3J_{HH}$ = $^3J_{HP}$ = 3.2 Hz, 1H, 3,4-pyrrole C*H*); 6.64 (ov br s, 1H, Pipp Ar *H*); 6.56 (br s, 1H, Pipp Ar *H*); 6.52 (s, 1H, Mes Ar *H*); 6.49 (t, $^3J_{HH}$ = $^3J_{HP}$ = 3.2 Hz, 1H, 3,4-pyrrole C*H*); 4.85 (d, $^2J_{HRh}$ = 7.47 Hz, 1H, C(Ph)-C(*H*)); 2.81 (sp, $^3J_{HH}$ = 6.89 Hz, 1H, Pipp C*H*$(CH_3)_2$); 2.69 (s, 3H, Mes C*H*$_3$); 2.66 (ov sp, $^3J_{HH}$ = 6.82 Hz, 1H, Pipp C*H*$(CH_3)_2$); 2.61 (ov sp, $^3J_{HH}$ = 6.70 Hz, 1H, PC*H*$(CH_3)_2$); 2.22 (m, 1H, PC*H*$(CH_3)_2$); 2.14 (s, 3H, Mes C*H*$_3$); 2.08 (ov d sp, $^3J_{HH}$ = $^2J_{HP}$ = 7.00 Hz, 1H, PC*H*$(CH_3)_2$); 2.01 (m, 1H, PC*H*$(CH_3)_2$); 1.78 (s, 3H, Mes C*H*$_3$); 1.43 (dd, $^3J_{HH}$ = 6.82 Hz, $^3J_{HP}$ = 15.86 Hz, 3H, PCH(C*H*$_3)_2$); 1.28-1.22 (ov dd, $^3J_{HH}$ = 6.82 Hz, 3H, PCH(C*H*$_3)_2$); 1.23 (ov d, $^3J_{HH}$ = 6.89 Hz, 6H, Pipp CH(C*H*$_3)_2$); 1.25-1.20 (ov ddd, $^3J_{HH}$ = 7.00 Hz, *J* = 2.00 Hz, 3H, PCH(C*H*$_3)_2$); 1.11 (d, $^3J_{HH}$ = 6.86, 6H, Pipp CH(C*H*$_3)_2$); 0.77 (dd, $^3J_{HH}$ = 7.00 Hz, $^3J_{HP}$ = 15.56 Hz, 3H, PCH(C*H*$_3)_2$). **^{13}C{^{1}H} NMR (benzene-d_6, 23 ºC):** δ 206.0 (d, $^1J_{CRh}$ = 21.0 Hz, Rh–*C*O); 148.7 (s, Rh–C(O)–*C*(Ph); 147.4 (d, ^2J = 1.8 Hz, Pipp Ar *C*); 142.6 (s, Ph *C*); 142.3 (d, ^2J = 3.3 Hz, Pipp Ar *C*); 140.8 (s, Mes Ar *C*); 140.3 (s, Mes Ar *C*); 138.7 (br s, Mes Ar *C*); 136.2 (dd, $^1J_{CP}$ = 143.1 Hz, $^4J_{CP}$ = 15.1 Hz, 2,5-pyrrole *C*); 134.4 (s, Mes Ar *C*); 133.3 (br s, Pipp Ar *C*); 130.1 (br s, Pipp Ar *C*); 128.6 (d, *J* = 5.9 Hz, Ph *C*H); 128.4 (ov s, identified through ^{13}C–^{1}H HSQC and HMBC experiments, Ar *C*H); 128.2 (ov s, identified through ^{13}C–^{1}H HSQC and HMBC experiments, Ar *C*H) 128.1 (ov s, identified through ^{13}C–^{1}H HSQC and HMBC experiments, Mes Ar *C*H); 128.0

(ov s, identified through ^{13}C–^{1}H HSQC and HMBC experiments, Mes Ar *C*H); 127.2 (s, Ar *C*H); 126.8 (s, Ar *C*H); 126.6 (d, J = 2.0 Hz, Ar *C*H); 124.6 (s, Ar *C*H); 121.1 (dd, $^{2}J_{CP}$ = 25.7 Hz, $^{3}J_{CP}$ = 10.2 Hz, 3,4-pyrrole *C*H); 120.3 (dd, $^{1}J_{CP}$ = 133.4 Hz, $^{4}J_{CP}$ = 13.3 Hz, 2,5-pyrrole *C*); 114.7 (dd, $^{2}J_{CP}$ = 24.6 Hz, $^{3}J_{CP}$ = 10.5 Hz, 3,4-pyrrole *C*H); 70.23 (br s, C(Ph)–*C*(H)); 34.0 (s, Pipp *C*H$(CH_3)_2$); 33.9 (s, Pipp *C*H$(CH_3)_2$); 28.4 (d, $^{1}J_{CP}$ = 56.3 Hz, P*C*H$(CH_3)_2$); 26.5 (d, $^{1}J_{CP}$ = 53.4 Hz, P*C*H$(CH_3)_2$); 26.0 (d, $^{1}J_{CP}$ = 53.0 Hz, P*C*H$(CH_3)_2$); 25.2 (s, Mes *C*H_3); 24.9 (d, $^{1}J_{CP}$ = 62.5 Hz, P*C*H$(CH_3)_2$); 24.8 (s, Pipp CH(*C*$H_3)_2$); 24.6 (s, Pipp CH(*C*$H_3)_2$); 24.4 (s, Mes *C*H_3); 24.2 (d, $^{2}J_{CP}$ = 3.7 Hz, PCH(*C*$H_3)_2$); 21.5 (s, Mes *C*H_3); 17.5 (d, $^{2}J_{CP}$ = 3.0 Hz, PCH(*C*$H_3)_2$); 16.3 (d, $^{2}J_{CP}$ = 1.9 Hz, PCH(*C*$H_3)_2$); 16.3 (d, $^{2}J_{CP}$ = 2.6 Hz, PCH(*C*$H_3)_2$); 16.1 (d, $^{2}J_{CP}$ = 3.5 Hz, PCH(*C*$H_3)_2$); 15.9 (d, $^{2}J_{CP}$ = 2.0 Hz, PCH(*C*$H_3)_2$); 15.8 (d, $^{2}J_{CP}$ = 2.6 Hz, PCH(*C*$H_3)_2$); 15.3 (d, $^{2}J_{CP}$ = 3.6 Hz, PCH(*C*$H_3)_2$). **$^{31}P\{^{1}H\}$ NMR (283.42 MHz, benzene-d_6, 23 °C):** δ 48.2 (s, 1P, *P*–N–Rh); 45.1 (s, 1P, *P*–N–B). **$^{11}B\{^{1}H\}$ NMR (224.63 MHz, benzene-d_6, 23 °C):** δ 14.9 (br, s). **IR (cm^{-1}):** 1724 (s, Rh–*C*=*O* stretch).

Preparation of κ^2-*L*Rh[C(O)C(Ph)C(Me)B(Mes)], Compound 13^{Me}. Recrystallized **3** (70 mg, 0.085 mmol) was dissolved in 5 mL of toluene. In a separate flask, excess 1-phenyl-1-propyne (46 mg, 0.40 mmol) was dissolved in 1 mL of toluene and then added to the solution of **3** dropwise over a minute. The mixture was allowed to stir at ambient temperature for 5 hours. After removal of the solvent under reduced pressure, the crude solid was recrystallized over 16 hours from 5 mL of Et_2O at –30 °C to yield 29 mg (36% yield) of $\mathbf{13^{Me}}$ as light yellow crystals. Anal Calcd. for $C_{54}H_{74}BN_3OP_2Rh$: C, 67.59; H, 7.60; N, 4.46. Found: C, 66.98; H, 7.65; N, 8.10.

^{1}H NMR (benzene-d_6, 23 °C): δ 8.27 (br s, 2H, Ph Ar *H*); 7.58 (dd, $^3J_{HH}$ = 8.37 Hz, *J* = 1.73, 2H, Pipp Ar *H*); 7.37 (t, $^3J_{HH}$ = 7.58 Hz, 2H, Ph *H*); 7.25 (tt, $^3J_{HH}$ = 7.33 Hz, $^4J_{HH}$ = 1.1 Hz, 1H, Ph *para H*); 7.08 (d, $^3J_{HH}$ = 8.25 Hz, 2H, Pipp Ar *H*); 7.05-7.00 (br m, 2H, Pipp Ar *H*); 6.91 (s, 1H, Mes Ar *H*); 6.68 (t, $^3J_{HH}$ = $^3J_{HP}$ = 3.51 Hz, 1H, 3,4-pyrrole C*H*); 6.64 (ov s, 1H, Mes Ar *H*); 6.62 (ov d, 1H, Pipp Ar *H*); 6.51 (ov d, 1H, Pipp Ar *H*); 6.51 (t, $^3J_{HH}$ = $^3J_{HP}$ = 3.34 Hz, 1H, 3,4-pyrrole C*H*); 2.76 (s, 3H, Mes CH_3); 2.72 (sp, $^3J_{HH}$ = 6.88 Hz, 1H, Pipp C*H*(CH_3)$_2$); 2.64 (sp, $^3J_{HH}$ = 6.84 Hz, 1H, Pipp C*H*(CH_3)$_2$); 2.42 (m, 1H, PC*H*(CH_3)$_2$); 2.26 (m, 1H, PC*H*(CH_3)$_2$); 2.17 (s, 3H, Mes CH_3); 2.16 (s, 3H, Mes CH_3); 2.12 (m, 1H, PC*H*(CH_3)$_2$); 2.03 (m, 1H, PC*H*(CH_3)$_2$); 1.33 (ov dd, $^3J_{HH}$ = 7.21 Hz, $^3J_{HP}$ = 15.59 Hz, 3H, PCH(CH_3)$_2$); 1.31 (ov dd, $^3J_{HH}$ = 7.09 Hz, $^3J_{HP}$ = 16.02 Hz, 3H, PCH(CH_3)$_2$); 1.14 (d, $^3J_{HH}$ = 6.89 Hz, 6H, Pipp CH(CH_3)$_2$); 1.09 (dd, $^3J_{HH}$ = 6.90 Hz, *J* = 1.69 Hz, 6H, Pipp CH(CH_3)$_2$); 1.01 (dd, $^3J_{HH}$ = 7.18 Hz, $^3J_{HP}$ = 16.16 Hz, 3H, PCH(CH_3)$_2$); 0.91 (ov dd, $^3J_{HH}$ = 7.10 Hz, $^3J_{HP}$ = 15.06 Hz, 3H, PCH(CH_3)$_2$); 0.89 (ov dd, $^3J_{HH}$ = 7.01 Hz, $^3J_{HP}$ = 15.49 Hz, 3H, PCH(CH_3)$_2$); 0.84 (d, *J* = 3.52 Hz, 3H, C(Ph)-C(CH_3)); 0.60 (ov dd, $^3J_{HH}$ = 7.02 Hz, $^3J_{HP}$ = 16.47 Hz, 3H, PCH(CH_3)$_2$); 0.56 (ov dd, $^3J_{HH}$ = 7.20 Hz, $^3J_{HP}$ = 16.82 Hz, 3H, PCH(CH_3)$_2$); 0.53 (ov dd, $^3J_{HH}$ = 7.17 Hz, $^3J_{HP}$ = 14.79 Hz, 3H, PCH(CH_3)$_2$). **^{13}C{^{1}H} NMR (benzene-d_6, 23 °C):** δ 206.5 (d, $^1J_{CRh}$ = 21.7 Hz, Rh–*C*O); 149.6 (s, Pipp Ar *C*); 147.3 (s, Pipp Ar *C*); 146.0 (d, $^2J_{CRh}$ = 4.7 Hz, Ph *C*); 144.5 (s, Mes Ar *C*); 144.1 (br s, *C*(Ph)); 143.7 (s, Mes Ar *C*); 141.9 (d, $^2J_{CP}$ = 2.9 Hz, Pipp Ar *C*); 140.6 (s, Mes Ar *C*); 139.7 (s, Pipp Ar *C*); 135.9 (dd, $^1J_{CP}$ = 145.0 Hz, $^4J_{CP}$ = 15.0 Hz, 2,5-

pyrrole *C*); 134.3 (s, Mes Ar *C*); 133.7 (br s, Pipp Ar *C*H); 131.9 (br s, Pipp Ar *C*H); 129.0 (s, Mes Ar *C*H); 128.5 (ov s, identified through ^{13}C–^{1}H HSQC and HMBC experiments, Ph *C*H); 128.3 (ov s, identified through ^{13}C–^{1}H HSQC and HMBC experiments, Mes Ar *C*H); 127.5 (d, J = 6.1 Hz, Pipp Ar *C*H); 127.3 (s, Ph *C*H); 126.5 (d, J = 1.9 Hz, Pipp Ar *C*H); 126.1 (br s, Pipp Ar *C*H); 125.9 (s, Ph *C*H); 125.5 (br s, Pipp Ar *C*H); 121.7 (dd, $^{1}J_{CP}$ = 132.1 Hz, $^{4}J_{CP}$ = 12.7 Hz, 2,5-pyrrole *C*); 120.6 (dd, $^{3}J_{CP}$ = 10.5 Hz, $^{2}J_{CP}$ = 26.1 Hz, 3,4-pyrrole *C*H); 114.7 (dd, $^{3}J_{CP}$ = 10.5 Hz, $^{2}J_{CP}$ = 25.1 Hz, 3,4-pyrrole *C*H); 93.1 (br s, identified through ^{13}C–^{1}H HMBC experiments, C(Ph)-*C*(CH_3)); 33.9 (s, Pipp *C*H(CH_3)$_2$); 33.8 (s, Pipp *C*H(CH_3)$_2$); 30.4 (d, $^{1}J_{CP}$ = 60.1 Hz, P*C*H(CH_3)$_2$); 27.1 (d, $^{1}J_{CP}$ = 53.2 Hz, P*C*H(CH_3)$_2$); 26.3 (d, $^{1}J_{CP}$ = 52.5 Hz, P*C*H(CH_3)$_2$); 26.1 (s, Mes *C*H_3); 26.1 (s, Mes *C*H_3); 25.3 (d, $^{1}J_{CP}$ = 58.7 Hz, P*C*H(CH_3)$_2$); 24.5 (d, J = 6.2 Hz, ???); 24.3 (s, Pipp CH(*C*H_3)$_2$); 24.2 (s, Pipp CH(*C*H_3)$_2$); 21.4 (s, Mes *C*H_3); 17.2 (br d, $^{2}J_{CP}$ = 1.1 Hz, PCH(C*H*$_3$)$_2$); 17.1 (br s, PCH(C*H*$_3$)$_2$); 16.5 (d, $^{2}J_{CP}$ = 1.7 Hz, PCH(C*H*$_3$)$_2$); 16.4 (d, $^{2}J_{CP}$ = 2.0 Hz, PCH(C*H*$_3$)$_2$); 16.4 (d, $^{2}J_{CP}$ = 3.3 Hz, PCH(C*H*$_3$)$_2$); 16.2 (d, $^{2}J_{CP}$ = 2.5 Hz, PCH(C*H*$_3$)$_2$); 16.1 (d, $^{2}J_{CP}$ = 2.0 Hz, PCH(C*H*$_3$)$_2$); 16.0 (d, $^{2}J_{CP}$ = 2.6 Hz, PCH(C*H*$_3$)$_2$); 10.6 (d, J = 2.8 Hz, C(Ph)-C(*C*H_3)). **$^{31}P\{^{1}H\}$ NMR (283.42 MHz, benzene-d_6, 23 °C):** δ 51.7 (s, 1P, *P*–N–Rh); 42.9 (s, 1P, *P*–N–B). **$^{11}B\{^{1}H\}$ NMR (224.63 MHz, benzene-d_6, 23 °C):** δ 10.7 (br s). **IR (cm^{-1}):** 1727 (s, Rh–*C*=*O* stretch).

Preparation of *L*(CO)Rh($\overline{\mathbf{PhCCH=BMesOC}}$), Compound $\mathbf{15^H}$. Recrystallized $\mathbf{13^H}$ (20 mg, 0.022 mmol) was dissolved in 2 mL of benzene-d_6 and added to a PTFE sealed Young NMR tube. The solution was then degassed with three freeze, pump, thaw cycles and allowed to warm to ambient temperature. Approximately 1 atm of CO gas was added to the vessel using a glass dual manifold vacuum/gas line. The tube was inverted every minute and turned from light yellow to bright orange after 5 minutes. Once the bright orange color was observed, the tube was inverted one more time and was left for an additional 5 minutes before the headspace was removed *in vacuo* and the sample degassed with three more freeze, pump, thaw cycles. Removal of solvent under reduced pressure lead to isolation of compound $\mathbf{15^H}$ (20 mg, 98% yield) as a bright orange solid. Anal Calcd. for $C_{53}H_{69}BN_3O_2P_2Rh$: C, 66.60; H, 7.28; N, 4.40. Found: C, 66.31; H, 7.34; N, 4.67.

^{1}H NMR (benzene-d_6, 23 °C): δ 8.62 (br s, 2H, *ortho*-Ph *H*); 7.43 (d, $^3J_{HH}$ = 7.76 Hz, 2H, Pipp Ar *H*); 7.22 (m, 3H, *meta/para*-Ph *H*); 7.15 (ov d, 1H, Pipp Ar *H*); 7.01 (d, $^3J_{HH}$ = 8.02 Hz, 2H, Pipp Ar *H*); 6.90 (s, 2H, Mes Ar *H*); 6.71 (d, $^3J_{HH}$ = 8.02 Hz, 1H, Pipp Ar *H*); 6.56 (ov d, 1H, Pipp Ar *H*); 6.55 (ov t, 1H, 3,4-pyrrole C*H*); 6.50 (t, $^3J_{HH}$ = $^3J_{HP}$ = 3.2 Hz; 1H, 3,4-pyrrole C*H*); 6.41 (d, $^3J_{HH}$ = 8.02 Hz, 1H, Pipp Ar *H*); 6.15 (s, 1H, PhC–C*H*); 2.95 (br s, 1H, PC*H*$(CH_3)_2$); 2.73 (sp, $^3J_{HH}$ = 6.83 Hz, 1H, Pipp C*H*$(CH_3)_2$); 2.66 (s, 6H, Mes *ortho*-CH_3); 2.54 (sp, $^3J_{HH}$ = 6.83 Hz, 1H, Pipp C*H*$(CH_3)_2$); 2.21 (s, 3H, Mes *para*-CH_3); 2.14 (m, 2H, PC*H*$(CH_3)_2$); 1.99 (dd, $^3J_{HH}$ = 6.69 Hz, $^3J_{HP}$ = 16.60 Hz, 3H, PCH(C$H_3)_2$); 1.91 (m, 1H, PC*H*$(CH_3)_2$); 1.26 (dd, $^3J_{HH}$ = 7.20 Hz, $^3J_{HP}$ = 15.37 Hz, 3H, PCH(C$H_3)_2$); 1.15 (dd, *J* = 1.96, $^3J_{HH}$ = 6.83 Hz, 6H, Pipp CH(C$H_3)_2$); 1.08 (ov dd, $^3J_{HH}$ = 7.00 Hz, $^3J_{HH}$ = 16.33 Hz, 3H, PCH(C$H_3)_2$); 1.04 (ov d, $^3J_{HH}$ = 6.83 Hz, 3H, Pipp CH(C$H_3)_2$); 1.02 (ov d, $^3J_{HH}$ = 6.83 Hz, 3H, Pipp CH(C$H_3)_2$); 0.88 (ov m, 12H, PCH(C$H_3)_2$); -0.01 (dd, $^3J_{HH}$ = 7.00 Hz, $^3J_{HP}$ = 14.87 Hz, 3H, PCH(C$H_3)_2$). **^{13}C{^{1}H} NMR (benzene-d_6, 23 °C):** δ 196.4 (d, $^1J_{CRh}$ = 83.0 Hz, Rh–*C*O); 175.1 (d, $^1J_{CRh}$ = 12.3 Hz, Rh–C(O)–*C*(Ph)); 151.4 (s, Pipp Ar *C*); 148.56 (s, Pipp Ar *C*); 143.6 (s, Mes Ar *C*); 141.3 (d, ^2J = 2.2 Hz, Pipp Ar *C*); 139.4 (s,Ph *C*); 137.7 (s, Mes Ar *C*); 135.7 (dd, $^1J_{CP}$ = 143.3 Hz, $^4J_{CP}$ = 15.6 Hz, 2,5-pyrrole *C*); 134.0 (br s, Mes Ar *C*); 133.9 (d, $^2J_{CP}$ =

5.1 Hz, Pipp Ar *C*); 133.3 (s, Pipp Ar *C*H); 132.2 (d, J_{CP} = 4.7 Hz, Pipp Ar *C*H); 130.5 (s, *ortho*-Ph *C*H); 128.4 (s, Mes Ar C*H*); 127.5 (s, Pipp Ar *C*H); 127.4 (s, Ph *C*H); 127.3 (s, Ph *C*H); 126.7 (s, Pipp Ar *C*H); 126.2 (s, Pipp Ar *C*H); 125.9 (s, Pipp Ar *C*H); 125.4 (s, Pipp Ar *C*H); 119.2 (br s, C(Ph)–*C*(H), identified through 2D ^{1}H–^{13}C HSQC experiments); 118.4 (dd, $^{1}J_{CP}$ = 131.1 Hz, $^{4}J_{CP}$ = 14.2 Hz, 2,5-pyrrole *C*); 117.2 (dd, $^{2}J_{CP}$ = 24.8 Hz, $^{3}J_{CP}$ = 10.4 Hz, 3,4-pyrrole *C*H); 114.9 (dd, $^{2}J_{CP}$ = 24.5 Hz, $^{3}J_{CP}$ = 10.2 Hz, 3,4-pyrrole *C*H); 105.7 (dd, $^{2}J_{CP}$ = 10.5 Hz, $^{1}J_{CRh}$ = 41.1 Hz, *C*(O)–C(Ph)–C(H), identified through 2D ^{13}C–^{1}H HMBC experiments and ^{13}C labelling experiments); 34.0 (s, Pipp *C*H(CH$_3$)$_2$); 33.8 (s, Pipp *C*H(CH$_3$)$_2$); 28.9 (d, $^{1}J_{CP}$ = 50.9 Hz, P*C*H(CH$_3$)$_2$); 27.8 (d, $^{1}J_{CP}$ = 52.7 Hz, P*C*H(CH$_3$)$_2$); 26.7 (d, $^{1}J_{CP}$ = 53.0 Hz, P*C*H(CH$_3$)$_2$); 24.4 (d, *J* = 37.4, Pipp CH(*C*H$_3$)$_2$); 24.2 (s, Pipp CH(*C*H$_3$)$_2$); 23.9 (s, Pipp CH(*C*H$_3$)$_2$); 23.8 (d, $^{1}J_{CP}$ = 63.1 Hz, P*C*H(CH$_3$)$_2$); 23.4 (s, *ortho*-Mes *C*H$_3$); 21.4 (s, *para*-Mes *C*H$_3$); 18.0 (d, $^{2}J_{CP}$ = 2.6 Hz, PCH(*C*H$_3$)$_2$);17.3 (s, PCH(*C*H$_3$)$_2$); 17.0 (d, $^{2}J_{CP}$ = 1.7 Hz, PCH(*C*H$_3$)$_2$); 16.8 (d, $^{2}J_{CP}$ = 2.6 Hz, PCH(*C*H$_3$)$_2$); 16.2 (d, $^{2}J_{CP}$ = 2.6 Hz, PCH(*C*H$_3$)$_2$); 16.1 (d, $^{2}J_{CP}$ = 2.3 Hz, PCH(*C*H$_3$)$_2$); 15.8 (d, $^{2}J_{CP}$ = 3.2 Hz, PCH(*C*H$_3$)$_2$); 14.7 (d, $^{2}J_{CP}$ = 3.9 Hz, PCH(*C*H$_3$)$_2$). **^{31}P{^{1}H} NMR (283.42 MHz, benzene-*d*$_6$, 23 ºC):** δ 54.6 (s, 1P, *P*–N–Rh); 45.0 (s, 1P, *P*–N–B). **^{11}B{^{1}H} NMR (benzene-*d*$_6$, 23 °C):** Unable to resolve from baseline. **IR (cm^{-1}):** 1914 (s, Rh–*C*=*O* stretch).

Preparation of PhC=C(Ph)B(Mes)OC(NPipp), Compound 16^{Ph}. A PTFE sealed Young NMR tube was charged with a sample of **13^{Ph}** (10 mg, 0.010 mmol) dissolved in 1 mL benzene-d_6. The solution was degassed with three freeze-pump-thaw cycles and allowed to warm to ambient temperature before approximately 1 atm of $CO_{(g)}$ was introduced to the system on a glass dual manifold gas/high-vacuum line. The NMR tube was heated at 45 °C for 14 hours, with occasional inversion of solution, resulting in a gradual color change from amber yellow to a deep orange-red. Due to the small scale of the reaction, as well as similar solubility profiles to the metal complex **14**, the organic product was characterized through 2D-(^{1}H^{1}H) COSY experiments as a reaction mixture, as well as high resolution mass spectroscopy experiments. **^{1}H NMR (benzene-d_6, 23 °C):** δ 7.62 (d, $^3J_{HH}$ = 7.6 Hz, 2H, Pipp Ar *H*); 7.21-7.17 (ov m, 4H, Ph *H*); 7.13-7.01 (ov m, 6H, Ph *H*); 6.94 (d, $^3J_{HH}$ = 7.6 Hz, 2H, Pipp Ar *H*); 6.58 (br s, Mes Ar *H*); 2.58 (sp, $^3J_{HH}$ = 6.9 Hz, 1H, Pipp C*H*(CH$_3$)$_2$); 2.06 (s, 6H, Mes *ortho*-C*H*$_3$); 2.01 (s, 3H, Mes *para*-C*H*$_3$); 1.00 (d, $^3J_{HH}$ = 6.9 Hz, 6H, Pipp CH(C*H*$_3$)$_2$). **^{11}B{^{1}H} NMR (224.63 MHz, benzene-d_6, 23 °C):** δ 53.0 (br s). **HRMS (ESI)**: m/z calcd for $C_{33}H_{32}BNO$ $[M+H]^+$ 470.2655, found 470.2660.

Preparation of PhC=C(CO$_2$Et)B(Mes)OC(NPipp), Compound 16^{CO2Et}. A PTFE sealed Young NMR tube was charged with a sample of **13^{CO2Et}** (15 mg, 0.015 mmol) dissolved in 1 mL benzene-d_6. The solution was degassed with three freeze-pump-thaw cycles and allowed to warm to ambient temperature before approximately 1 atm of $CO_{(g)}$ was introduced to the system on a glass dual manifold gas/high-vacuum line. The NMR tube was left at ambient temperature for 2 hours, resulting in a gradual color change from bright yellow to a deep orange-red. Due to the small scale of the reaction, as well as similar solubility profiles to the metal complex **14**, the organic product was characterized through 2D-(^{1}H^{1}H) COSY experiments as a reaction mixture, as well as high resolution mass spectroscopy experiments. **^{1}H NMR (benzene-d_6, 23 °C):** δ 7.93 (d, $^3J_{HH}$ = 7.4 Hz, 2H, Pipp Ar *H*); 7.24 (d, $^3J_{HH}$ = 7.3 Hz, 2H, Ph *H*); 7.19 (ov d, 2H, Pipp Ar *H*); 6.87 (t, $^3J_{HH}$ = 7.3 Hz, 1H, Ph *H*); 6.78 (t, 2H, $^3J_{HH}$ = 7.3 Hz Ph *H*); 6.72 (s, 2H, Mes Ar *H*); 3.85 (q, $^3J_{HH}$ = 7.1 Hz,

2H, OCH_2CH$_3$); 2.65 (sp, $^3J_{HH}$ = 6.9 Hz, 1H, Pipp CH(CH$_3$)$_2$); 2.38 (s, 6H, Mes *ortho*-CH_3); 2.11 (s, 3H, Mes *para*-CH_3); 1.08 (d, $^3J_{HH}$ = 6.9 Hz, 6H, Pipp CH(CH_3)$_2$); 0.70 (t, $^3J_{HH}$ = 7.1 Hz, 3H, OCH$_2$CH_3). **^{11}B{^{1}H} NMR (224.63 MHz, benzene-d_6, 23 °C):** δ 49.1 (br s). **HRMS (ESI)**: m/z calcd for $C_{30}H_{32}BNO_3$ $[M+H]^+$ 466.2553, found 466.2546.

Preparation of PhC=C(H)B(Mes)OC(NPipp), Compound 16^H. A PTFE sealed Young NMR tube was charged with a sample of **13^H** (15 mg, 0.016 mmol) dissolved in 1 mL benzene-d_6. The solution was degassed with three freeze-pump-thaw cycles and allowed to warm to ambient temperature before approximately 1 atm of $CO_{(g)}$ was introduced to the system on a glass dual manifold gas/high-vacuum line. The NMR tube was left at ambient temperature for 2 hours, resulting in a gradual color change from bright yellow to a deep orange-red. Due to the small scale of the reaction, as well as similar solubility profiles to the metal complex **14**, the organic product was characterized through 2D-(^{1}H^{1}H) COSY experiments as a reaction mixture, as well as high resolution mass spectroscopy experiments. **^{1}H NMR (benzene-d_6, 23 °C):** δ 8.14 (d, $^3J_{HH}$ = 7.6 Hz, 2H, Ph *H*); 7.59 (d, $^3J_{HH}$ = 8.2 Hz, 2H, Pipp Ar *H*); 7.24 (t, $^3J_{HH}$ = 7.3 Hz, 2H, Ph *H*); 7.18-7.15 (ov m, 1H, Ph *H*); 7.14 (ov d, $^3J_{HH}$ = 8.2 Hz, Pipp Ar *H*); 6.89 (s, 1H, C*H*, identified through 2D ^{1}H–^{13}C HSQC experiments); 6.75 (s, 2H, Mes Ar *H*); 2.71 (ov sp, $^3J_{HH}$ = 6.9 , 1H, Pipp CH(CH$_3$)$_2$); 2.42 (s, 6H, Mes *ortho*-CH_3); 2.12 (s, 3H, Mes *para*-CH_3); 1.08 (ov d, $^3J_{HH}$ = 6.9, 6H, Pipp CH(CH_3)$_2$). **^{11}B{^{1}H} NMR (224.63 MHz, benzene-d_6, 23 °C):** δ 48.7 (br s). **HRMS (ESI)**: m/z calcd for $C_{27}H_{28}BNO$ $[M]^+$ 393.2264, found 393.2244.

Preparation of PhC=C(Me)B(Mes)OC(NPipp), Compound 16^{Me}. A PTFE sealed Young NMR tube was charged with a sample of **13^{Me}** (10 mg, 0.010 mmol) dissolved in 1 mL benzene-d_6. The solution was degassed with three freeze-pump-thaw cycles and allowed to warm to ambient temperature before approximately 1 atm of $CO_{(g)}$ was introduced to the system on a glass dual manifold gas/high-vacuum line. The NMR tube was left at ambient temperature for 2 hours, resulting in a gradual color change from orange yellow to a deep orange-red. Due to the small scale

of the reaction, as well as similar solubility profiles to the metal complex **14**, the organic product was characterized through 2D-(^{1}H^{1}H) COSY experiments as a reaction mixture, as well as high resolution mass spectroscopy experiments. **^{1}H NMR (benzene-d_6, 23 °C):** δ 7.75 (d, $^3J_{HH}$ = 8.3 Hz, 2H, Pipp Ar *H*); 7.20 (d, $^3J_{HH}$ = 7.2 Hz, 2H, Ph *H*); 7.13 (d, $^3J_{HH}$ = 8.3 Hz, 2H, Pipp Ar *H*); 7.04 (t, $^3J_{HH}$ = 7.5 Hz, 2H, Ph *H*); 6.99 (ov t, 1H, Ph *H*); 6.67 (s, 2H, Mes Ar *H*); 2.70 (sp, $^3J_{HH}$ = 6.9 Hz, 1H, Pipp C*H*(CH$_3$)$_2$); 2.32 (s, 3H, C*H*$_3$); 2.14 (s, 6H, Mes *ortho*-C*H*$_3$); 2.09 (s, 3H, Mes *para*-C*H*$_3$); 1.13 (d, $^3J_{HH}$ = 6.9 Hz, 6H, Pipp CH(C*H*$_3$)$_2$). **^{11}B{^{1}H} NMR (224.63 MHz, benzene-d_6, 23 °C):** Unable to resolve from baseline. **HRMS (ESI)**: m/z calcd for $C_{30}H_{32}BNO_3$ $[M+H]^+$ 407.2420, found 407.2425.

Appendix III. II NMR Spectra

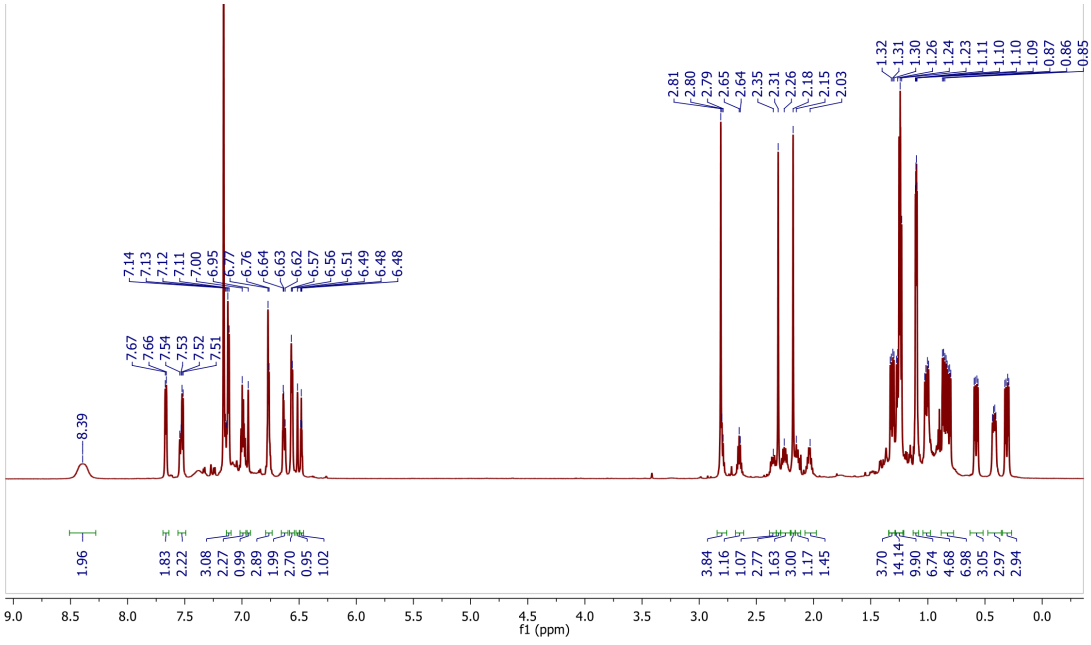

Appendix Figure III.1. ^{1}H NMR (700 MHz) spectrum of complex **13^{Ph}** in benzene-d_6 at 22 °C

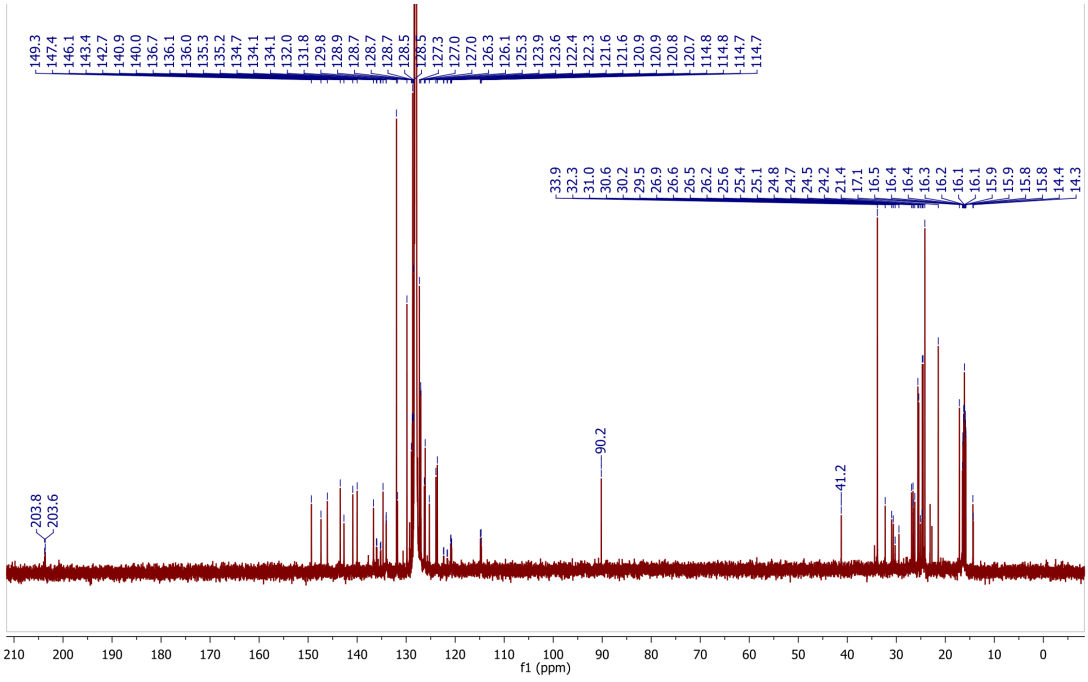

Appendix Figure III.2. ^{13}C{^{1}H} NMR (176 MHz) spectrum of complex **13^{Ph}** in benzene-d_6 at 22 °C

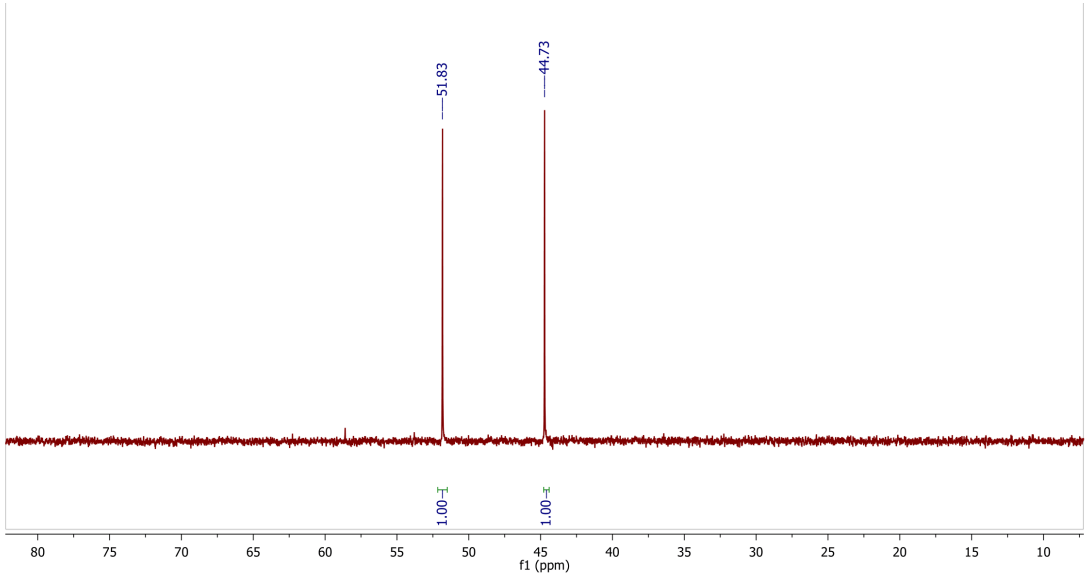

Appendix Figure III.3. $^{31}P\{^{1}H\}$ NMR (283.5 MHz) spectrum of complex **13^{Ph}** in benzene-d_6 at 22 °C

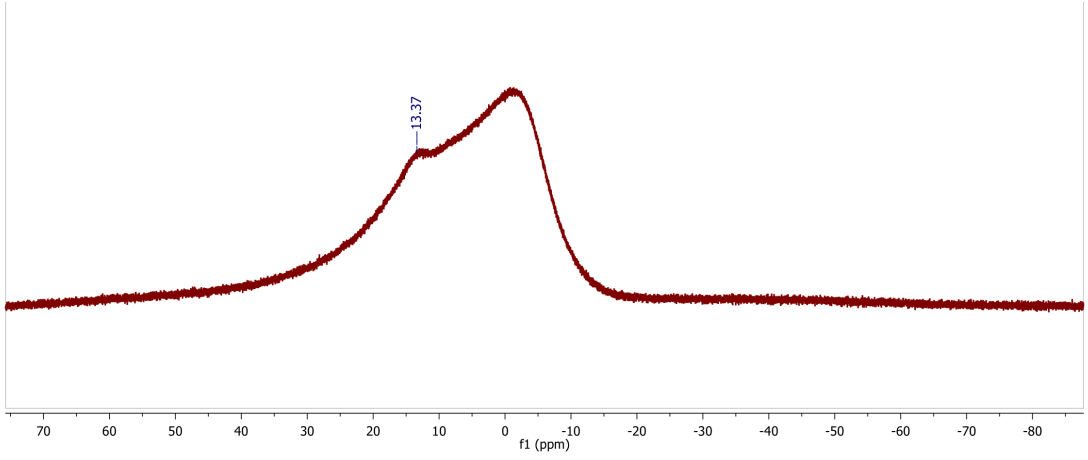

Appendix Figure III.4. $^{11}B\{^{1}H\}$ NMR (224.6 MHz) spectrum of complex **13^{Ph}** in benzene-d_6 at 22 °C

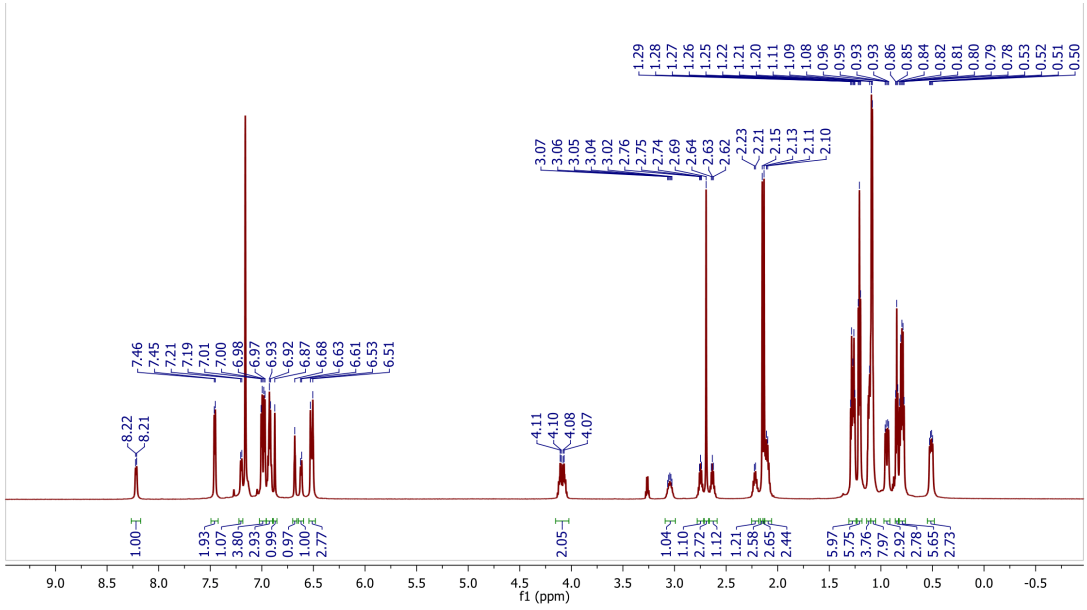

Appendix Figure III.5. ^{1}H NMR (700 MHz) spectrum of complex **13**$^{\mathbf{CO2Et}}$ in benzene-d_6 at 22 °C

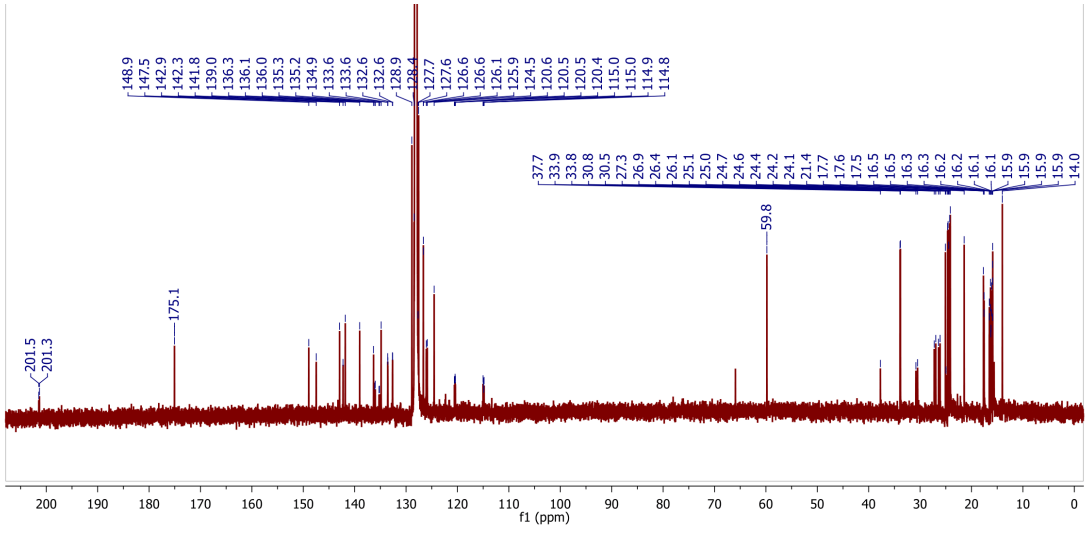

Appendix Figure III.6. ^{13}C{^{1}H} NMR (176 MHz) spectrum of complex **13**$^{\mathbf{CO2Et}}$ in benzene-d_6 at 22 °C

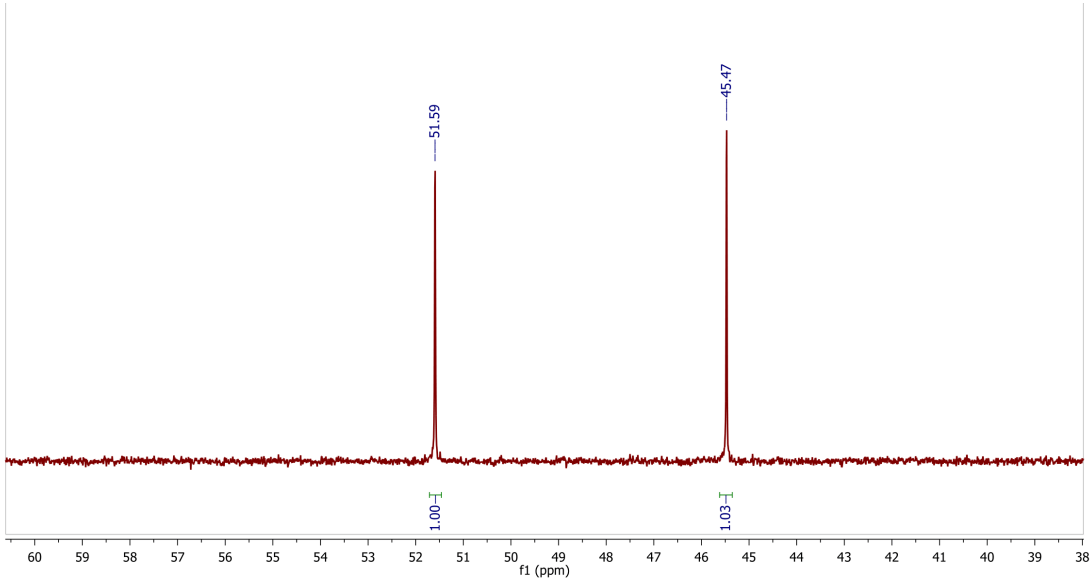

Appendix Figure III.7. $^{31}P\{^{1}H\}$ NMR (283.5 MHz) spectrum of complex **13**$^{\mathbf{CO2Et}}$ in benzene-d_6 at 22 °C

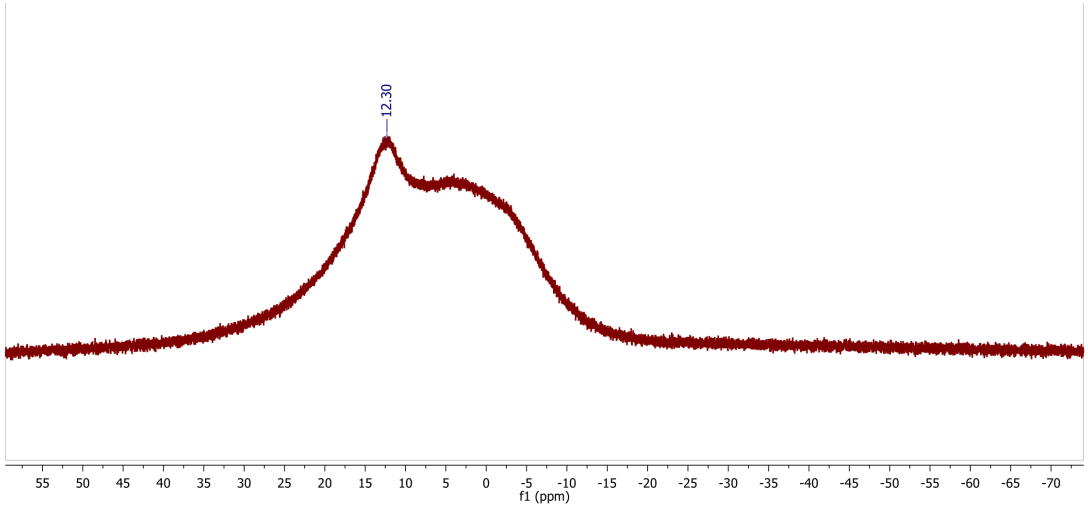

Appendix Figure III.8. $^{11}B\{^{1}H\}$ NMR (224.6 MHz) spectrum of complex **13**$^{\mathbf{CO2Et}}$ in benzene-d_6 at 22 °C

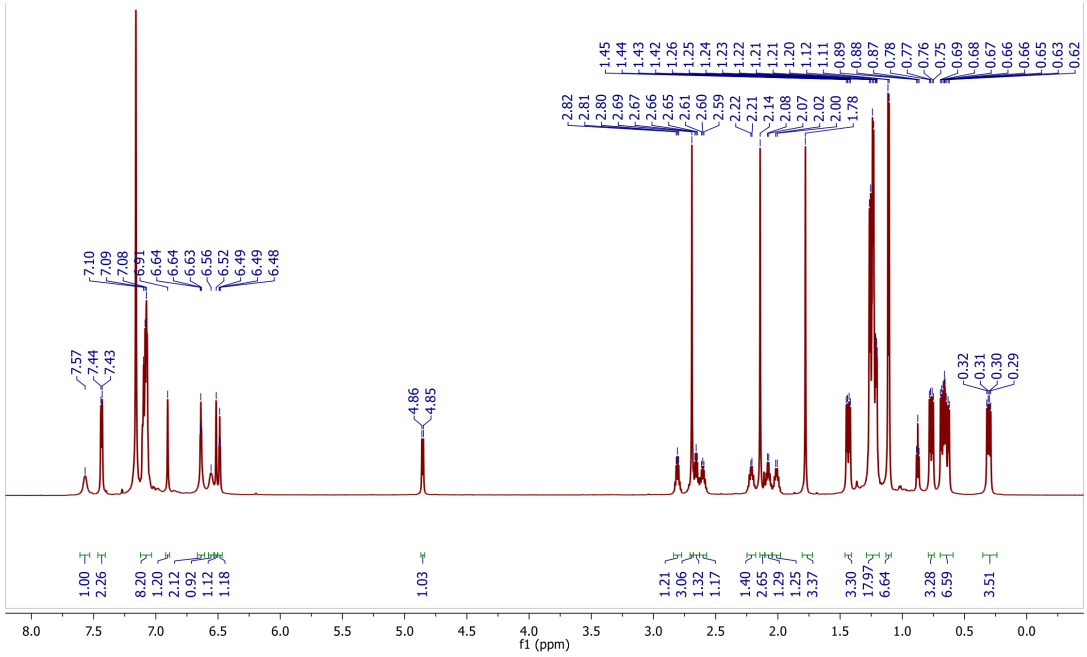

Appendix Figure III.9. ^{1}H NMR (700 MHz) spectrum of complex **13^{H}** in benzene-d_6 at 22 °C

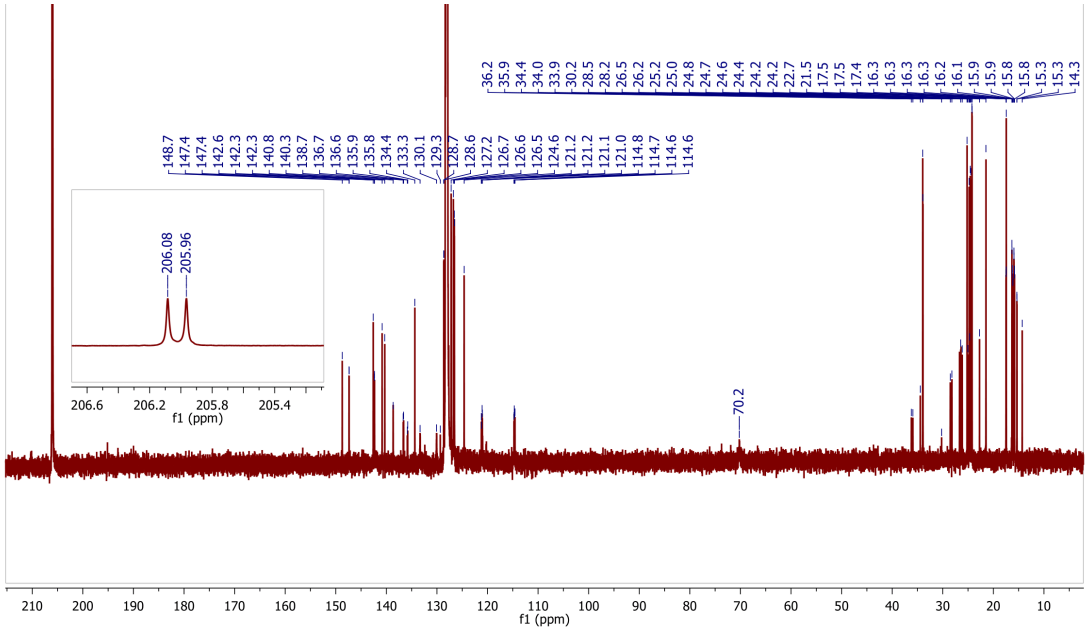

Appendix Figure III.10. ^{13}C{^{1}H} NMR (176 MHz) spectrum of ^{13}CO enriched complex **13^{H}** in benzene-d_6 at 22 °C

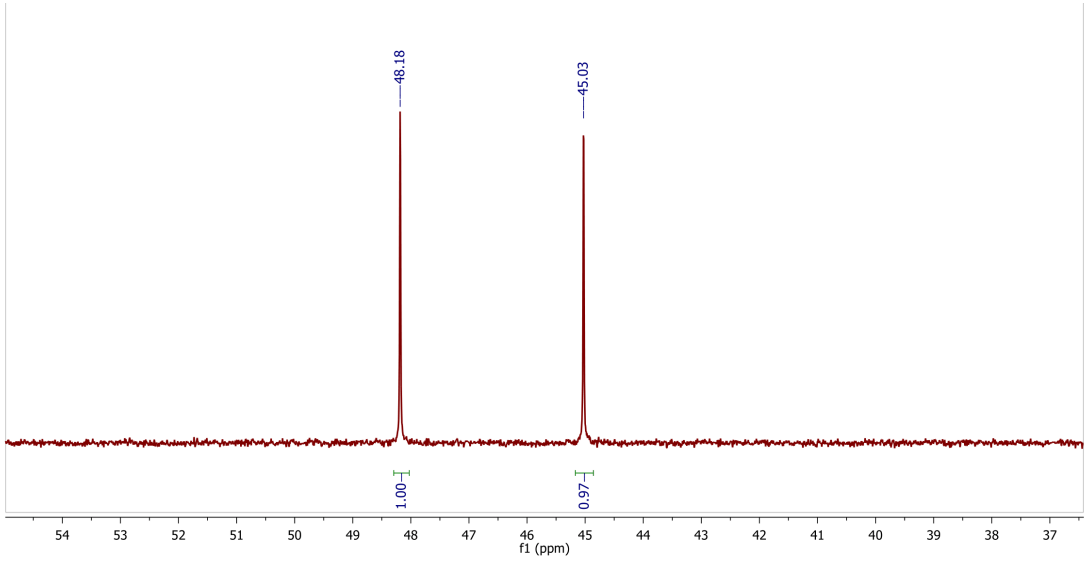

Appendix Figure III.11. $^{31}P\{^{1}H\}$ NMR (283.5 MHz) spectrum of complex **13^{H}** in benzene-d_6 at 22 °C

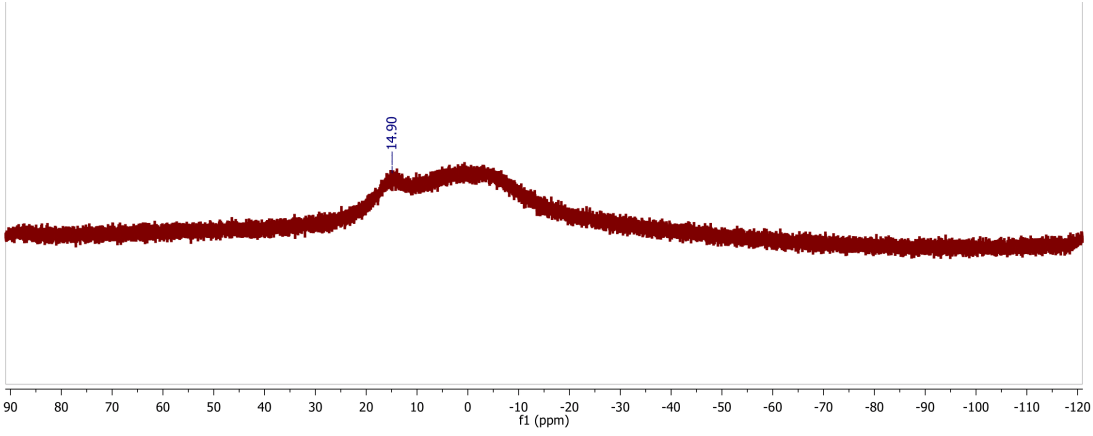

Appendix Figure III.12. $^{11}B\{^{1}H\}$ NMR (224.6 MHz) spectrum of complex **13^{H}** in benzene-d_6 at 22 °C

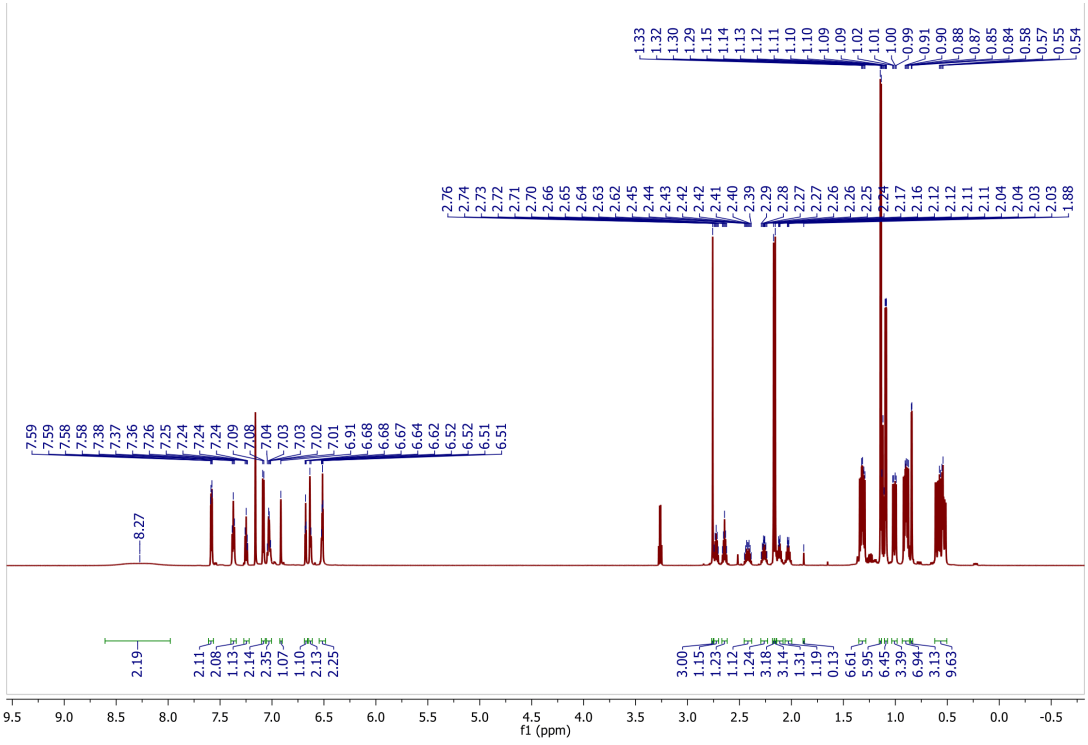

Appendix Figure III.13. ^{1}H NMR (700 MHz) spectrum of complex **13^{Me}** in benzene-d_6 at 22 °C

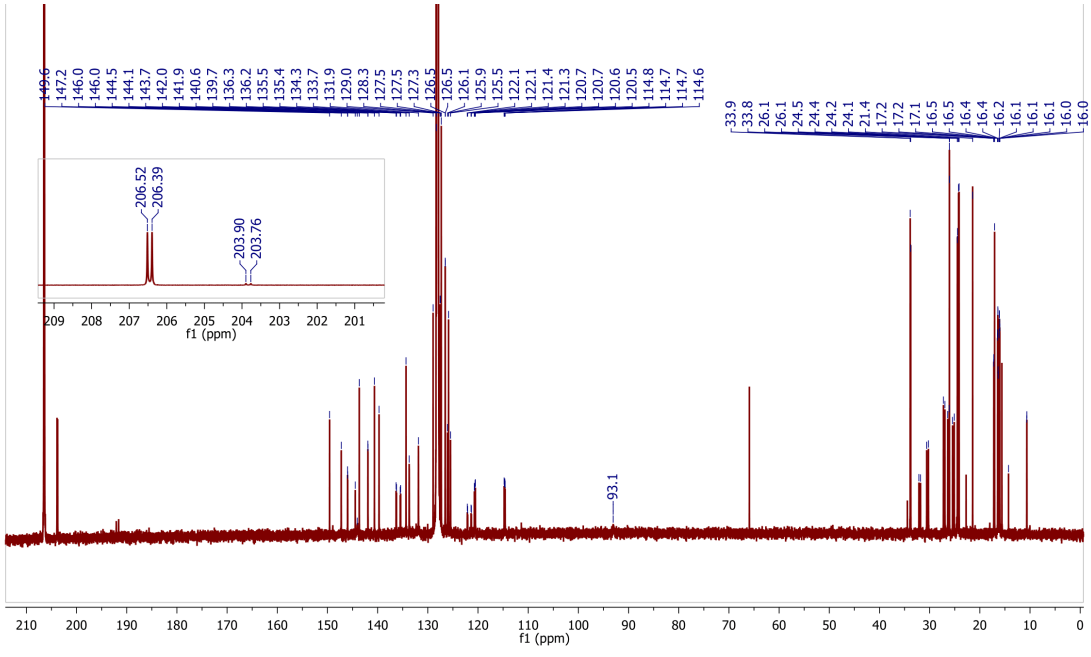

Appendix Figure III.14. ^{13}C{^{1}H} NMR (176 MHz) spectrum of complex ^{13}CO enriched **13^{Me}** in benzene-d_6 at 22 °C

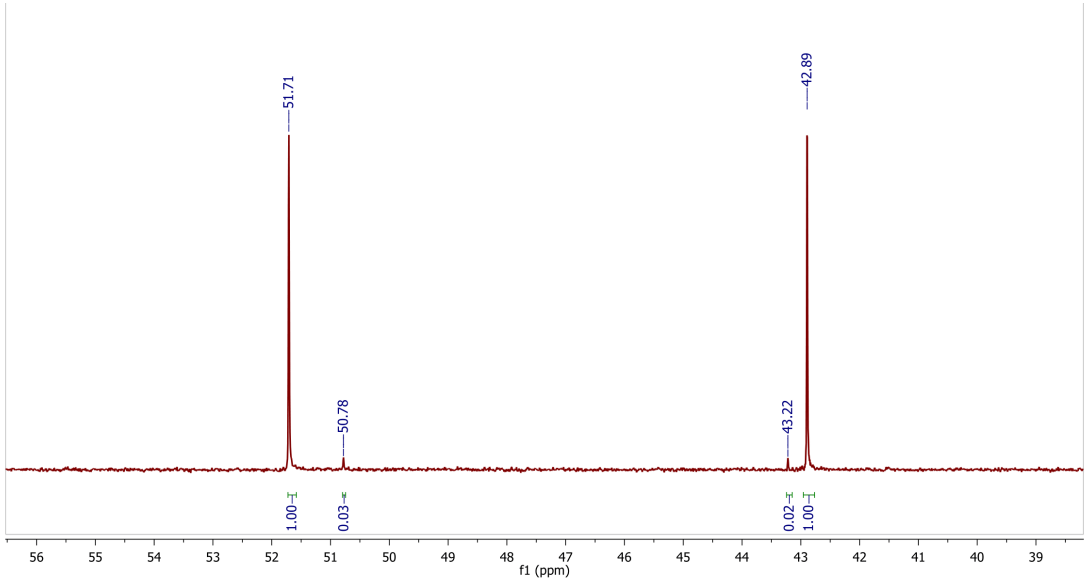

Appendix Figure III.15. $^{31}P\{^{1}H\}$ NMR (283.5 MHz) spectrum of complex **13**$^{\mathbf{Me}}$ in benzene-d_6 at 22 °C

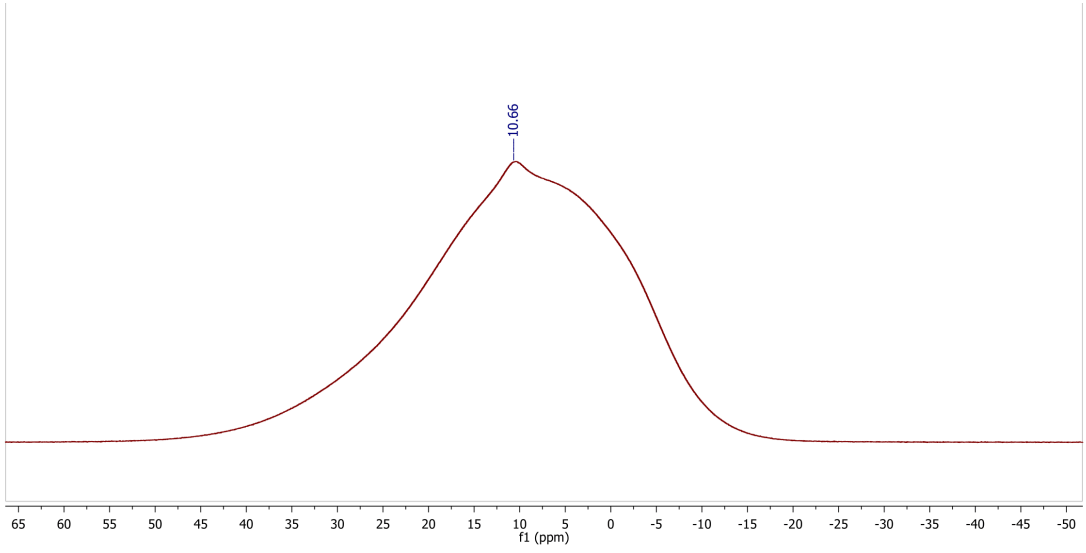

Appendix Figure III.16. $^{11}B\{^{1}H\}$ NMR (224.6 MHz) spectrum of complex **13**$^{\mathbf{Me}}$ in benzene-d_6 at 22 °C

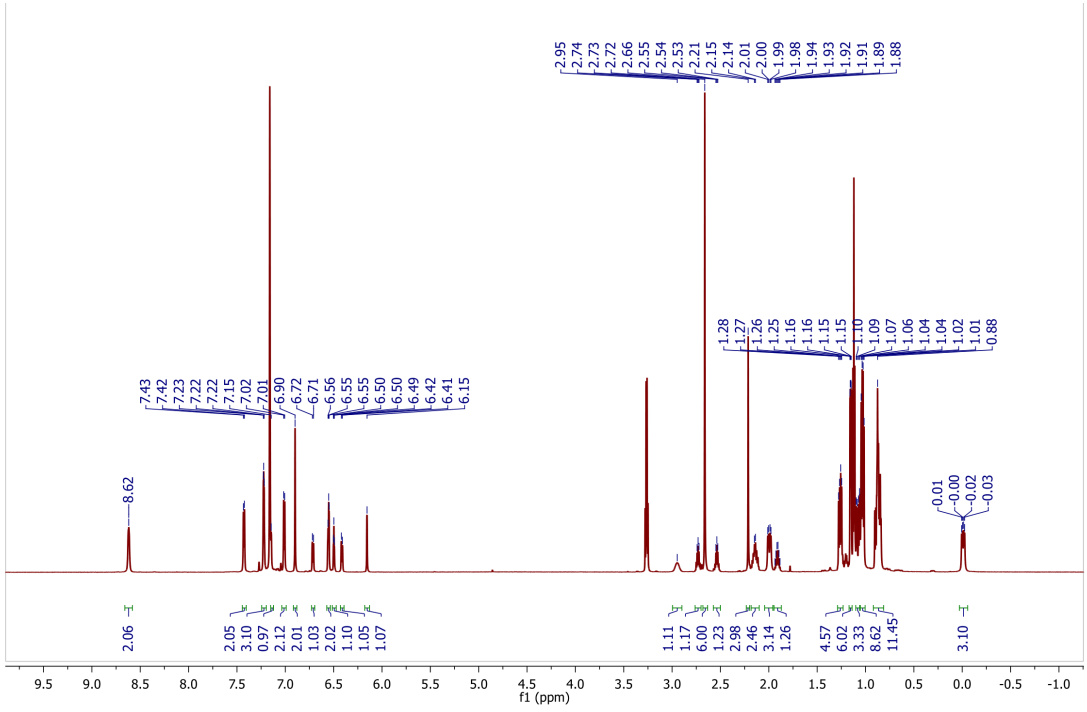

Appendix Figure III.17. ^{1}H NMR (700 MHz) spectrum of complex **15^{H}** in benzene-d_6 at 22 °C

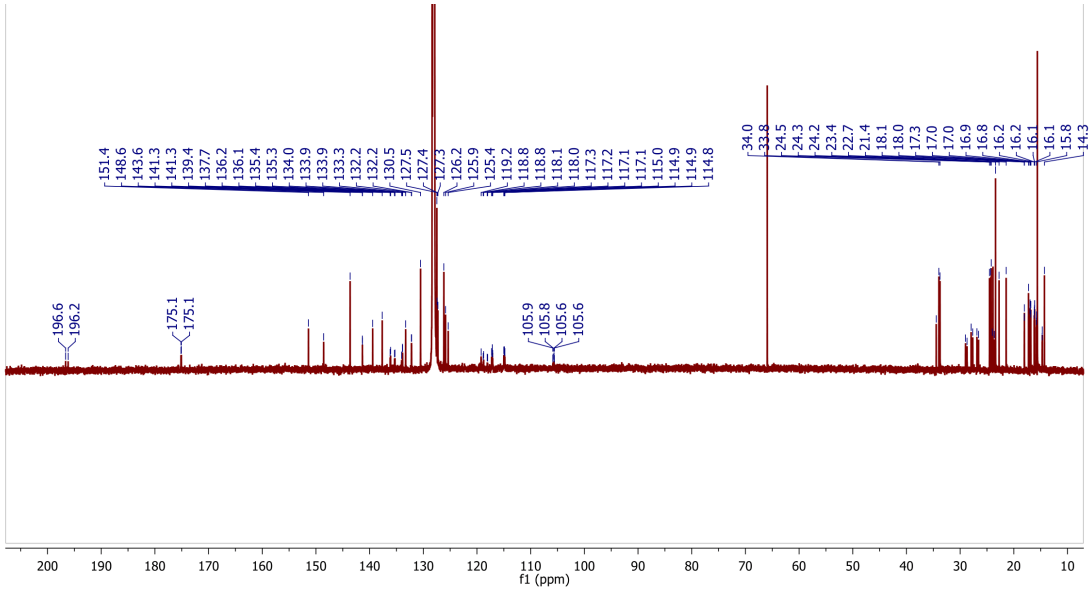

Appendix Figure III.18. ^{13}C{^{1}H} NMR (176 MHz) spectrum of complex **15^{H}** in benzene-d_6 at 22 °C

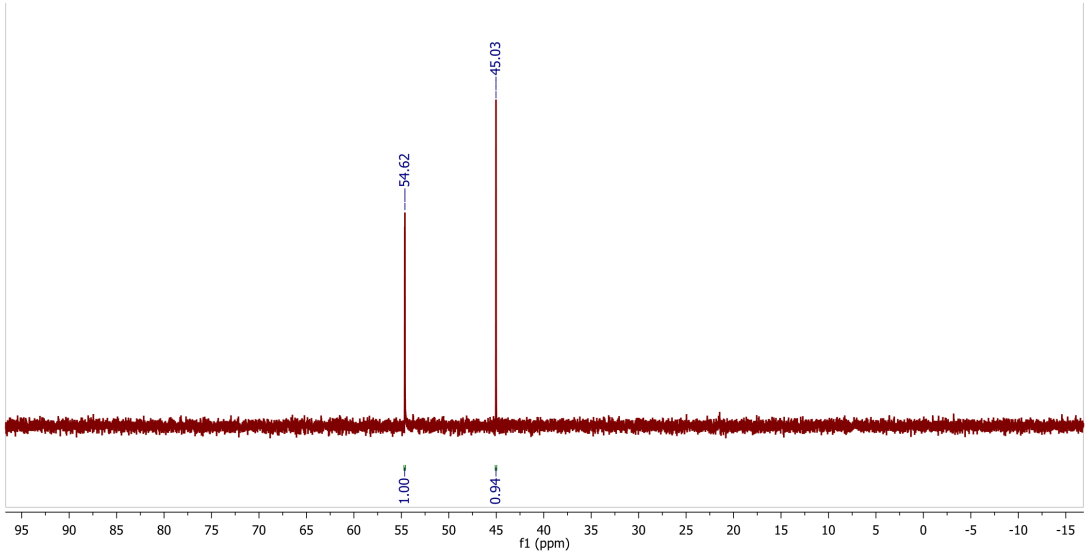

Appendix Figure III.19. $^{31}P\{^{1}H\}$ NMR (283.5 MHz) spectrum of complex **15^{H}** in benzene-d_6 at 22 °C

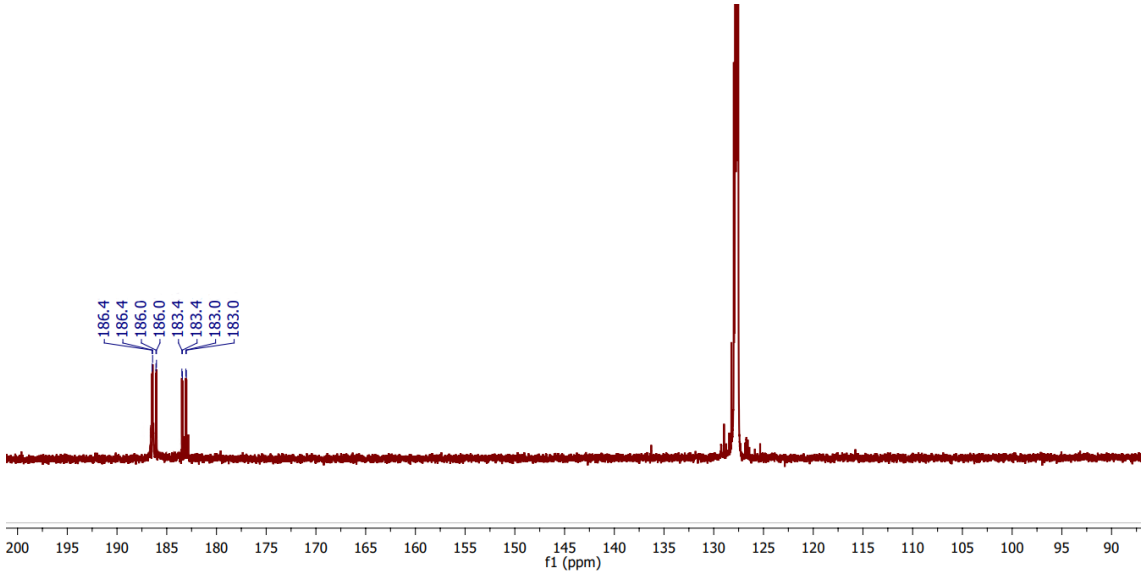

Appendix Figure III.20. $^{13}C\{^{1}H\}$ NMR (176 MHz) spectrum of complex **14** resulting from addition of ^{13}CO to natural ^{13}C abundant **13^{H}** in benzene-d_6 at 22 °C

Appendix III. III Mass Spectra

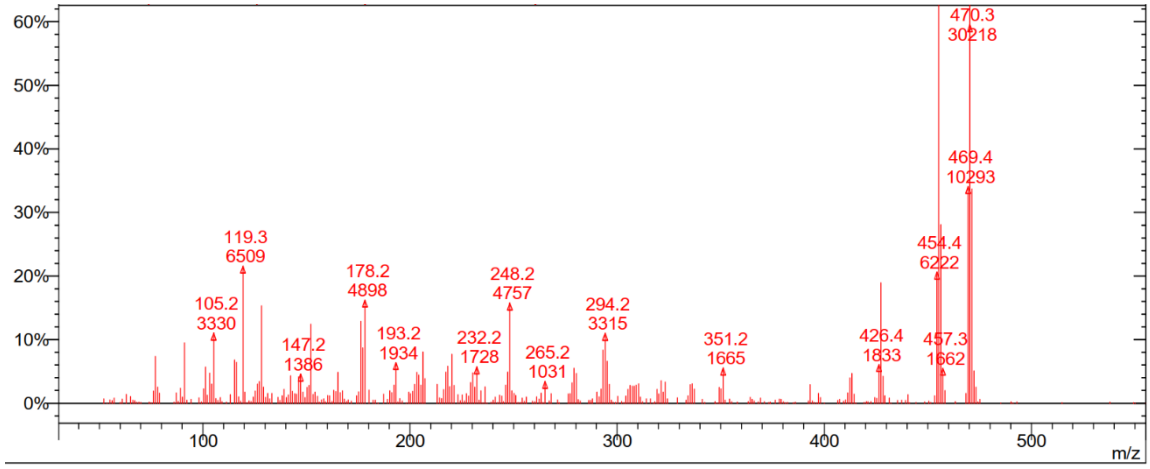

Appendix Figure III.21. Mass Spectra of **16**^{Ph} obtained from electron impact (EI) ionization showing fragmentation pattern

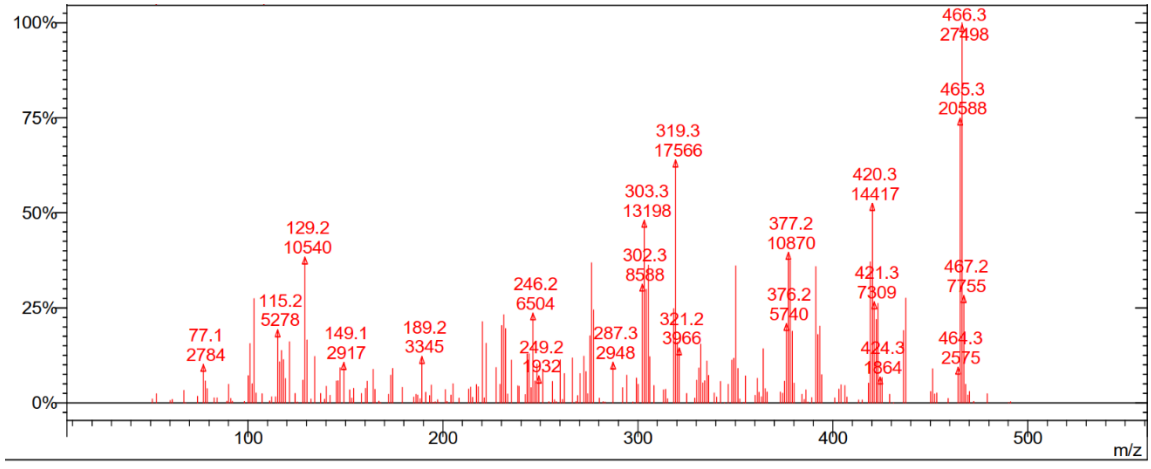

Appendix Figure III.22. Mass Spectrum of **16**^{CO2Et} obtained from electron impact (EI) ionization showing fragmentation pattern

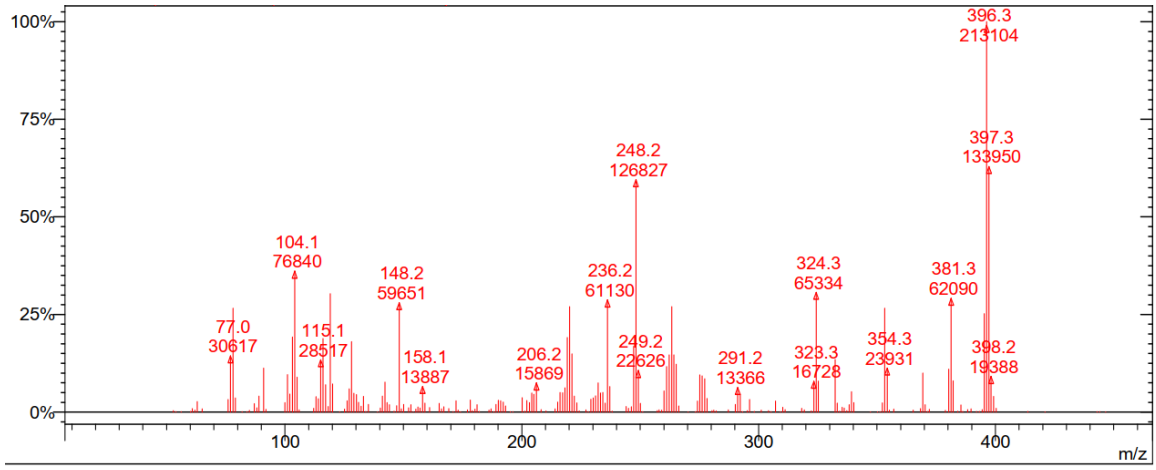

Appendix Figure III.23. Mass Spectrum of **16^{H}** obtained from electron impact (EI) ionization showing fragmentation pattern

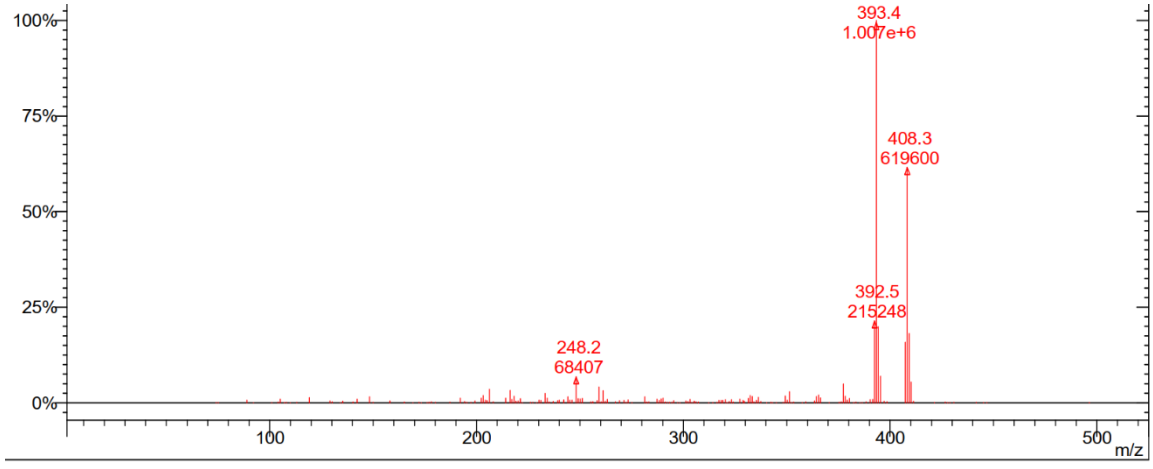

Appendix Figure III.24. Mass Spectrum of **16^{Me}** obtained from electron impact (EI) ionization showing fragmentation pattern

Appendix III. IV Crystallographic Details

X-Ray Diffraction Techniques. All structures were collected on a Rigaku SuperNova diffractometer equipped with a Dectris Pilatus 3R 200K-A hybrid-pixel-array detector, a four-circle κ goniometer, sealed graphite-monochromated Mo Kα (λ = 0.71073 Å) and Cu Kα (λ = 1.54178 Å) X-ray sources, and an Oxford cryostream-cooling device fixed at 100 K. Single crystals suitable for X-ray diffraction studies were mounted on a MiTiGen cryo-loop using desiccated Paratone–N oil stored in a glove box. The structures were solved by the Intrinsic Phasing methods and refined by least-squares methods using SHELXT-2014 and SHELXL-2014 with the OLEX2 interface.[2] All non-H atom were located in difference Fourier maps, and then refined anisotropically. Outlier reflections were omitted from refinement when appropriate. Hydrogen atoms on C atoms were placed at idealized positions and refined using a riding model. Crystallographic refinement details, including disorder modeling and software employed, have been delineated within each crystallographic information file (*.cif) and are available via the CCDC database. Molecular graphics were generated using ORTEP and Adobe Illustrator.

Appendix Table III.1. X-ray Crystallographic Details for Reported Compounds. *Connectivity structures were not submitted to the CCDC database on account of complete datasets being impossible to complete in reasonable collection timeframes (>500 hours in all cases). In **13^{Ph}** and **13^{H}** the quality of data also did not meet publication standards but was deemed sufficient to demonstrate connectivity.

	13^{Ph}	**13^{CO2Et}**	**13^{H}**
CCDC Entry ID	Connectivity*	Connectivity*	Connectivity*
Crystal System	Triclinic	Triclinic	Monoclinic
Formula	$C_{58}H_{73}BN_3OP_2Rh$	$C_{55}H_{73}BN_3O_3P_2Rh$	$C_{53}H_{72}BN_3OP_2Rh$
Formula weight (g/mol)	1003.8	999.85	942.84
Space Group	P-1	P-1	C2/c
a (Å)	12.3593(6)	11.9598(6)	41.203(5)
b (Å)	14.1095(7)	19.7293(14)	13.196(6)
c (Å)	19.0979(6)	25.334(3)	20.2697(17)
α (deg)	93.276(3)	71.496(9)	90
β (deg)	91.270(3)	76.362(7)	100.930(9)
γ (deg)	105.821(4)	76.500(6)	90
Z	2	4	8
V (Å^3)	3196.5(3)	5426.8(9)	10821(5)
Indep. Reflections	12812	7454	3895
R(int)	0.1416	0.0287	0.0541
R1(%)	13.34	5.10	13.38
wR2	0.3793	0.1249	0.3619
GoF	1.693	1.024	1.560

	13^{Me}	**14** ($L^2Rh(CO)_2$)	**15**^{Me}
CCDC Entry ID	Connectivity*	2387421	Connectivity*
Crystal System	Monoclinic	Orthorhombic	Triclinic
Formula	$C_{53}H_{71}BN_3OP_2Rh$	$C_{27}H_{41}N_2O_2P_2Rh$	$C_{54}H_{71}BN_3O_2P_2Rh$
Formula weight (g/mol)	941.78	590.47	969.84
Space Group	$P2_1/c$	$P2_12_12_1$	P-1
a (Å)	12.9701(5)	9.37500(10)	12.1584(16)
b (Å)	19.3528(11)	9.79560(10)	14.100(2)
c (Å)	19.5260(9)	31.7302(3)	16.268(2)
α (deg)	90	90	98.558(12)
β (deg)	91.786(4)	90	105.860(12)
γ (deg)	90	90	106.064(13)
Z	4	4	2
V ($Å^3$)	4898.8(4)	2913.90(5)	2500.8(7)
Indep. Reflections	3386	6037	4388
R(int)	0.0280	0.0386	0.1028
R1(%)	3.34	2.89	8.10
wR2	0.0828	0.0735	0.1949
GoF	1.039	1.085	1.058

Appendix Table III.2. Selected bond distances and angles for complexes **13** and **15**^{Me}. Note that these data are included for completion, but should be considered low quality.

	3^{Ph}	**3**^{CO2Et}	**3**^{H}	**3**^{Me}	**5**^{Me}
Rh–C1 (Å)	1.90(1)	1.941(9)	1.91(2)	1.927(7)	2.36(1)
C1–O (Å)	1.20(1)	1.17(1)	1.26(3)	1.207(8)	1.38(2)
C1–C2 (Å)	1.43(1)	1.45(2)	1.40(4)	1.434(9)	1.52(2)
C2–C3 (Å)	1.44(1)	1.52(1)	1.48(3)	1.435(8)	1.55(2)
C3–B (Å)	1.55(1)	1.42(2)	1.56(7)	1.538(8)	1.35(2)
B–N (Å)	1.56(1)	1.57(1)	1.63(3)	1.587(8)	-
C1–C2–C3 ∠ (°)	112.8(8)	111.2(9)	111(2)	114.2(5)	97(1)
C2–C3–B ∠ (°)	114.6(9)	116(1)	118(2)	114.0(5)	110(1)
C3–B–N ∠ (°)	120.7 (8)	119 (1)	106(3)	117.8(5)	-
B (Σ_{angles}) (°)	353.6	347.2	151.1	351.4	360
Rh–C2 (Å)	-	-	-	-	2.23(1)
B–O (Å)	-	-	-	-	1.38(2)

Appendix III. V Computational Details

All density functional theory (DFT) calculations in this study were conducted with the Gaussian 16 C.01 suite of programs.[3] Geometry optimizations of all the intermediates were carried out with the Minnesota functional M06[4] with the double-ζ basis set def2SVP[5] and Grimme's dispersion (GD3).[6] Solution phase interactions were calculated with Truhlar and workers' SMD model.[7] Cartesian coordinates were obtained from X-ray diffraction analysis or based off of analogous structures. Harmonic vibrational frequencies were computed to verify the absence of imaginary frequencies. Wiberg bond indices, natural bond orbital (NBO) analyses and second order perturbation analyses were determined using NBO 3.1 at the triple-ζ Def2TZVPP level of theory.[5]

Solid state metrics acquired through X-Ray crystallography was compared to the optimized solution phase geometry of each complex in the series $\mathbf{13^{Ph}}$, $\mathbf{13^{Me}}$, $\mathbf{13^{CO2Et}}$, $\mathbf{13^{H}}$. Table below details select parameters compared for complex $\mathbf{13^{Ph}}$ as an example.

Appendix Table III.3. Comparison of calculated (def2svpp) and experimental structural parameters in $\mathbf{13^{Ph}}$.

Parameter	Experimental	Calculated	% Difference
d(Rh–C1) (Å)	1.90(1)	1.95	2.6
d(Rh–C2) (Å)	2.11(1)	2.13	0.94
d(Rh–C3) (Å)	2.11(1)	2.14	1.4
d(Rh–B) (Å)	2.31(1)	2.31	0
d(C2–C3) (Å)	1.44(1)	1.45	0.69
d(N1–B) (Å)	1.56(1)	1.58	1.3
∠(C2–C3–B) (deg)	114.6(9)	115.1	0.44
∠(C1–C2–C3) (deg)	112.8(8)	114.3	1.3
∠(C3–B–N1) (deg)	120.7(8)	119.8	0.75

Appendix III. VI References

[1] C. S. MacNeil, S.-J. Hsiang, P. G. Hayes, *Chem. Commun.* **2020**, *56*, 12323-12326.

[2] a) G. M. Sheldrick, *Acta Crystallogr., Sect. A: Found. Adv.* **2015**, *71*, 3-8; b) G. M. Sheldrick, *Acta Crystallogr., Sect. C: Struct. Chem.* **2015**, *71*, 3-8.

[3] Gaussian 16 C.01. M. J. Frisch, G. W. Trucks, H. B. Schlegel, G. E. Scuseria, M. A. Robb, J. R. Cheeseman, G. Scalmani, V. Barone, G. A. Petersson, H. Nakatsuji, X. Li, M. Caricato, A. V. Marenich, J. Bloino, B. G. Janesko, R. Gomperts, B. Mennucci, H. P. Hratchian, J. V. Ortiz, A. F. Izmaylov, J. L. Sonnenberg, Williams, F. Ding, F. Lipparini, F. Egidi, J. Goings, B. Peng, A. Petrone, T. Henderson, D. Ranasinghe, V. G. Zakrzewski, J. Gao, N. Rega, G. Zheng, W. Liang, M. Hada, M. Ehara, K. Toyota, R. Fukuda, J. Hasegawa, M. Ishida, T. Nakajima, Y. Honda, O. Kitao, H. Nakai, T. Vreven, K. Throssell, J. A. Montgomery Jr., J. E. Peralta, F. Ogliaro, M. J. Bearpark, J. J. Heyd, E. N. Brothers, K. N. Kudin, V. N. Staroverov, T. A. Keith, R. Kobayashi, J. Normand, K. Raghavachari, A. P. Rendell, J. C. Burant, S. S. Iyengar, J. Tomasi, M. Cossi, J. M. Millam, M. Klene, C. Adamo, R. Cammi, J. W. Ochterski, R. L. Martin, K. Morokuma, O. Farkas, J. B. Foresman, D. J. Fox, Wallingford, CT, **2016**.

[4] Y. Zhao, D. G. Truhlar, *Theor. Chem. Acc.* **2008**, *120*, 215-241.

[5] a) F. Weigend, *Phys. Chem. Chem. Phys.* **2006**, *8*, 1057-1065; b) F. Weigend, R. Ahlrichs, *Phys. Chem. Chem. Phys.* **2005**, *7*, 3297-3305.

[6] S. Grimme, J. Antony, S. Ehrlich, H. Krieg, *J. Chem. Phys.* **2010**, *132*.

[7] A. V. Marenich, C. J. Cramer, D. G. Truhlar, *J. Phys. Chem. B* **2009**, *113*, 6378-6396.

Appendix IV. Supporting Information for Chapter 5

Reformatted from submitted supporting information associated with “Hsiang, S.J.; Hayes, P.G.*, Synthesis and Reaction Chemistry of a Rhodium Silylyne Complex.” Accepted for publication in the *Canadian Journal of Chemistry,* **2025**.

Table of Contents

Appendix IV. I NMR Spectra

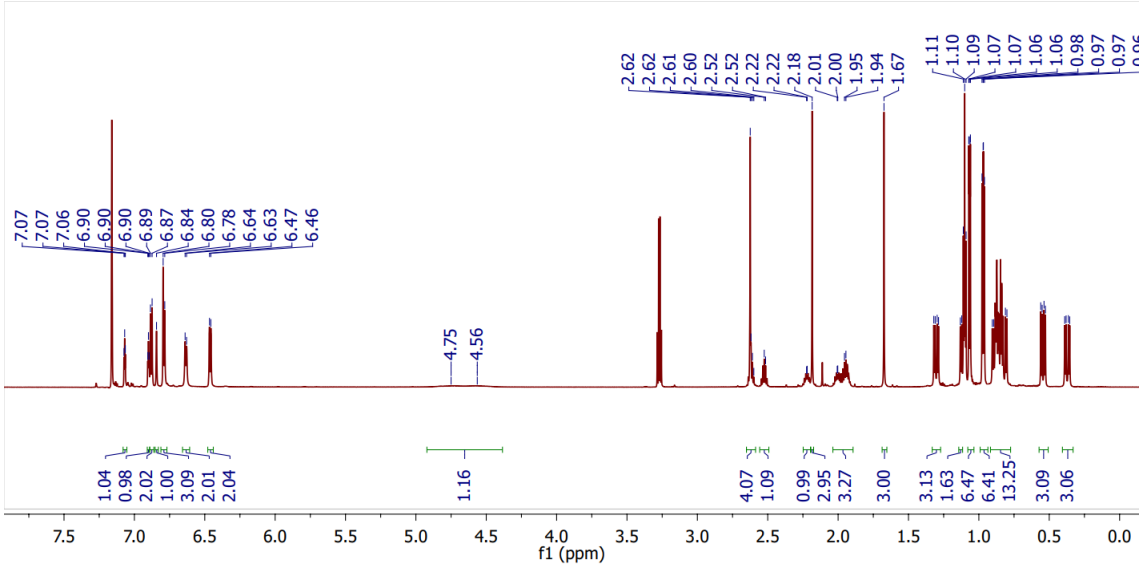

Appendix Figure IV.1. ^{1}H NMR (700 MHz) spectrum of complex **17^{Mes}** in benzene-d_6 at 22 °C.

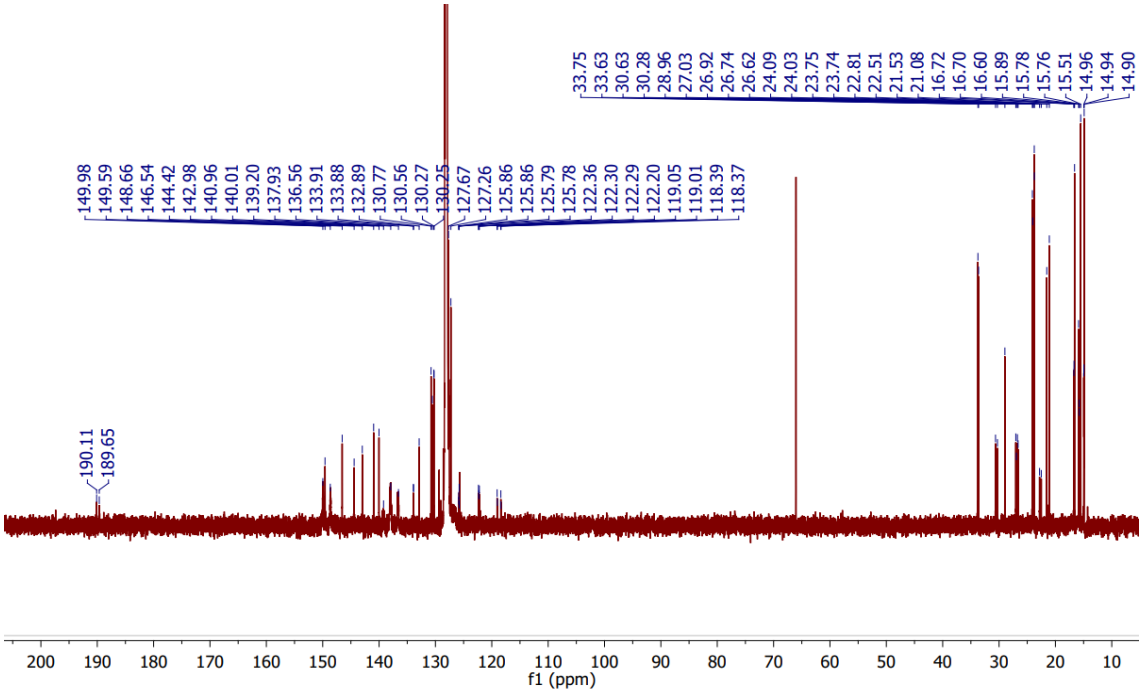

Appendix Figure IV.2. ^{13}C{^{1}H} NMR (176 MHz) spectrum of complex **17^{Mes}** in benzene-d_6 at 22 °C

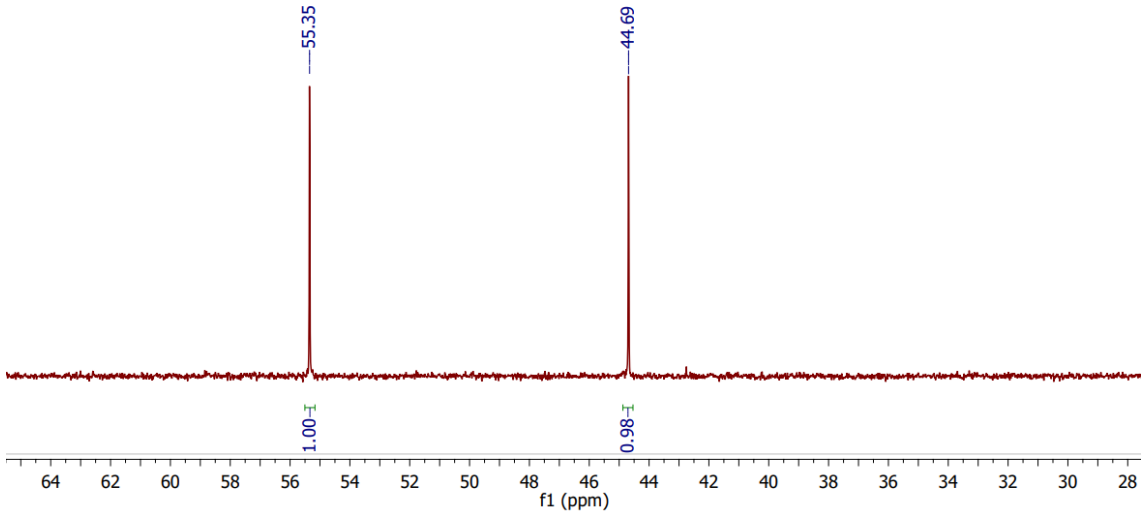

Appendix Figure IV.3. $^{31}P\{^{1}H\}$ NMR (283.5 MHz) spectrum of complex **17**$^{\mathbf{Mes}}$ in benzene-d_6 at 22 °C

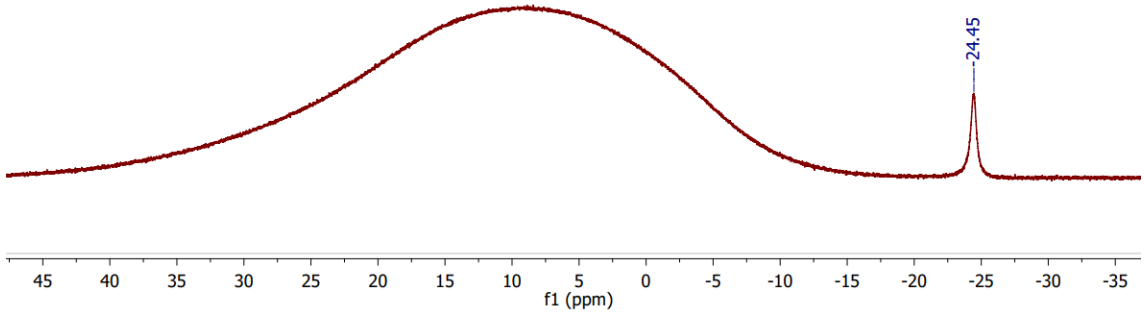

Appendix Figure IV.4. $^{11}B\{^{1}H\}$ NMR (224.6 MHz) spectrum of complex **17**$^{\mathbf{Mes}}$ in benzene-d_6 at 22 °C

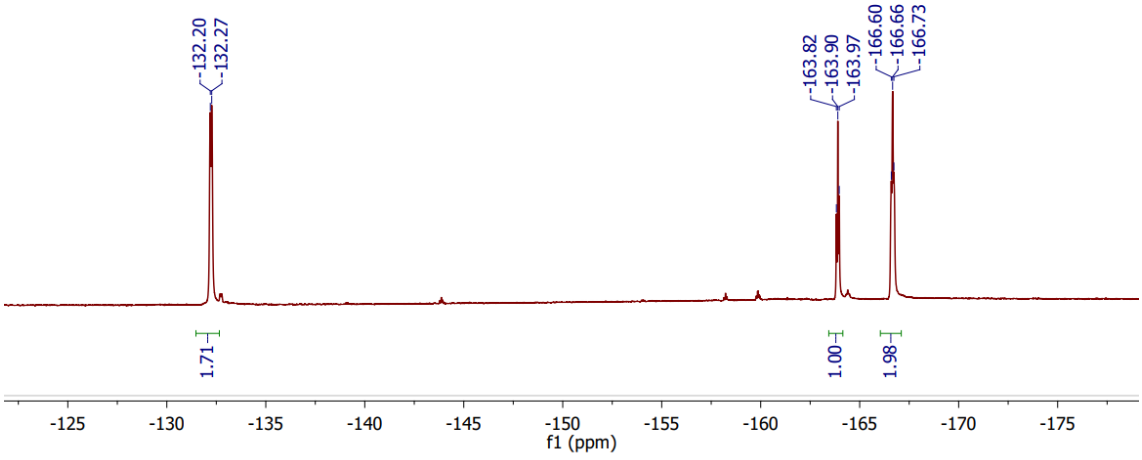

Appendix Figure IV.5. $^{19}F\{^{1}H\}$ NMR (282.43 MHz) Spectrum of **17**$^{\mathbf{Mes}}$ in benzene-d_6 at 22 °C

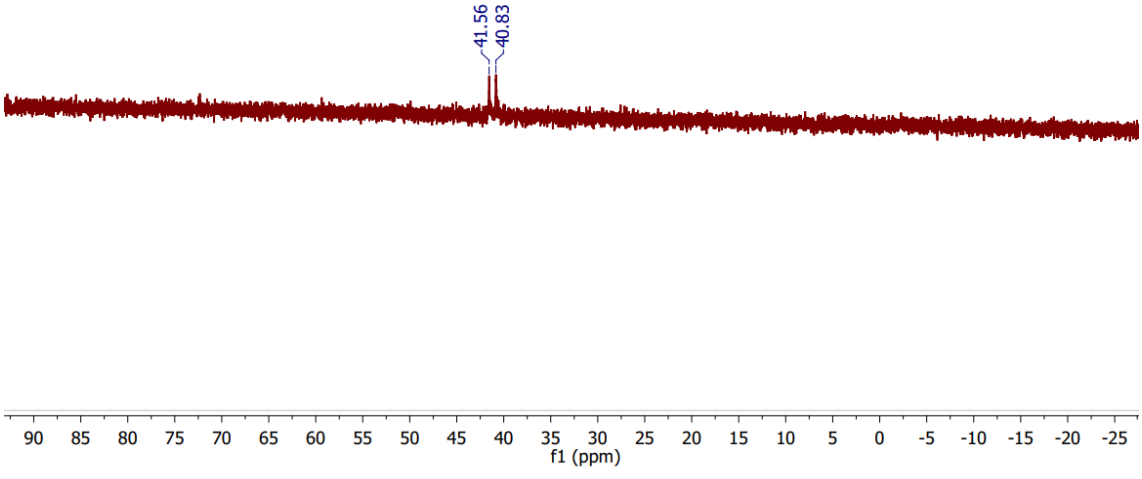

Appendix Figure IV.6. $^{29}Si\{^{1}H\}$ NMR (139.10 MHz) Spectrum of **17**$^{\mathbf{Mes}}$ in benzene-d_6 at 22 °C

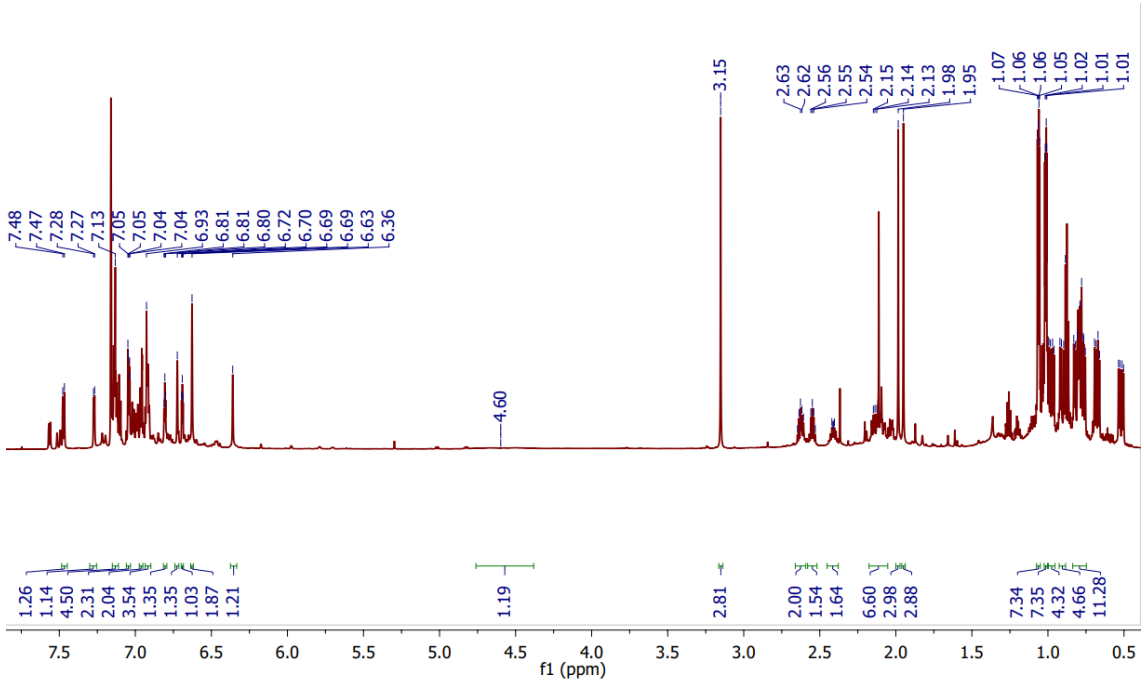

Appendix Figure IV.7. ^{1}H NMR (700 MHz) spectrum of complex **18**$^{\mathbf{Mes}}$ in benzene-d_6 at 22 °C

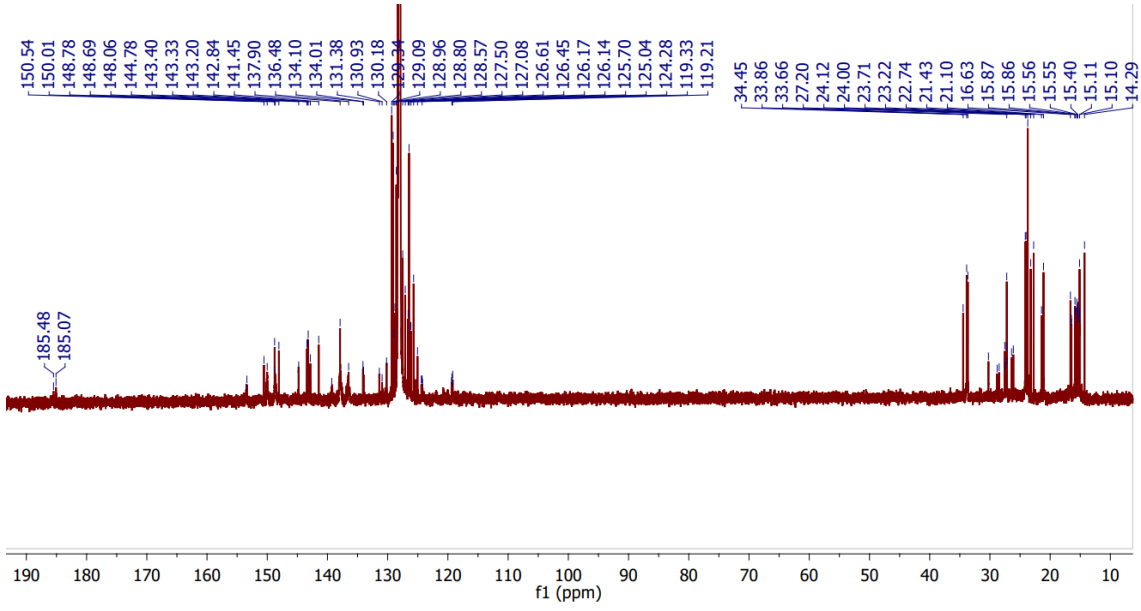

Appendix Figure IV.8. ^{13}C{^{1}H} NMR (176 MHz) spectrum of complex **18**$^{\mathbf{Mes}}$ in benzene-d_6 at 22 °C

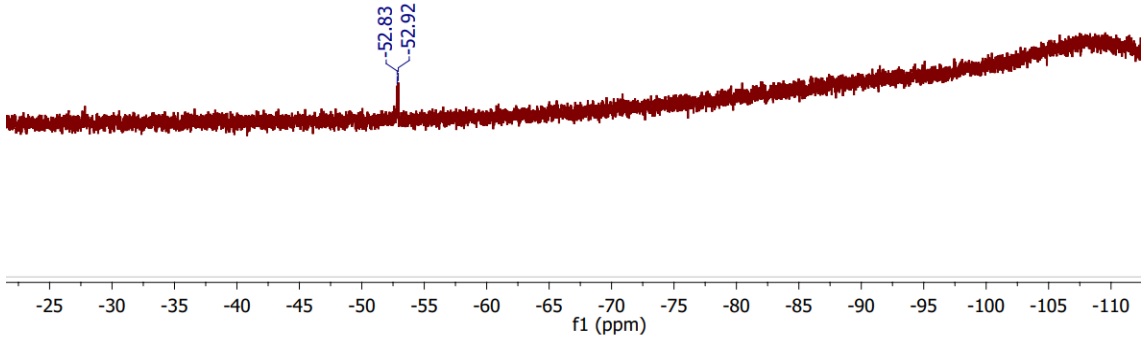

Appendix Figure IV.9. $^{29}Si\{^{1}H\}$ NMR (139.10 MHz) Spectrum of **18^{Mes}** in benzene-d_6 at 22 °C

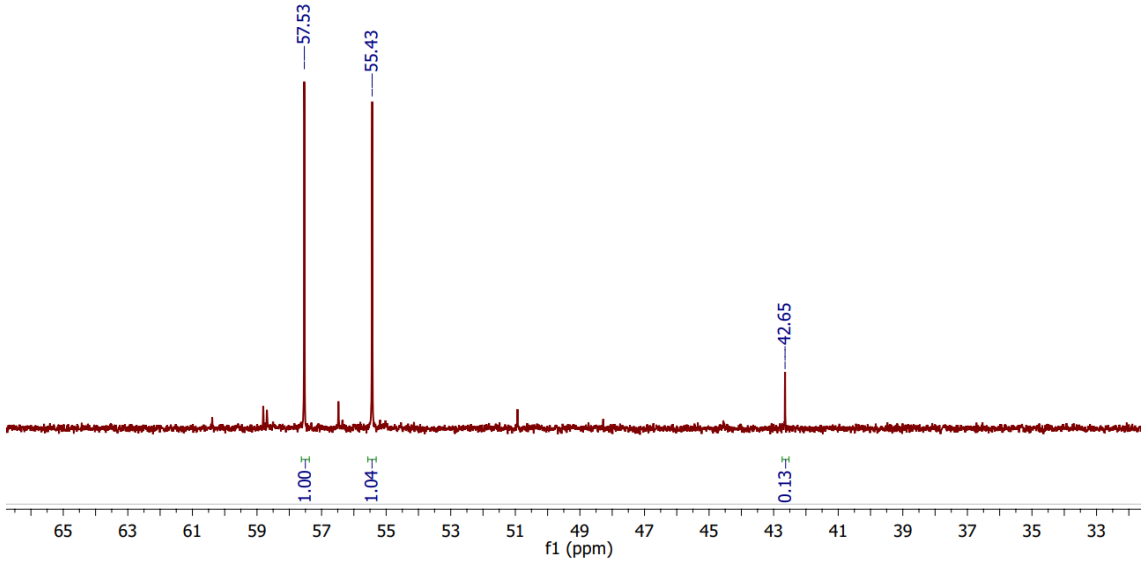

Appendix Figure IV.10. $^{31}P\{^{1}H\}$ NMR (283.5 MHz) spectrum of complex **18^{Mes}** in benzene-d_6 at 22 °C showing minor impurity

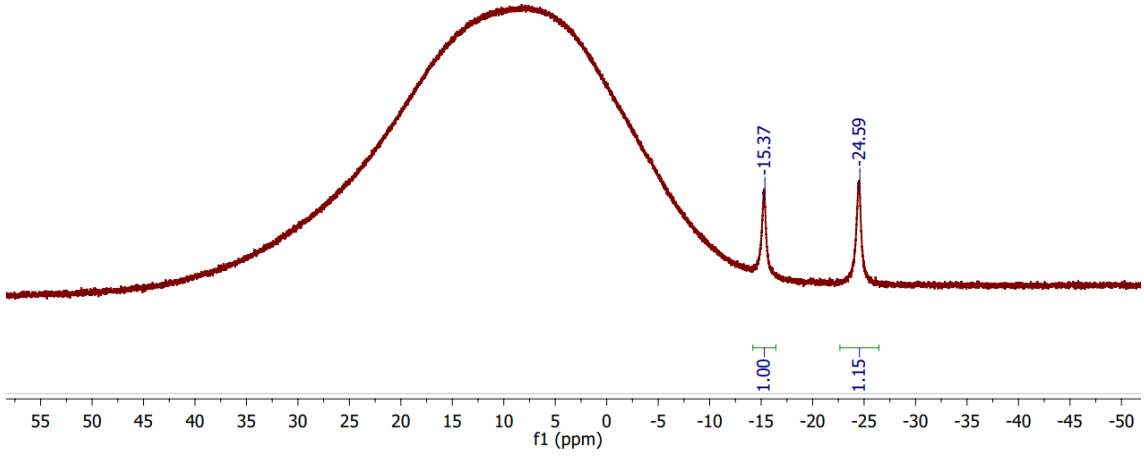

Appendix Figure IV.11. $^{11}B\{^{1}H\}$ NMR (224.6 MHz) spectrum of complex **18**^{Mes} in benzene-d_6 at 22 °C

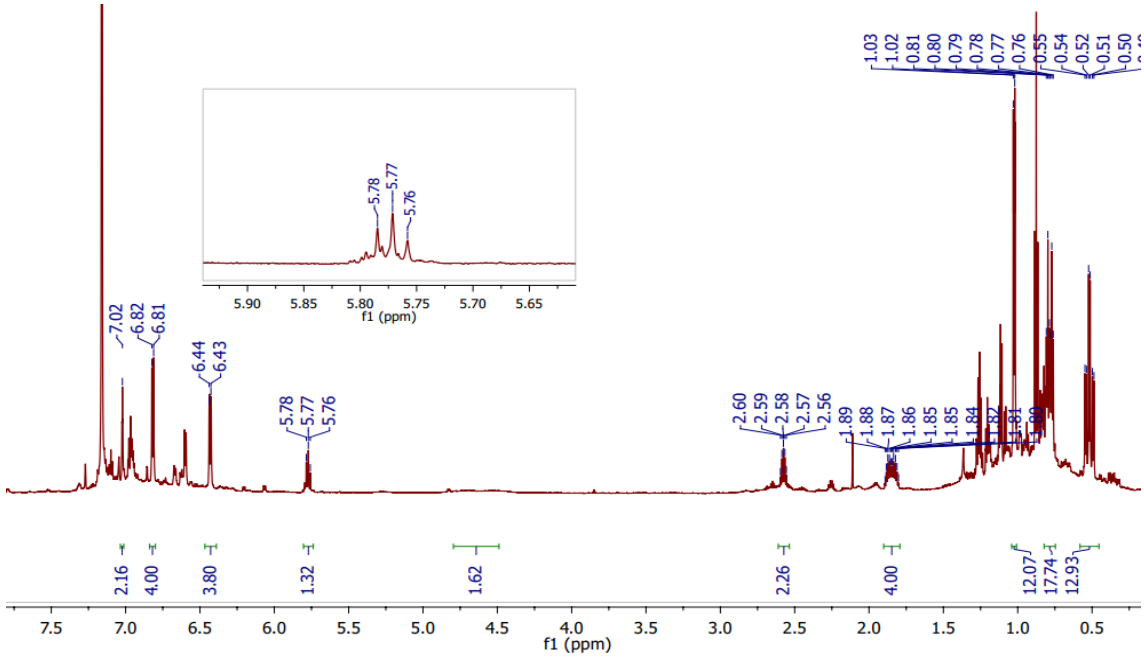

Appendix Figure IV.12. ^{1}H NMR (700 MHz) spectrum for the reaction between **2**^{Ph} and $B(C_6F_5)_3$ in benzene-d_6 at 22 °C

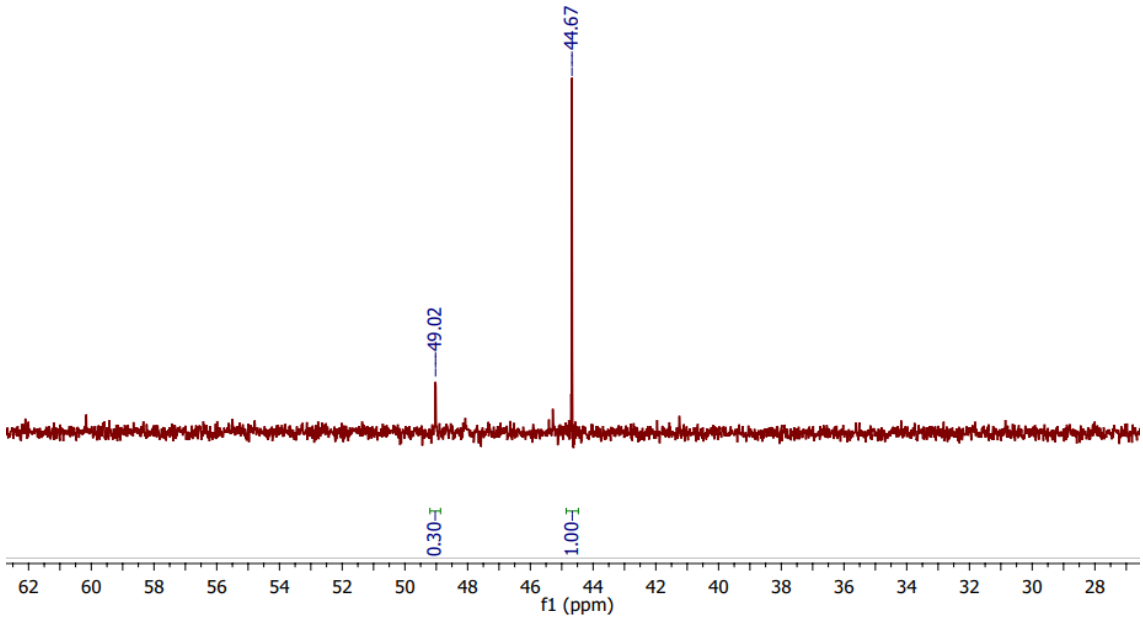

Appendix Figure IV.13. $^{31}P\{^{1}H\}$ NMR (283.5 MHz) spectrum for the reaction between $\mathbf{2^{Ph}}$ and $B(C_6F_5)_3$ in benzene-d_6 at 22 °C

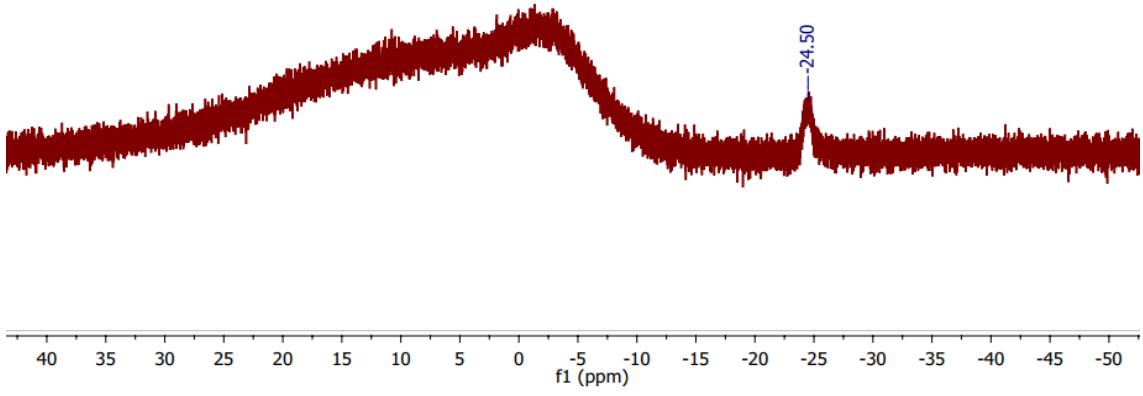

Appendix Figure IV.14. $^{11}B\{^{1}H\}$ NMR (224.6 MHz) spectrum for the reaction between $\mathbf{2^{Ph}}$ and $B(C_6F_5)_3$ in benzene-d_6 at 22 °C

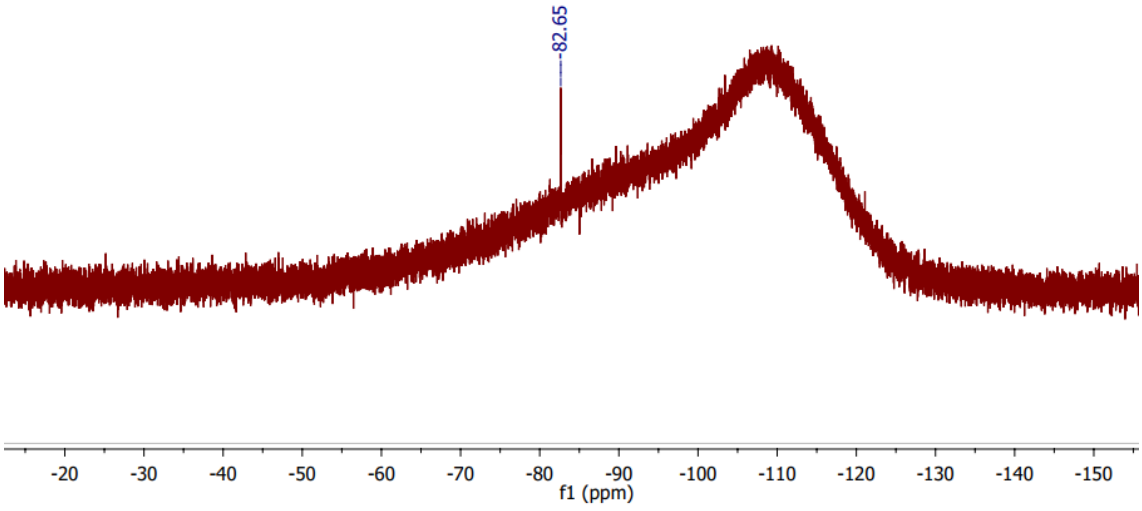

Appendix Figure IV.15. $^{29}Si\{^{1}H\}$ NMR (139.10 MHz) Spectrum for the reaction between **2^{Ph}** and $B(C_6F_5)_3$ benzene-d_6 at 22 °C

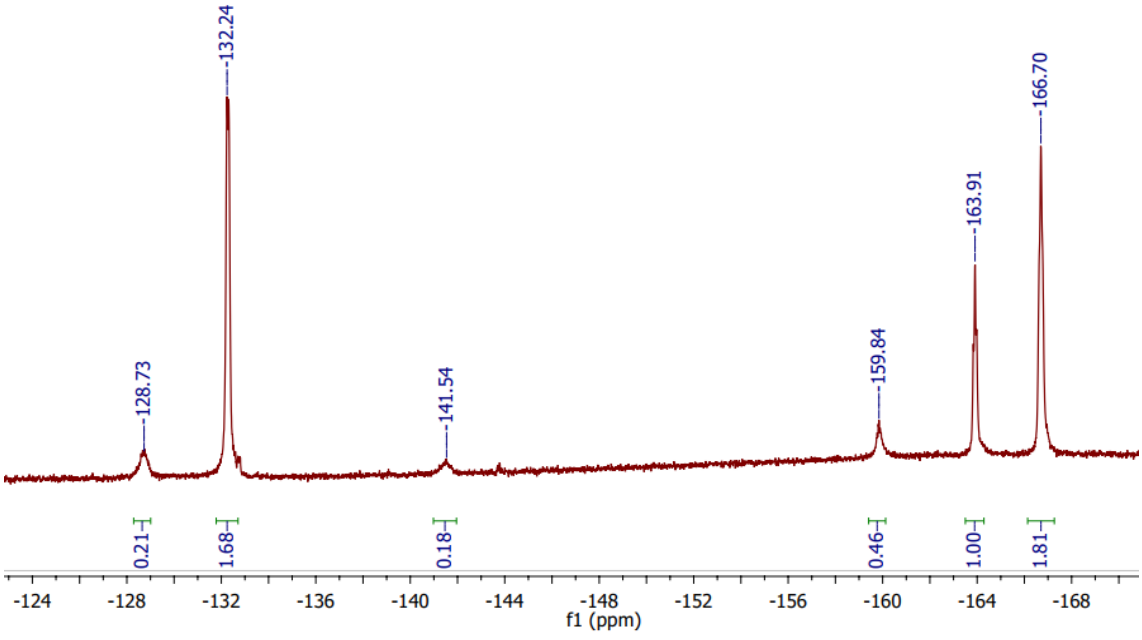

Appendix Figure IV.16. $^{19}F\{^{1}H\}$ NMR (282.43 MHz) Spectrum for the reaction between **2^{Ph}** and $B(C_6F_5)_3$ in benzene-d_6 at 22 °C